Coordination of cell envelope biogenesis and cell division by an essential two-component signaling system in Alphaproteobacteria

By

Bryan D. Lakey

A dissertation submitted in partial fulfillment of the requirements for the degree of

Doctor of Philosophy

(Genetics)

at the

UNIVERSITY OF WISCONSIN-MADISON

2022

Date of final oral examination: July 7, 2022

This dissertation is approved by the following members of the final oral committee:

Timothy J. Donohue, Professor, Bacteriology
Daniel R. Noguera, Professor, Civil and Environmental Engineering
Nicole T. Perna, Professor, Genetics
Chris T. Hittinger, Associate Professor, Genetics
Katrina T. Forest, Professor, Bacteriology

ABSTRACT

Abstract

Prokaryotes depend on a number of two-component systems (TCSs) to rapidly sense and respond to environmental stimuli. These TCSs, comprised of a signaling histidine kinase and cognate response regulator, are critical for bacterial signal integration and cellular response to external or internal cues. Commonly, these systems function to regulate the expression of target genes, or initiate larger regulatory cascades, to coordinate this response. Bacteria rely on several well-studied envelope stress response TCSs to monitor extracytoplasmic and cell envelope homeostasis as well as respond to antibiotics, toxins, host immune factors, osmotic and desiccation stress to promote survival. Other TCSs are important regulators of essential processes including cell cycle dynamics and cell wall biosynthesis. However, these systems tend to be poorly conserved and/or studied in Gram-negative bacteria. As a result, little is known about this regulation in α-proteobacteria. Therefore, one goal of my thesis project was to provide insight into these processes using the Gram-negative α-proteobacterium *Rhodobacter sphaeroides* as a model. This purple non-sulfur bacterium remodels the cell envelope under low oxygen conditions by increasing lipid content and creating intracytoplasmic membrane invaginations (ICM) that protrude from the cytoplasmic membrane and house the cell's photosynthetic machinery. Thus, we hypothesized that *Rb. sphaeroides* would be amenable to perturbation to identify the genetic basis and regulation of cell envelope remodeling and biosynthesis.

First, I characterized a previously unidentified histidine kinase (CenK) with no known cognate response regulator that when disrupted, produced cells with altered cell morphology and

hypersensitivity to compounds inhibiting peptidoglycan synthesis. This work defined the TCS that this kinase belongs in and identified an essential response regulator (CenR) as its cognate pair. Utilizing gain of function and loss of function alleles, I assayed the predicted function of CenR in transcriptional regulation and determined that this TCS regulates the expression of cell division, outer membrane biogenesis, and peptidoglycan cell wall biosynthesis and assembly. Consistent with its activity in *Rb. sphaeroides*, I found that many α-proteobacteria contain a homologous TCS and provide evidence for its conserved function in these microbes.

Expanding on this work, I utilized the cell morphological changes produced by increasing the activity of the CenKR TCS to probe poorly understood spatial and temporal cell division processes in *Rb. sphaeroides*. I showed that the localization of the outer membrane lipoprotein Pal is key to proper localization of peptidoglycan biosynthesis and the coordination of bacterial cytoskeletal proteins MreB and FtsZ. By monitoring the localization of these essential proteins, I developed a model for how these systems function in wild type cells as well as how their disruption leads to TCS mutant phenotypes. Therefore, I propose CenKR is an unusual and essential regulator of outer membrane homeostasis and division. I further propose that genetic manipulation of this TCS has and can continue to provide new insights into poorly understood process of cell elongation, cell division, and cell envelope biogenesis in *Rb. sphaeroides* and other α-proteobacteria.

ACKNOWLEDGEMENTS

This work is dedicated in its entirety to my wife, Katie (PhD). It is hard to find the words to define the support, patience, thoughtfulness, love, and patience from you over this long six years apart: You go there, and I'll go too, I'll be the one that follows you.

I am thankful for Timothy Donohue's guidance, encouragement, and passion for answering emails. I have truly enjoyed my time in the lab and am thankful for the freedom that was given to me to explore projects, pursue my thesis work, and develop as a scientist. Thanks to everyone in the Donohue lab past and present. Specific thanks to Wayne Kontur, Kimberly Lemmer, Kevin Myers, and François Alberge for everything they taught me along the way and willingness to help me troubleshoot experiments. Thanks to Rachelle Lemke for being the lab manager every lab deserves. Big thanks to the WEI support and custodial staff, sorry for always being in the way at night.

Shout out the Volleyball Squad (BackToLab), UW BBall Crew, Joel, Blake, Nate, and Adam. Thanks to everyone I've met in Grad school for forcing me to have a work life balance. Tons of memories and good times, appreciate you boys.

Lastly thanks to my family. My parents and grandparents for instilling in me a passion to learn and the toughness and perseverance to finish this PhD.

TABLE OF CONTENTS

CHAPTER 1:

Introduction – From cell membranes to biofuels

Summary

My thesis sought to understand how changes in cell membranes could impact the ability to generate new types of oleaginous microbes as a source of renewable fuels and chemicals. In the end, this work was productive by identifying and characterizing an essential regulatory system for cell envelope biogenesis and division in *Rhodobacter sphaeroides*. Before describing the results of my experiments, this chapter provides an overview on motivations for the generation of sustainable biofuels and strategies for the generation of oleaginous microbes. I will outline some features of *Rhodobacter sphaeroides* that make it attractive as a chassis microbe for the production of lipids and other hydrophobic compounds, and the potential for the regulation of this production by two-component systems in this and other bacteria. I will end with a brief summary of the major findings of my studies and introduction to the main body of the thesis.

On the production of oleochemicals and biofuels by microbes.

The increase in energy and petroleum prices, rising concerns over global crude oil supplies, the need for environmental conservation, a desire to increase economic opportunities to underserved communities, as well as climate change are major drivers for the development of a sustainable source of renewable biodiesel and bioproducts. According to the International Energy Agency, biofuels represents only 3% of total transport fuel demand in 2019 and this fraction of the total must grow to represent 12% of total usage by 2030 in order to achieve net zero carbon emission goals [1]. In the United States, ethanol, produced by microbial fermentation, is currently being blended into traditional gasoline and represents 94% of this biofuel production and demand [2]. Ethanol production, which has already met 2030 net zero emission goals, is limited by a 10% (v/v) cap in gasoline blends in many countries due to its low energy density, hygroscopicity, and the need for oxygenation in many automotive engines [1–3]. Consequently, current research has shifted to the development of a new generation of biofuel that can be used in multiple engine types and overcomes environmental and food issues associated ethanol production from starch.

These next-generation of fuel additives, similar to ethanol (C2), consist of higher carbon alcohols (C4-C6). One of which, isobutanol (C4) can be blended into existing gasoline, diesel, and aviation fuels either directly or after upgrading, with the advantage of being less hygroscopic and volatile, while offering higher energy output upon combustion [4,5]. These traits together with its higher octane number makes isobutanol a preferred option for blending into gasoline reaching ~16% of total fuel volume [4,5]. Congruent to the successful metabolic engineering strategies that have been implemented for the fermentation of ethanol, much work has been directed towards engineer a variety of model organisms, including bacteria like *Escherichia coli*, for the

production of industrial relevant quantities of isobutanol [4–7]. While this enteric bacterium is not considered to be an industrial chassis of choice for bioalcohol synthesis in the same way as sugar fermenting *Saccharomyces cerevisiae* and *Zymomonas mobilis* or the cellulose degrading C*lostridium thermocellum* [5], *E. coli* offers a rapid growth rate (doubling time of ~20 minutes) and the use of inexpensive growth media or waste streams for the fermentation of bioalcohols. Moreover, model systems like *E. coli* boast an impressive array of genetic and genome tools and editing techniques allowing for rapid engineering compared to other fermenters. This allows for non-native pathways from other organisms, like *Z. mobilis*, to be easily ported into *E. coli* for metabolic reprogramming and the fermentation of plant biomass [8]. While use of *E. coli* for the production of isobutanol has led to increased yields at faster rates, it also offers a robust experimental platform for understanding and overcoming other limitation associated with bioalcohol production such as carbon source utilization, resistance to inhibitor molecules sometimes present in feedstocks, and tolerance of high bioalcohol concentrations [5]. These insights can then be used to improve bioalcohol production in chassis microbes that are favored for industrial applications.

Today nearly all commercially available gasoline contains a 10% blend of ethanol as an oxygenate (E10) with the remaining 90% representing a complex blend of hydrocarbon molecules that are typically derived from petroleum [9]. Gasoline contains both linear and aromatic C4-C12 hydrocarbon molecules, while diesel fuels are composed of higher molecular weight molecules in the range of C8-C21. Thus, fatty acids, phospholipids, and triacylglycerides (TAGs) that can be chemically or enzymatically modified to produce fatty acyl alkyl esters (Fig 1-1A) offer a route for the production of higher molecular weight hydrocarbon molecules

necessary for gasoline and diesel production [3]. These compounds (typically C16-C22 alkyl chains) look structurally similar to diesel hydrocarbon molecules and therefore are marketed as an alternative biodiesel (Fig 1-1A). Additionally, longer chain aliphatic molecules can be used for industrial scale production of oleochemicals for the renewable and sustainable production of lubricants, surfactants, and bioplastics that are typically synthesized from crude oil [10]. One focus on the alternative synthesis of oleochemicals has relied on the chemical processing of plant biomass derived oils such as soybeans, sugarcane, etc. [11]. By doing so, biofuels reduce/offset CO_2 emissions from fuel combustion due to carbon capture in plant biomass during photosynthesis (Fig 1-1B). However, this production is limited by land mass required for production of these crops raising concerns regarding habitat destruction, water usage, competition with food production, and other ethical considerations [12–14]. In addition, agricultural production of these crops often requires the use of fertilizer and pesticides that can have negatively impact on greenhouse gas emissions, water quality and eutrophication, or other environmental issues. Similar to metabolic engineering strategies used to increase the production of isobutanol, the extensive advances in genomics, metabolic engineering, and system biology, allows for the microbial synthesis of petroleum derived oleochemicals from oleaginous microbes [15–18].

Natural and engineered oleaginous microbes

An oleaginous microbe is defined as a species with an oil content representing >20% cell biomass. Indeed, a number of oleaginous phototrophic or heterotrophic microalgal, yeast, mold, and bacterial species have been shown to accumulate lipids under a variety of conditions [15,16]. However, the accumulation of microbial lipids typically requires the use of nutrient rich or well-

Figure 1-1. Utilization microbial factories for bioproduct synthesis.

A. The structure of oleochemicals and bioalcohols. Biodiesels (green box) are structurally similar to lipids that are naturally produced by oleaginous microbes (yellow box). Modifications to fatty acids including the addition of double bonds, hydroxyl groups, branching alkyl chains, and rings produce a variety of designer lipid molecules (blue box). The molecular structure of the two main bioalcohols ethanol and isomers of butanol, including isobutanol, are shown (red box). **B.** The carbon cycle of biofuel production. Carbon emissions from fuel combustion is captured by plants during photosynthesis. Oil containing seeds can been used to product biodiesel through processing and chemical extraction. Synthetic biology approaches allow for the utilization of plant biomass by microbial communities or genetically engineered microbes for the fermentation of bioalcohols, the synthesis of biodiesel, or the specialized production of chemicals. Diverse microbial metabolism facilitates the use of other available feedstocks as well as different modes of carbon sequestration to offset CO_2 emissions. (Image created using BioRender.com).

A

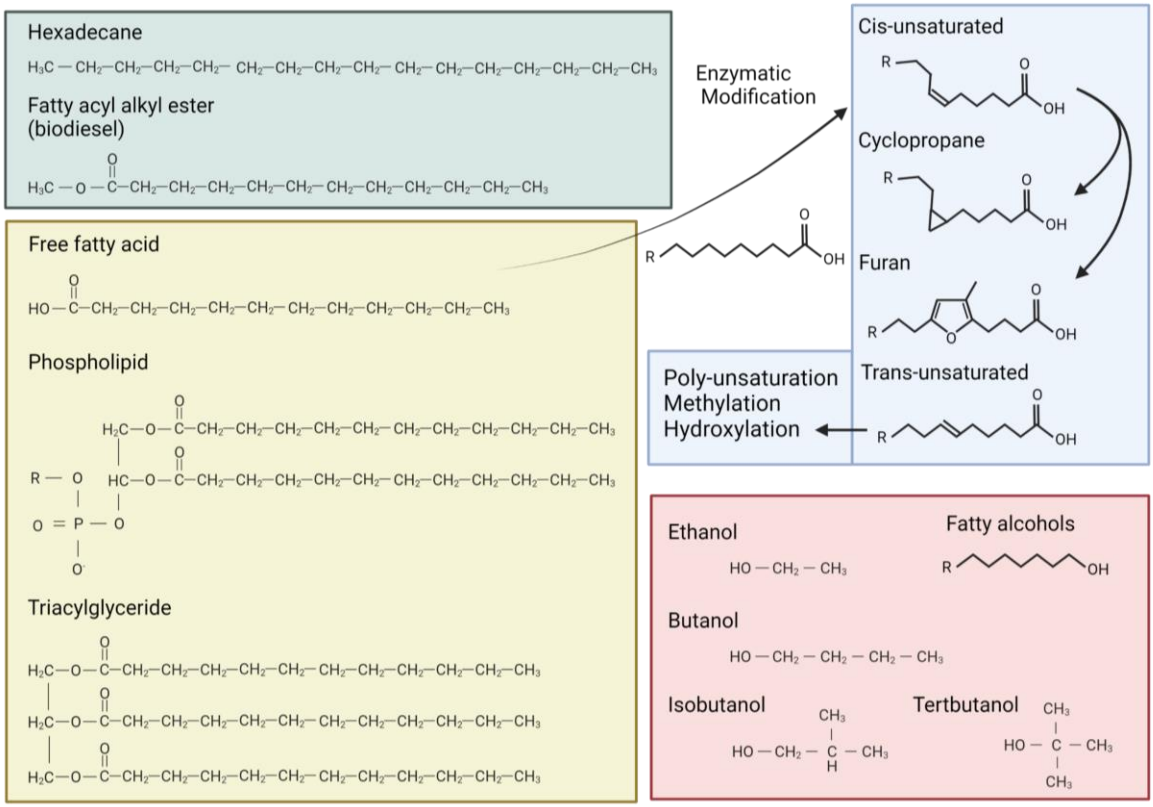
Hexadecane
Fatty acyl alkyl ester (biodiesel)
Free fatty acid
Phospholipid
Triacylglyceride
Enzymatic Modification
Cis-unsaturated
Cyclopropane
Furan
Trans-unsaturated
Poly-unsaturation
Methylation
Hydroxylation
Ethanol
Fatty alcohols
Butanol
Isobutanol
Tertbutanol

B

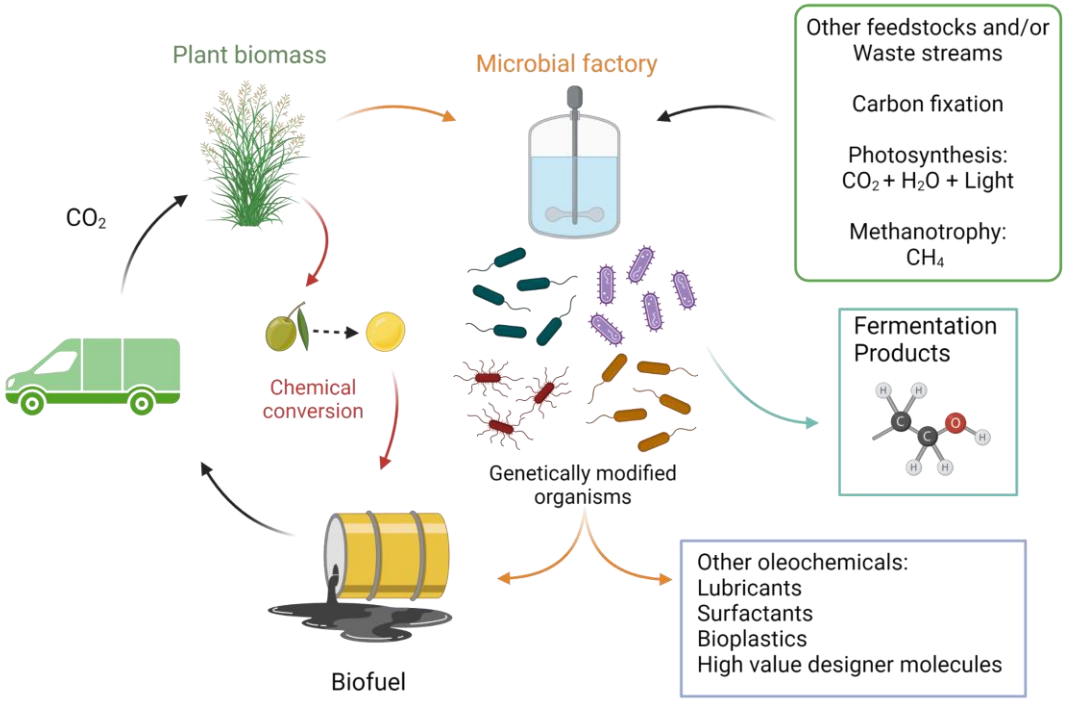
Plant biomass
Microbial factory
Other feedstocks and/or Waste streams
Carbon fixation
Photosynthesis: $CO_2 + H_2O$ + Light
Methanotrophy: CH_4
CO_2
Chemical conversion
Fermentation Products
Genetically modified organisms
Other oleochemicals:
Lubricants
Surfactants
Bioplastics
High value designer molecules
Biofuel

defined media, each of which can limit the potential for using abundant renewable agricultural or industrial waste streams to lower the cost and the environmental impact of these molecules [16,19]. In other organisms, synthesis of high levels of biodiesels can require nitrogen starvation, pH or temperature stress, or other conditions that can limit cellular growth and microbial biomass accumulation [15,17,19]. Thus, a key component for the development of industrially relevant oleaginous microbes is genetic and metabolic engineering to allow accumulation of these molecules using conditions that will allow synthesis at high titers, rates and yields from abundant resources at low cost without limiting cell titers or metabolism.

To this end, much progress has been made towards building a comprehensive understanding of the pathways for fatty acid, lipid, and triacylglycerol biosynthesis as well as the control of the genes and gene products that synthesize these molecules in oleaginous microbes, particularly in response to environmental or stress signals [16,19,20]. What's more, understanding the synthesis and regulation of these pathways in oleaginous microbes - many of which have traditionally not been well studied – can allow for application of engineering principles that are derived within non-oleaginous systems. This can lead to the development of new oleaginous producing microbial chassis and the combination or 'stacking' of industrially relevant processes within one organism [21]. Broadly speaking, these engineering approaches have sought to maximize a pathway's potential for the synthesis of a desired product by reducing competition for pathway intermediates, deregulating feedback inhibition or allosteric regulation within the pathway, balancing enzyme expression levels with activity, optimizing cofactor production to facilitate energetically expensive processes, and/or preventing reverse pathway flux [12]. Coupled together, these approaches have been shown to be effective in engineering Actinomycetes [22]

and species of microalgae [23] to accumulate 55-75% and 25-50% of dry cell weight as TAGs, respectively. Some of these differences in productivity between these organisms can be attributed to variations in growth rates and biomass accumulation, the energetics of carbon fixation (CO_2) in phototrophic microbes [23], compared to heterotrophic pathways that can sequester carbon from abundant lignocellulosic biomass (or other organic residue streams) for synthesis of TAGs and other oleaginous molecules (Fig 1-1B). Furthermore, the use of microaerophilic heterotrophs to produce oleaginous molecules has some advantages over algae or other organisms when one considers the need for space, oxygen, light, or water by this and other microbes [20,23]. Consequently, bacteria may offer another or even a better alternative for the synthesis of lipid-based biofuels, at industrial and economically feasible quantities, especially if these can be derived from renewable resources and produced in a manner that allows low-cost growth of the microbial chassis and isolation of the product.

Secretion of oleochemicals as a strategy to reduce product toxicity and cost.

While TAG storage granules (also known as lipid droplets) are common to oleaginous and other eukaryotic organisms like microalgae, yeast, and fungi, they are found only in a small group of bacteria, with the majority of prokaryotes synthesizing fatty acids, phospholipids or other specialty lipids for the production and/or maintenance of cell membrane(s). This makes bacteria attractive hosts for the synthesis of specific lipids or other oleochemicals. However, unlike TAGs that are neutral storage lipids and do not typically result in toxicity when accumulated internally, often the overproduction of polar lipid at similar levels results in membrane disfunction, permeabilization, and/or cell death [24]. Therefore, an additional engineering strategy that should be considered for the industrial scale production of bacterial lipids is the transport or secretion of

these molecules into the media. Examples of lipid transport strategies have relied on the overexpression of bacterial drug efflux pumps and outer membrane channel proteins in *E. coli* to move free fatty acids to the exterior of the cell [25]. Other approaches have blocked reuptake and extracellular degradation of secreted free fatty acids by inhibiting FadL a long-chain fatty acid transporter in *E. coli* [26]. It has been also shown the co-culturing fatty acid secreting bacteria in dodecane improved production and allows for nearly 100% product recovery by phase separation of extracellular lipids from the culture media and cells [27]. Since isolation or extraction of products from cells or media is often a major cost, secretion and real time recovery of lipids from the media represent additional strategies that should be considered to further lower cost and increase efficacy of industrial oleochemical production.

The major roles of bacterial lipids are to provide membrane structure and function, regulate its fluidity as a function of changes in temperature or osmolarity, or respond to laboratory or environmental stresses [28]. Given their chemical properties, the last steps of lipid synthesis typically occurs at the cell membrane and are catalyzed by integral membrane proteins with others membrane associated proteins required for specific modifications [28]. Therefore the vast majority of saturated, unsaturated, branched, cyclopropane, and furan containing ‘specialty’ fatty acyl chains in bacterial lipids are found as part of membrane phospho- or other lipids and are not easily secreted from the cell [12,29,30]. Recent work to increase fatty acid secretion has included expression of a foreign phospholipase in the purple non-sulfur bacterium *Rhodobacter sphaeroides* [31]. This phospholipase (taken from *Arabidopsis thalinana*) was trafficked to the periplasmic space and was able to cleave the ester bond(s) of phospholipids fatty acyl chains. This strain was shown to secrete free fatty acids into the media that were recovered by growing

cells in media containing dodecane to prevent fatty acid toxicity [31]. As the cell membranes of bacteria represent the largest store of lipids within cells, controlled release of oleaginous molecules (specialty and otherwise) across the bacterial cell envelope offers a potentially new avenue for the production and secretion of lipid-derived bioproducts.

Overview of the Gram-negative bacterial cell envelope.

Any successful strategy to secrete lipids or other molecules into the media as a way to increase their production and overcome toxicity must not interfere with normal function of the cell envelope. The cell envelope of Gram-negative bacteria consists of three distinct, but highly connected, layers: the inner membrane (IM), outer membrane (OM), peptidoglycan (PG) cell wall, and periplasmic space (Fig 1-2).

The IM surrounds the cytoplasm and is home to several important functions including energy conservation, lipid biosynthesis, protein secretion, and transporters that facilitate the influx of nutrients or the efflux of toxins/waste products. In *Rb. sphaeroides*, the organism that is the subject of my thesis research, the IM is a phospholipid bilayer composed primarily of phosphatidylglycerol, phosphatidylethanolamine, phosphatidylcholine, and cardiolipin [32–34] with primarily 18:1, 18:0, and 16:0 acyl chains [35]. Furthermore, *Rb. sphaeroides* is capable of producing glycoglycerolipids, sulfolipids, and betaine lipids that are present in smaller quantities, may serve specialized roles, and are present at higher levels under phosphate-limiting conditions [35,36]. In addition, when *Rb. sphaeroides* cells are grown at low oxygen tensions (< 1%), there are reports of increased levels of phosphatidylglycerol and cardiolipin in the membrane compared to highly aerated cells, presumably due to proportions of these phospholipids present

in the ICM [34]. Under high osmotic conditions, it has been reported that *Rb. sphaeroides* cells have elevated cardiolipin levels [37]. In addition, cardiolipin has been shown to be important for maintaining *Rb. sphaeroides* shape and transport of PG cell wall precursor molecules to the periplasm, suggesting a role for cardiolipin in the envelope function that has not been observed in well-studied Gram-negative bacteria such as *E. coli* [38,39].

The OM is comprised of an inner leaflet of phospholipids and an outer leaflet of glycolipids which in most Gram-negative species are lipopolysaccharide (LPS) molecules [40]. This asymmetric membrane encircles the cell and forms the outer most barrier that separates the cell from the environment. The OM includes lipoproteins anchored into the inner leaflet that serve structural and other roles within the periplasmic space, as well as so-called porins - beta-barrel proteins that serve are size-controlled pores for selective diffusion of substrates into the cell or export of toxins into the media. Recently, the OM has been shown to be the key contributor to cell rigidity and the load bearing function of the cell envelope rather than the PG cell wall [41]. Specifically, LPS, and to a lesser extent OM proteins, have been shown to be key for maintain OM stiffness [41]. These amphipathic LPS molecules have negative charges at the cell surface, but they are packed into the OM via their fatty acyl chains [40]. The presence of divalent cations, like magnesium (Mg^{2+}) neutralize the negative charge of the LPS allowing non-covalent interactions between neighboring molecules to exclude hydrophobic molecules [40]. Together, the OM is selectively permeable and makes Gram-negative bacteria inherently resistant to many antibiotic treatments and more resilient to environmental or host agitates.

Figure 1-2. The Gram-negative cell envelope.

A model of the three layers of the cell envelope. The OM consists of an inner leaflet of phospholipids and an outer leaflet of protective, rigid lipopolysaccharide molecules anchored into the outer leaflet by lipid A. The OM is separated from the IM, a phospholipid bilayer, by the PG cell wall. The cell wall consists of repeating disaccharide units crosslinked via short peptide sidechains. The OM and PG layers are closely associated by lipoproteins that anchor the two together. (Image created using BioRender.com).

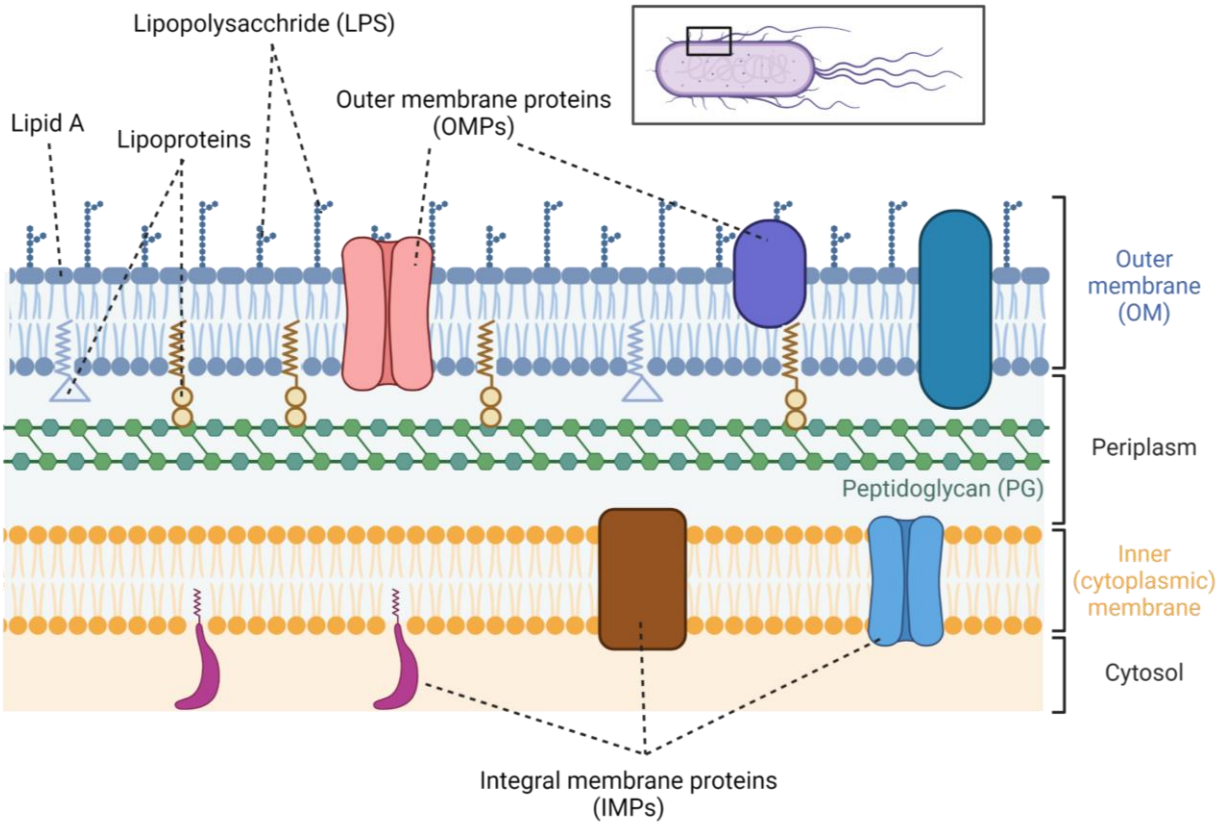

The Gram-negative PG is a single-layered polymer consisting of repeating disaccharides N-acetyl glucosamine-N-acetyl muramic acid that are crosslinked via pentapeptide sidechains [42,43]. This interconnection forms a mesh-like structure that encases the cell and determines cell shape. The glycan strands are organized perpendicular to the length of the cell and contain pores allowing for the diffusion of nutrients or polymers such as proteins and nucleic acids [44]. In order to maintain viability, the cell wall is an elastic structure allowing the cell to synthesize, remodel, and adapt to defects and damages arising from environmental stressors, as well as coordinate normal processes like cell elongation and division [42,44,48]. The robustness of the PG is a key part of the cell wall's role in resisting internal osmotic pressure as well as formation of a cell septum and seperation of daughter cells during cell division. Given the relative thinness of the Gram-negative PG compared to that found in Gram-positive bacteria, coordination between the synthesis and autolysis of the PG strands in the cell wall during division, repair or response to environmental stress must be tightly regulated to maintain viability, growth, and prevent cell lysis.

The OM and PG layers are linked through the abundant lipoproteins, like Lpp in *E. coli*, that are both anchored in the OM and covalently bound to the peptide stem of PG molecules [40]. Other noncovalent interactions between OM β-barrel proteins like OmpA or lipoproteins like Pal also contribute to forming OM-PG interactions and cell envelope stability [49,50]. Disrupting the interconnection between the OM and PG layers as a consequence of loss of Lpp, OmpA, or Pal lead to the increased production of OM blebs or vesicles due to OM instability [50]. For α-proteobacteria, which lack Lpp homologues, this function and stability is proposed to be

substituted by covalent crosslinks between β-barrel proteins and the PG cell wall to facilitate cell envelope stability [51].

The OM and IM and separated by a viscous periplasmic space that houses the PG cell wall as well as many proteins with functions in mitigating or sensing extracytoplasmic stress, protein folding, transport, cell envelope assembly, and energy conservation. In some species, like *Rb. sphaeroides*, periplasmic proteins can function in both aerobic and anaerobic respiration [52–54]. Importantly, the fundamental nature of the periplasmic space also allows for the compartmentalization of specialized activities that otherwise might be detrimental to cell survival in nature, such as the production of DNases or broad specificity phosphatases [40]. This compartmentalization of functions in Gram-negative bacteria is long thought to be the predecessor of eukaryotic organelles acquired via independent endosymbiotic acquisition events. Finally, the presence of this compartment requires additional coordination between the IM and OM-PG layers to ensure proper division and represents an additional obstacle for recognizing environmental cues.

The cell envelope is also the site of cell elongation and division (Fig 1-3). Much of what is understood about cell elongation and division and the regulation of these processes has been derived from studies in γ-proteobacteria, like *E. coli* and other pathogenic bacteria. In these species, synthesis of the PG cell wall is performed by bifunctional penicillin binding proteins (PBPs) 1A and 1B that have both glycosyltransferase (GTase) and transpeptidase (TPase) activity. These bifunctional PBPs link nascent glycan strains and polymerize peptide crosslinks, respectively, and in concert with monofunctional TPase (PBP2, PBP3) or GTase (RodA, FtsW)

enzymes [42,43,55,56]. In these cells, nascent PG synthesis is known to occur in two stages to facilitate cell elongation (at an elongasome) and division (in the divisome). Localization of the elongasome is mediated by the actin homolog MreB that polymerizes within the cytoplasmic at the membrane into short filaments along the length of *E. coli* [57] and other α-proteobacteria [58], or at the midcell in *Rb. sphaeroides* [59]. To direct nascent PG synthesis, MreB recruits the GTase RodA [57], the TPase PBP2, and MreCD, which modulate the activity of PBP2/RodA, to balance synthesis and crosslinking of the cell polymer [45,60]. The dual function PBP1A has also been implicated in this process by interacting with PBP2 and contributing strength to the growing lateral PG cell wall [43,45]. Localization of the divisome is initiated by polymerization of the Z-ring, comprised of the tubulin homolog FtsZ, at the midcell in many organisms[57]. Once polymerized FtsZ rings recruit other divisome proteins, including the GTase FtsW and TPase PBP3/FtsI as well as the dual functioning PBP1B [47,48] whose activity is regulated by the FtsQLB complex and FtsN [48,61]. Alphaproteobacteria, while retaining homologues of many of the core proteins predicted to be needed for cell elongation and division, lack a number of components that are key to these processes in other Gram-negative bacteria. For example, the lipoproteins LpoA and LpoB that have been shown in *E. coli* to regulate the activity of bifunctional PBPs are not found in many α-proteobacteria, so it is not known if and how PBP activity is regulated in α-proteobacteria [62]. Additional, some members of the *Rhizobiales*, like *Agrobacterium tumerfaciens* rely solely on polar growth and elongation strategies and do no encode genes for MreB or other elongasome machinery, instead relying solely upon FtsZ directed PG synthesis [63,64]. Recent work has also shown that the essentiality, conservation, number, and structure of PBPs varies significantly throughout α-proteobacteria [63,65,66].

Figure 1-3. Core constituents of the *Escherichia coli* divisome and elongasome.

In the Gram-negative bacterium *E. coli*, separate multiprotein machines are used to synthesize nascent PG cell wall during growth (elongasome [45]) and division (divisome [46]) [43]. **A.** Divisome assembly is initiated by FtsZ polymerization at the midcell to allow cell septum formation. FtsZ polymerization results in the recruitment of the cytoplasmic domains of FtsA, ZipA, and FtsK transmembrane proteins (not shown) thereby anchoring FtsZ to the midcell. This FtsZ-containing complex recruits the regulatory FtsQLB subcomplex, as well as the FtsW and PBP3 (FtsI) for PG polymerization and crosslinking, respectively. FtsN is the last protein recruited to the divisome, activating the FtsQLB complex to initiate PG synthesis. FtsQLB activity also coincides with PBP1b activation. Regulation of PBP1b TP activity is also modulated by the lipoprotein LpoB in tandem with CpoB and members of the Tol-Pal complex. **B.** Polymerization of MreB filaments organize and direct localization of the elongasome (also known as the Rod complex) for the synthesis, polymerization (RodA and PBP1a), and crosslinking (PBP2 and PBP1a) of PG cell wall along the length of the cell. The activity of PBP1a is regulated by interactions with PBP2 and the lipoprotein LpoB which affects TP activity [REF]. The MreCD subcomplex regulate the activity of the PBP3-RodA, and functions in conjunction with RodZ to stabilize MreB polymerization and interactions with the rod complex. TP, transpeptidase domain; GT, glycosyltransferase domain. L, FtsL; B, FtsB; n-PBD, non-penicillin binding domain. This figure was adopted from Leclercq *et al* 2017 [47].

Major components of the Divisome

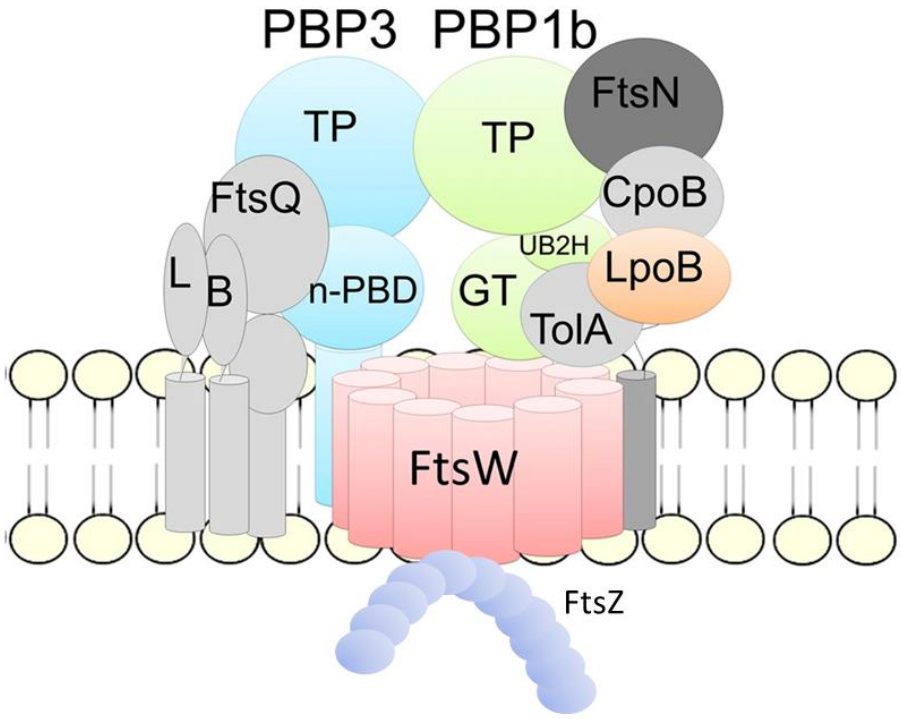

Major components of the Elongasome

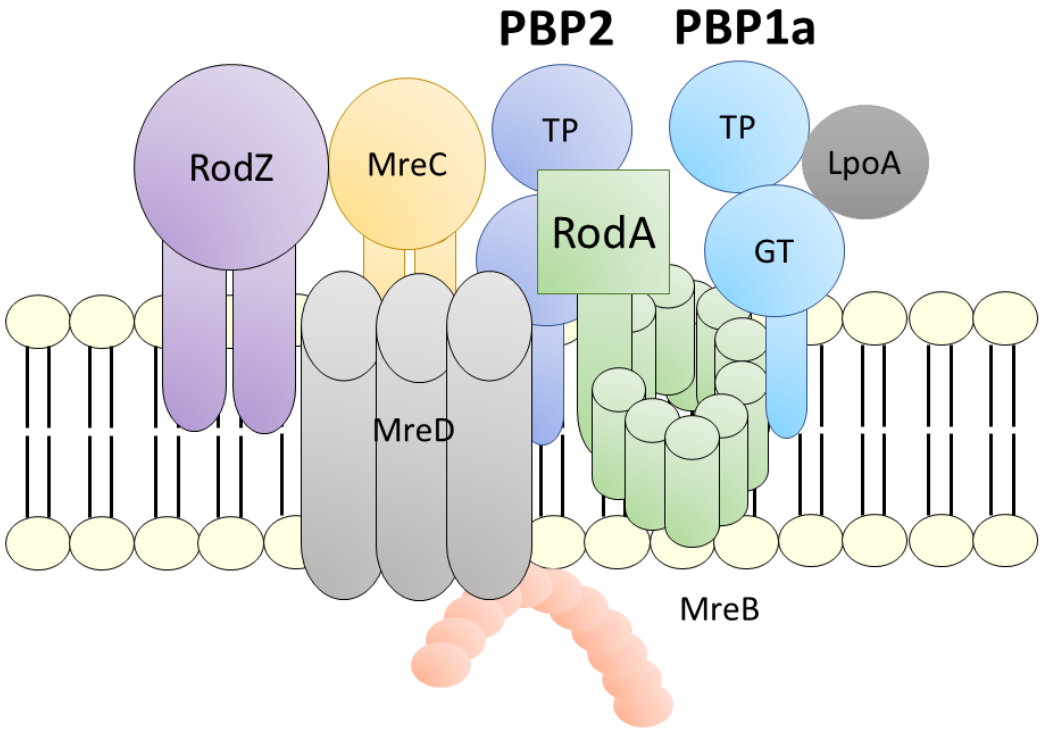

It has also been shown in *E. coli* that certain PBPs are essential for resistance to acidic or alkaline pH, suggesting that they can serve specialized roles [67]. This adaptation of specialized function of PBPs may be extended to some of the duplicated α-proteobacterial homologues that have yet to be studied in these organisms. Similarly, differences in the subcellular positioning of MreB and FtsZ between α-proteobacteria and other Gram-negative species suggests they do not use the same strategies for cell elongation and division [58,68–72]. Indeed, α-proteobacteria display a variety of cell elongation and division strategies including stalked budding in the *Caulobacterales* and *Rhizobiales*, lateral growth by members of the *Caulobacterales*, unipolar elongation in *Rhizobiales*, prosthecate budding by members of the *Rhizobiales* and *Rhodospirillales*, as well as poorly or uncharacterized growth patterns throughout these clades, including for *Rb. sphaeroides* [73]. These various cell elongation and division patterns underscores why elucidating the processes of cell elongation and division are key to understanding and altering bacterial cell envelope structure to balance viability with secretion of valuable molecules.

Outer membrane vesicles as candidate hydrocarbon secretion systems.

The OM of Gram-negative bacteria can also serve as a site for the production of outer membrane vesicles (OMVs) that bud from the cell surface and are released into in the media. This is a natural phenomenon in some Gram-negative species where it is proposed to serve a variety of functions including: removal of toxic compounds or misfolded proteins from the periplasmic space, increase survival under stress, aid in nutrient capture or iron scavenging, avoid antibiotics or phages, promote horizontal gene transfer, and release of virulence factors, toxins, or antigens

by pathogenic species [50,74]. While OMVs can be enriched with certain cargo, as a rule, OMVs contain lipids, LPS, and proteins normally found in the OM of whole cells [50,74].

In some cases, the release of OMVs can be modulated by affecting the stability and interconnection between cell envelope layers, often OM-PG connection, or by events or chemicals that create an imbalance between OM and PG synthesis (Fig 1-4). For example, when normal lipoprotein-mediated linkages between the OM and PG layers are disrupted, cells produce more vesicles, likely stemming from continued biogenesis of OM that is not properly linked to the cell wall resulting in the formation, bulging, and subsequent release of excess membrane as vesicles or blebbs [50,74,75]. Increased PBP autolysin (i.e. PBP4, 5, and 7 [76]) activity can also promote OMV production, presumably by digestion of pentapeptide crosslinks in PG, thereby preventing Lpp-OM or other interactions that are needed for cell envelope integrity [50,74,77]. Additionally, conditions that cause an increase in the release of PG disaccharide subunits (from PG digestion, mis-assembly, and/or damage) or the stress of accumulating misfolded extracytoplasmic proteins from similar stressors, can promote secretion of OMVs as a means of removing unwanted materials from the periplasmic space [50,74].

It has also been shown that changes in the state of the LPS layer from loss of divalent cations, enzymatic modifications, or antibiotic treatment leads to the accumulation of negatively charged LPS in the outer leaflet of the OM promoting OMV formation due to charge repulsion on the surface of the envelope [50,78]. More recently, the engineering of OMV production by bacteria have been used as delivery vehicles for cancer treatments, vaccine production, and other drugs [79,80]. In the context of bioproduct production, OMV secretion allows for accumulation of

extracellular lipids, other membrane soluble materials (quinones, carotenoids) and any hydrophilic molecules trapped in the lumen of extracellular vesicles that could be recovered by a variety of aqueous or other separation systems. Engineering strategies for the secretion of these vesicles have and will likely continue to rely on the principles discussed above to subtly disrupt OM integrity and stability to further improve oleaginous microbes.

A growing body of data suggests phospholipid trafficking between the IM and OM plays a role in OMV production [81]. Specifically, the Maintenance of Lipid Asymmetry (Mla) complex is proposed to allow bi-directional transport of lipids between the IM and OM [82]. However, Mla function is only essential for the retrograde transport of lipids back to the IM [82]. Loss of Mla function leads to the accumulation of OM phospholipids in the outer leaflet, a state that is proposed to compromise membrane rigidity leading to OMV [83].

Figure 1-4. Destabilization of the outer membrane leads to vesicle production.

Factors that influence OMV production. Loss of lipoproteins and breakdown of the PG cell wall leads to OM-PG instability resulting in membrane blebbing. Endopeptidase (denoted by the blue Pacman) cleaves PG peptide stems disturpting its interactions with OM lipoproteins. PG disaccharides or periplasmic proteins can be found in OMV, along with OM components. Loss of the normal OM asymmetry (peach) can increase cellular lipid content and form lipid-rich microdomains leading to OMV formation. (Image created in BioRender.com)

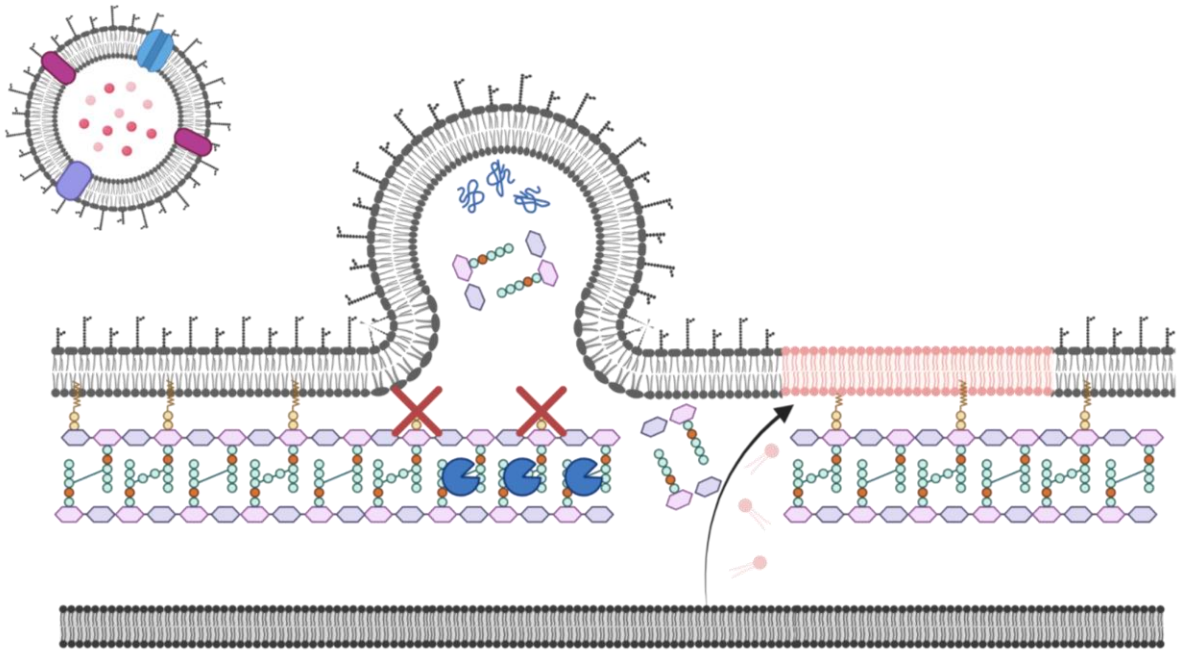

Other events that disrupt the membrane lipid composition or the interactions of the OM with cell envelope components have been reported to lead to membrane vesicle formation. For example the accumulation of phospholipid-enriched 'microdomains' is reported to significantly alter membrane fluidity and curvature, leading to membrane budding, vesicles, invaginations, and division across bacteria and in eukaryotic organelle cristae [84]. OMV release can also be driven by accumulation of cardiolipin, or other non-cylindrical lipids that generate negative membrane curvature like those normally found at cell division sites and poles of rod shaped microbes [85]. Transport of cardiolipin to the OM in γ-proteobacteria is performed by PbgA that also plays secondary roles in LPS transport [86,87]. Furthermore, the Tol-Pal system has been shown to be involved in antegrade phospholipid movement, however this appears to be an indirect effect of the role Pal has in OM stability leading to increased phospholipid antegrade movement in order to replace lost OMVs [88]. In sum, many chemical, genetic or environmental changes that lead to increased OMV production do not necessarily lead to cell lysis [89]. The overproduction of OMV leads to loss of OM phospholipids and LPS that must be replaced by phospholipids from the IM. If the balance is not restored, cell lysis occurs through loss of IM integrity and shrinkage [89]. Mla mutants produce large amounts of OMVs from the cell division septum prior to lysis, a process that can be delayed by stalling cell division and Z-ring formation suggesting a role in OM to IM retrograde lipid trafficking in this process [89]. Given the ability of *Rb. sphaeroides* to remodel its cell envelope and increase production of IM phospholipids for ICM synthesis (described below), it would be interesting to test the impact of Mla and other mutations in processes that lead to increased phospholipids, loss of OM bilayer asymmetry, and OMV production from the sites of cell division or due to envelope destabilization.

***Rhodobacter sphaeroides* as an industrial chassis microbe.**

My thesis sought to leverage the properties of *Rb. sphaeroides* as a chassis to produce lipids and other hydrocarbons by analyzing the genetic features of previously characterized high lipid producing mutants [90]. Before expanding on this, I will introduce this model organism and highlight key features that make it an intriguing candidate for understanding cell envelope changes that lead to lipid accumulation and secretion.

Rb. sphaeroides is a Gram-negative purple non-sulfur α-proteobacterium, that historically has been studied extensively as a model of photosynthesis [91–94]. Additionally, this organism can utilize an extensive variety of metabolic modes including photoautotrophy, photoheterotrophy, chemolithotrophy, chemoheterotrophy, aerobic and anaerobic respiration, and fermentation [94,95]. This myriad of metabolic modes likely contributes to the wide distribution of natural habitats occupied by *Rb. sphaeroides*.

Recently, biotechnological application of *Rb. sphaeroides* as a microbial factory to produce several bioproducts has come to the forefront of interest in this and related α-proteobacteria. Strains of *Rb. sphaeroides* have been engineered to produce antioxidant ubiquinone [96,97], various isoprenoids (such as β-carotene a precursor for vitamin A synthesis) [98], polyhydroxybutyrate (a potential alternative for the synthesis of plastics) [99,100], hydrogen gas (‘biogas’) [100,101], furan fatty acids (antioxidant compounds with potential as a fuel additive) [102], as well as others [103]. Moreover, the metabolic and respiratory versatility of *Rb. sphaeroides* allows it to be grown in bioreactors fed with various feedstocks and waste streams at

different oxygen tensions, expanding the options for valorizing the synthesis of bioproducts during industrial scale production [100,103].

In addition to the ability to synthesize these specialized products, *Rb. sphaeroides* naturally increases its cellular membrane content under anaerobic growth conditions (Fig 1-5) [104]. In the presence of oxygen, *Rb. sphaeroides* morphology resembles that of many other Gram-negative organisms. When oxygen tensions decrease, *Rb. sphaeroides* cells produce internal membrane vesicles that invaginate and bud from the IM [93,105]. These intracytoplasmic membranes (ICM) house photosystems, light harvesting complexes, and other photosynthetic machinery for the light reactions of photosynthesis. Thus, the production of ICMs and expansion in membrane surface area under microaerophilic conditions, results in a threefold increase in lipids and an increase in the cellular levels of other membrane bound products (quinones, carotenoids, etc) compared to highly aerated cells [104]. Efforts to understand the regulation of ICM development and lipid synthesis in *Rb. sphaeroides* has revealed global regulators of this membrane differentiation process [92,105–109].

In many other microbes, the energetic favorable flow of cellular reducing power to oxygen during aerobic respiration competes with the synthesis of lipids and other highly reduced products. Thus, understanding the molecular mechanisms driving increase in fatty acids, lipids and other hydrophobic compound levels in *Rb. sphaeroides* under low or anoxygenic conditions presents an opportunity to develop new strategies for producing these and other molecules in bacteria. Published research has shown that mutations exist which promote secretion of sufficient lipids to designate these *Rb. sphaeroides* mutants as oleaginous bacteria [90]. Below I

Figure 1-5. *Rhodobacter sphaeroides* produces ICM vesicles in response to reduced oxygen tensions resulting in lipid accumulation, pigment production, and cell envelope remodeling. In the presence of oxygen *Rhodobacter sphaeroides* resembles other rod-shaped Gram-negative microbes in appearance (A) and overall shape (B). In microaerobic or anaerobic conditions, cells are capable of anaerobic photosynthesis producing invaginations of the IM (arrows in A) to increase membrane surface area per cell and store light gathering machinery giving cells their characteristic colors (D). Production of these invaginations increased the fatty acid content per cell due to the accumulation of intercellular lipids (C) and generates longer, wider cells that resemble coccoid bacteria (B). Images in panel A courtesy of Timothy J. Donohue, University of Wisconsin-Madison. (and can also be found at https://fr.wikipedia.org/wiki/Rhodobacter)

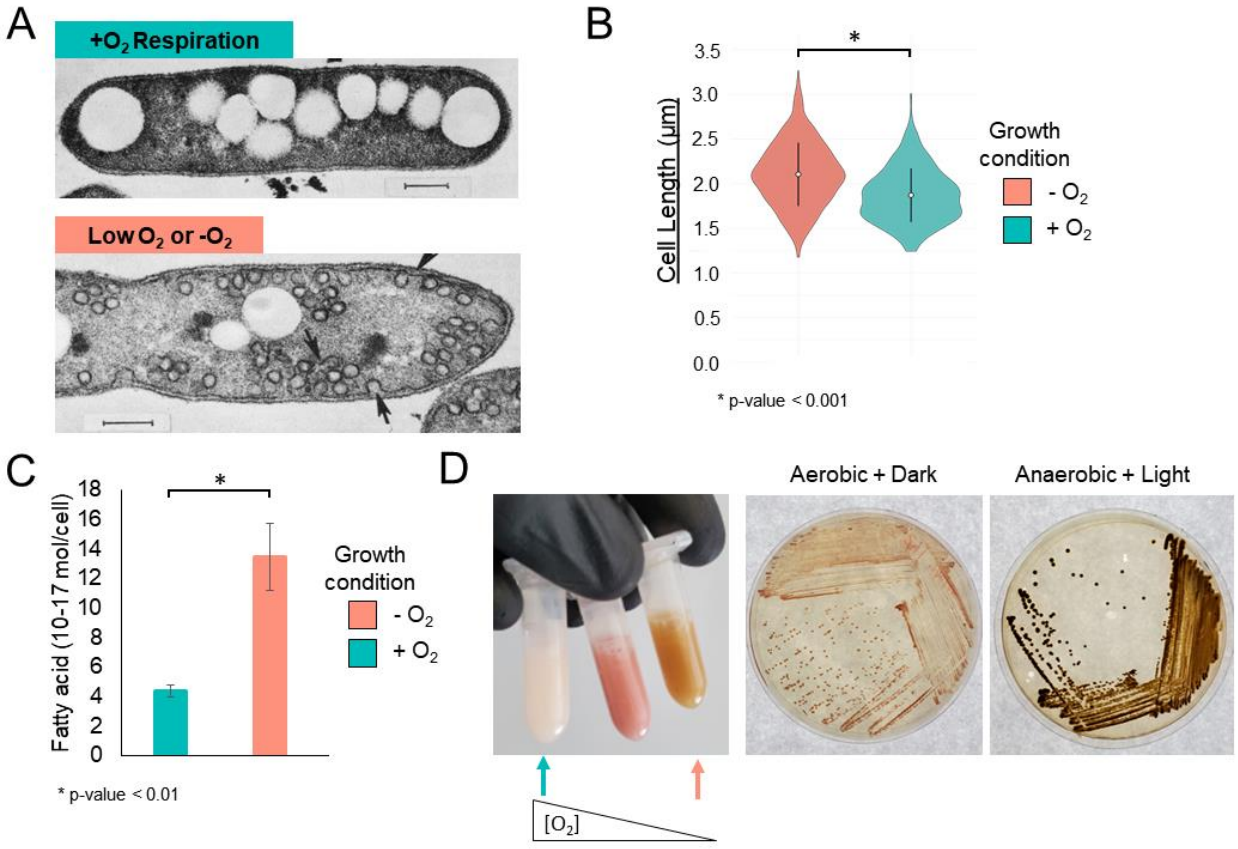

introduce *Rb. sphaeroides* lipid overproducing mutants containing lesions that directly impact function the of the bacterial cell envelope and lead to secretion of oleochemicals into the media.

Rhodobacter sphaeroides high lipid mutants as a potential source of extracellular lipids

We previously reported on a series of *Rb. sphaeroides* mutants that produced higher yields of lipids under aerobic conditions when cells normally do not produce ICM vesicles [90]. It was later shown that none of the causal mutations mapped to genes known to be involved in the process or regulation of lipid or fatty acid synthesis, suggesting that there were other causes for the high lipid phenotype. In fact, all of the high lipid mutants had altered cell morphology (shorter or longer cell lengths) and were found to be sensitive to drugs that target the cell wall, OM, and/or acted as polar detergents suggesting that these mutations altered proteins that impacted the permeability of the OM and LPS and more broadly affects overall cell envelope homeostasis [90]. Interestingly, three of these strains that secreted lipids into the media had lesions within genes encoding two different two-component systems (TCSs). Two of these genes encoded the NtrY-NtrX TCS and the third gene was *RSP_1056* that was predicted to encode a histidine kinase. Together, this suggests that each of these two putative TCS may play a previously unrealized role in the regulation of cell envelope processes that somehow lead to lipid overproduction and secretion. Indeed, previous analysis of the NtrYX TCS shows that it is a global regulator of genes encoding PG and LPS biosynthesis enzymes and transport machinery as well as other proteins that function in cell envelope or division processes [110]. My thesis research focused on analyzing the function of RSP_1056 in order to explain how insertions in this gene led to a high-lipid phenotype. Before doing this, I will next discuss features of TCSs, how they can function in bacteria, and their role in the regulation of cell envelope events.

Figure 1-6. High lipid mutant strains of *Rhodobacter sphaeroides*.

A. Transposon mutagenesis produced ten high lipids mutants with fatty acid contents greater that parent cells grown at high oxygen conditions [104]. The fatty acid content of parent and high lipid mutants separated by cellular and medium content shown as a stacked bar graph. This analysis identified several strains that secrete lipids (as measured by fatty acids; dashed lines). Of particular interest for this thesis is strain HLM04 containing a transposon insertion within the gene *RSP_1056* encoding a putative histidine kinase. Data represents the mean value measured from >3 biological replicates. Error bars represent standard deviation. **B.** Transposon insertion sites identified within each high lipid mutant. This figure was adopted from Lemmer *et al* 2017 [90].

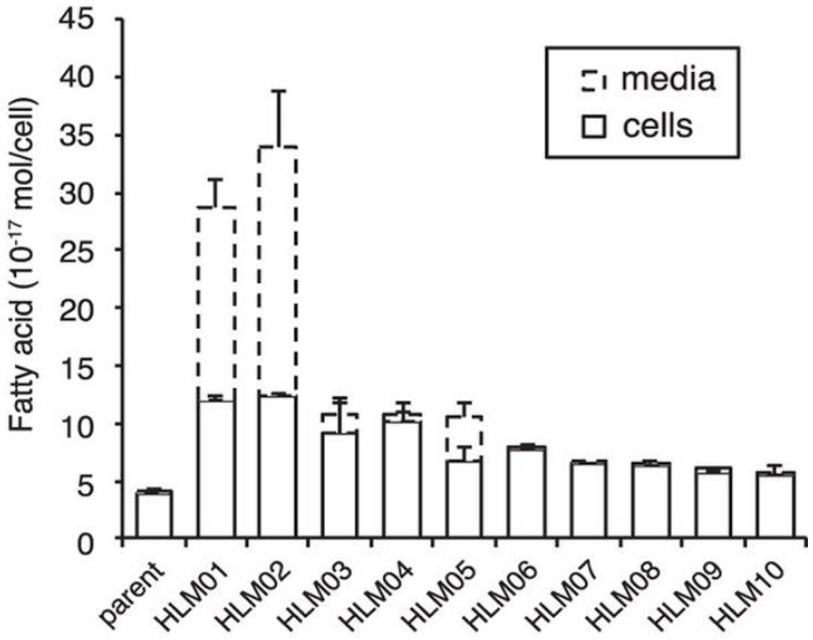

Strain	FA inc. (fold)	Insertion site	ORF(s) disrupted, with annotation	Sig. pep.	TM helix
HLM01	6.7	Chr1: 1471645	RSP2839, NtrY sensor signal transduction histidine kinase	No	5
			RSP2840, NtrX response regulator	No	None
HLM02	6.1	Chr1: 1469665	RSP2840, NtrX response regulator	No	None
HLM03	2.7	Chr2: 274987	RSP3218, cob(II)yrinic acid a,c-diamide reductase/5,6-dimethylbenzimidazole synthase	No	None
HLM04	2.7	Chr1: 2814885	RSP1056, signal transduction histidine kinase	No	2
HLM05	2.6	Chr1: 2970757	RSP1200, uncharacterized conserved protein YkwD	Yes	None
HLM06	1.8	Chr2: 938456	RSP1422, chromosome partitioning protein, ParB family	No	None
HLM07	1.7	Chr1: 2086261	RSP0355, periplasmic serine protease DegP	No	1
HLM08	1.7	Chr1: 1189239	RSP2545, stationary-phase survival protein SurE	No	None
			RSP2544, protein-L-isoaspartate *O*-methyltransferase (pcm)	No	None
			RSP2543, peptidoglycan D,D-endopeptidase	Yes	None
HLM09	1.5	Chr1: 1395725	RSP2745, Stealth protein	No	None
HLM10	1.5	Chr1: 916649	RSP2293, ClpA, ATP-dependent Clp protease ATP-binding subunit	No	None

[a] Strains are sorted from highest to lowest fold increase in total fatty acid (FA inc.) compared to the parent strain. The presence of a signal peptide (Sig. pep.) was predicted by SignalP 4.1 (http://www.cbs.dtu.dk/services/SignalP/), and the number of predicted transmembrane helixes (TM helix) was determined by TMHMM Server v.2.0 (http://www.cbs.dtu.dk/services/TMHMM/).

The function and role of bacterial two-component systems.

Two-component systems (TCSs) are a large and highly conserved family of signal transduction pathways facilitating bacterial response to external as well as internal stimuli [111]. Canonical TCSs consist of a histidine kinase (HK) and response regulator (RR) the latter often functions as a DNA binding protein to positively or negatively impact transcription upon activation (phosphorylation) by the former.

HKs contain an N-terminal sensory domain and a C-terminal dimerization/histidine phosphorylation (DHp) and catalytic-ATP binding (CA) domain [112]. Nearly all HKs form homodimers through specific amino acid interactions in the DHp domain and the vast majority of these kinases are membrane bound (~65%) [112,113]. The sensory domain of a HK is variable to allow recognition of an impressive array of stimuli from light, pH, metal ions, redox states, small molecules, antibiotics, peptides, proteins, and host signals as well as others [114]. Membrane associated HKs relay the signal through structural changes in the downstream transmembrane domain that is amplified into a larger conformational change and activation of the C-terminal portion of the protein by either a PAS (Per-ARNT-Sim), HAMP (histidine kinase, adenyl cyclase, methyl-accepting proteins, and phosphatases), or less common GAF (cGMP-specific phosphodiesterase, adenylyl cyclase, and FhlA) domain [111,112]. The number of PAS, HAMP, or GAF domains or the presence of some combination of the three, as well as, the specific structural changes that occur within a HK for signal transduction, dictate subfamily classifications and vary between kinases, likely explaining the observed high variety of input stimuli [112].

Figure 1-7 Canonical bacterial two-component sensory systems. Most common bacterial TCSs are comprised of an integral membrane HK and a soluble cytoplasmic RR. Upon activation, the HK autophosphorylates a conserved histidine (H) residue within the cytoplasmic DHp domain. This phosphoryl group is then transferred to a cognate RR, phosphorylating a conserved aspartate (D) residue in the REC domain, resulting in conformational changes and activation of a downstream effector domain. Most RRs act as transcriptional regulators therefore phosphorylation allows for RR-promoter interaction and the modulation of transcription. Repression and/or activation of transcription produces a tailored cellular response based on the input stimuli that are recognized by the HK. (Imaged created using Biorender.com)

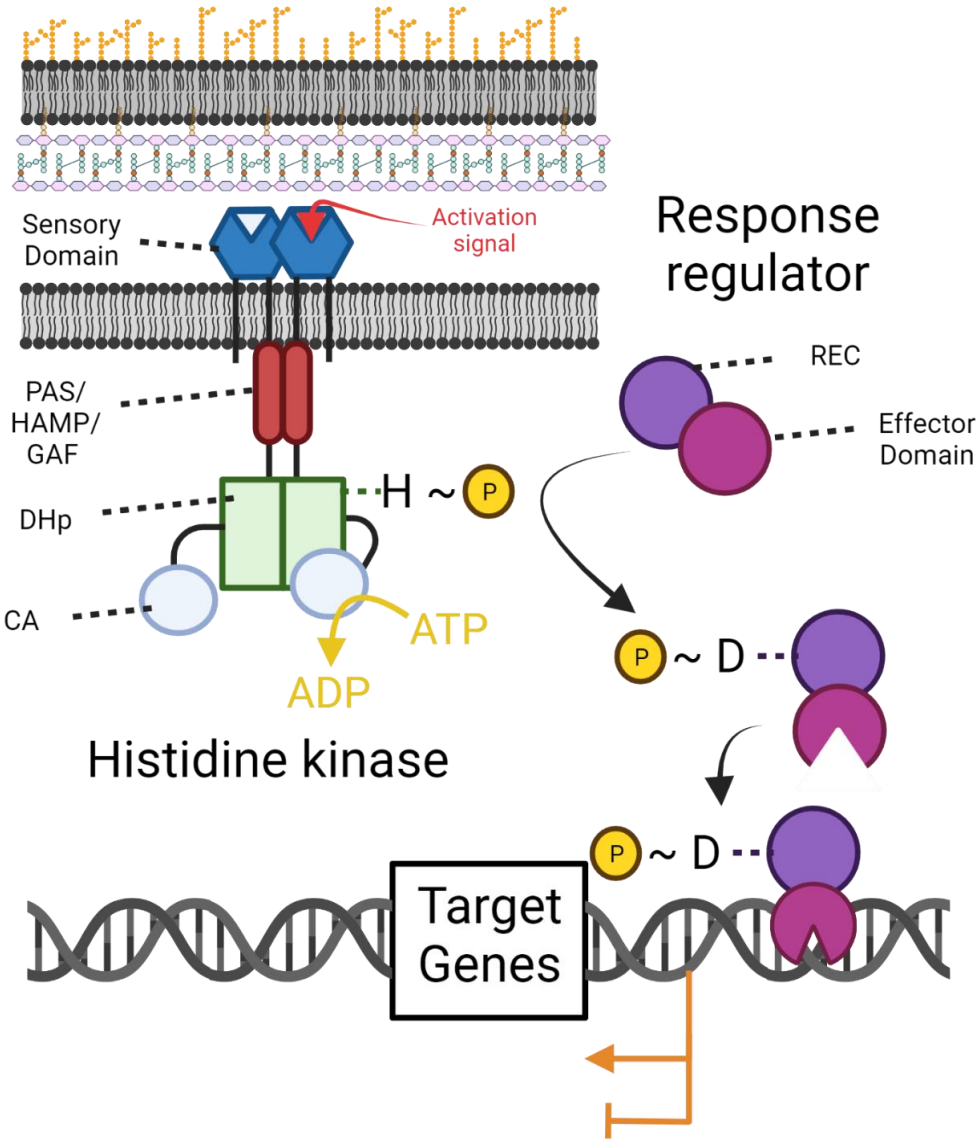
Sensory Domain
Activation signal
Response regulator
REC
Effector Domain
PAS/ HAMP/ GAF
DHp
H ~ P
CA
ATP
ADP
P ~ D
Histidine kinase
P ~ D
Target Genes

Overall, signal-mediated HK conformational changes serve to bring the CA domain containing ATP close to the DHp domain containing the phospho-accepting histidine residue enabling coordination of Mg^{2+} by catalytic (often acidic) residues in both domains for successful autophosphorylation [111,112].

Upon autophosphorylation, specific RR and HK interactions are facilitated by interactions between amino acids at the surface of the RR REC (receiver domain) and HK DHp domains [112]. While exceptions exists, the residues involved in HK-RR interactions are co-evolutionarily conserved to insulate cognate TCS pairs and to prevent unwanted cross-talk between other HK-RR pairs [113]. Cognate HR-RR TCS pairs are often encoded within the same transcriptional unit, but there are numerous instances of 'orphaned' HK-RR pairs that are encoded at distinct genomic loci but still exhibit a high degree of specificity for their cognate protein partners [113,115].

Allosteric interactions with the REC domain rotates the CA region of the HK to its original position allowing phosphotransfer to a conserved aspartate residue in the REC domain of the RR [111,112]. By analogy to HK autophosphorylation, acidic residues proximal to the phospho-accepting aspartate within the REC domain of the RR facilitate phosphotransfer [116]. Phosphorylation of the RR aspartate results in conformational changes and activation of a downstream effector domain to elicit a specific cellular response. Most often the RR effector domain contains a DNA-binding motif (~61%), but examples of RR with cyclic-di-GMP synthesis, methyltransferase, kinase, RNA-binding, or protein binding have been described [117]. Of the DNA-binding domains in known RR proteins, the winged helix-turn-helix and

helix-turn-helix represent over 75% of DNA-binding motifs indicating that many of these transcription factors bind tandem direct repeat sequences as oligomers [117].

The half-life of REC phosphorylation varies widely among RRs [117] and can be shortened by the phosphatase activity of some cognate HKs in the absence of the input stimulus [112]. These features contribute to maintain TCS activity under the appropriate conditions, and to prevent unwanted activity of an RR that may become aberrantly phosphorylated by small molecule donors [118] or a non-cognate HK [119]. Loss of phosphorylation returns the RR to an inactive state by inhibiting DNA recognition or enzymatic activity. In summary, the ubiquitous nature of TCS and the specificity of HK-RR interactions coupled with the versatility of signal recognition by the HK and the cellular response of the RR, allows TCSs to naturally control a myriad of cellular functions and opens the possibility of using these systems as master regulators in the bioengineering of microbial cell factories.

Rhodobacter sphaeroides two-component systems.

Rhodobacter sphaeroides 2.4.1 is somewhat unusual as it contains a bipartite genome consisting of two circular chromosomes that each encode essential genes (3.19 Mb and 0.94 Mb) as well as five plasmids (0.11-0.05 Mb) [91]. In general, the number of TCS genes found in a bacterium appears to be positively correlated with genome size and niche, with organisms occupying diverse or changing environments encoding more TCS genes [113]. Similarly, *Rb. sphaeroides* 2.4.1, which is found in a variety of environments and displays considerable metabolic versatility, encodes many 94 TCS genes (45 HKs and 49 RRs) on chromosome I and 21 (10 HKs and 11 RRs) on chromosome 2 with at most two on some of the plasmids [91,120].

Of the characterized *Rb. sphaeroides* TCS, the most well-studied is the photosynthetic response regulatory pair, PrrBA, which is essential for photosynthetic growth (anaerobic conditions in the presence of light) [121]. The membrane-bound HK PrrB is involved in sensing a redox signal derived from the cbb_3 cytochrome *c* oxidase thereby using electron flow through the aerobic respiration to control activity of this TCS as a proxy for oxygen tension [122,123]. Under anaerobic conditions, the kinase activity of PrrB phosphorylates PrrA, a DNA-binding RR, which directly regulates a total of 34 operons that include over 250 genes [92]. Specifically, PrrA activates expression of the so-called photosynthetic gene cluster (~67 kb genomic region containing 10 operons), electron transport, tetrapyrrole and terpenoid biosynthesis genes [92]. Furthermore, oxygen-regulated lipid accumulation was suggested to be controlled in part by PrrA as Δ*prrA* mutants fail to accumulate lipids under microaerobic (0.5% O_2) conditions [104]. However, it is not clear which differentially expressed genes under direct, or indirect control, allow PrrA to impact lipid production. Therefore, how *Rb. sphaeroides* directly regulates increased lipid accumulation that accompanies membrane invagination and ICM formation during cell envelope remodeling is still an unanswered question.

Given the essential role of many cell envelope processes, it is not surprising that bacteria have evolved several two-component regulatory systems to ensure normal assembly and function of the PG, periplasm and OM. In *E. coli* and other γ-proteobacteria, the Cpx and Rcs TCSs have been shown to monitor and regulate cell envelope biosynthetic processes [124–128]. These TCSs respond to defects in assembly of OM β-barrel proteins (Bam complex), lipoprotein trafficking (Lol complex), or LPS assembly (Lpt complex) [124,129]. Combined these TCSs use positive

and negative regulators of HK activity to maintain envelope homeostasis, mitigate stress, and prevent lysis by controlling the expression of chaperons, proteases, lipases, exopolysacchride production, antibiotic resistance genes, as well as PG remodeling pathways and other cell envelope maintenance processes [126,128,130,131]. Some other γ-proteobacteria employ the conserved PhoPQ TCS, to directly activate the expression of genes for synthesis of cardiolipin, glycolipids, or other non-phosphate lipids, to maintain cell envelope integrity when starved for phosphate or to decrease LPS synthesis as a mechanism to evade host defense systems [132]. However, none of these characterized TCSs are found in α-proteobacteria, so it is likely these organisms use other TCS(s) or transcription factors to ensure normal assembly and function of the PG, periplasm and OM. Most recently, the ChvGI and NtrYX TCSs have been identified as regulators of cell envelope biogenesis in *Caulobacter crescentus* [133] and *Rb. sphaeroides* [110]. However, their cellular roles do not appear to be conserved across all α-proteobacteria, since there are reports of ChvGI and NtrYX regulating pathogenesis and nitrogen fixation, respectively, in *Rhizobiales* [110,133].

The isolation of *Rb. sphaeroides* high lipid mutants identified a gene (*RSP_1056*) encoding a previously uncharacterized HK that was not a homologue of ChvG or NtrY. [90,110,133]. Cells lacking RSP_1056 also had an altered cell shape and were sensitive to chemicals and antibiotics that act at the cell surface [90]. Combined, these facts predicted that RSP_1056 was a member of a previously uncharacterized α-proteobacterial TCS that, when mutated, leads to the overproduction and secretion of lipids. However, the cognate RR for RSP_1056 in this putative TCS was unknown making it impossible to predict how insertions in the gene for this newly discovered HK led to these phenotypes. Given the natural ability of *Rb. sphaeroides* to remodel

its cell envelope in response to environmental conditions, and its ability to produce lipids and other valuable hydrocarbons, I choose to focus my research on characterizing the TCS controlled by this HK and understand the role of RSP_1056 in this bacterium and possibly other α-proteobacteria.

Introduction to Thesis

In Chapter 2, I demonstrate that RSP_1056 is indeed a HK and used its activity to identify its cognate response regulator. Interestingly, this RR (encoded at *RSP_0847*) is an essential gene in *Rb. sphaeroides*. By combining genetic, biochemical, and genomic approaches, I was able to specifically manipulate the activity of this RR and use this approach to identify the direct targets controlled by this DNA-binding transcription factor. I show that both direct and indirect members of this TCS's regulon encode many proteins that are required for cell shape, elongation, and division. Consequently, we refer to this TCS as CenKR to denote the role in **c**ell **en**velope function as a **k**inase-**r**egulator pair.

In Chapter 3, I expand on the functional characterization of this TCS by overexpressing *cenK* in order to increase CenKR activity. I then used this overexpression strain to examine morphological differences stemming from cell elongation and division defects compared to wild type cells and to model how CenKR activity affects this process and develop hypotheses for the secretion of lipids in these strains. Furthermore, examining these processes in wild type cells offers the first comprehensive description cell wall biosynthesis dynamics in *Rb. sphaeroides* and how it differs from *E. coli* or other well studied α-proteobacteria.

In the final Chapter of this thesis, I summarize how my findings have shed new light on the process and control of cell envelope functions in α-proteobacteria, suggest additional experiments to dissect cell elongation and division in *Rb. sphaeroides* and other Gram-negative bacteria and inform future studies on the generation of this and other oleaginous microbes for the production and secretion of biofuels and designer lipids.

In the appendix, I outline additional experimental data as it relates to the study of the CenKR TCS. I also provide a brief overview to experiments that I have performed to characterize the iron-sulfur cluster transcriptional regulator (IscR) in *Rb. sphaeroides*. I highlight deletion phenotypes, suppressor analysis, the regulon of IscR, as well as experiments to characterize the novel metal coordination site in the N-terminus. These experiments provide important insight into the metabolic regulation of iron-sulfur clusters in photosynthetic bacteria.

References

1. IEA (2021), Transport Biofuels, IEA, Paris https://www.iea.org/reports/transport-biofuels
2. USDA ERS (2022), U.S. Bioenergy Statistics. https://www.ers.usda.gov/data-products/u-s-bioenergy-statistics/
3. d'Espaux L, Mendez-Perez D, Li R, Keasling JD. Synthetic biology for microbial production of lipid-based biofuels. Current Opinion in Chemical Biology. 2015;29: 58–65. doi:10.1016/j.cbpa.2015.09.009
4. Chen C-T, Liao JC. Frontiers in microbial 1-butanol and isobutanol production. FEMS Microbiology Letters. 2016;363: fnw020. doi:10.1093/femsle/fnw020
5. Liang L, Liu R, Freed EF, Eckert CA. Synthetic Biology and Metabolic Engineering Employing Escherichia coli for C2–C6 Bioalcohol Production. Frontiers in Bioengineering and Biotechnology. 2020;8. Available: https://www.frontiersin.org/article/10.3389/fbioe.2020.00710
6. Sherkhanov S, Korman TP, Chan S, Faham S, Liu H, Sawaya MR, et al. Isobutanol production freed from biological limits using synthetic biochemistry. Nat Commun. 2020;11: 4292. doi:10.1038/s41467-020-18124-1
7. Baez A, Cho K-M, Liao JC. High-flux isobutanol production using engineered Escherichia coli: a bioreactor study with in situ product removal. Appl Microbiol Biotechnol. 2011;90: 1681–1690. doi:10.1007/s00253-011-3173-y
8. Flores AD, Ayla EZ, Nielsen DR, Wang X. Engineering a Synthetic, Catabolically Orthogonal Coculture System for Enhanced Conversion of Lignocellulose-Derived Sugars to Ethanol. ACS Synth Biol. 2019;8: 1089–1099. doi:10.1021/acssynbio.9b00007
9. UEIA (2016), Almost all U.S. gasoline is blended with 10% ethanol. https://www.eia.gov/todayinenergy/detail.php?id=26092
10. Biermann U, Bornscheuer U, Meier MAR, Metzger JO, Schäfer HJ. Oils and Fats as Renewable Raw Materials in Chemistry. Angewandte Chemie International Edition. 2011;50: 3854–3871. doi:10.1002/anie.201002767
11. Sawangkeaw R, Ngamprasertsith S. A review of lipid-based biomasses as feedstocks for biofuels production. Renewable and Sustainable Energy Reviews. 2013;25: 97–108. doi:10.1016/j.rser.2013.04.007
12. Pfleger BF, Gossing M, Nielsen J. Metabolic engineering strategies for microbial synthesis of oleochemicals. Metabolic Engineering. 2015;29: 1–11. doi:10.1016/j.ymben.2015.01.009
13. Fargione J, Hill J, Tilman D, Polasky S, Hawthorne P. Land Clearing and the Biofuel Carbon Debt. Science. 2008;319: 1235–1238. doi:10.1126/science.1152747
14. Thompson PB. The Agricultural Ethics of Biofuels: The Food vs. Fuel Debate. Agriculture. 2012;2: 339–358. doi:10.3390/agriculture2040339
15. Liang M-H, Jiang J-G. Advancing oleaginous microorganisms to produce lipid via metabolic engineering technology. Progress in Lipid Research. 2013;52: 395–408. doi:10.1016/j.plipres.2013.05.002

16. Levering J, Broddrick J, Zengler K. Engineering of oleaginous organisms for lipid production. Current Opinion in Biotechnology. 2015;36: 32–39. doi:10.1016/j.copbio.2015.08.001

17. Meng X, Yang J, Xu X, Zhang L, Nie Q, Xian M. Biodiesel production from oleaginous microorganisms. Renewable Energy. 2009;34: 1–5. doi:10.1016/j.renene.2008.04.014

18. Koreti D, Kosre A, Jadhav SK, Chandrawanshi NK. A comprehensive review on oleaginous bacteria: an alternative source for biodiesel production. Bioresources and Bioprocessing. 2022;9: 47. doi:10.1186/s40643-022-00527-1

19. Kosa M, Ragauskas AJ. Lipids from heterotrophic microbes: advances in metabolism research. Trends in Biotechnology. 2011;29: 53–61. doi:10.1016/j.tibtech.2010.11.002

20. Muñoz CF, Südfeld C, Naduthodi MIS, Weusthuis RA, Barbosa MJ, Wijffels RH, et al. Genetic engineering of microalgae for enhanced lipid production. Biotechnology Advances. 2021;52: 107836. doi:10.1016/j.biotechadv.2021.107836

21. Singh D, Sharma D, Soni SL, Sharma S, Kumar Sharma P, Jhalani A. A review on feedstocks, production processes, and yield for different generations of biodiesel. Fuel. 2020;262: 116553. doi:10.1016/j.fuel.2019.116553

22. Alvarez H, Steinbüchel A. Triacylglycerols in prokaryotic microorganisms. Appl Microbiol Biotechnol. 2002;60: 367–376. doi:10.1007/s00253-002-1135-0

23. Hwangbo M, Chu K-H. Recent advances in production and extraction of bacterial lipids for biofuel production. Science of The Total Environment. 2020;734: 139420. doi:10.1016/j.scitotenv.2020.139420

24. Sheibani S, Richard V, Beach A, Leonov A, Feldman R, Mattie S, et al. Macromitophagy, neutral lipids synthesis, and peroxisomal fatty acid oxidation protect yeast from “liponecrosis”, a previously unknown form of programmed cell death. Cell Cycle. 2014;13: 138–147. doi:10.4161/cc.26885

25. Lennen RM, Politz MG, Kruziki MA, Pfleger BF. Identification of Transport Proteins Involved in Free Fatty Acid Efflux in Escherichia coli. Journal of Bacteriology. 2013;195: 135–144. doi:10.1128/JB.01477-12

26. Liu H, Yu C, Feng D, Cheng T, Meng X, Liu W, et al. Production of extracellular fatty acid using engineered Escherichia coli. Microbial Cell Factories. 2012;11: 41. doi:10.1186/1475-2859-11-41

27. Youngquist JT, Schumacher MH, Rose JP, Raines TC, Politz MC, Copeland MF, et al. Production of medium chain length fatty alcohols from glucose in Escherichia coli. Metabolic Engineering. 2013;20: 177–186. doi:10.1016/j.ymben.2013.10.006

28. Zhang Y-M, Rock CO. Membrane lipid homeostasis in bacteria. Nat Rev Microbiol. 2008;6: 222–233. doi:10.1038/nrmicro1839

29. Lemke RAS, Peterson AC, Ziegelhoffer EC, Westphall MS, Tjellström H, Coon JJ, et al. Synthesis and scavenging role of furan fatty acids. Proceedings of the National Academy of Sciences. 2014;111: E3450–E3457. doi:10.1073/pnas.1405520111

30. Buist PH. Exotic biomodification of fatty acids. Nat Prod Rep. 2007;24: 1110–1127. doi:10.1039/B508584P

31. Tong X, Oh EK, Lee B, Lee JK. Production of long-chain free fatty acids from metabolically engineered Rhodobacter sphaeroides heterologously producing periplasmic phospholipase A2 in dodecane-overlaid two-phase culture. Microbial Cell Factories. 2019;18: 20. doi:10.1186/s12934-019-1070-8

32. Cain BD, Deal CD, Fraley RT, Kaplan S. In vivo intermembrane transfer of phospholipids in the photosynthetic bacterium Rhodopseudomonas sphaeroides. Journal of Bacteriology. 1981;145: 1154–1166. doi:10.1128/jb.145.3.1154-1166.1981

33. Marinetti GV, Cattieu K. Lipid analysis of cells and chromatophores of Rhodopseudomonas sphaeroides. Chemistry and Physics of Lipids. 1981;28: 241–251. doi:10.1016/0009-3084(81)90011-6

34. Russell NJ, Harwood JL. Changes in the acyl lipid composition of photosynthetic bacteria grown under photosynthetic and non-photosynthetic conditions. Biochem J. 1979;181: 339–345.

35. Imhoff JF. Polar Lipids and Fatty Acids in the Genus Rhodobacter. Systematic and Applied Microbiology. 1991;14: 228–234. doi:10.1016/S0723-2020(11)80373-5

36. Tamot B, Benning C. Membrane Lipid Biosynthesis in Purple Bacteria. In: Hunter CN, Daldal F, Thurnauer MC, Beatty JT, editors. The Purple Phototrophic Bacteria. Dordrecht: Springer Netherlands; 2009. pp. 119–134. doi:10.1007/978-1-4020-8815-5_7

37. Catucci L, Depalo N, Lattanzio VMT, Agostiano A, Corcelli A. Neosynthesis of cardiolipin in Rhodobacter sphaeroides under osmotic stress. Biochemistry. 2004;43: 15066–15072. doi:10.1021/bi048802k

38. Lin T-Y, Santos TMA, Kontur WS, Donohue TJ, Weibel DB. A Cardiolipin-Deficient Mutant of Rhodobacter sphaeroides Has an Altered Cell Shape and Is Impaired in Biofilm Formation. Journal of Bacteriology. 2015;197: 3446–3455. doi:10.1128/JB.00420-15

39. Lin T-Y, Gross WS, Auer GK, Weibel DB. Cardiolipin Alters Rhodobacter sphaeroides Cell Shape by Affecting Peptidoglycan Precursor Biosynthesis. mBio. 2019;10: e02401-18. doi:10.1128/mBio.02401-18

40. Silhavy TJ, Kahne D, Walker S. The Bacterial Cell Envelope. Cold Spring Harb Perspect Biol. 2010;2: a000414. doi:10.1101/cshperspect.a000414

41. Rojas ER, Billings G, Odermatt PD, Auer GK, Zhu L, Miguel A, et al. The outer membrane is an essential load-bearing element in Gram-negative bacteria. Nature. 2018;559: 617–621. doi:10.1038/s41586-018-0344-3

42. Vollmer W, Blanot D, De Pedro MA. Peptidoglycan structure and architecture. FEMS Microbiology Reviews. 2008;32: 149–167. doi:10.1111/j.1574-6976.2007.00094.x

43. Egan AJF, Errington J, Vollmer W. Regulation of peptidoglycan synthesis and remodelling. Nat Rev Microbiol. 2020;18: 446–460. doi:10.1038/s41579-020-0366-3

44. Huang KC, Mukhopadhyay R, Wen B, Gitai Z, Wingreen NS. Cell shape and cell-wall organization in Gram-negative bacteria. Proceedings of the National Academy of Sciences. 2008;105: 19282–19287. doi:10.1073/pnas.0805309105

45. Liu X, Biboy J, Consoli E, Vollmer W, Blaauwen T den. MreC and MreD balance the interaction between the elongasome proteins PBP2 and RodA. PLOS Genetics. 2020;16: e1009276. doi:10.1371/journal.pgen.1009276

46. Levin PA, Janakiraman A. Localization, Assembly, and Activation of the Escherichia coli Cell Division Machinery. EcoSal Plus. 2021;9: eESP00222021. doi:10.1128/ecosalplus.ESP-0022-2021

47. Leclercq S, Derouaux A, Olatunji S, Fraipont C, Egan AJF, Vollmer W, et al. Interplay between Penicillin-binding proteins and SEDS proteins promotes bacterial cell wall synthesis. Sci Rep. 2017;7: 43306. doi:10.1038/srep43306

48. Egan AJF, Errington J, Vollmer W. Regulation of peptidoglycan synthesis and remodelling. Nat Rev Microbiol. 2020;18: 446–460. doi:10.1038/s41579-020-0366-3

49. Bernadac A, Gavioli M, Lazzaroni J-C, Raina S, Lloubès R. Escherichia coli tol-pal Mutants Form Outer Membrane Vesicles. Journal of Bacteriology. 1998;180: 4872–4878. doi:10.1128/JB.180.18.4872-4878.1998

50. Avila-Calderón ED, Ruiz-Palma M del S, Aguilera-Arreola MaG, Velázquez-Guadarrama N, Ruiz EA, Gomez-Lunar Z, et al. Outer Membrane Vesicles of Gram-Negative Bacteria: An Outlook on Biogenesis. Frontiers in Microbiology. 2021;12. Available: https://www.frontiersin.org/article/10.3389/fmicb.2021.557902

51. Godessart P, Lannoy A, Dieu M, Van der Verren SE, Soumillion P, Collet J-F, et al. β-Barrels covalently link peptidoglycan and the outer membrane in the α-proteobacterium Brucella abortus. Nat Microbiol. 2021;6: 27–33. doi:10.1038/s41564-020-00799-3

52. Cox RL, Patterson C, Donohue TJ. Roles for the Rhodobacter sphaeroides CcmA and CcmG Proteins. J Bacteriol. 2001;183: 4643–4647. doi:10.1128/JB.183.15.4643-4647.2001

53. Sturm G, Richter K, Doetsch A, Heide H, Louro RO, Gescher J. A dynamic periplasmic electron transfer network enables respiratory flexibility beyond a thermodynamic regulatory regime. ISME J. 2015;9: 1802–1811. doi:10.1038/ismej.2014.264

54. Arai H. Regulation and Function of Versatile Aerobic and Anaerobic Respiratory Metabolism in Pseudomonas aeruginosa. Frontiers in Microbiology. 2011;2. Available: https://www.frontiersin.org/article/10.3389/fmicb.2011.00103

55. Cho H, Wivagg CN, Kapoor M, Barry Z, Rohs PDA, Suh H, et al. Bacterial cell wall biogenesis is mediated by SEDS and PBP polymerase families functioning semi-autonomously. Nat Microbiol. 2016;1: 1–8. doi:10.1038/nmicrobiol.2016.172

56. Vigouroux A, Cordier B, Aristov A, Alvarez L, Özbaykal G, Chaze T, et al. Class-A penicillin binding proteins do not contribute to cell shape but repair cell-wall defects. Akhmanova A, Xiao J, Xiao J, Dörr T, editors. eLife. 2020;9: e51998. doi:10.7554/eLife.51998

57. Wagstaff J, Löwe J. Prokaryotic cytoskeletons: protein filaments organizing small cells. Nat Rev Microbiol. 2018;16: 187–201. doi:10.1038/nrmicro.2017.153

58. Figge RM, Divakaruni AV, Gober JW. MreB, the cell shape-determining bacterial actin homologue, co-ordinates cell wall morphogenesis in Caulobacter crescentus. Molecular Microbiology. 2004;51: 1321–1332. doi:10.1111/j.1365-2958.2003.03936.x

59. Slovak PM, Wadhams GH, Armitage JP. Localization of MreB in Rhodobacter sphaeroides under Conditions Causing Changes in Cell Shape and Membrane Structure. Journal of Bacteriology. 2005;187: 54–64. doi:10.1128/JB.187.1.54-64.2005

60. Rohs PDA, Buss J, Sim SI, Squyres GR, Srisuknimit V, Smith M, et al. A central role for PBP2 in the activation of peptidoglycan polymerization by the bacterial cell elongation machinery. PLOS Genetics. 2018;14: e1007726. doi:10.1371/journal.pgen.1007726

61. Liu B, Persons L, Lee L, de Boer PAJ. Roles for both FtsA and the FtsBLQ subcomplex in FtsN-stimulated cell constriction in Escherichia coli. Molecular Microbiology. 2015;95: 945–970. doi:10.1111/mmi.12906

62. Typas A, Banzhaf M, van den Berg van Saparoea B, Verheul J, Biboy J, Nichols RJ, et al. Regulation of peptidoglycan synthesis by outer membrane proteins. Cell. 2010;143: 1097–1109. doi:10.1016/j.cell.2010.11.038

63. Williams MA, Aliashkevich A, Krol E, Kuru E, Bouchier JM, Rittichier J, et al. Unipolar Peptidoglycan Synthesis in the Rhizobiales Requires an Essential Class A Penicillin-Binding Protein. mBio. 2021;12: e02346-21. doi:10.1128/mBio.02346-21

64. Zupan JR, Cameron TA, Anderson-Furgeson J, Zambryski PC. Dynamic FtsA and FtsZ localization and outer membrane alterations during polar growth and cell division in Agrobacterium tumefaciens. Proceedings of the National Academy of Sciences. 2013;110: 9060–9065. doi:10.1073/pnas.1307241110

65. Atwal S, Chuenklin S, Bonder EM, Flores J, Gillespie JJ, Driscoll TP, et al. Discovery of a Diverse Set of Bacteria That Build Their Cell Walls without the Canonical Peptidoglycan Polymerase aPBP. mBio. 2021;12: e0134221. doi:10.1128/mBio.01342-21

66. Strobel W, Möll A, Kiekebusch D, Klein KE, Thanbichler M. Function and localization dynamics of bifunctional penicillin-binding proteins in Caulobacter crescentus. J Bacteriol. 2014;196: 1627–1639. doi:10.1128/JB.01194-13

67. Mueller EA, Levin PA. Bacterial Cell Wall Quality Control during Environmental Stress. mBio. 11: e02456-20. doi:10.1128/mBio.02456-20

68. Cameron TA, Anderson-Furgeson J, Zupan JR, Zik JJ, Zambryski PC. Peptidoglycan Synthesis Machinery in Agrobacterium tumefaciens During Unipolar Growth and Cell Division. mBio. 2014;5: e01219-14. doi:10.1128/mBio.01219-14

69. Slovak PM, Porter SL, Armitage JP. Differential Localization of Mre Proteins with PBP2 in Rhodobacter sphaeroides. Journal of Bacteriology. 2006;188: 1691–1700. doi:10.1128/JB.188.5.1691-1700.2006

70. Chiu S-W, Roberts MAJ, Leake MC, Armitage JP. Positioning of chemosensory proteins and FtsZ through the Rhodobacter sphaeroides cell cycle. Molecular Microbiology. 2013;90: 322–337. doi:10.1111/mmi.12366

71. Biteen JS, Goley ED, Shapiro L, Moerner WE. Three-Dimensional Super-Resolution Imaging of the Midplane Protein FtsZ in Live Caulobacter crescentus Cells Using Astigmatism. ChemPhysChem. 2012;13: 1007–1012. doi:10.1002/cphc.201100686

72. Caccamo PD, Brun YV. The Molecular Basis of Noncanonical Bacterial Morphology. Trends Microbiol. 2018;26: 191–208. doi:10.1016/j.tim.2017.09.012

73. Williams MA, Kysela DT, Brown PJB. Diversity of Growth Patterns in the Alphaproteobacteria. In: Biondi E, editor. Cell Cycle Regulation and Development in Alphaproteobacteria. Cham: Springer International Publishing; 2022. pp. 185–220. doi:10.1007/978-3-030-90621-4_7

74. Schwechheimer C, Kuehn MJ. Outer-membrane vesicles from Gram-negative bacteria: biogenesis and functions. Nat Rev Microbiol. 2015;13: 605–619. doi:10.1038/nrmicro3525

75. Mashburn-Warren LM, Whiteley M. Special delivery: vesicle trafficking in prokaryotes. Molecular Microbiology. 2006;61: 839–846. doi:10.1111/j.1365-2958.2006.05272.x

76. Sauvage E, Kerff F, Terrak M, Ayala JA, Charlier P. The penicillin-binding proteins: structure and role in peptidoglycan biosynthesis. FEMS Microbiology Reviews. 2008;32: 234–258. doi:10.1111/j.1574-6976.2008.00105.x

77. Hayashi J, Hamada N, Kuramitsu HK. The autolysin of Porphyromonas gingivalis is involved in outer membrane vesicle release. FEMS Microbiology Letters. 2002;216: 217–222. doi:10.1111/j.1574-6968.2002.tb11438.x

78. Nguyen TT, Saxena A, Beveridge TJ. Effect of surface lipopolysaccharide on the nature of membrane vesicles liberated from the Gram-negative bacterium Pseudomonas aeruginosa. Microscopy. 2003;52: 465–469. doi:10.1093/jmicro/52.5.465

79. Gujrati V, Kim S, Kim S-H, Min JJ, Choy HE, Kim SC, et al. Bioengineered Bacterial Outer Membrane Vesicles as Cell-Specific Drug-Delivery Vehicles for Cancer Therapy. ACS Nano. 2014;8: 1525–1537. doi:10.1021/nn405724x

80. Wang S, Gao J, Wang Z. Outer Membrane Vesicles (OMVs) for Vaccination and Targeted Drug Delivery. Wiley Interdiscip Rev Nanomed Nanobiotechnol. 2019;11: e1523. doi:10.1002/wnan.1523

81. Shrivastava R, Chng S-S. Lipid trafficking across the Gram-negative cell envelope. Journal of Biological Chemistry. 2019;294: 14175–14184. doi:10.1074/jbc.AW119.008139

82. Malinverni JC, Silhavy TJ. An ABC transport system that maintains lipid asymmetry in the Gram-negative outer membrane. Proceedings of the National Academy of Sciences. 2009;106: 8009–8014. doi:10.1073/pnas.0903229106

83. Roier S, Zingl FG, Cakar F, Durakovic S, Kohl P, Eichmann TO, et al. A novel mechanism for the biogenesis of outer membrane vesicles in Gram-negative bacteria. Nat Commun. 2016;7: 10515. doi:10.1038/ncomms10515

84. McMahon HT, Gallop JL. Membrane curvature and mechanisms of dynamic cell membrane remodelling. Nature. 2005;438: 590–596. doi:10.1038/nature04396

85. Renner LD, Weibel DB. Cardiolipin microdomains localize to negatively curved regions of Escherichia coli membranes. Proceedings of the National Academy of Sciences. 2011;108: 6264–6269. doi:10.1073/pnas.1015757108

86. Cian MB, Giordano NP, Masilamani R, Minor KE, Dalebroux ZD. Salmonella enterica Serovar Typhimurium Uses PbgA/YejM To Regulate Lipopolysaccharide Assembly during Bacteremia. Infect Immun. 2019;88: e00758-19. doi:10.1128/IAI.00758-19

87. Dong H, Zhang Z, Tang X, Huang S, Li H, Peng B, et al. Structural insights into cardiolipin transfer from the Inner membrane to the outer membrane by PbgA in Gram-negative bacteria. Sci Rep. 2016;6: 30815. doi:10.1038/srep30815

88. Szczepaniak J, Press C, Kleanthous C. The multifarious roles of Tol-Pal in Gram-negative bacteria. FEMS Microbiol Rev. 2020;44: 490–506. doi:10.1093/femsre/fuaa018

89. Sutterlin HA, Shi H, May KL, Miguel A, Khare S, Huang KC, et al. Disruption of lipid homeostasis in the Gram-negative cell envelope activates a novel cell death pathway. Proceedings of the National Academy of Sciences. 2016;113: E1565–E1574. doi:10.1073/pnas.1601375113

90. Lemmer KC, Zhang W, Langer SJ, Dohnalkova AC, Hu D, Lemke RA, et al. Mutations That Alter the Bacterial Cell Envelope Increase Lipid Production. mBio. 8: e00513-17. doi:10.1128/mBio.00513-17

91. Mackenzie C, Eraso JM, Choudhary M, Roh JH, Zeng X, Bruscella P, et al. Postgenomic Adventures with *Rhodobacter sphaeroides.* Annu Rev Microbiol. 2007;61: 283–307. doi:10.1146/annurev.micro.61.080706.093402

92. Imam S, Noguera DR, Donohue TJ. Global Analysis of Photosynthesis Transcriptional Regulatory Networks. PLOS Genetics. 2014;10: e1004837. doi:10.1371/journal.pgen.1004837

93. Kiley PJ, Kaplan S. Molecular genetics of photosynthetic membrane biosynthesis in Rhodobacter sphaeroides. 1988;52: 20.

94. The Purple Phototrophic Bacteria. Available: https://link.springer.com/book/10.1007/978-1-4020-8815-5

95. Imam S, Noguera DR, Donohue TJ. Global insights into energetic and metabolic networks in Rhodobacter sphaeroides. BMC Systems Biology. 2013;7: 89. doi:10.1186/1752-0509-7-89

96. Zhu Y, Pan M, Wang C, Ye L, Xia C, Yu H. Enhanced CoQ10 production by genome modification of Rhodobacter sphaeroides via Tn7 transposition. FEMS Microbiol Lett. 2022;369: fnab160. doi:10.1093/femsle/fnab160

97. Zidwick MJ, Sanchez-Riera F. Process for the preparation of coenzyme qlo by culturing rhodobacter sphaeroides in a defined medium. WO2008100782A2, 2008. Available: https://patents.google.com/patent/WO2008100782A2/en

98. Qiang S, Su AP, Li Y, Chen Z, Hu CY, Meng YH. Elevated β-Carotene Synthesis by the Engineered Rhodobacter sphaeroides with Enhanced CrtY Expression. J Agric Food Chem. 2019;67: 9560–9568. doi:10.1021/acs.jafc.9b02597

99. Kobayashi J, Kondo A. Disruption of poly (3-hydroxyalkanoate) depolymerase gene and overexpression of three poly (3-hydroxybutyrate) biosynthetic genes improve poly (3-hydroxybutyrate) production from nitrogen rich medium by Rhodobacter sphaeroides. Microbial Cell Factories. 2019;18: 40. doi:10.1186/s12934-019-1088-y

100. Ghimire A, Valentino S, Frunzo L, Pirozzi F, Lens PNL, Esposito G. Concomitant biohydrogen and poly-β-hydroxybutyrate production from dark fermentation effluents by adapted Rhodobacter sphaeroides and mixed photofermentative cultures. Bioresource Technology. 2016;217: 157–164. doi:10.1016/j.biortech.2016.03.017

101. Kontur WS, Noguera DR, Donohue TJ. Maximizing reductant flow into microbial H2 production. Current Opinion in Biotechnology. 2012;23: 382–389. doi:10.1016/j.copbio.2011.10.003

102. Lemke RAS, Olson SM, Morse K, Karlen SD, Higbee A, Beebe ET, et al. A bacterial biosynthetic pathway for methylated furan fatty acids. J Biol Chem. 2020;295: 9786–9801. doi:10.1074/jbc.RA120.013697

103. Orsi E, Beekwilder J, Eggink G, Kengen SWM, Weusthuis RA. The transition of Rhodobacter sphaeroides into a microbial cell factory. Biotechnology and Bioengineering. 2021;118: 531–541. doi:10.1002/bit.27593

104. Lemmer KC, Dohnalkova AC, Noguera DR, Donohue TJ. Oxygen-Dependent Regulation of Bacterial Lipid Production. Journal of Bacteriology. 2015;197: 1649–1658. doi:10.1128/JB.02510-14

105. Zeilstra-Ryalls J, Gomelsky M, Eraso JM, Yeliseev A, O'Gara J, Kaplan S. Control of Photosystem Formation in Rhodobacter sphaeroides. J Bacteriol. 1998;180: 2801–2809.

106. Gomelsky L, Moskvin OV, Stenzel RA, Jones DF, Donohue TJ, Gomelsky M. Hierarchical Regulation of Photosynthesis Gene Expression by the Oxygen-Responsive PrrBA and AppA-PpsR Systems of Rhodobacter sphaeroides. Journal of Bacteriology. 2008;190: 8106–8114. doi:10.1128/JB.01094-08

107. Elsen S, Jaubert M, Pignol D, Giraud E. PpsR: a multifaceted regulator of photosynthesis gene expression in purple bacteria. Molecular Microbiology. 2005;57: 17–26. doi:10.1111/j.1365-2958.2005.04655.x

108. Zeilstra-Ryalls JH, Kaplan S. Aerobic and anaerobic regulation in Rhodobacter sphaeroides 2.4.1: the role of the fnrL gene. Journal of Bacteriology. 1995;177: 6422–6431. doi:10.1128/jb.177.22.6422-6431.1995

109. Dufour YS, Imam S, Koo B-M, Green HA, Donohue TJ. Convergence of the Transcriptional Responses to Heat Shock and Singlet Oxygen Stresses. PLOS Genetics. 2012;8: e1002929. doi:10.1371/journal.pgen.1002929

110. Lemmer KC, Alberge F, Myers KS, Dohnalkova AC, Schaub RE, Lenz JD, et al. The NtrYX Two-Component System Regulates the Bacterial Cell Envelope. Harwood CS, editor. mBio. 2020;11. doi:10.1128/mBio.00957-20

111. Gao R, Stock AM. Biological Insights from Structures of Two-Component Proteins. Annual Review of Microbiology. 2009;63: 133–154. doi:10.1146/annurev.micro.091208.073214

112. Jacob-Dubuisson F, Mechaly A, Betton J-M, Antoine R. Structural insights into the signalling mechanisms of two-component systems. Nat Rev Microbiol. 2018;16: 585–593. doi:10.1038/s41579-018-0055-7

113. Capra EJ, Laub MT. Evolution of Two-Component Signal Transduction Systems. Annual Review of Microbiology. 2012;66: 325–347. doi:10.1146/annurev-micro-092611-150039

114. Lazar JT, Tabor JJ. Bacterial two-component systems as sensors for synthetic biology applications. Current Opinion in Systems Biology. 2021;28: 100398. doi:10.1016/j.coisb.2021.100398

115. Skerker JM, Prasol MS, Perchuk BS, Biondi EG, Laub MT. Two-Component Signal Transduction Pathways Regulating Growth and Cell Cycle Progression in a Bacterium: A System-Level Analysis. PLOS Biology. 2005;3: e334. doi:10.1371/journal.pbio.0030334

116. Zschiedrich CP, Keidel V, Szurmant H. Molecular Mechanisms of Two-Component Signal Transduction. Journal of Molecular Biology. 2016;428: 3752–3775. doi:10.1016/j.jmb.2016.08.003

117. Gao R, Mack TR, Stock AM. Bacterial Response Regulators: Versatile Regulatory Strategies from Common Domains. Trends Biochem Sci. 2007;32: 225–234. doi:10.1016/j.tibs.2007.03.002

118. Lukat GS, McCleary WR, Stock AM, Stock JB. Phosphorylation of bacterial response regulator proteins by low molecular weight phospho-donors. Proc Natl Acad Sci USA. 1992;89: 718–722. doi:10.1073/pnas.89.2.718

119. Laub MT, Goulian M. Specificity in Two-Component Signal Transduction Pathways. Annu Rev Genet. 2007;41: 121–145. doi:10.1146/annurev.genet.41.042007.170548

120. Galperin MY, Higdon R, Kolker E. Interplay of heritage and habitat in the distribution of bacterial signal transduction systems. Mol BioSyst. 2010;6: 721–728. doi:10.1039/B908047C

121. Eraso JM, Roh JH, Zeng X, Callister SJ, Lipton MS, Kaplan S. Role of the Global Transcriptional Regulator PrrA in Rhodobacter sphaeroides 2.4.1: Combined Transcriptome and Proteome Analysis. J Bacteriol. 2008;190: 4831–4848. doi:10.1128/JB.00301-08

122. Kim Y-J, Ko I-J, Lee J-M, Kang H-Y, Kim YM, Kaplan S, et al. Dominant Role of the cbb3 Oxidase in Regulation of Photosynthesis Gene Expression through the PrrBA System in Rhodobacter sphaeroides 2.4.1. J Bacteriol. 2007;189: 5617–5625. doi:10.1128/JB.00443-07

123. Eraso JM, Kaplan S. From Redox Flow to Gene Regulation: Role of the PrrC Protein of Rhodobacter sphaeroides 2.4.1. Biochemistry. 2000;39: 2052–2062. doi:10.1021/bi9923858

124. Saha S, Lach SR, Konovalova A. Homeostasis of the Gram-negative cell envelope. Current Opinion in Microbiology. 2021;61: 99–106. doi:10.1016/j.mib.2021.03.008

125. Raivio TL, Silhavy TJ. Transduction of envelope stress in Escherichia coli by the Cpx two-component system. Journal of Bacteriology. 1997;179: 7724–7733. doi:10.1128/jb.179.24.7724-7733.1997

126. Price NL, Raivio TL. Characterization of the Cpx regulon in Escherichia coli strain MC4100. J Bacteriol. 2009;191: 1798–1815. doi:10.1128/JB.00798-08

127. Wall E, Majdalani N, Gottesman S. The Complex Rcs Regulatory Cascade. Annual Review of Microbiology. 2018;72: 111–139. doi:10.1146/annurev-micro-090817-062640

128. Laubacher ME, Ades SE. The Rcs Phosphorelay Is a Cell Envelope Stress Response Activated by Peptidoglycan Stress and Contributes to Intrinsic Antibiotic Resistance. Journal of Bacteriology. 2008;190: 2065–2074. doi:10.1128/JB.01740-07

129. Grabowicz M, Silhavy TJ. Envelope Stress Responses: An Interconnected Safety Net. Trends in Biochemical Sciences. 2017;42: 232–242. doi:10.1016/j.tibs.2016.10.002

130. García-Calderón CB, Casadesús J, Ramos-Morales F. Rcs and PhoPQ regulatory overlap in the control of Salmonella enterica virulence. J Bacteriol. 2007;189: 6635–6644. doi:10.1128/JB.00640-07

131. Masi M, Pinet E, Pagès J-M. Complex Response of the CpxAR Two-Component System to β-Lactams on Antibiotic Resistance and Envelope Homeostasis in Enterobacteriaceae. Antimicrobial Agents and Chemotherapy. 2020;64: e00291-20. doi:10.1128/AAC.00291-20

132. Dalebroux ZD, Edrozo MB, Pfuetzner RA, Ressl S, Kulasekara BR, Blanc M-P, et al. Delivery of cardiolipins to the Salmonella outer membrane is necessary for survival within host tissues and virulence. Cell Host Microbe. 2015;17: 441–451. doi:10.1016/j.chom.2015.03.003

133. Stein BJ, Fiebig A, Crosson S. The ChvG-ChvI and NtrY-NtrX Two-Component Systems Coordinately Regulate Growth of Caulobacter crescentus. Journal of Bacteriology. 2021;203: e00199-21. doi:10.1128/JB.00199-21

CHAPTER 2:

The essential *Rhodobacter sphaeroides* CenKR two-component system regulates cell division and envelope biosynthesis

This chapter is published under the same title:

Lakey, B.D., Myers, K.S., Alberge, F., Mettert, E.L., Kiley, P.J., Noguera, D.R., Donohue, T.J. (2022) *PLOS Genetics* 18(6): e1010270. https://doi.org/10.1371/journal.pgen.1010270.

BDL was responsible for conceptualization, construction of all plasmids and strains used in this analysis, protein purification and radioactivity kinase assays, RNA and ChIP isolation and analysis, electromobility shift assays, microscopy, phylogenetic analysis. KSM was responsible for RNA-seq and ChIP-seq data processing and analysis, MEME and PatSer analyses. FA was responsible for microscopy analysis. ELM assisted in troubleshooting EMSA, providing reagents. The manuscript was written by BDL and TJD. Editing and revision provided by all.

Abstract

Bacterial two-component systems (TCSs) often function through the detection of an extracytoplasmic stimulus and the transduction of a signal by a transmembrane sensory histidine kinase. This kinase then initiates a series of reversible phosphorylation modifications to regulate the activity of a cognate, cytoplasmic response regulator as a transcription factor. Several TCSs have been implicated in the regulation of cell cycle dynamics, cell envelope integrity, or cell wall development in *Escherichia coli* and other well-studied Gram-negative model organisms. However, many α-proteobacteria lack homologs to these regulators, so an understanding of how α-proteobacteria orchestrate extracytoplasmic events is lacking. In this work we identify an essential TCS, CenKR (Cell envelope Kinase and Regulator), in the α-proteobacterium *Rhodobacter sphaeroides* and show that modulation of its activity results in major morphological changes. Using genetic and biochemical approaches, we dissect the requirements for the phosphotransfer event between CenK and CenR, use this information to manipulate the activity of this TCS *in vivo*, and identify genes that are directly and indirectly controlled by CenKR in *Rb. sphaeroides*. Combining ChIP-seq and RNA-seq, we show that the CenKR TCS plays a direct role in maintenance of the cell envelope, regulates the expression of subunits of the Tol-Pal outer membrane division complex, and indirectly modulates the expression of peptidoglycan biosynthetic genes. CenKR represents the first TCS reported to directly control the expression of Tol-Pal machinery genes in Gram-negative bacteria, and we predict that homologs of this TCS serve a similar function in other closely related organisms. We propose that *Rb. sphaeroides* genes of unknown function that are directly regulated by CenKR play unknown roles in cell envelope biosynthesis, assembly, and/or remodeling in this and other α-proteobacteria.

Summary

The bacterial cell envelope is home to an array of important functions including, energy conservation, motility, influx/efflux of nutrients and toxins, modulation of cell morphology and division, cell-cell interaction, and biofilm formation. Consequently, it is a major target of antibiotics and antimicrobial agents that inhibit these essential processes. Key to the recognition of environmental stressors or stimuli are bacterial TCSs, however systems that monitor or directly regulate cell envelope assembly and homeostasis are not widely conserved amongst bacteria. Here, we use *Rhodobacter sphaeroides* as a model to investigate the function of the CenKR TCS in this and other α-proteobacteria. We show that this essential TCS plays a key role in maintenance of the cell envelope through the regulation of outer membrane integrity and division, cell wall remodeling and homeostasis, and an alternate sigma factor that controls global cellular stress response. We provide evidence that this TCS and its function is widely conserved in α-proteobacteria and identify genes of unknown function as candidates for the study of cell envelope assembly in this and related bacteria.

Introduction

The Gram-negative cell envelope serves as a selectively permeable barrier to separate and protect a cell from its external environment. This inter-connected compartment is comprised of an inner membrane (IM), the periplasmic space, a thin layer of peptidoglycan (PG), and an outer membrane (OM) [1]. The IM is a phospholipid bilayer separating the cytoplasm from the periplasmic space. Encircling the periplasm is the OM, composed of an inner leaflet of phospholipids and an outer leaflet of protective, charged lipopolysaccharides (LPS) that acts a rigid, semi-permeable barrier [2,3]. Closely associated to the OM is the PG cell wall, a load bearing, mesh-like structure composed of repeating disaccharide units that are cross-linked via short peptide side chains [4,5]. Together, the cell envelope is critical for maintaining cell shape, organizing and facilitating cell division, and protecting cells from deleterious environmental threats such as antibiotics, desiccation, and osmotic stress. Given the many essential functions of the cell envelope, a wide range of naturally occurring toxins, host defense systems, and clinically important antibiotics target cell envelope biosynthetic machinery.

To combat these threats, the Gram-negative cell envelope also serves as a major control center for sensing and rapidly responding to environmental stimuli. Fundamental to this activity are two-component systems (TCSs) which rely on regulated, transmitter-receiver protein communication to monitor cell homeostasis and adjust cell structure, physiology, and behavior in response to internal or external cues [6]. Canonical TCS are comprised of a transmembrane histidine kinase (HK) that upon recognizing an envelope or extracellular derived signal autophosphorylates a cytoplasmic C-terminal histidine residue [6–8]. The phosphate of the activated HK is then transferred to its cytoplasmic, cognate response regulator (RR), often

resulting in conformational changes and activation of an effector domain to elicit a specific cellular response [6–8]. Commonly, RRs are DNA binding proteins that directly control the transcription of target genes [9]. Several TCSs which regulate envelope functions and mitigate a variety of membrane or cell wall perturbations have been described in Gram-negative bacteria such as *Escherichia coli* Cpx [10–12], Rcs [11–13], and BaeSR [14] and *Caulobacter crescentus* ChvGI [15]. However, these characterized TCS are not generally conserved across bacterial phyla and typically control the transcription of genes whose products are envelope proteases, periplasmic chaperones, function in antibiotic catabolism, or produce alternate PG crosslinks to maintain cell wall integrity [11,16–21]. Moreover, examples of TCS in *Vibrio cholerae* (WigRK [22]) and *Mycobacterium tuberculosis* (MtrAB [23,24]) that directly regulate cell wall metabolism are specific to each respective bacterial genus and are necessary for the individual pathogenic lifestyles of these bacteria. Therefore, conserved systems that directly regulate the expression of cell envelope biosynthetic genes remain elusive. Previously, Lemmer *et. al.* identified a HK (encoded at the *RSP_1056* locus) in the Gram-negative α-proteobacterium *Rhodobacter sphaeroides* that when disrupted, resulted in cell envelope changes that included alterations in shape, increased phospholipid content, and sensitivity to detergents and β-lactam antibiotics that target the cell envelope and wall [25]. Together, these results suggested that RSP_1056 is a *trans*-membrane HK that plays a previously unknown role in cell envelope homeostasis [25].

In this study, we demonstrate the predicted kinase activity of RSP_1056 and identify RSP_0847 as the essential cognate RR for this TCS. We apply a systems biology approach, combining genome-scale chromatin immunoprecipitation followed by high-throughput sequencing (ChIP-

seq) and analysis of strain specific changes in global transcript abundance (RNA-seq), to identify genes whose expression are directly and indirectly impacted *in vivo* by genetically altering TCS activity. From these data, we identify the direct targets of RSP_0847 and make predictions for how the altered transcription of these genes lead to the observed phenotypes of strains with changes in activity of this TCS. Based on these data, we propose that the RSP_1056-RSP_0847 TCS, renamed CenK-CenR based on homology with a described TCS in *C. crescentus* [26], is henceforth a regulator of cell division, bacterial envelope development and homeostasis, and OM integrity, specifically through the regulation of the Tol complex. Finally, we show that other α-proteobacteria of agricultural, industrial, and medical relevance, lacking well-studied cell envelope development and stress responses, contain homologs of this TCS.

Results

RSP_1056 is a histidine kinase that phosphorylates the response regulator RSP_0847. To determine how disruption of *RSP_1056* impacts cellular events [25], we sought to identify the predicted phosphorylation target of RSP_1056. To test that RSP_1056 is indeed a HK, we expressed the predicted cytoplasmic portion of this putative *trans*-membrane protein in *E. coli*. After purification, this recombinant form of a truncated RSP_1056 was incubated with [γ^{32}P]-ATP, and a stable autophosphorylated species corresponding to the molecular weight of the truncated RSP_1056 protein was observed (Fig 2-1 A, lane 1), confirming the prediction that RSP_1056 is a kinase.

Genes encoding TCS pairs are often found in the same transcriptional unit. However, genomic neighborhood analysis did not identify any putative RR genes in the vicinity of the gene

encoding the RSP_1056 HK. The *Rb. sphaeroides* genome encodes 27 predicted RRs that are unpaired with corresponding HK genes that could be phosphoacceptors of RSP_1056. To identify potential candidate RRs for the RSP_1056 kinase, we used a publicly available *in silico* prediction tool (SwissRegulon -TCS [27]) to infer potential HK-RR orphaned pairs based on conserved sequence-specific interactions between protein domains and specific residues that are canonically involved in phosphotransfer by TCS [27–29]. This approach produced three candidate RRs as phosphoacceptors for RSP_1056. One of these, RSP_0847, had a high Bayesian probability (>0.80) as a phosphoaccepting partner for RSP_1056, while two others (RSP_1274 and RSP_1083) had probabilities of 0.14 and 0.05 [27], respectively (Fig 2-2 A). Therefore, we hypothesized that RSP_1056 and RSP_0847 most likely formed a TCS in *Rb. sphaeroides*.

To test whether RSP_0847 was the cognate response regulator, we assayed time-dependent *in vitro* phosphotransfer activity from the ^{32}P-labeled RSP_1056 to a purified, recombinant form of the predicted RR RSP_0847 *in vitro* (Fig 2-1 A). Detectable phosphate transfer was observed in reactions containing RSP_0847 (Fig 2-1 A, white arrow), with the appearance of radiolabeled RSP_0847 after one minute of incubation (Fig 2-1 A, lane 2). Such rapid phosphotransfer from a HK to a RR is characteristic of an interaction between members of known TCSs, as HKs exhibit strong kinetic preference for their *in vivo* cognate RR target *in vitro* [26,30–32]. Using this same assay, we found that phosphotransfer was not observed between RSP_1056 and the other two candidate RRs (RSP_1083 and RSP_1274, Fig 2-2 B). Together, the rapid and specific *in vitro* phosphotransfer between RSP_1056 and RSP_0847 provides strong support that these two proteins form a TCS in *Rb. sphaeroides*.

Figure 2-1: RSP1056-RSP0847 comprise an essential TCS.

(A) RSP_1056 is phosphorylated after incubation with [γ^{32}P]-ATP (lane 1). When recombinant response regulator (RR) RSP_0847 was added, phosphotransfer between RSP_1056 (black arrow) and RSP_0847 (white arrow) was detected by the presence of two radiolabeled species. **(B)** Attempts to produce an in-frame, markerless deletion of *RSP_0847* were unsuccessful. Double crossover events were scored (phenotype), and deletions confirmed by PCR (genotype). **(C)** Structural modeling of RSP_0847 using I-TASSER TM-align [34–36]. The RR N-terminus containing the receiver domain (grey) and C-terminal DNA-binding winged helix-turn-helix motif (black) are shown. Predicted Mg^{2+} coordinating aspartate residues between α-helix 1 and β-sheet 1 (orange, D11-D13), aspartate 56 (magenta) on the C-terminal end of β-sheet 3, and aspartate 51 (cyan) on the N-terminal end of β-sheet 3, are labeled in the RR receiver domain (zoomed image). The amino acid sequence of the receiver domain, aspartates of interest, and β3 is shown. **(D)** Recombinant RSP_0847 harboring an alanine substitution at aspartate position 56 (D56A) was tested for *in vitro* phosphotransfer from radiolabeled RSP_1056. Phosphotransfer between radiolabeled RSP_1056 and RSP_0847(D56A) was not detected. Control reactions containing only [γ^{32}P]-ATP and RSP_0847 (lane 5) and autophosphorylated RSP_1056 incubated for 10 minutes (lane 6) are shown.

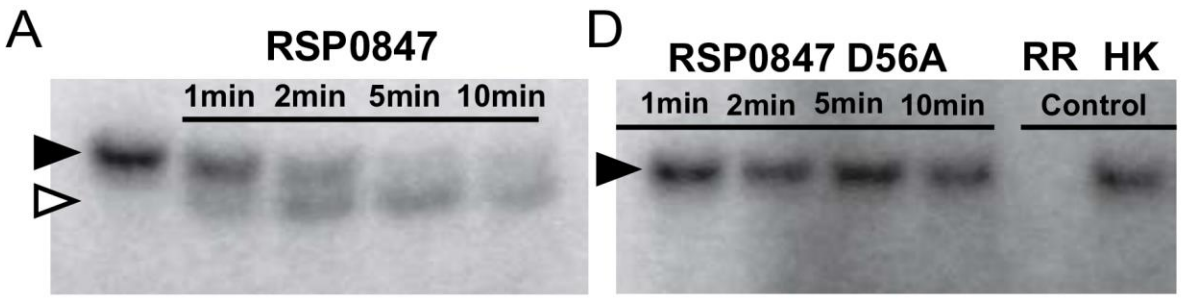

B

Strain Construction	Total Colonies Screened	Genotype: Δ	Genotype: WT	Phenotype: *sacB* inactivation
Deletion of *RSP0847* (*cenR*)	200	0	157	43
Deletion of *RSP1056* (*cenK*)	50	24	17	9

C RSP0847:

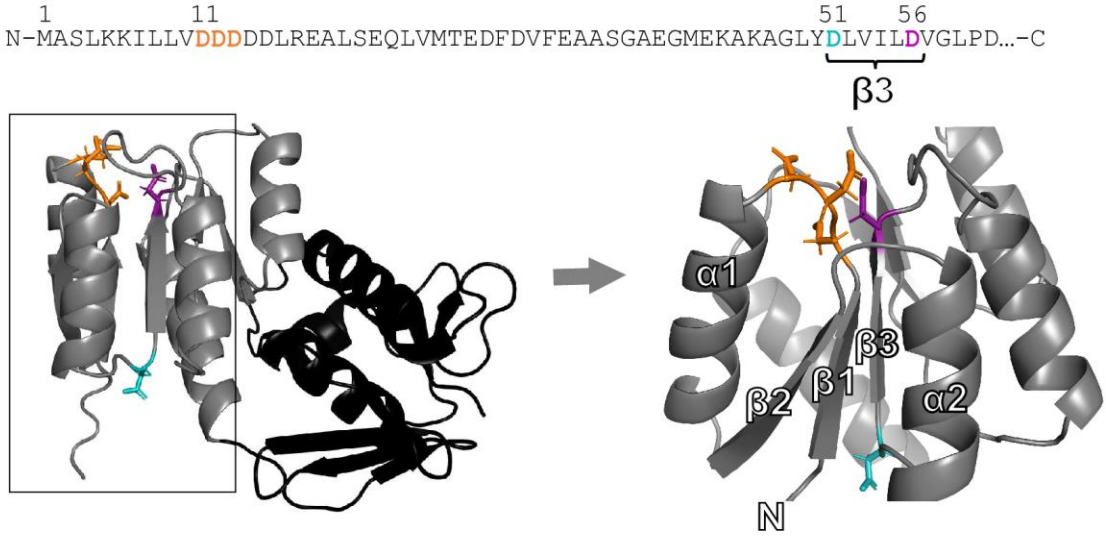

Figure 2-2. Other predicted partners of CenK are not phosphorylated *in vitro*.

(A) Bayesian probabilities for the highest ranked predicted cognate response regulator of RSP_1056. Reciprocal search of this database for cognate kinases of RSP_0847 also identified RSP_1056 as the highest ranked partner. The Bayesian algorithm models amino acid composition of interacting kinase/regulator pairs to predict specific interaction networks for orphaned TCSs across bacterial genomes [27]. **(B)** Phosphotransfer between phosphorylated RSP_1056 and the candidate recombinant response regulators RSP_1083 and RSP_1274 was not detected. (In Lakey *et al* 2022 as Supplemental Figure 1, S1).

A

Kinase	Predicted Regulator	Probability
RSP1056	RSP0847	0.80122
RSP1056	RSP1274	0.14385
RSP1056	RSP1083	0.05493

Regulator	Predicted Kinase	Probability
RSP0847	RSP1056	0.80122
RSP0847	RSP3217	0.00046
RSP0847	RSP0491	0.00013

B

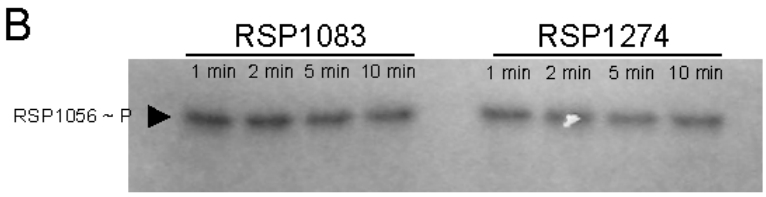

The gene encoding the RR RSP_0847 is essential in *Rb. sphaeroides*. A query of the NCBI protein database identified the HK CenK (CCNA_00564) and RR CenR (CCNA_03859), **Cell envelope Kinase and Regulator**, in the α-proteobacterium *C. crescentus* as potential homologs of RSP_1056 (35% amino acid identify, E-value 1e-76) and RSP_0847 (69.5% amino acid identity, E-value 2e-107), respectively. In *C. crescentus*, both *cenK* and *cenR* are reported to be essential genes encoded at separate genomic loci, with depletion of either protein resulting in severe OM blebbing and cell lysis through unknown mechanisms [26]. Consistent with the previously proposed essential nature of CenKR, genome-scale Tn-seq analysis of *Rb. sphaeroides* (Fig 2-3 A-B) predicted that the gene encoding the RR RSP_0847 was essential [33]. However, unlike in *C. crescentus*, this analysis identified transposon insertions in *RSP_1056* suggesting this gene is not essential in the conditions tested [25,33].

To independently test if *RSP_0847* is an essential gene, we attempted to construct an in-frame deletion of this gene using the same method that we used to generate an in-frame deletion of *RSP_1056* (Fig 2-1 B). We were unable to recover a strain containing a chromosomal deletion of *RSP_0847*, confirming its essentiality in *Rb. sphaeroides*. To independently confirm the functionality of the recombineering plasmid, we attempted to recover a chromosomal deletion of *RSP_0847* in a strain constitutively expressing *RSP_0847* from an ectopic plasmid (Fig 2-4 B-E). We were able to efficiently recover in-frame deletions of the genomic copy of *RSP_0847* in this background (Fig 2-4 C) confirming the efficacy of our plasmid to inactivate this locus. Together, these biochemical and genetic analyses provide evidence that the *Rb. sphaeroides* RSP_1056-RSP_0847 TCS is likely a homolog of *C. crescentus* CenKR [26]. Therefore, we will hereafter refer to *RSP_1056* as *cenK* and *RSP_0847* as *cenR*.

Figure 2-3. Analysis of genome-wide transposon insertions within the *cenR* and *cenK* loci. Transposon insertion data determined previously by Burger *et. al.* (2017) [33]. The *Rb. sphaeroides* Tn5 mutant library was grown aerobically in Sistrom's minimal medium and split into two replicates (aliquots 1 and 2). Insertion positions and read count data for each genomic region are shown. **(A)** The genomic regions surrounding the nonessential gene *cenK* (*RSP_1056*). **(B)** The genomic region surrounding the essential gene *cenR* (*RSP_0847*). (In Lakey *et al* 2022 as Supplemental Figure 2, S2)

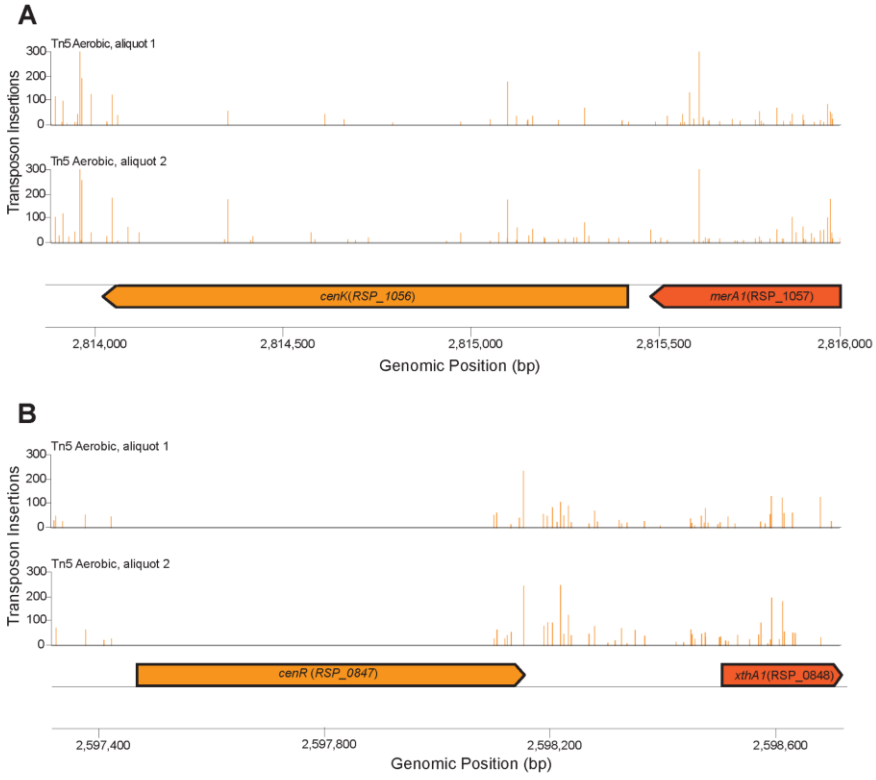

Figure 2-4. Use of pk18mobsacB-ΔcenR supports essentiality of this RR in Rb. sphaeroides. **(A)** Schematic for the workflow of recombineering in *Rb. sphaeroides*. Cloned into the suicide vector, pk18mobsacB, are 1kb DNA fragments corresponding to the sequences immediately 5' (upstream) and 3' (downstream) of the desired recombination site. Following successful mating, stable integration of the plasmid into the genome by recombination is selected for first by resistance to kanamycin. The second crossover is initiated by counter selection with sucrose as cells harboring *sacB* do not survive in the presence of sucrose. Thus, a successful double crossover is identified by screening for $Kan^{S}Suc^{R}$ colonies. This double crossover can occur at either the original integration site resulting in no change to the chromosome or within the second homologous region resulting in allelic exchange within the target region. **(B)** Deletion of *cenR* is possible in the presence of an ectopic copy of *cenR*. The results of colony PCR screening for the loss of *cenR* (lane 1-3) in strains containing $pIND5_{spec}$-*cenR* (lanes 4-6) relative to WT (lanes 3,6). Colony 1 represents the first possible outcome of the double crossover workflow and colony 2 represents the second possible outcome and successful deletion of *cenR*. **(C)** Deletion of *cenR* in the presence of ectopically expressed *cenR* was successful. Double crossover events were scored (phenotype: $Spec^{R}Kan^{S}Suc^{R}$), and deletions confirmed by PCR (genotype). **(D)** Plasmid map of $pIND5_{spec}$-*cenR* showing the location of primers used to confirm the presence of the plasmid by colony PCR. **(E)** Genomic positions and distances for the primers used in colony PCR to confirm the deletion of *cenR* (WT = 1,837 bp; Δ*cenR* = 1,150 bp). (In Lakey *et al* 2022 as Supplemental Figure 3, S3).

A

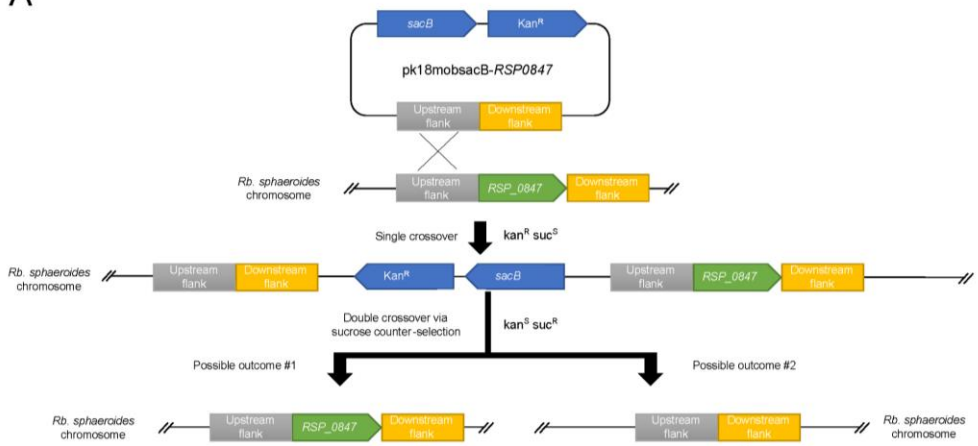

B

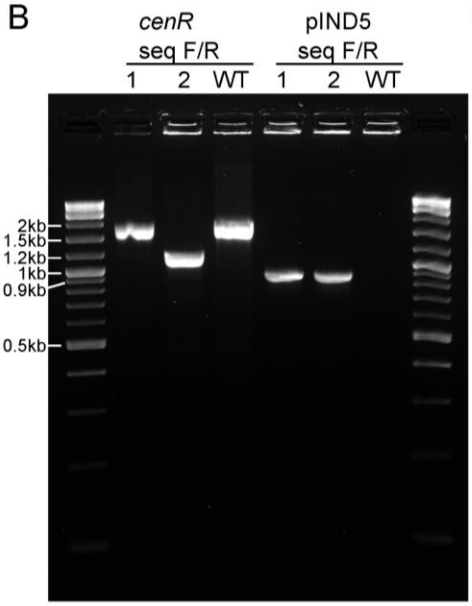

C

Strain Construction	Total Colonies Screened	Genotype		Phenotype
		Δ	WT	*sacB* inactivation
Deletion of *cenR* in the presence of pIND5$_{spec}$-*cenR*	50	16	19	15

D

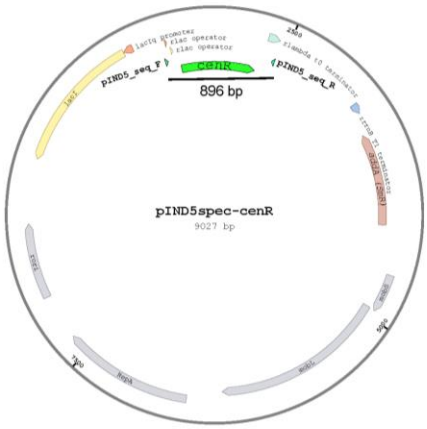

E

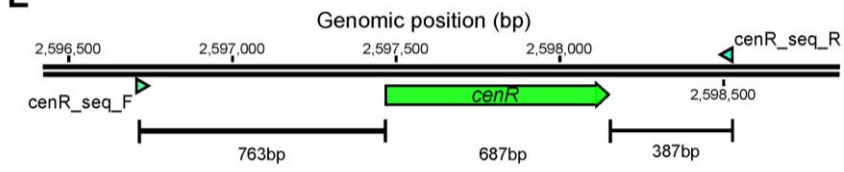

Aspartate 56 in CenR is critical for phosphorylation by CenK. To further explore the impact and mechanism of phosphotransfer from CenK to CenR, we sought to identify the CenR residue that was required for phosphorylation by CenK. To do this, we used the I-TASSER homology modeling tool [34–36] to predict which CenR aspartate residue acts as a phosphoacceptor from CenK. The receiver domain of OmpR-family RRs, like CenR, contains five-stranded parallel β-sheets flanked by two α-helices on the N-terminus and three α-helices on the other, with the canonical phosphoaccepting aspartate residue located at the end of the third β-sheet [7,8]. This residue is located proximal to negatively charged residues between α1 and β1, which coordinate a Mg^{2+} ion to catalyze phosphorylation [7,8]. The I-TASSER structural model of CenR (Fig 2-1 C) we used was assembled based on similarity to the structure of a RR in *M. tuberculosis* (PDB accession number: 1YS6; identity 0.31, coverage 0.97, TM-score 0.87, RMSD 2.16). This model predicts that residue D56 in CenR (Fig 2-1 C, magenta) is proximal to the three aspartate residues, D11-D13, that coordinate Mg^{2+} (Fig 2-1 C, orange), and likely the residue that participates in phosphotransfer from CenK.

To assess if an aspartate at residue D56 is needed for CenR phosphorylation, we expressed and purified a variant RSP_0847 protein containing an alanine substitution (D56A) and tested for activity in a phosphotransfer assay with ^{32}P-labeled CenK (Fig 2-1 D). We observed no transfer between ^{32}P-labeled CenK and CenR(D56A) under the same conditions where wild-type RR was phosphorylated, demonstrating that an aspartate at residue 56 is necessary for this protein to serve as a phosphoacceptor from phosphorylated CenK. Previously, it had been proposed that *Rb. sphaeroides* CenR residue D51 is a site of phosphorylation [37]. However, given the predicted orientation of the CenR D51 side chain away from the catalytic phosphorylation site at

the N-terminus of β1, and the inability of CenR(D56A) to be phosphorylated by CenK *in vitro*, we propose that D56 is the site of phosphorylation of this RR (Fig 2-1 C).

Modulation of the activity of CenR results in cell length defects. Using this *cenR*(D56A) allele, we asked if we could disrupt phosphorylation of CenR *in vivo*. As we were able to delete *cenK* (Fig 2-1 B), we hypothesized that a non-phosphorylatable form of CenR would be sufficient to support cell viability and would phenocopy cells containing the Δ*cenK* allele. To test this hypothesis, we successfully created a strain containing an alanine codon at residue D56 of the native *cenR* locus (*cenR*(D56A)), using the same methods that were unable to produce a strain containing an in-frame deletion of *cenR*.

As previous studies showed that loss of CenK had an observable impact on cell shape [25], we tested the impact of the CenR D56A substitution *in vivo* by measuring cell dimensions using bright-field microscopy. We observed that cells containing the *cenR*(D56A) allele were short (length: WT = 1.98 ± 0.11 μm; *cenR*(D56A) = 1.63 ± 0.10 μm; Δ*cenK* = 1.62 ± 0.13 μm) and more spherical (width: WT = 0.66 ± 0.04 μm; *cenR*(D56A) = 0.80 ± 0.04 μm; Δ*cenK* = 0.82 ± 0.05 μm) in comparison to wild-type cells (Fig 2-5 A-C). As the *cenR*(D56A) allele phenocopied the features of the Δ*cenK* strain, this supports the conclusion that reduction in activity of this TCS is the cause of the observed changes in cell shape. Furthermore, *Rb. sphaeroides* cells containing either the Δ*cenK* or *cenR*(D56A) alleles grew at a similar rate compared to wild-type cells (~2.5 hrs) and reached a similar final cell density (Fig 2-5 D). From our *in vitro* and *in vivo* data, we conclude that the CenR D56A amino acid substitution reduces, but does not completely abolish, activity of the CenKR TCS.

It has been established that substitution of the phosphoaccepting aspartate residue with a glutamate can sterically mimics phosphorylation of other RRs [38,39]. Therefore, we hypothesized that introduction of the phosphomimetic amino acid change D56E in CenR would result in a cell elongation phenotype. We generated a strain containing a glutamate codon at position 56 of the native *cenR* locus (*cenR*(D56E)), and measured cell dimensions finding that *cenR*(D56E) cells were longer (2.91 ± 0.17 μm) than wild-type cells (Fig 2-5 A, C). We also observed that cells containing the *cenR*(D56E) allele grew slower than wild-type cells (*cenR*(D56E) ~3.5 hrs, WT ~ 2.5 hrs, Fig 2-5 D) suggesting that constitutive activity of CenR has pleiotropic effects on growth and/or cell division rates. To test if the impact of the *cenR*(D56E) allele is independent of CenK activity, we introduced this mutation in a Δ*cenK* strain. We observed Δ*cenK cenR*(D56E) also produced longer cells than those containing a wild-type CenR protein (Fig 2-6, 2.91 ± 0.06 μm), confirming that the D56E substitution in CenR is sufficient to increase the activity of the RR and change cell length and growth rate.

Figure 2-5. Impact of changes in CenKR activity on cell dimensions. (Panels A-C) Bright-field microscopy measurements of the length and width of exponential phase cells displayed as beeswarms plots [133]. Mean values from each of the three biological replicates (grey circles, yellow triangles, and blue squares, respectively) and mean values for each strain are shown (black bar). For each biological replicate, >1000 cells were analyzed. Unpaired t-tests were used to compare pooled cell dimension data from the mean values of each biological replicates (n = 3) [133]. Significant *P* values < 0.05 are indicated by an asterisk. **(A)** Cell length measurements of wild-type (WT) and indicated CenKR mutants: (mean ± SD) WT = 1.98 ± 0.11 µm; Δ*cenK* = 1.62 ± 0.13 µm; *cenR*(D56A) = 1.63 ± 0.10 µm; *cenR*(D56E) = 2.91 ± 0.17 µm (see text for explanation of individual alleles). **(B)** Cell width measurements of WT and indicated CenKR mutants: WT = 0.66 ± 0.04 µm; Δ*cenK* = 0.82 ± 0.05 µm; *cenR*(D56A) = 0.80 ± 0.04 µm; *cenR*(D56E) = 0.57 ± 0.01 µm. **(C)** Bright-field microscopy images of wild-type and indicated CenKR mutant strains (scale bar = 3 µm). **(D)** Growth curve of *Rb. sphaeroides* strains. Hyperactivation of CenR results in slower growth rate compared to WT cells (3.5 hours vs 2.5 hour doubling time, respectively).

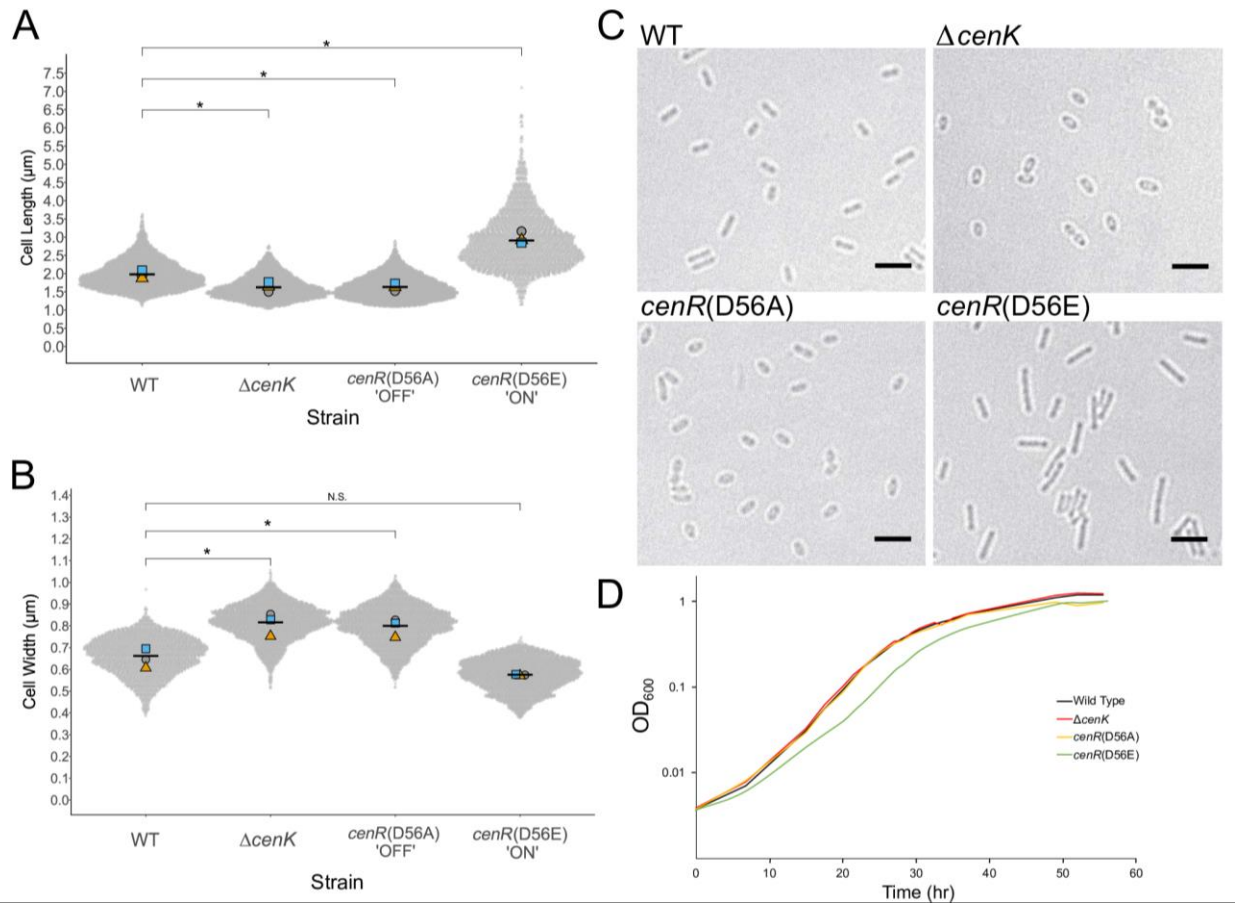
A
Cell Length (μm)
WT
ΔcenK
cenR(D56A) 'OFF'
cenR(D56E) 'ON'
Strain
B
Cell Width (μm)
N.S.
Strain
C
WT
ΔcenK
cenR(D56A)
cenR(D56E)
D
OD600
Time (hr)
Wild Type
ΔcenK
cenR(D56A)
cenR(D56E)

Figure 2-6. CenR(D56E) hyperactivity and cell elongation is independent of CenK activity. Bright-field microscopy measurements of the length of exponential phase cells displayed as beeswarm plots [133]. Mean values from each of the three biological replicates (grey circles, yellow triangles, and blue squares, respectively) and the mean value of cell length for each strain is shown (black bar). For each replicate n > 1000 cells were analyzed. Unpaired t-tests were used to compare pooled cell dimension data from the mean values of each biological replicate (n = 3, * *P* value < 0.05). (Mean ± SD) Wild-type: 2.09 ± 0.13 µm; *cenR*(D56E) Δ*cenK*: 2.91 ± 0.05 µm. (In Lakey *et al* 2022 as Supplemental figure 4, S4)

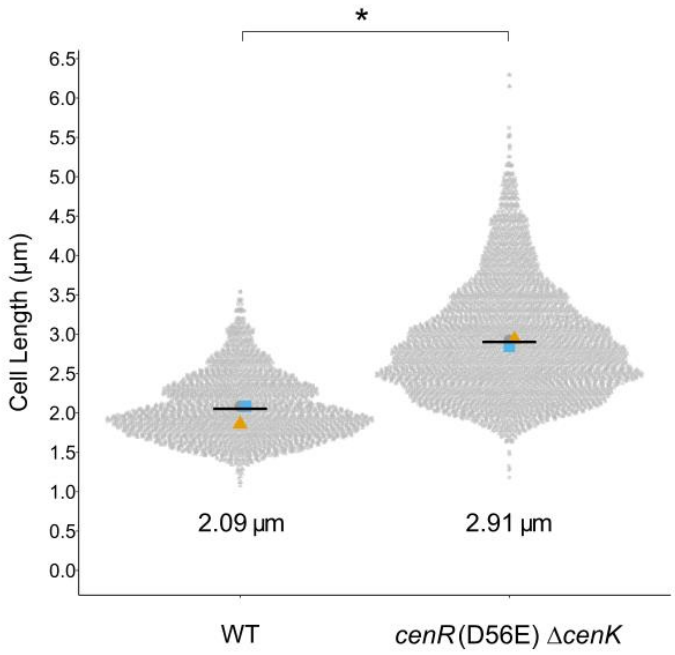

Characterization of the genome-wide binding sites of CenR. To understand how changes in CenKR activity led to the observed cellular changes, we sought to identify genes comprising the direct regulon for this TCS (Fig 2-7). We expected CenR to bind DNA since it is predicted to be within the OmpR RR family and contains a characteristic winged helix-turn-helix motif in the C-terminal effector domain of the protein (Fig 2-1 C) [6]. To identify potential CenR binding sites, we used ChIP-seq to map the *in vivo* DNA binding by this protein in strains containing wild-type, increased (*cenR*(D56E)), and decreased (Δ*cenK* or *cenR*(D56A)) activity of this TCS. Using the MOSAiCS [40] peak finding algorithm, we identified 458 sites across the *Rb. sphaeroides* genome as putative CenR binding sites (S1 Data). Of these, ~60% (273) were present in three or more biological replicates and were located near previously mapped transcription start sites (TSSs) of cells grown under the same conditions used to monitor DNA binding by this RR [41]. The remaining ~40%, found in less than three biological replicates, located in intragenic regions, or between coding regions of convergent genes, were not used in the subsequent analysis.

To identify the CenR binding events which led to changes in gene expression, we used RNA-seq to compare global transcript levels in the same strains used for ChIP-seq experiments (S2 Data). A total of 597 genes were differentially expressed in at least two strains with $\log_2$ fold change greater than 0.5 or less than -0.5 and a false discovery rate (FDR) of less than 0.05. Based on the impact of CenR amino acid changes at residue D56 on cells, we predicted that genes with increased transcript levels in a strain containing a hyperactive TCS (CenR D56E) should show decreased expression in cells containing reduced CenKR activity (CenR D56A), and vice versa. Of the 597 differentially expressed genes (DEGs) among these data sets, 275 showed opposing

expression patterns when comparing strains with increased and decreased CenKR activity relative to wild-type (S2 Data). Combing the ChIP-seq results mapping CenR binding sites and transcriptomic analysis of CenKR dependent changes in gene expression, we identified 59 potential transcriptional units (101 DEGs) that both showed CenR DNA binding and differential transcripts levels between wild-type cells and TCS mutants (Table 2-2). Of the 59 potential transcriptional units identified, we predict that CenR activates the expression of 42 (71%), while repressing transcription of the other 17 (29%).

Figure 2-7. Strategy used to define members of the CenKR regulon. The *in vivo* genome-wide CenR binding sites and CenKR-dependent transcriptomic data were generated from strains with a hyperactive (CenR D56E), wild-type (WT), and low activity (CenR D56A and ΔCenK) TCS. Combined data sets were used to identify genes directly regulated by CenR and the mode of regulation of each candidate gene. Genomic CenR binding sites were then analyzed for a putative DNA binding motif recognized by CenR to further refine the predicted CenR regulon.

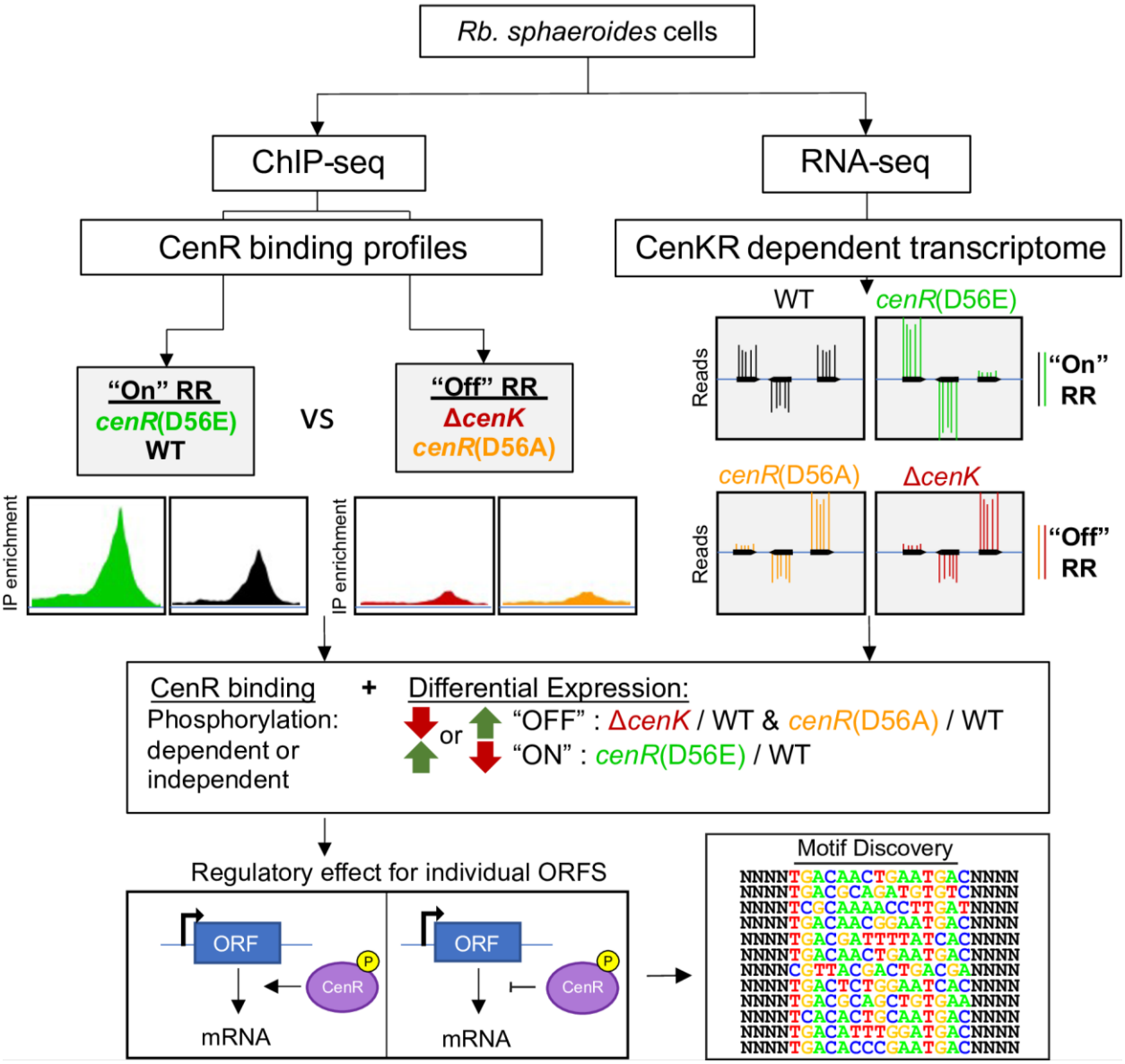
Rb. sphaeroides cells
ChIP-seq
RNA-seq
CenR binding profiles
CenKR dependent transcriptome
"On" RR
cenR(D56E)
WT
VS
"Off" RR
ΔcenK
cenR(D56A)
WT
cenR(D56E)
Reads
"On" RR
cenR(D56A)
ΔcenK
Reads
"Off" RR
IP enrichment
IP enrichment
CenR binding
Phosphorylation:
dependent or
independent
+
Differential Expression:
or
"OFF" : ΔcenK / WT & cenR(D56A) / WT
"ON" : cenR(D56E) / WT
Regulatory effect for individual ORFS
ORF
CenR
P
mRNA
ORF
CenR
P
mRNA
Motif Discovery
NNNNTGACAACTGAATGACNNNN
NNNNTGACGCAGATGTGTCNNNN
NNNNTCGCAAAACCTTGATNNNN
NNNNTGACAACGGAATGACNNNN
NNNNTGACGATTTTATCACNNNN
NNNNTGACAACTGAATGACNNNN
NNNNCGTTACGACTGACGANNNN
NNNNTGACTCTGGAATCACNNNN
NNNNTGACGCAGCTGTGAANNNN
NNNNTCACACTGCAATGACNNNN
NNNNTGACATTTGGATGACNNNN
NNNNTGACACCCGAATGACNNNN

Identification of a CenR binding motif. We used MEME [42,43] to identify a conserved DNA sequence logo enriched in regions defined by the 59 ChIP-seq peaks mentioned above. This analysis identified the motif sequence TGA-N_8-TGA (Fig 2-8A), a tandem direct repeat within <100 bp upstream of 31 of these 59 putative CenR regulated transcriptional units (Table 2-2). Identification of a direct repeat is consistent with other OmpR family transcription factors that often bind DNA as oligomers by recognizing direct repeat sequence motifs [9]. Additionally, the 10 bp distance between the start of each half-site is consistent with that of other known RR that bind B-form DNA [9,44].

We compared the position of each identified CenR binding site to the TSS of each transcriptional unit to make predictions on the role of this RR in controlling expression of these genes (Fig 2-8 C-D). Based on this analysis, we found that 28 of the 31 CenR binding sites are located directly upstream of the promoter -35 element (Fig 2-8 C-D, green) and oriented co-directionally with the direction of transcription. The location of these predicted CenR binding sites relative to the promoter of these transcription units is consistent with our hypothesis that this RR activates transcription of these genes, likely through interacts with the α subunit of RNA polymerase analogous to other OmpR-family RRs [9]. Of the transcriptional units that we predicted are directly repressed by CenR, the predicted RR binding site is located between the -35 promoter element and known TSS (Fig 2-8 C-D, red), with two of the predicted binding sites oriented in the opposite direction of transcription, and one co-directional. This suggests that CenR binding to these sites represses transcription by competing for RNA polymerase binding to promoter elements. Together, we propose that the 31 transcriptional units that contain the conserved TGA-N_8-TGA motif are members of the CenKR direct regulon (Table 2-1). While we were unable to

find this putative CenR binding site upstream of the other 28 transcriptional units, this does not necessarily mean that these transcriptional units are not direct members of this regulon. However, for this study, we only considered transcriptional units with CenR binding sites in the subsequent analyses.

To test the role of the TGA-N_8-TGA direct repeat in CenR binding to promoter regions, we assayed the ability of phosphorylated CenR (CenR~P) to bind to DNA fragments containing the promoter regions of *rpoH1* and *tolQRAB* which are predicted to contain a related sequence (Table 2-1) and *RSP_2157* which lacks any similarity to this motif. When we assayed binding of CenR~P to each DNA fragment in a gel electromobility shift assay, we found that the presence of CenR~P in reactions containing DNA fragments of either *rpoH1* or *tolQRAB* transcriptional units resulted in delayed migration through the gel, relative to reactions containing no protein, which is indicative of DNA-protein interaction (Fig 2-9). Furthermore, we observed no change in migration patterns of the DNA fragment of the *RSP_2157* promoter suggesting that the shift in *rpoH1* or *tolQRAB* promoter DNA was dependent on the presence of the TGA-N_8-TGA direct repeat sequence. The binding patterns observed in this EMSA were similar to what has been previously reported for other OmpR family response regulators, like ArcA, which recognizes a series of three direct repeat motifs [45,46]. Together, this bioinformation and *in vitro* data suggest that this direct repeat is likely the DNA binding motif recognized by CenR *in vivo*.

Figure 2-8. Identification of the CenR DNA binding motif.

(A) WebLogo [132] representation of CenR consensus sequence determined using the MEME motif finder. Of the 59 promoters identified in ChIP-seq experiments, 31 operons contained the putative CenR consensus sequence TGA-(N8)-TGA. **(B)** Location and orientation of the 31 identified CenR binding sites, in respect to the previously determined TSS [41] and promoter -35 and -10 elements [124] for directly activated (green) and repressed (red) transcription units. The DNA sequence of each binding motif is listed in Table 2-1. **(C)** Histogram of the distance from the center of each putative CenR binding site and the TSS of the respective transcription unit mapped in (B). Operons predicted to be activated have CenR binding sites upstream of the -35 promoter element, whereas operons predicted to be repressed have CenR binding sites that overlap either the TSS or the predicted promoter elements.

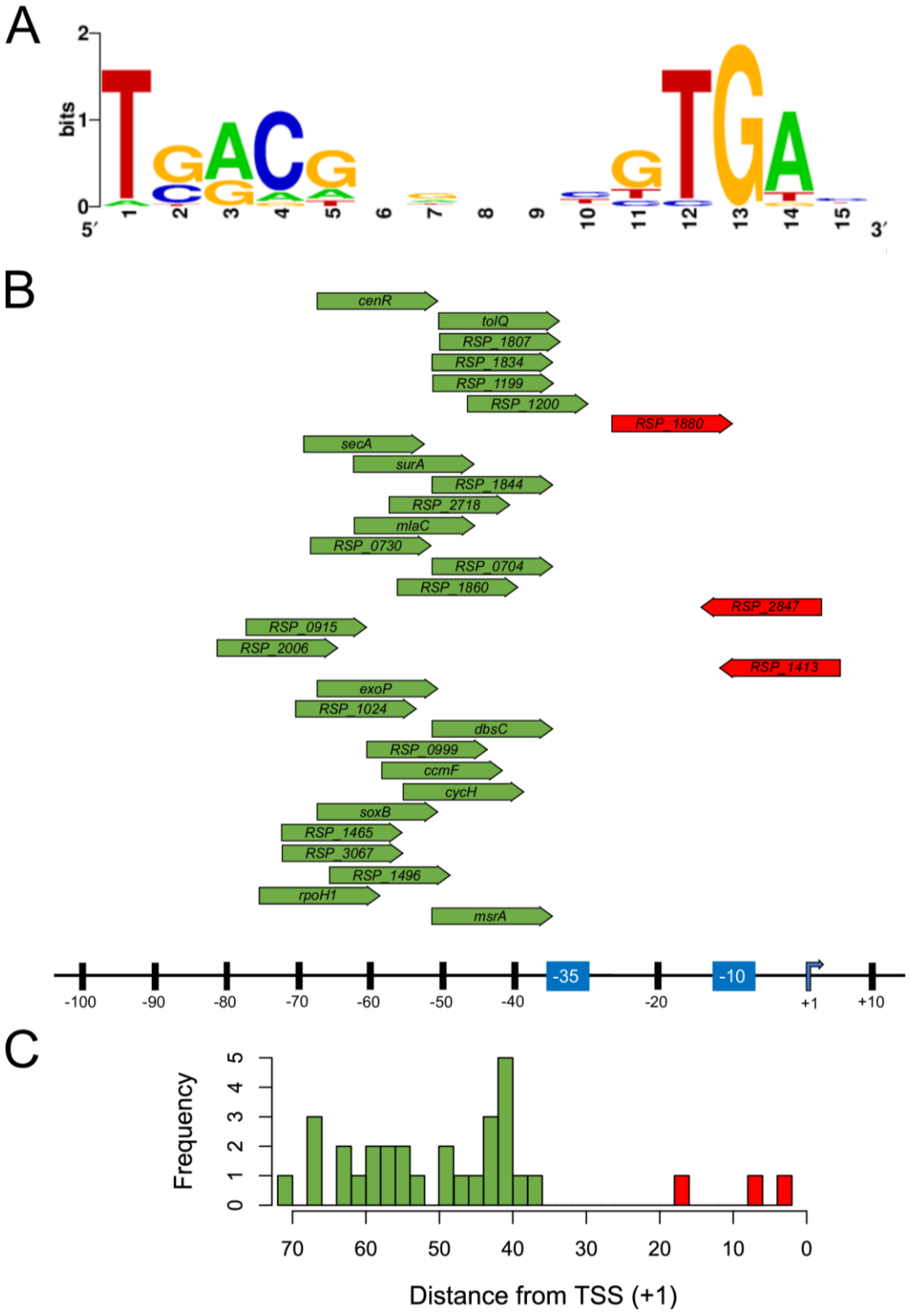
A
bits
5′
3′
B
cenR
tolQ
RSP_1807
RSP_1834
RSP_1199
RSP_1200
RSP_1880
secA
surA
RSP_1844
RSP_2718
mlaC
RSP_0730
RSP_0704
RSP_1860
RSP_2847
RSP_0915
RSP_2006
RSP_1413
exoP
RSP_1024
dbsC
RSP_0999
ccmF
cycH
soxB
RSP_1465
RSP_3067
RSP_1496
rpoH1
msrA
-35
-10
-100
-90
-80
-70
-60
-50
-40
-20
+1
+10
C
Frequency
Distance from TSS (+1)

Figure 2-9. CenR binds the promoters of *tolQRAB* and *rpoH1 in vitro.*

Gel mobility shift assays containing DNA sequences directly upstream of *tolQ* (lanes 1-5), *rpoH1* (lanes 6-10), or *RSP_2157* (lanes 11-15) transcription start sites [41]. To each reaction, 0, 125, 250, 500, or 1000 nM of phosphorylated CenR (CenR~P) was used to shift DNA. (In Lakey *et al* 2022 as Supplemental Figure 5, S5).

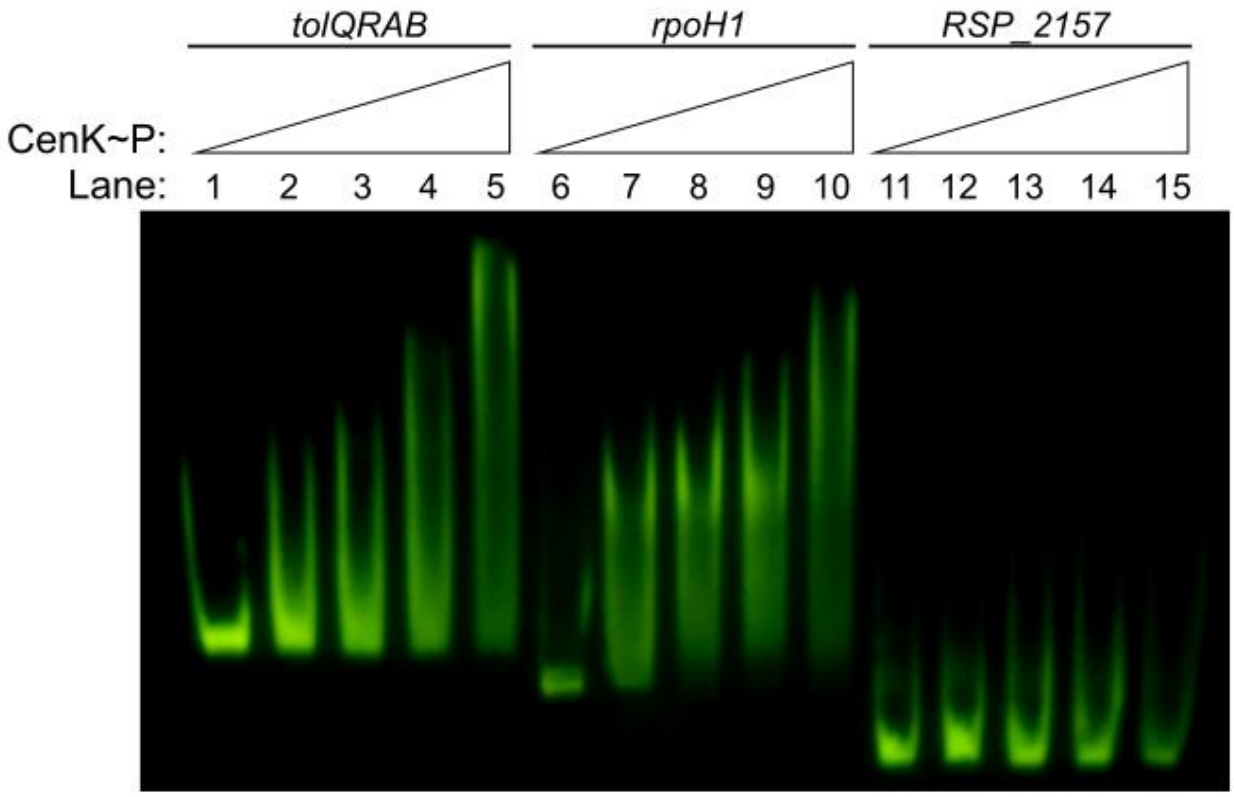

CenKR directly activates the expression of genes for envelope stress, remodeling, and cell division. We used the known or predicted function of the DEGs to gain insight into cellular functions that are directly controlled by CenR. Of the 31 transcriptional units which we predict are direct targets for control by CenR, 29 encode protein products that are targeted to the cell envelope or periplasmic space (Table 2-1), illustrating this TCS plays a broad role in the function of this cellular compartment. For example, we identified CenR as a direct activator of the transcriptional unit that encodes the Tol proteins of the Tol-Pal complex. CenR enrichment was identified upstream of *tolQ*, the first gene in the *tolQRAB* operon, in all strains analyzed, with decreased occupancy of this RR in Δ*cenK* and *cenR*(D56A) strains (Fig 2-10 A). We found increased abundance of *tolQRAB* transcripts in cells with increased CenKR activity relative to wild-type cells and a slight, yet significant decrease in abundance of the same transcripts in cells with reduced activity of this TCS (Fig 2-10 A).

We found that the expression of other genes known or predicted to function in cell envelope maintenance in other bacteria was predicted to be directly activated by CenR (Table 2-1). For example, *RSP_1834* encodes a predicted β-lactamase that in other bacteria degrades antibiotics that target penicillin binding proteins thereby preventing inhibition of PG synthesis [47], and *RSP_1199* which encodes a putative L,D-transpeptidase that forms crosslinks between peptide sidechains of PG either in response to OM/LPS assembly defects, osmotic stress, or in response to β-lactam antibiotics that inhibit D,D-transpeptidases [5,48,49]. Moreover, *Rb. sphaeroides* genes encoding proteins that function in autolysis to digest glycan chains of PG such as *RSP_1496* (a putative lysozyme-like lipoprotein), and *RSP_1860* (a putative cell wall hydrolase) are among those that we predict are directly regulated by CenKR (Table 2-1). We also identified

CenR as a direct transcriptional regulator of the gene encoding the periplasmic retrograde lipid trafficking protein MlaC (RSP_0890), a member of the mla complex (maintenance of lipid asymmetry) and functions to transport lipids away from the OM [50]. *RSP_0915, RSP_1200, RSP_1844, RSP_2006, RSP_2718*, and *RSP_3067* are genes of unknown function that encode proteins targeted to the OM or periplasmic space in other bacteria, suggesting that these predicted members of the direct CenR regulon may have heretofore untested roles in cell envelope biology in *Rb. sphaeroides* and other related α-proteobacteria.

This analysis also predicted that several of the gene products in the direct CenR regulon aid in the mitigation of misfolded proteins. These include the homolog of the *E. coli* periplasmic chaperon, SurA, which functions to facilitate the folding and assembly of OM proteins [51], and the alternate sigma factor RpoHI (Fig 2-10 B). *Rb. sphaeroides* RpoHI directly controls genes encoding protein that are involved in protein homeostasis, maintenance of membrane integrity, and DNA repair [52], and we identified many of these genes as DEGs in our RNA-seq datasets (S2 Data). This later result suggests that CenKR initiates a global response to general stress. Furthermore, we predict that CenR directly regulates genes that mitigate oxidative and disulfide bond protein stresses *dsbC, msr*A [53,54], and cytochrome biogenesis operons *ccmF-ccmH* as well as *cycH*. Finally, RRs often regulate their own transcription [9,29]. Consistent with this, we observed CenR binding upstream of *cenR* (Fig 2-10 C), but not upstream of *cenK*. Accordingly, we observed no change in transcription of *cenK*, suggesting expression of *cenK* is not dependent on CenKR activity (Fig 2-10 C).

Figure 2-10. CenKR activity directly regulates the *tolQRAB* operon, the gene encoding the alternate sigma factor *rpoH1*, and indirectly affects the expression of cell wall biosynthesis genes.

(A-C) Shown are the ChIP-seq data traces of CenR binding upstream of an indicated promoter in TCS "on" strains (*cenR*(D56E) in green, and WT in black) and TCS "low activity" strains (Δ*cenK* in red, and *cenR*(D56A) in orange). ChIP-seq peak heights are represented on the y-axis (fold-enrichment of IP vs input DNA). The chromosomal location is shown on the x-axis with genes represented by arrows pointing in the direction of transcription. TSSs of known promoter(s) are represented as green arrows [41,124]. This inset shows the $\log_2$ fold change in transcript levels determined from RNA-seq experiments showing change in abundance of the indicated gene in TCS mutant strains relative to WT cells. Non-significant (N.S.) changes in gene expression (FDR > 0.05) are indicated with a grey box **(A)** CenR autoregulates its own expression. CenR binding was detected upstream of *cenR* and increased *cenR* transcripts were found in strains with a hyperactive TCS. No detectable CenR binding was identified upstream of *cenK* and there was no significant change in *cenK* transcript levels in CenR mutants compared to wild-type cells. **(B)** CenR binding enriched upstream of the *tol* operon is predicted to correlate with increased transcript levels. No CenR binding or CenR-dependent change in transcript levels was detected upstream of the operon containing *pal*. **(C)** CenR binding and predicted activation of *rpoHI* expression by this RR. **(D)** Heat map of the effect CenKR TCS activity on expression of PG biosynthesis, division, and elongation machinery. CenKR activity is predicted to indirectly repress PG biosynthesis and cell division related machinery while indirectly activating the expression of the cell elongation machinery (Rod complex). (In Lakey *et al* 2022 as Supplemental Figure 6, S6)

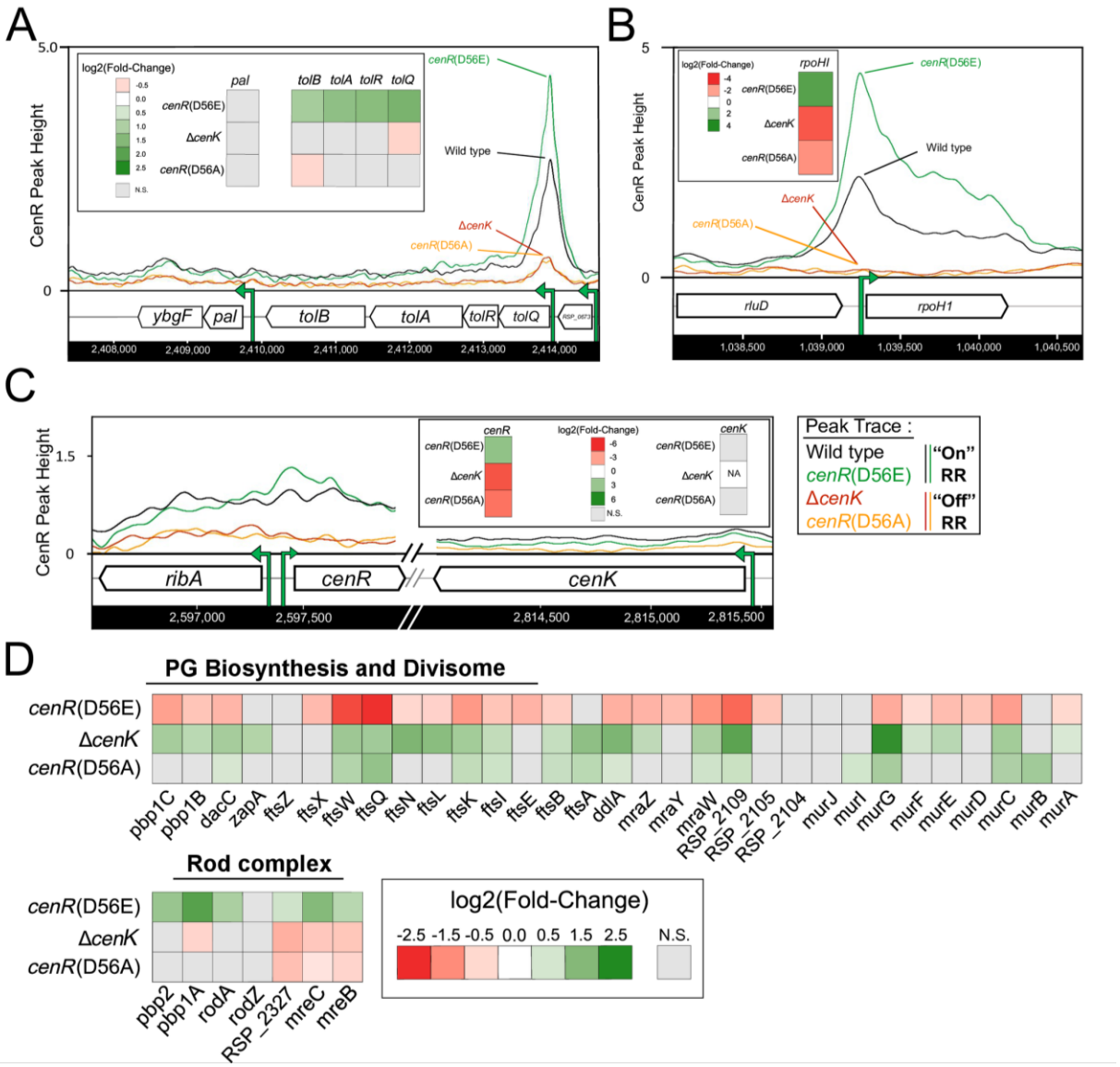
A
CenR Peak Height
5.0
0
log2(Fold-Change)
pal
tolB tolA tolR tolQ
cenR(D56E)
ΔcenK
cenR(D56A)
N.S.
Wild type
ybgF pal tolB tolA tolR tolQ
2,408,000 2,409,000 2,410,000 2,411,000 2,412,000 2,413,000 2,414,000
B
CenR Peak Height
5
0
rpoHI
Wild type
rluD rpoH1
1,038,500 1,039,000 1,039,500 1,040,000 1,040,500
C
CenR Peak Height
1.5
0
cenR
cenK
NA
ribA cenR cenK
2,597,000 2,597,500 2,814,500 2,815,000 2,815,500
Peak Trace :
Wild type
cenR(D56E)
ΔcenK
cenR(D56A)
"On" RR
"Off" RR
D
PG Biosynthesis and Divisome
pbp1C pbp1B dacC zapA ftsZ ftsX ftsW ftsQ ftsN ftsL ftsK ftsI ftsE ftsB ftsA ddlA mraZ mraY mraW RSP_2109 RSP_2105 RSP_2104 murJ murI murG murF murE murD murC murB murA
Rod complex
pbp2 pbp1A rodA rodZ RSP_2327 mreC mreB
log2(Fold-Change)
-2.5 -1.5 -0.5 0.0 0.5 1.5 2.5 N.S.

Figure 2-11. Putative CenR binding and regulation of the division and cell wall gene cluster.

Shown are the ChIP-seq data traces of CenR binding upstream of an indicated promoter in TCS "on" strains (*cenR*(D56E) in green, and WT in black) and TCS "low activity" strains (Δ*cenK* in red, and *cenR*(D56A) in orange). ChIP-seq peak heights are represented on the y-axis (fold-enrichment of IP vs input DNA). The chromosomal location is shown on the x-axis with genes represented by arrows pointing in the direction of transcription. TSSs of known promoter(s) are represented as green arrows [41,124]. This inset shows the $\log_2$ fold change in transcript levels determined from RNA-seq experiments showing change in abundance of the indicated gene in TCS mutant strains relative to WT cells. Non-significant (N.S.) changes in gene expression (FDR > 0.05) are indicated with a grey box. **(A)** The first half of the *dcw* operon showing putative CenR enrichment within of the promoter region of *mraZ*. **(B)** The second half of the *dcw* operon showing CenR enrichment within the promoter regions of *ftsW* / *RSP_2105* and *ddlA*. CenKR TCS activity is predicted to repress the transcription of genes in the *dcw* operon.

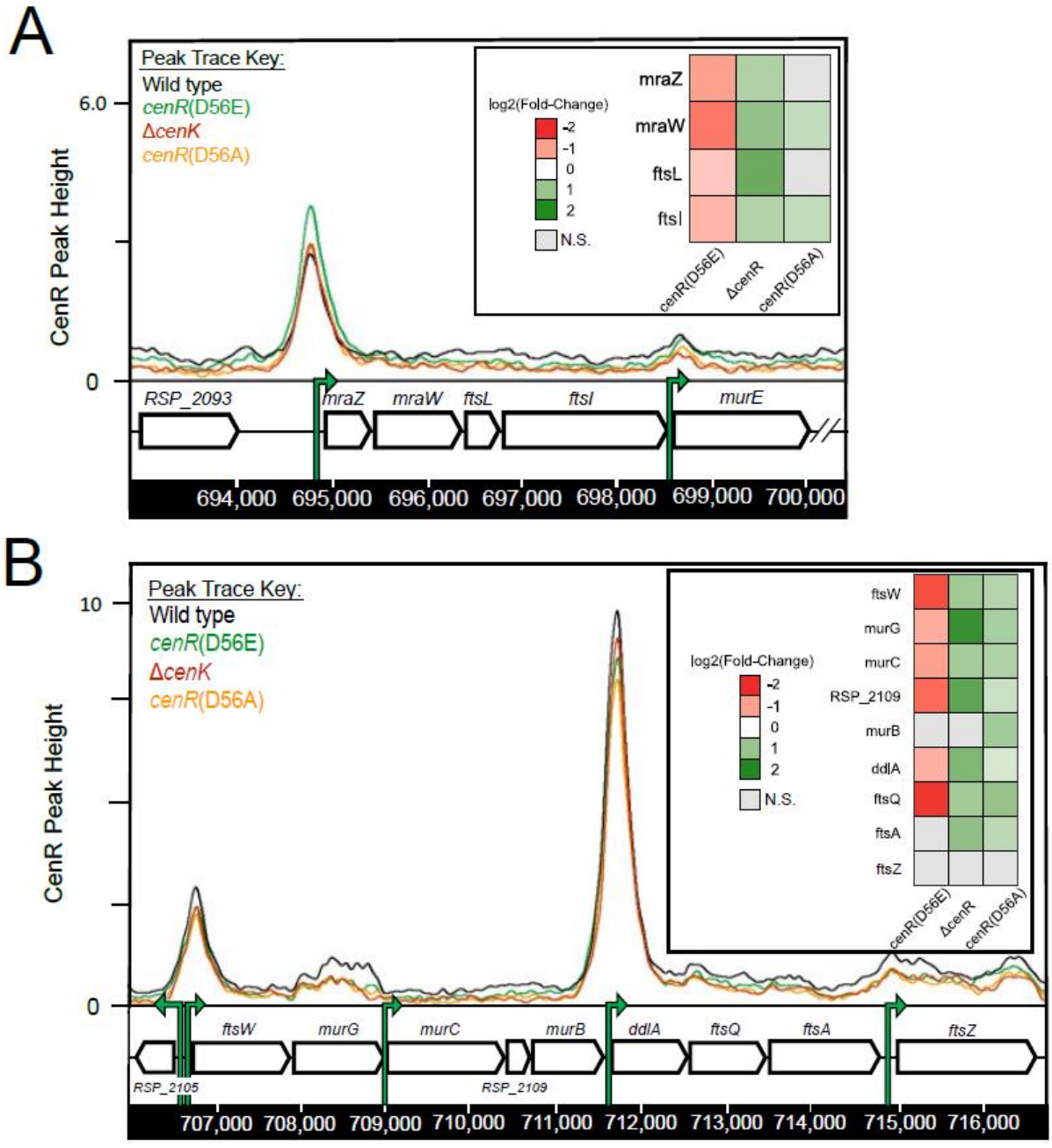
A
Peak Trace Key:
Wild type
cenR(D56E)
ΔcenK
cenR(D56A)
CenR Peak Height
6.0
0
log2(Fold-Change)
-2
-1
0
1
2
N.S.
mraZ
mraW
ftsL
ftsI
cenR(D56E)
ΔcenR
cenR(D56A)
RSP_2093
mraZ
mraW
ftsL
ftsI
murE
694,000 695,000 696,000 697,000 698,000 699,000 700,000
B
Peak Trace Key:
Wild type
cenR(D56E)
ΔcenK
cenR(D56A)
CenR Peak Height
10
0
log2(Fold-Change)
-2
-1
0
1
2
N.S.
ftsW
murG
murC
RSP_2109
murB
ddlA
ftsQ
ftsA
ftsZ
cenR(D56E)
ΔcenR
cenR(D56A)
RSP_2105
ftsW
murG
murC
RSP_2109
murB
ddlA
ftsQ
ftsA
ftsZ
707,000 708,000 709,000 710,000 711,000 712,000 713,000 714,000 715,000 716,000

Cell wall biosynthetic machinery indirectly responds to changes in CenKR activity.

Transcripts from genes encoding PG biosynthesis machinery critical for division and elongation were differentially expressed in cells with altered CenKR activity (Fig 2-10 D). Cells containing the *cenR*(D56E) allele had reduced levels of transcripts from genes whose products are predicted to function in synthesis of cytoplasmic PG precursor molecules (*murB, murC, murD, murE, ddlA*, *murF*, *mraY*, and *murG*), their transport across the inner membrane (*ftsW*), and their subsequent assembly into nascent peptide chains (*ftsA*, *ftsQLB*, *ftsK* (*RSP_1495*), *ftsX* (*RSP_0734*), *ftsN* (*RSP_6008*), *pbp1B* (*RSP_0887*), *pbp1C* (*RSP_1355*)) [5,55]. We also found an effect of the *cenR*(D56E) allele on the abundance of transcripts from genes whose products are predicted to function in the divisome (Fig 2-10 D), the complex involved in septal PG synthesis during the latter stages of cell division [5,55]. We found that cells containing the *cenR*(D56E) allele had increased levels of transcripts from genes predicted to encode subunits of the Rod complex (Fig 2-10 D) that synthesizes PG along the lateral cell wall to facilitate cell elongation [5,55]. Combined, these changes in transcript abundance provide a possible explanation for the cell length changes observed in cells that contain the *cenR*(D56E) allele which we predicted increased CenKR TCS activity.

Using ChIP-seq analysis, CenR binding was detected upstream of three (*mraZ, ftsW, ddlA*) of the seven highly conserved promoters within the division and cell wall biosynthesis (*dcw*) gene cluster (*RSP_2095-RSP_2114*) [56], suggesting that this TCS plays a direct role in repressing the transcription of these genes (Table 2-2 and Fig 2-11). However, these promoter regions did not contain the predicted binding motif for this RR in the vicinity of the known TSS, and no decline in CenR enrichment was detected in strains harboring an inactive TCS (Fig 2-11). Therefore, we

propose that CenR either requires another DNA binding protein to alter transcription, plays an indirect role in the regulation of these genes though hierarchical regulation of other transcription factors, or this represents an artifact in ChIP-seq analysis. In any case, further experiments are required to resolve this. Related to the differential expression of the *dcw* cluster, other genes encoding PG remodeling proteins such as the lytic transglycosylase *mltB* (increased by CenR activity) and D-alanine-D-alanine carboxypeptidase *dacC* (decreased by CenR activity) [5] were predicted to be indirectly regulated by CenR since they were among our list of DEGs in TCS mutants, but lacked any evidence for binding of this RR by ChIP-seq analysis.

The CenKR TCS is conserved in α-proteobacteria. Given the high degree of amino acid sequence similarity between *Rb. sphaeroides* and *C. crescentus* CenKR proteins and the impact of altered activity of their respective TCSs on cell shape, we sought to determine if aspects of this system were conserved in other bacteria. To probe the conservation of CenKR in other organisms, we constructed separate maximum-likelihood (ML) phylogenies of both CenK and CenR. The topology of both trees was identical and could be combined (Fig 2-12, node support for CenK/CenR trees, respectively) into a tree that predicts evolutionary relationships agreeing with other α-proteobacteria phylogenies [57–60]. From this analysis, we identified homologs of CenK and CenR within eight orders in the α-proteobacteria phylogeny. These eight formed six, well supported clades consisting of *Rhizobiales* (bootstrap = 98/84), *Hyphomicrobiales* (bs = 98/85) *Caulobacterales*/*Parvularculales* (bs = 85/81), *Rhodobacterales* (bs = 100/98), *Sneathiellales* (bs = 100/100), and *Rhodospirillales*/*Kiloniellales* (bs = 95/98) representing the *Caulobacteridae* subclass [59,60]. Homologs of CenK or CenR were not identified in organisms belonging to the *Sphingomonadales* (subclass *Caulobacteridae*), orders with in the *Rickettsiidae*

subclass (encompassing the *Rickettsiales*, *Pelagibacterales*, and *Holosporales* orders), or the *Magnetococcales* at the base of the α-proteobacterial phylogeny [57–60], in members of other proteobacterial groups, or elsewhere in the bacterial phylogeny.

The conservation of CenKR homologs in other α-proteobacteria, as well as the proposed conserved role of the TCS in cell envelope regulation in *C. crescentus* [26] leads us to hypothesize that the genes we identified as direct members of this regulon might also be evolutionarily conserved in other related bacteria. To test this hypothesis, we sought to identify predicted CenR DNA binding sites in the genome of other well-studied organisms such as *Agrobacterium tumerfaciens* (*Rhizobiales*), *Brucella aborus* (*Rhizobiales*), *C. crescentus* (*Caulobacterales*), and *Rhodopseudomonas palustris* (*Hyphomicrobiales*) that contain this TCS. To do so, we compared the mapped CenR binding sites upstream of *cenR*, *tolQ*, *RSP_1860*, *RSP_1807*, *surA* and *msrA* (Table 2-1) in *Rb. sphaeroides*, with regions 300 bp upstream of each of these operons in these four related species (Table 2-5). This analysis identified the conserved direct repeat TGA-N_8-TGA upstream of each operon in each analyzed species (Fig 2-12, bottom panel), supporting the hypothesis that CenKR plays a conserved role in cell envelope regulation in α-proteobacteria.

Figure 2-12. Homologs of CenKR are found in several other α-proteobacteria.

(Phylogeny) Combined maximum likelihood phylogenetic tree of CenK and CenR identified in α-proteobacteria which had identical topologies. Support values (ML bootstrap) for CenK/CenR are listed for each node. Support values under 50 are labeled NS. **(Bottom panel)** Putative sequence logo of the CenR DNA binding motif derived from analyzing the regions upstream of transcriptional units directly controlled by CenR in indicated α-proteobacteria.

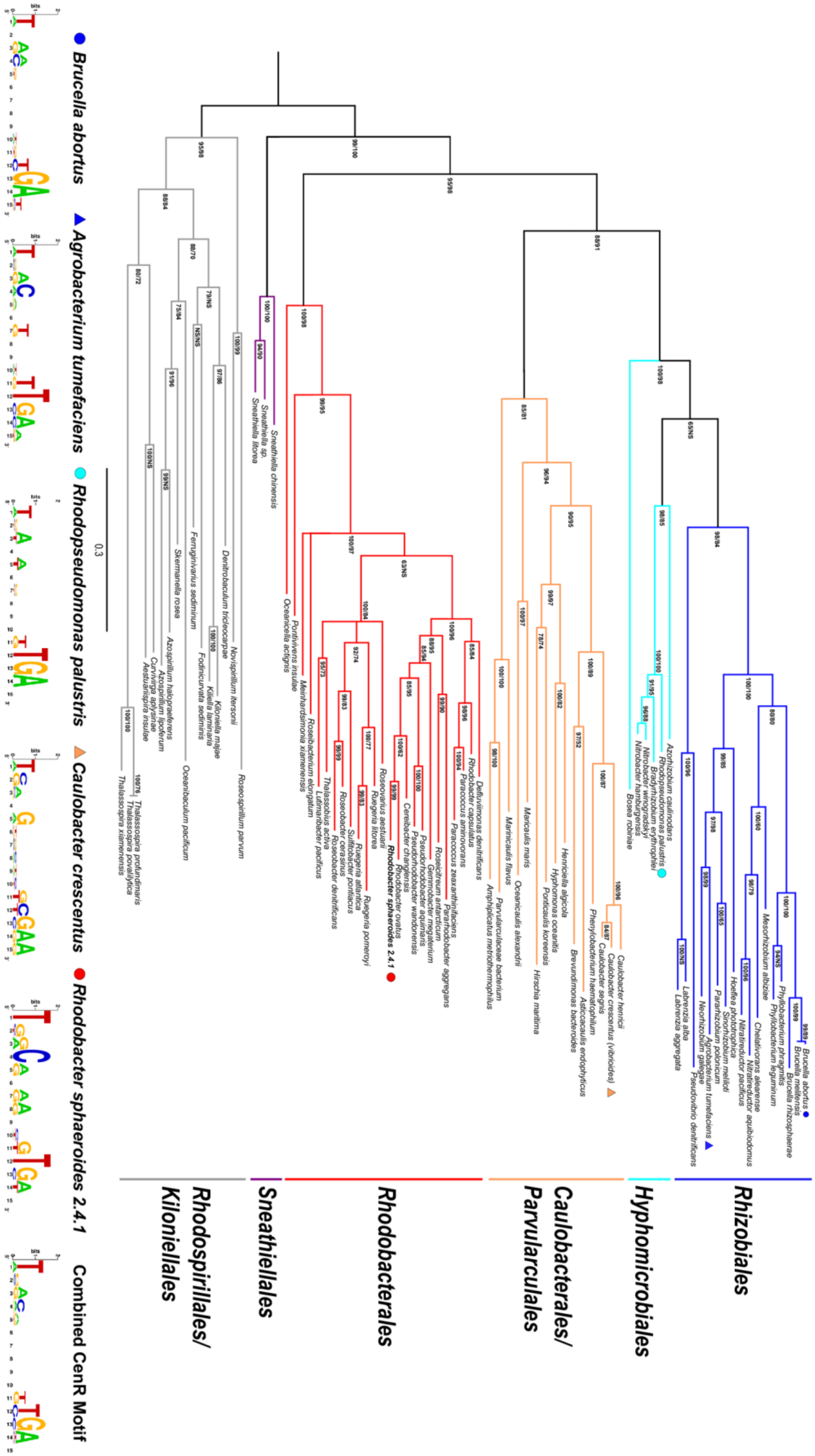

Brucella abortus
Agrobacterium tumefaciens
Rhodopseudomonas palustris
Caulobacter crescentus
Rhodobacter sphaeroides 2.4.1
Combined CenR Motif
Rhizobiales
Hyphomicrobiales
Caulobacterales/
Parvularculales
Rhodobacterales
Sneathiellales
Rhodospirillales/
Kiloniellales
0.3

Discussion

This work sought to increase our understanding of bacterial cell envelope assembly as well as modifications to this essential cellular compartment. Little is known about these processes in α-proteobacteria since these organisms lack well-studied regulators of cell envelope processes that are known in other proteobacteria. We showed that the α-proteobacterium *Rb. sphaeroides* protein RSP_1056 (CenK) is a HK that phosphorylates an OmpR-family RR, RSP_0847 (CenR), and these two proteins comprise a TCS with a high degree of amino acid similarity to *C. crescentus* CenKR. We combined genome-scale ChIP-seq with transcript abundance data from cells predicted to have different levels of CenKR activity to identify the direct CenR targets and make predict how this TCS impacts cell envelope functions in this and other α-proteobacteria (Fig 2-13). Below we highlight new information provided by our analysis of the *Rb. sphaeroides* CenKR TCS.

CenKR comprise an essential TCS in *Rb. sphaeroides*. It is known that genes encoding CenK and CenR are essential, encoded at separate loci, and comprise a TCS in *C. crescentus* [26]. In contrast, insertions in *Rb. sphaeroides cenK* (*RSP_1056*) were identified in two separate transposon insertion libraries, suggesting that unlike in *C. crescentus*, this gene is not essential in this α-proteobacterium [33]. However, the saturating genome-wide transposon library that identified *cenK*, did not contain insertions in *cenR* suggesting that this predicted RR is essential in *Rb. sphaeroides* (Fig 2-3) [25]. Similarly, a Tn-seq screen performed in α-proteobacterium *Rhodopseudomonas palustris* (Fig 2-12, *Hyphomicrobiales*) identified insertions in the homolog of *cenK* (*RPA0635*), but not *cenR* (*RPA0283*) suggesting that this RR is also essential in this bacterium [61]. To date, only a few bacterial TCSs are known to be essential. Indeed, systematic

disruption of the 106 TCS genes in *C. crescentus* identified only four essential TCS pairs. Three of these, CenK-CenR, CtrA-CckA, and DivK-DivJ, are known or predicted to be involved in cell cycle or cell envelope processes [26]. Another essential *C. crescentus* gene identified in this study was *ntrX,* encoding the RR in the NtrYX TCS that regulates LPS, exopolysaccharide synthesis, and cell wall composition in *Rb. sphaeroides* [62]. Other essential TCSs that directly regulate crucial cell wall biosynthesis machinery include WalKR in the Gram-positive organisms *Streptococcus pneumoniae* (also known as VicKR) [63] and *Bacillus subtilis* [64], WigRK in the pathogenic Gram-negative bacterium *V. cholerea* [22], and MtrAB in the pathogenic bacterium *Mycobacterium tuberculosis* [23,24]. In contrast, the cell envelope stress response TCSs, Cpx and Rcs in Gram-negative γ-proteobacteria like *E. coli* are not essential, and regulate genes that mitigate OM/LPS, OM protein, or lipoprotein stress rather than directly regulating cell envelope biogenesis machinery [11,65].

C. crescentus ntrX, *M. tuberculosis mtrA*, *S. pneumoniae vicR* (*walR*), and *Rb. sphaeroides*/*C. crescentus cenR* each are examples of essential RRs linked to non-essential HKs, suggesting that loss of the HK reduces TCS activity and that these RRs have some critical function in the absence of phosphorylation [24,26,63]. Supporting this, our *in vivo* analysis of a *cenR*(D56A) allele that abolishes phosphotransfer between CenK and CenR *in vitro* (Fig 2-1 D) suggests that this mutation diminishes CenR activity as the *cenR*(D56A) allele phenocopies the Δ*cenK* strain (Fig 2-5). Furthermore, in strains with low CenKR activity (Δ*cenK* and *cenR*(D56A)), we detected CenR binding to some promoters by ChIP-seq (Fig 2-10 A). Based on these observations, we propose that CenR has basal activity in the absence of phosphorylation that is

sufficient to promote transcription of essential genes and/or pathways, comparable to other TCS [32,63].

***Rb. sphaeroides* CenKR regulates essential division, cell wall and other envelope processes.** Genetic and biochemical characterization of *Rb. sphaeroides* CenKR allowed us to identify direct and indirect targets of this TCS. Our data predict that most members of the direct CenR regulon encode proteins that contain signal peptides and are predicted to be targeted to the OM or periplasmic space. These direct CenKR regulon members prominently included predicted OM structural or transport proteins, PG binding proteins, and periplasmic chaperones or proteases. Of the genes predicted to be direct targets of CenR, ~42% are annotated as either hypothetical proteins or have generic descriptions of their function, thus we propose these represent candidates for the future study of envelope components that are controlled by the CenKR TCS. For example, α-proteobacteria lack homologs of the well-studied spatial regulators of *E. coli* PG biosynthesis LpoA and LpoB [55,66], so it is possible that one or more members of the CenKR direct regulon provide this function. Our data also predict that CenR indirectly regulates genes encoding PG biosynthesis enzymes that promote lateral cell wall synthesis (Fig 2-10 D). This, plus the observed changes in cell shape when CenKR activity is increased or decreased (Fig 2-5 A-C) make testable predictions that one or more direct, or indirect, targets of CenKR may have a role in the spatial regulation of cell wall synthesis. Given the relatively thin cell wall of Gram-negative bacteria, precise control of PG synthesis, turnover, and repair is essential, and in other bacterial cells, redundant pathways exist to maintain cell wall integrity in response to environmental signals and membrane-active agents [5]. Furthermore, the number of PG cleavage or crosslinking enzymes (amidases, lytic transglycosylases, carboxypeptidases, and DD-endopeptidases or DD/LD-transpeptidases and glycosyltransferases) vary among bacteria

Figure 2-13. Model for the cellular impacts of direct and indirect CenKR transcriptional regulation.

CenK autophosphorylation occurs at a conserved histidine residue within its cytoplasmic domain in response to an unknown signal. CenK then phosphorylates CenR at aspartate 56 within the receiver domain, resulting in conformational changes that allow CenR to bind the promoter regions of direct target genes, repressing transcription by binding within the promoter elements (red) or activating transcription by binding upstream of promoter elements (green). Phosphorylated CenR directly upregulates (green box) genes and pathways that function in the mitigation of cellular or cell envelope stresses, maintenance of the envelope, the Tol complex that plays a vital role in OM division and stability, and other genes of unknown function predicted to be involved in the assembly or repair of cell envelope components. Indirectly, increased activity of CenR results in the increased expression of genes that function in an osmotic stress response and synthesis/remodeling of lateral cell wall (green oval). Phosphorylated CenR directly reduces transcription (red box) of gene products of unknown function that are predicted to be targeted to the cell envelope. Indirectly, increased activity of CenR decreases expression of genes within the *dcw* gene cluster that function in septal PG and cell wall biosynthesis, and genes whose products cleave PG, synthesize flagellar, and are vital for cell growth such as ribosome biosynthesis (red oval).

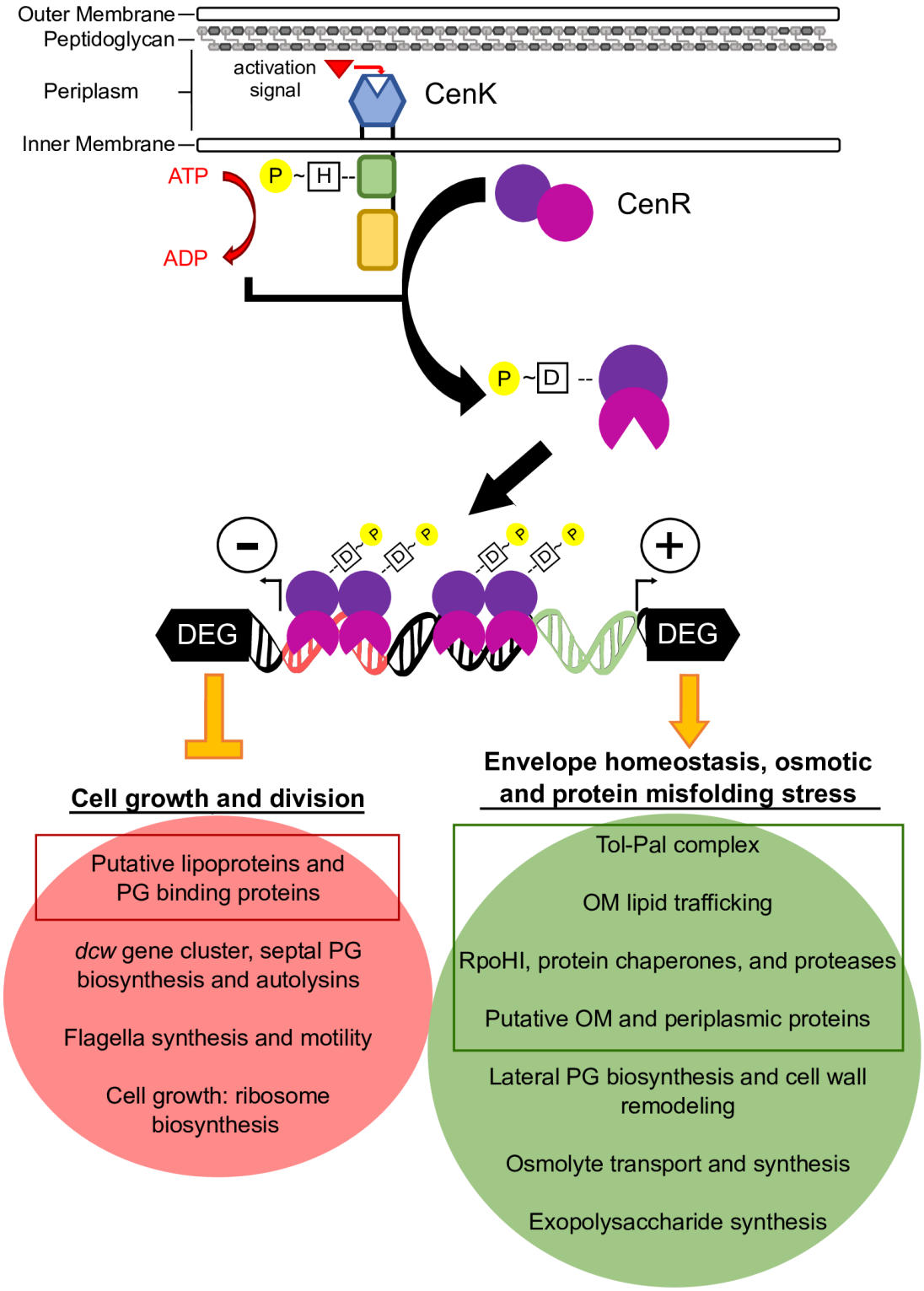
Outer Membrane
Peptidoglycan
Periplasm
Inner Membrane
activation signal
CenK
ATP
ADP
P ~ H --
CenR
P ~ D --
DEG
DEG
Cell growth and division
Putative lipoproteins and PG binding proteins
dcw gene cluster, septal PG biosynthesis and autolysins
Flagella synthesis and motility
Cell growth: ribosome biosynthesis
Envelope homeostasis, osmotic and protein misfolding stress
Tol-Pal complex
OM lipid trafficking
RpoHI, protein chaperones, and proteases
Putative OM and periplasmic proteins
Lateral PG biosynthesis and cell wall remodeling
Osmolyte transport and synthesis
Exopolysaccharide synthesis

[48,49]. *Rb. sphaeroides* contains nine predicted lytic transglycosylases and nine predicted L,D-transpeptidases compared to the eight and six, respectively, that have been identified in *E. coli* [48,49]. Our datasets identify *Rb. sphaeroides* candidates for gene products that may fill some of these roles or occupy other cellular niches including *RSP_1199,* annotated to encode a predicted L,D-transpeptidase (upregulated by CenKR), and *RSP_1880,* encoding a putative PG binding protein that may have autolytic activity since it is downregulated by CenKR. Thus, we predict that analyzing genes that are direct or indirect CenKR targets will shed new light on the process and control of PG biosynthesis across α-proteobacteria.

We also identified CenR as a direct regulator of the Tol subunits of the Tol-Pal complex (Fig 2-10 A), a system that has been implicated in envelope processes such as OM migration during septal constriction [67,68], coordination of PG remodeling/cleavage at the site of cell division [69,70], and polar localization of proteins [71]. It has also been proposed that Tol-Pal is important for maintaining noncovalent OM-PG interactions in Gram-negative bacteria like *Rb. sphaeroides* that lack a homolog of the Braun's lipoprotein [72]. Recently, it has been shown that the function of Braun's lipoprotein in α-proteobacteria is facilitated by other OM ß-barrel proteins that are covalently bound to PG through the activity of L,D-transpeptidases in α-proteobacteria [72]. Given the effects of disruption of Tol-Pal on OM integrity, leakiness, and OM vesicle production in other organisms [73], we propose that Tol-Pal, or Tol-Pal associated proteins, may coordinate one or more of these process in α-proteobacteria. In other bacteria, a reduction or loss of Tol-Pal components also increases cell permeability and OM fluidity due to an increase in OM phospholipid and a reduction or loss of LPS [73,74]. This also appears to be the case in *Rb. sphaeroides* since disruption of *cenK* resulted in increased cellular phospholipids,

lipid secretion, and enhanced sensitivity to detergents (like SDS and polymyxin B) which are normally excluded by LPS [25]. We also found that cells containing a phosphomimetic *cenR* allele, *cenR*(D56E), that is predicted to increase activity of this TCS *in vivo*, resulted in cell filamentation, suggesting that CenKR activity coordinates cell division and/or cytokinesis.

It is known that *tol* operon genes encoding IM subunits of the Tol complex are essential in *Rb. sphaeroides*, *C. crescentus*, and other α-proteobacteria [71,75]. In other bacteria where the Tol system has been well-studied, the IM Tol complex (TolQRA) facilitates Pal localization and PG binding at the septum during cell division, by regulating the interaction between the OM lipoprotein Pal and the periplasmic TolB protein [68,76]. In *E. coli* and related organisms, *tolQRA* and *tolB-pal-cpoB* make up two transcriptional units [77]. However, in *Rb. sphaeroides*, *C. crescentus*, and other α-proteobacteria *tolB* is part of the *tolQRAB* transcriptional unit, and *pal-cpoB* are in a separate transcriptional unit [41,71]. Our analysis indicates that CenR acts directly at *tolQRAB* but, does not directly or indirectly regulate the expression of *pal-cpoB* (Fig 2-10 A). As the function of Pal and TolQRAB are proposed to be essential in several α-proteobacteria [33,61,71,73], we propose that organisms with the same *tol-pal* synteny rely on CenKR to regulate the activity of Tol-Pal by direct control of *tolQRAB* transcription. Such a mechanism would allow for the regulation of essential Tol driven cell division processes while allowing Pal to maintain other functions independent of the subunits of Tol.

The many roles of Tol-Pal complex as well as the essential role of this machine in several α-proteobacteria [71,73,75] likely contributes to CenR essentiality and further supports our hypothesis that CenKR regulates functions necessary for cell division. To our knowledge,

CenKR is the first TCS in Gram-negative bacteria that directly regulates genes encoding Tol complex proteins. Mutations that impact the *E. coli* Rcs are reported to increase expression of the Tol-Pal genes [78], and inactivation of the *C. crescentus* ChvGI altered expression of genes encoding subunits of the Tol-Pal complex [15]. However, it is unclear in these organisms if these TCSs directly or indirectly regulate the expression of these genes.

The CenKR TCS also controls cellular stress responses. We identified CenR as a direct activator of *rpoHI* expression (Fig 2-10 B), one of two *Rb. sphaeroides* σ^{32} alternate sigma factors, that control transcription of gene products that function in protein quality control and turnover, ion transport, and oxidative stress responses (i.e. disulfide bond and peroxide reduction) [52,79]. Previously, it was proposed that CenR negatively regulates *rpoHI* expression [52]. However, we found reduced levels of transcripts of both *rpoHI* and known RpoHI regulon members in cells containing low CenKR activity (Δ*cenK* or *cenR*(D56A)) and increased levels of these transcripts in cells containing increased activity of this TCS (*cenR*(D56E)). Direct activation of *rpoHI* transcription by CenR suggests that CenKR activates expression, in a hierarchical fashion, of a large set of genes that encode proteins functioning to mitigate general, cytoplasmic, or membrane stress responses.

The *E. coli* RseA-σ^E system is another master regulator of both unique genes encoding proteins with cell envelope functions and some genes which also are members of the Cpx or Rcs regulons, thereby functioning broadly to monitor extracytoplasmic homeostasis [11,65]. In *E. coli* it is proposed that accumulation of unfolded or mislocalized OM proteins activates proteases that degrade the anti-σ^E factor RseA, allowing σ^E to promote transcription of envelope stress

response genes [76]. *Rb. sphaeroides* lacks homologs of *E. coli* RseA-σ^E, but it is known that RpoHI is a direct regulator of *cenR* transcription in response to heat shock, oxidative and/or membrane stress signals [52,80]. Thus, we propose the existence of a positive CenR-RpoHI feedback loop that allows a robust, synergistic response to agents that act at the cell envelope. Given the lack of homologs of *E. coli* Cps, Rcs, and RseA-σ^E in *Rb. sphaeroides* and other α-proteobacteria, it is likely that CenKR is a major contributor to a transcriptional response to envelope derived signals.

Other likely indirect effects of changes in CenKR activity include repression of genes involved in chemotaxis, motility, flagellar machinery, and those encoding ribosomal proteins, the latter is consistent with the slow growth rate of strains harboring the hyperactive CenR(D56E) protein (S2 Data). Low CenKR activity in Δ*cenK* or *cenR*(D56A) is also associated with an increase in transcripts from genes encoding proteins that function in polysaccharide production, sarcosine/glycine biosynthesis, and transport of osmolytes which, together, mitigate osmotic stress within the cell [81] and the periplasmic space [82]. Given the role of the OM LPS and the cell wall in resistance to turgor pressure [3] and the altered levels of transcripts from genes whose products are predicted to function in assembly or maintenance of these structures in cells with low CenKR activity, we propose this results in the responsive expression of these osmotic stress response genes. Together, the CenKR TCS is a heretofore unknown regulator of cell envelope changes necessary to combat internal/external turgor pressures.

The presence and role of CenKR is predicted to be conserved across α-proteobacteria. We identified homologs of CenK and CenR within the *Caulobacteridae* sub-class of α-

proteobacteria, including free-living, commensal, and pathogenic organisms. Many of the α-proteobacteria that contain CenKR homologs undergo morphological changes throughout their lifecycle. Purple non-sulfur bacteria like *Rb. sphaeroides* and *Rp. palustris*, under low oxygen conditions, produce intracytoplasmic membranes as cell envelope invaginations that bud inward from the IM and house the machinery for the light reactions of photosynthesis [83,84]. *C. crescentus* and *Rp. palustris*, and other members of the *Rhizobiales* that contain CenKR homologs, have a dimorphic life cycle that requires changes in cell envelope, loss of flagella, and the formation of stalks that differentiate free-living swarmer cells to an anchored sessile form [85,86]. The animal parasite *B. abortus* relies on membrane changes for macrophage internalization and pathogenesis [87], and the plant pathogen *A. tumefaciens*, as well as other members of the *Rhizobiales*, exhibit polar growth and utilize polar budding for division and exhibits a range of morphologies when cell division is altered [88]. These examples showcase some of the cell envelope and cell cycle alterations that are characteristic of α-proteobacteria containing CenKR homologs. We propose that these lifestyles are one reason why these organisms contain cell envelope TCSs and stress response machinery different from those classically studied in *E. coli* and other bacteria. We note that we were unable to identify homologues of CenKR in the *Sphingomonadales* or *Rickettsiales* clades (Fig 2-12), α-proteobacteria that are known to exhibit unusual cell envelope features. *Sphingomonades* contain sphingolipids in the outer leaflet of the OM rather than LPS [89], and members of the *Rickettsiales* include many obligate parasitic bacteria that lack complete cell wall biosynthetic pathways or known membrane-bound enzymes to polymerize PG precursor molecules into the nascent cell wall [90,91]. The existence of CenKR across the *Caulobacteridae* subclass of α-proteobacteria supports a hypothesis that this TCS coordinates a myriad of activities that reside

in the OM, LPS, or PG cell wall. There is no recognizable ligand-binding domain in the N-terminal periplasmic or IM region of the CenK HK, so further experiments are needed to identify the signal(s) that controls CenK kinase activity to determine if CenKR responds to signals derived from these cell envelope components.

In closing, we have shown that CenKR is one of several identified TCSs that regulates cell envelope homeostasis in α-proteobacteria [15,62]. However, the function(s) of these other recently identified cell envelope regulators are not necessarily conserved across α-proteobacteria. For example, NtrYX has been implicated as a regulator of root nodule formations that are involved in nitrogen fixations, carbon/nitrogen metabolism, transport systems [92–94], regulation of anaerobic processes [93,95,96], as well as exopolysaccharide biosynthesis, cell envelope composition, and growth [15,62,93,97]. Similarly, in some α-proteobacteria, ChvIG has been linked to growth [15], pathogenesis [98,99], motility [100], and pH sensitivity [101]. In contrast, the presence of a putative *Rb. sphaeroides* CenR binding motif (TGA-N_8-TGA), upstream of several conserved transcriptional units across α-proteobacteria (including the *tol* operon), suggests a similar role for the CenKR in these species. While further study of the signals that control CenKR kinase and DNA binding activity are required to better understand the role of this TCS, we have shown that CenKR is an essential TCS, defined the regulon controlled by this regulatory system, and we predict that it plays a conserved and central role in envelope, cell division, and other processes that are crucial to viability in *Rb. sphaeroides* and other α-proteobacteria.

Materials and Methods

Bacterial strains and growth conditions. *Rb. sphaeroides* strains (Table 2-3) were grown in Sistrom's (SIS) minimal medium [102]. Unless specified, aerobic cultures of 10 mL were grown in 125 mL flasks with shaking at 200 rpm, at 30°C for ~18 hours until cells reached an OD_{600} of ~0.5. *Escherichia coli* strains were grown at 37°C in Luria-Bertani medium. As needed, media was supplemented with 50 μg/mL kanamycin, 25 ug/mL spectinomycin, or 10 uM isopropyl β-D-1-thiogalactopyranoside (IPTG).

Strain construction. All strains, primers, and plasmids used in this study are listed in Table 2-3 (A,B). In-frame, markerless deletion of *RSP_1056* and allelic exchange within *RSP_0847* was performed via the integration of the suicide vector pk18mobsacB [103]. The genomic regions corresponding to ~1 Kb immediately upstream of the start and downstream of the stop codons of each gene was PCR amplified using Herculase II Fusion DNA Polymerase (Agilent). These PCR products were assembled into PCR linearized pk18mobsacB via Gibson Assembly (New England BioLabs), transformed in DH5α cells (New England BioLabs), and screened by colony PCR of the cloning site and sequenced. Assembled plasmids were mobilized into *Rb. sphaeroides* via conjugal mating with *E. coli* S17-1 [104]. Single crossover transconjugants were selected for by kanamycin resistance followed by sucrose counter-selection to induce double crossovers. Strains with the desired double crossover were identified by isolation of colonies sensitive to kanamycin and resistant to sucrose (Fig 2-4 A). The locus-specific genotype of each strain was confirmed by colony PCR of chromosomal loci and sequenced with specific primers (Table 2-3). Construction of $pIND5_{spec}$-*cenR* was achieved by co-transformation of PCR amplified *cenR* and linearized $pIND5_{spec}$ into *E. coli* DH5α (New England BioLabs). Assembled

plasmids were mobilized into *Rb. sphaeroides* via conjugal mating with *E. coli* S17-1 [104]. Markerless deletion of *RSP_0847* was attempted in the presence of pIND5$_{sepc}$-cenR as described above except in the presence of spectinomycin antibiotic and IPTG through the selections.

***Microscopy*.** All strains were grown as described above to an OD_{600} ~ 0.5. Images were acquired on an EVOS FL microscope with 100X oil immersion plan apochromat objective (numerical aperture, 1.40). To facilitate cell segmentation, all bright-field pictures were treated in FIJI [105] with the same process: bandpass filter (large filter, 40 pixels (pxs); small filter, 2 pxs), background subtraction (rolling ball radius = 20 pxs), and contrast enhancing with normalization (0.1%). Segmentation was performed using the plugin MicrobeJ [106] and cell segmentation errors were removed. Cell shape parameters were extracted, figures and statistical analysis were performed in Rstudio using ggplot2 package [107].

***Protein purification and RSP_0847 (CenR) antibody production*.** The cytosolic domains of the RSP_1056 (CenK) coding sequence (truncated after the second predicted transmembrane helix at residue M195) was PCR amplified and ligated into linearized pVP302K [108] via HiFi Gibson Assembly (New England BioLabs), generating an N-terminal His_8-tagged protein containing a TEV protease cleave site (H_8-TEV-HK_{cyto}). Candidate RR genes (RSP_0847, RSP_1083, RSP_1247) were ligated into the same expression vector containing a C-terminal His_8 tag and TEV cleavage site (RR-TEV-H_8). Candidate TCS expression plasmids were transformed into B834 *E. coli* harboring pRARE2 (Novagen) [109,110]. Cells were grown in 500 mL of ZMS-80155 auto-inducing media supplemented with 10 µg/mL kanamycin and 20 µg/mL chloramphenicol for ~24 hours with shaking at room temperature. Cells were harvested by

centrifugation, resuspended in 10 mL of lysis buffer (20 mM HEPES-KOH [pH 7.5], 0.5 M NaCl, 5 mM imidazole, 1% glycerol, 1 mM TCEP, 0.1% Triton X-100) and 100 µL of HALT Protease Inhibitor (Thermo), lysed by sonication, and centrifuged at 4°C for 30 min at 20,000 x *g* to generate a lysate. The lysate was added to 5 mL washed Ni-NTA agarose slurry (Qiagen) and loaded into a gravity-flow column (BioRad). After passaging the lysate, the column was washed with 2 column volumes of wash buffer (20 mM HEPES-KOH [pH 7.5], 500 mM NaCl, 40 mM imidazole, 1 mM TCEP, 1% glycerol) and protein was eluted with 10 mL elution buffer (20 mM HEPES-KOH [pH 7.5], 300 mM NaCl, 400 mM imidazole, 1 mM TCEP, 1% glycerol). Fractions containing the most protein were combined and concentrated using a YM10 centrifugal filter (Millipore) before being dialyzed using a 10,000 molecular weight cut-off Slide-a-Lyzer dialysis cassette (Thermo Scientific) into storage buffer (20 mM HEPES-KOH [pH 7.5], 300 mM NaCl, 50 mM KCl, 1 mM TCEP, 5% glycerol, 0.1 mM EDTA). Protein was aliquoted and stored at −80 °C. Protein concentration was estimated using the Bradford Assay (Bio-Rad).

To obtain RSP_0847 for antibody production (used in ChIP-seq), after dialysis of RSP_0847-TEV-H_8, the H_8 tag was cleaved by incubation with H_6-TEV protease. The cleaved H_8 tag and H_6-TEV protease were removed with a second round of Ni-NTA chromatography. A 5 mL RSP_0847 protein fraction was subjected to size exclusion chromatography in storage buffer through a GE Healthcare HiLoad 16/600 Superdex 75 pg 120mL XK column (Milipore) at a flow rate on 0.5 mL/min controlled by a GE Healthcare ÄKTA Prime Plus FPLC system. Two mL fractions were collected, and sample purity was analyzed by loading ~250 ng of protein on a 12% SDS-PAGE gel. Fractions enriched for RSP_0847 (MW = 28.2 kDa) were combined and

concentrated, as above, to ~2 mg/mL. Purified RSP_0847 protein was sent to Covance (Denver, PA) to raise a rabbit polyclonal antibody.

***Phosphotransfer assay*.** Purified, truncated RSP_1056 (5 µM) was incubated at 30°C for 30 minutes in storage buffer supplemented with 50mM Tris-HCl pH 7.5, 50 mM KCl, 5 mM $MgCl_2$, 50 µM ATP, 1 µCi [γ^{32}P] ATP (6.16 µCi/µL, [Perkin Elmer]). Purified candidate response regulator proteins were diluted to 5 µM in storage buffer. For each phosphotransfer assays, 5 µL phosphorylated kinase (from the above reaction) and 5 µL response regulator (2.5 µM each protein in storage buffer) were incubated at 30°C. Reactions were stopped with 5 µL 3x NuPAGE LDS (Thermo Fisher) containing 10 mM DTT and stored on ice until samples were loaded, without heating, onto a NuPAGE 4-12% Bis-Tris Protein gel (Invitrogen). Samples were electrophoresed at room temperature for 50 minutes at 150 V. Regions of the gel below the dye front were removed with a razor blade, and the gel was placed between saran wrap and dried for 30 minutes. The dried gel was exposed to a phosphor screen for 3 hours at room temperature before imaging with a Typhoon phosphorimager at 50 µm resolution.

***RNA isolation and sequencing*.** *Rb. sphaeroides* was grown aerobically in 500 mL cultures bubbled with 69% N_2, 30% O_2, and 1% CO_2. 44 mL of cells were harvested when the culture reached an OD_{600} ~0.5 (mid-log), combined with 6 mL of ice-cold stop solution (95% EtOH and 5% acid phenol:chloroform (5:1, pH 4.5)), and centrifuged at 4°C for 10 minutes at 6,000 x *g*. Cell pellets were resuspended in 2 mL of lysis solution (2% sodium dodecyl sulfate, 16mM EDTA, RNase-free water) and heated at 65°C for 5 minutes. Nucleic acids were extracted using 2 mL of acidic phenol:chloroform heated to 65°C, mixed by inversion, incubated at 65°C for 5

minutes, and centrifuged at room temperature for 7 minutes at 20,000 x *g*. The aqueous phase was removed, extracted twice more, before addition of 2 mL of chloroform, mixed, and centrifuged once more at room temperature for 7 minutes at 20,000 x *g*. The aqueous layer was removed and mixed with 1/10 volume of 3M sodium acetate and equal volume of isopropanol, and incubated at -20°C for >1 hour to precipitate nucleic acids that were collected by centrifugation at 4°C for 30 minutes at 16,000 x *g*. The pellet was washed twice with 1 mL of 75% EtOH (prepared with RNase-free water). Once residual ethanol was removed by evaporation, the pellet was resuspended in 85 µL of RNase-free water. Samples were treated with RNase-free DNase (10 µL 10x DNase buffer, 2 µL DNase, 3 µL RNasin (Promega)) and purified using RNeasy kit (Qiagen).

RNA-seq library preparation and sequencing were performed at the Joint Genome Institute. Sequencing libraries were created using the Illumina TruSeq Stranded Total RNA kit (Illumina) and sequenced on an Illumina NextSeq in 2x151 reads using the manufacturers protocol. The resulting paired-end FASTQ files were split into R1 and R2 files, and R1 files were retained for processing through the same pipeline. Reads were trimmed using Trimmomatic version 0.3 [111] with the default settings except for a HEADCROP of 5, LEADING of 3, TRAILING of 3, SLIDINGWINDOW of 3:30, and MINLEN of 36. After trimming, the reads were aligned to the *Rb. sphaeroides* 2.4.1 genome sequence (GenBank accession number GCA_000012905.2) using Bowtie2 version 2.2.2 [112] with default settings except that the number of mismatches was set at 1. Aligned reads were mapped to gene locations using HTSeq version 0.6.0 [113] using default settings except that the “reverse” strandedness argument was used. edgeR version 3.26.8 [114,115] was used to identify significantly differentially expressed genes from pairwise

analyses, using Benjamini and Hochberg [116] false discovery rate (FDR) of less than 0.05 as a significance threshold. Raw sequencing reads were normalized using the reads per kilobase per million mapped reads (RPKM). Pathway enrichment was performed using the SmartTable enrichment function at biocyc.org [117] using a P value of ≤ 0.05 as significant.

Chromatin immunoprecipitation, sequencing, and CenR binding site analysis. *Rb. sphaeroides* strains (Table 2-3) were grown aerobically in 500 mL culture bubbled (69% N_2, 30% O_2, and 1% CO_2). To each 500 mL culture, 5 mL of 1M sodium phosphate mix (0.85 M Na_2HPO_4, 0.15 M NaH_2PO_4) and 13 mL of 37% formaldehyde was added. Crosslinking was allowed to continue with continuous bubbling of the culture for 5 minutes. Each culture was placed into an ice bath and 20 mL of ice cold 2.5 M glycine was added and incubated with bubbling for 30 minutes to quench crosslinking. Cells were pelleted in 50 mL portions by centrifugation at 3500 x *g* for 10 minutes at 4°C, washed twice with 100 mL of phosphate buffered saline (PBS), resuspended in 1 mL of PBS, and flash frozen. DNA was isolated in tandem and pooled from technical replicates to improve DNA yields. For DNA isolation, cell pellets were resuspended in 500 µL RIPA buffer (Sigma) supplemented with 50 µL HALT Protease Inhibitor (Thermo). Cells were lysed at 4°C by water bath sonication for 30 cycles at 25% pulsed 25 seconds on and 35 seconds off. To each lysate, 2 µL of micrococcal nuclease (Pierce), 10 µL $CaCl_2$ mix (15 mM Tris-HCl pH 8, 1 mM $CaCl_2$, 60 mM KCl, 15 mM NaCl, 300 mM sucrose, 0.5 mM DTT), and 10 µL RNase A (0.1 mg/mL final (Fisher)) was added and the mixture was incubated at 4°C for 1 hour. Each nuclease reaction was stopped with 15 mM EDTA and lysate was centrifuged at 16,000 x *g* at 4°C to remove cell debris. DNA fragmentation (major band between 200-400bp) was check by gel electrophoresis on a 1.5% agarose gel. For immunoprecipitation, 1/10 of the volume was

taken from each lysate and mixed with an equal volume Protein A sepharose beads (Sigma) to be used as input and negative control. After preclearing the remaining lysate volume with 50 µL Sepharose beads, 5 µL of polyclonal anti-RSP_0847 antibody was added to each sample and incubated at 4°C overnight. Sepharose beads (60 µL) were added to each lysate, the volume was adjusted to ~750 µL with RIPA buffer, and samples were centrifuged for 2 minutes at 1,000 x *g* at 4°C to pellet antibody-protein-DNA complexes bound to the beads. The pelleted beads were washed twice with 1 mL LiCl Wash Solution (100 mM Tris-HCl pH 8, 250 mM LiCl, 2% TritionX-100), twice with 1 mL 600 mM NaCl Wash Buffer (100 mM Tris-HCl pH 8, 600 mM NaCl, 2% TritionX-100), twice with 1 mL 300 mM NaCl Wash Buffer (100 mM Tris-HCl pH 8, 300 mM NaCl, 2% TritionX-100) and twice with TE Buffer (10 mM Tris-HCl pH8, 1 mM EDTA). 150 µL Elution Buffer (50 mM Tris-HCl pH 8, 10 mM EDTA, 1% SDS) was added to the pelleted Sepharose beads and incubated for 1 hour at 65°C. The mixture was centrifuged (1,000 x *g* at 4°C) and the supernatant was removed and incubated overnight at 65°C to reverse-crosslinking. DNA was purified using QIAquick PCR Purification Kit (Qiagen), eluted into a volume of 50 µL and quantified using Qubit Fluorometer 1x dsDNA HS kit (Invitrogen, CA) for sequencing.

ChIP-seq library preparation (starting with at least 20 ng DNA per sample) and sequencing was performed by GeneWiz (South Plainfield, NJ) using an Illumina ChIP-seq Library kit for sequencing with Illumina HiSeq 2x150 bp configuration, single index. The paired-end FASTQ files were trimmed with Trimmomatic version 0.3 [111] with default settings except for LEADING:3, TRAILING:3, SLIDINGWINDOW:3:30, and MINLEN:36. The trimmed paired-end reads were aligned to the *Rb. sphaeroides* genome sequence (GenBank accession Chr1:

NC_007493.2, Chr2: NC_007494.2) using Bowtie2 version 2.2.2 [112] with default settings except the number of mismatches was set to 1. Picard-tools version 1.98 [118] and Samtools version 1.2 [119] were used to clean, sort, and index the alignment file using default settings. Areas of enrichment of immunoprecipitated over INPUT (peaks) were identified using MOSAiCS version 2.28 using two factor analysis and an analysis type of "IO" [120]. Conversion of BAM to ELAND format for MOSAiCS was performed using Pyicos version 2.0.6 [121] and default settings. WIG files were generated for each sample using QuEST version 2.4 [122] and default settings. WIG files were visualized on MochiView version 1.46 [123].

To identify a potential consensus CenR binding site, sequences 200bp upstream of the translational start site of candidate transcriptional units (Table 2-2) were selected and MEME [42,43] was used to search for an enriched motif present in these 59 sequences using the following parameters: -objfun classic -dna -mod zoops -minw 10 -maxw 20 -allw -revcomp. The PWM (Table 2-5B) generated from this alignment was used to produce the candidate CenR motif (Fig 2-8 A, E-value 2.6e-10). MEME identified this motif in 31 sequences with a p-value < 0.001 for each individual sequence. Orientation and proximity of each candidate sequence to mapped TSS [41] and predicted promoter elements [124] was assessed within the *Rb. sphaeroides* 2.4.1 genome.

***Data availability*.** All raw and processed ChIP-seq and RNA-seq data are available at NCBI GEO: https://www.ncbi.nlm.nih.gov/geo/query/acc.cgi?acc=GSE186600. (S1 Data and S2 Data omitted for brevity, see published manuscript S1 and S2 Data)

***Electromobility Shift Assays*.** DNA fragments (250-300bp) were PCR amplified from genomic DNA and purified via gel excision (Qiagen). H_8-TEV-CenR was purified as described above and the H_8 tag was cleaved with H_6-TEV protease and removed via gravity flow nickel agarose column. 20 µM CenR was phosphorylated in storage buffer supplemented with 25 mM acetyl-phosphate and 20 mM $MgCl_2$ and incubated at 37°C for 1.5hrs. EMSA reactions (10 µL total) consisted of a final concentration of 25 mM Tris-HCl pH 7.9, 5 mM EDTA, 10% glycerol, 40 mM potassium glutamate, 20 µg/mL BSA, 1 mM DTT, 200 mM NaCl, and 15 nM DNA substrate. Appropriate dilutions of phosphorylated CenR were made in storage buffer and 1 µL was added to each reaction for a final monomer protein concentration indicated in the figure. Reactions were incubated at 30°C for 30 min, stopped by addition of 5x loading dye (Invitrogen), and loaded onto a 6% nondenaturing polyacrylamide TBE gel, and electrophoresed in 0.5x TBE with 10% glycerol for 2 hours at 100V. Following electrophoresis, the gel was stained with SYBR green (Invitrogen) 1:10,000 in 1x TBE for 30 min in the dark and imaged on a Visi-Blue transilluminator.

***Phylogenetic analysis and identification of CenR binding sites in other Alphaproteobacteria*.** Amino acid sequences of RSP_1056 (CenK) and RSP_0847 (CenR) were used from the *Rb. sphaeroides* 2.4.1 genome (Genbank accession numbers ABA80240.1 and ABA80028.1, respectively) and homologs in other α-proteobacteria were identified via BLASTP of non-redundant sequences in Genbank (E-value >1e-70 with a percent identity match >30%) [125,126]. Gene sequences were then aligned in MEGA version 6.06 [127] using MUSCLE [128] and trimmed using Gblocks [129]. Phylogenetic trees were constructed using the Maximum-Likelihood (ML) methods of analysis. The ML analyses for all genes were performed

using FastTree 2 [130] with the parameters: –wag, –gamma, –pseudo. Bootstrap values (bs) are reported for the ML trees. Trees were rooted with the *Rhodospirillales* clade to match established α-proteobacteria relationships [57–60]. Trees were colored by order: Grey – *Rhodospirillales*/*Kiloniellales*; Purple – *Sneathiellales*; Red – *Rhodobacterales*; Orange – *Caulobacterales*/*Parvularculales*; Cyan – *Hyphomicobiales*; Blue – *Rhizobiales*.

To investigate possible CenR regulation in other α-proteobacteria, we identified potential homologs of *R. sphaeroides* CenR regulated genes in four well studied organisms: *C. crescentus* (NA1000, RefSeq accession number GCF_000022005.1), *B. abortus* (2308, RefSeq accession number GCF_000054005.1), *A. tumefaciens* (BIM B-1315G, RefSeq accession number GCF_014489975.1), and *Rp. palustris* (RCB100, RefSeq accession number GCA_000195775.1). Homologs were identified using BLASTn (version 2.9.0, default settings) [125,126]. For each identified homolog from each organism, 300 bp upstream of the translation start site was selected and searched for a match to the *Rb. sphaeroides* CenR PWM using PatSer (version 3f, default settings) [131]. For each sequence, the single site with the highest PatSer score was retained. Logos were constructed from the PatSer identified CenR sites using WebLogo [132].

Acknowledgments.

We thank Kemardo K. Henry and the Gourse Lab (University of Wisconsin – Madison) for help setting up the phosphotransfer assays. Specific thank you to Sarah E. Moskal (UW – Madison), Rachelle A. Lemke (UW – Madison), Wayne S. Kontur (UW – Madison), Kimberly C. Lemmer (UW – Madison), and Katherine J. Wozniak (University of Michigan), as well as other members of the Donohue/Noguera group for helpful discussion and feedback.

This work was supported by the Great Lakes Bioenergy Research Center (https://www.glbrc.org), U.S. Department of Energy, Office of Science, Office of Biological and Environmental Research (https://www.energy.gov/science/ber/biological-and-environmental-research) (award DE-SC0018409 to T.J.D.), and by the National Institutes of General Medical Sciences to (Grant R01 GM115894 to from P.J.K.) RNA sequencing was conducted by the U.S. Department of Energy Joint Genome Institute, a DOE Office of Science User Facility, which is supported by the Office of Science of the U.S. Department of Energy under contract DE-AC02-05CH11231 (https://jgi.doe.gov/). Additional funding provided by the National Science Foundation Graduate Research Fellowship Program (Grant No. DGE-1747503 to B.D.L. (https://www.nsfgrfp.org)), National Institute of Health Genetics Predoctoral Training Program award (T32 GM007133 to B.D.L.), and the Foster Wisconsin Idea Fellowship, UW-Madison, Department of Bacteriology (to B.D.L.). The funders had no role in study design, data collection and analysis, decision to publish, or preparation of the manuscript.

References

1. Silhavy TJ, Kahne D, Walker S. The Bacterial Cell Envelope. Cold Spring Harb Perspect Biol. 2010;2: a000414. doi:10.1101/cshperspect.a000414
2. Whitfield C, Trent MS. Biosynthesis and Export of Bacterial Lipopolysaccharides. Annual Review of Biochemistry. 2014;83: 99–128. doi:10.1146/annurev-biochem-060713-035600
3. Rojas ER, Billings G, Odermatt PD, Auer GK, Zhu L, Miguel A, et al. The outer membrane is an essential load-bearing element in Gram-negative bacteria. Nature. 2018;559: 617–621. doi:10.1038/s41586-018-0344-3
4. Vollmer W, Seligman SJ. Architecture of peptidoglycan: more data and more models. Trends in Microbiology. 2010;18: 59–66. doi:10.1016/j.tim.2009.12.004
5. Egan AJF, Errington J, Vollmer W. Regulation of peptidoglycan synthesis and remodelling. Nat Rev Microbiol. 2020;18: 446–460. doi:10.1038/s41579-020-0366-3
6. Stock AM, Robinson VL, Goudreau PN. Two-Component Signal Transduction. Annual Review of Biochemistry. 2000;69: 183–215. doi:10.1146/annurev.biochem.69.1.183
7. Jacob-Dubuisson F, Mechaly A, Betton J-M, Antoine R. Structural insights into the signalling mechanisms of two-component systems. Nat Rev Microbiol. 2018;16: 585–593. doi:10.1038/s41579-018-0055-7
8. Zschiedrich CP, Keidel V, Szurmant H. Molecular Mechanisms of Two-Component Signal Transduction. Journal of Molecular Biology. 2016;428: 3752–3775. doi:10.1016/j.jmb.2016.08.003
9. Gao R, Stock AM. Biological Insights from Structures of Two-Component Proteins. Annual Review of Microbiology. 2009;63: 133–154. doi:10.1146/annurev.micro.091208.073214
10. Raivio TL, Silhavy TJ. Transduction of envelope stress in Escherichia coli by the Cpx two-component system. Journal of Bacteriology. 1997;179: 7724–7733. doi:10.1128/jb.179.24.7724-7733.1997
11. Grabowicz M, Silhavy TJ. Envelope Stress Responses: An Interconnected Safety Net. Trends in Biochemical Sciences. 2017;42: 232–242. doi:10.1016/j.tibs.2016.10.002
12. May KL, Lehman KM, Mitchell AM, Grabowicz M. A Stress Response Monitoring Lipoprotein Trafficking to the Outer Membrane. mBio. 2019;10: e00618-19. doi:10.1128/mBio.00618-19
13. Wall E, Majdalani N, Gottesman S. The Complex Rcs Regulatory Cascade. Annual Review of Microbiology. 2018;72: 111–139. doi:10.1146/annurev-micro-090817-062640
14. Raffa RG, Raivio TL. A third envelope stress signal transduction pathway in Escherichia coli. Molecular Microbiology. 2002;45: 1599–1611. doi:10.1046/j.1365-2958.2002.03112.x

15. Stein BJ, Fiebig A, Crosson S. The ChvG-ChvI and NtrY-NtrX Two-Component Systems Coordinately Regulate Growth of Caulobacter crescentus. Journal of Bacteriology. 2021;203: e00199-21. doi:10.1128/JB.00199-21

16. Price NL, Raivio TL. Characterization of the Cpx regulon in Escherichia coli strain MC4100. J Bacteriol. 2009;191: 1798–1815. doi:10.1128/JB.00798-08

17. Guest RL, Rutherford ST, Silhavy TJ. Border Control: Regulating LPS Biogenesis. Trends in Microbiology. 2021;29: 334–345. doi:10.1016/j.tim.2020.09.008

18. García-Calderón CB, Casadesús J, Ramos-Morales F. Rcs and PhoPQ regulatory overlap in the control of Salmonella enterica virulence. J Bacteriol. 2007;189: 6635–6644. doi:10.1128/JB.00640-07

19. Callewaert L, Vanoirbeek KGA, Lurquin I, Michiels CW, Aertsen A. The Rcs Two-Component System Regulates Expression of Lysozyme Inhibitors and Is Induced by Exposure to Lysozyme. Journal of Bacteriology. 2009;191: 1979–1981. doi:10.1128/JB.01549-08

20. Bernal-Cabas M, Ayala JA, Raivio TL. The Cpx Envelope Stress Response Modifies Peptidoglycan Cross-Linking via the l,d-Transpeptidase LdtD and the Novel Protein YgaU. Journal of Bacteriology. 2015;197: 603–614. doi:10.1128/JB.02449-14

21. Laubacher ME, Ades SE. The Rcs Phosphorelay Is a Cell Envelope Stress Response Activated by Peptidoglycan Stress and Contributes to Intrinsic Antibiotic Resistance. Journal of Bacteriology. 2008;190: 2065–2074. doi:10.1128/JB.01740-07

22. Dörr T, Alvarez L, Delgado F, Davis BM, Cava F, Waldor MK. A cell wall damage response mediated by a sensor kinase/response regulator pair enables beta-lactam tolerance. Proc Natl Acad Sci U S A. 2016;113: 404–409. doi:10.1073/pnas.1520333113

23. Gorla P, Plocinska R, Sarva K, Satsangi AT, Pandeeti E, Donnelly R, et al. MtrA Response Regulator Controls Cell Division and Cell Wall Metabolism and Affects Susceptibility of Mycobacteria to the First Line Antituberculosis Drugs. Front Microbiol. 2018;9: 2839. doi:10.3389/fmicb.2018.02839

24. Zahrt TC, Deretic V. An Essential Two-Component Signal Transduction System in Mycobacterium tuberculosis. Journal of Bacteriology. 2000;182: 3832–3838. doi:10.1128/JB.182.13.3832-3838.2000

25. Lemmer KC, Zhang W, Langer SJ, Dohnalkova AC, Hu D, Lemke RA, et al. Mutations That Alter the Bacterial Cell Envelope Increase Lipid Production. mBio. 8: e00513-17. doi:10.1128/mBio.00513-17

26. Skerker JM, Prasol MS, Perchuk BS, Biondi EG, Laub MT. Two-Component Signal Transduction Pathways Regulating Growth and Cell Cycle Progression in a Bacterium: A System-Level Analysis. PLOS Biology. 2005;3: e334. doi:10.1371/journal.pbio.0030334

27. Burger L, Erik van N. Accurate prediction of protein–protein interactions from sequence alignments using a Bayesian method. Molecular Systems Biology. 2008;4: 165. doi:10.1038/msb4100203

28. Shoemaker BA, Panchenko AR. Deciphering Protein–Protein Interactions. Part II. Computational Methods to Predict Protein and Domain Interaction Partners. PLOS Computational Biology. 2007;3: e43. doi:10.1371/journal.pcbi.0030043

29. Capra EJ, Laub MT. Evolution of Two-Component Signal Transduction Systems. Annual Review of Microbiology. 2012;66: 325–347. doi:10.1146/annurev-micro-092611-150039

30. Igo MM, Ninfa AJ, Stock JB, Silhavy TJ. Phosphorylation and dephosphorylation of a bacterial transcriptional activator by a transmembrane receptor. Genes Dev. 1989;3: 1725–1734. doi:10.1101/gad.3.11.1725

31. Fisher SL, Kim S-K, Wanner BL, Walsh CT. Kinetic Comparison of the Specificity of the Vancomycin Resistance Kinase VanS for Two Response Regulators, VanR and PhoB. Biochemistry. 1996;35: 4732–4740. doi:10.1021/bi9525435

32. Comolli JC, Carl AJ, Hall C, Donohue T. Transcriptional Activation of the Rhodobacter sphaeroides Cytochrome c2 Gene P2 Promoter by the Response Regulator PrrA. J Bacteriol. 2002;184: 390–399. doi:10.1128/JB.184.2.390-399.2002

33. Burger BT, Imam S, Scarborough MJ, Noguera DR, Donohue TJ. Combining Genome-Scale Experimental and Computational Methods To Identify Essential Genes in Rhodobacter sphaeroides. mSystems. 2: e00015-17. doi:10.1128/mSystems.00015-17

34. Yang J, Yan R, Roy A, Xu D, Poisson J, Zhang Y. The I-TASSER Suite: protein structure and function prediction. Nat Methods. 2015;12: 7–8. doi:10.1038/nmeth.3213

35. Roy A, Kucukural A, Zhang Y. I-TASSER: a unified platform for automated protein structure and function prediction. Nat Protoc. 2010;5: 725–738. doi:10.1038/nprot.2010.5

36. Zhang Y. I-TASSER server for protein 3D structure prediction. BMC Bioinformatics. 2008;9: 40. doi:10.1186/1471-2105-9-40

37. Zhao Z, Peng T, Oh J-I, Glaeser J, Weber L, Li Q, et al. A response regulator of the OmpR family is part of the regulatory network controlling the oxidative stress response of Rhodobacter sphaeroides. Environmental Microbiology Reports. 2019;11: 118–128. doi:10.1111/1758-2229.12718

38. Smith JG, Latiolais JA, Guanga GP, Pennington JD, Silversmith RE, Bourret RB. A search for amino acid substitutions that universally activate response regulators. Molecular Microbiology. 2004;51: 887–901. doi:10.1046/j.1365-2958.2003.03882.x

39. Klose KE, Weiss DS, Kustu S. Glutamate at the Site of Phosphorylation of Nitrogen-regulatory Protein NTRC Mimics Aspartyl-Phosphate and Activates the Protein. Journal of Molecular Biology. 1993;232: 67–78. doi:10.1006/jmbi.1993.1370

40. Kuan PF, Chung D, Pan G, Thomson JA, Stewart R, Keleş S. A Statistical Framework for the Analysis of ChIP-Seq Data. J Am Stat Assoc. 2011;106: 891–903. doi:10.1198/jasa.2011.ap09706

41. Myers KS, Vera JM, Lemmer KC, Linz AM, Landick R, Noguera DR, et al. Genome-Wide Identification of Transcription Start Sites in Two Alphaproteobacteria, Rhodobacter sphaeroides 2.4.1 and Novosphingobium aromaticivorans DSM 12444. Microbiology Resource Announcements. 9: e00880-20. doi:10.1128/MRA.00880-20

42. Bailey TL, Boden M, Buske FA, Frith M, Grant CE, Clementi L, et al. MEME Suite: tools for motif discovery and searching. Nucleic Acids Research. 2009;37: W202–W208. doi:10.1093/nar/gkp335

43. Bailey TL, Williams N, Misleh C, Li WW. MEME: discovering and analyzing DNA and protein sequence motifs. Nucleic Acids Research. 2006;34: W369–W373. doi:10.1093/nar/gkl198

44. Wang JC. Helical repeat of DNA in solution. Proc Natl Acad Sci U S A. 1979;76: 200–203.

45. Jeon Y, Lee YS, Han JS, Kim JB, Hwang DS. Multimerization of Phosphorylated and Non-phosphorylated ArcA Is Necessary for the Response Regulator Function of the Arc Two-component Signal Transduction System. Journal of Biological Chemistry. 2001;276: 40873–40879. doi:10.1074/jbc.M104855200

46. Park DM, Akhtar MS, Ansari AZ, Landick R, Kiley PJ. The Bacterial Response Regulator ArcA Uses a Diverse Binding Site Architecture to Regulate Carbon Oxidation Globally. PLOS Genetics. 2013;9: e1003839. doi:10.1371/journal.pgen.1003839

47. Jacoby GA. AmpC beta-lactamases. Clin Microbiol Rev. 2009;22: 161–182, Table of Contents. doi:10.1128/CMR.00036-08

48. Mueller EA, Levin PA. Bacterial Cell Wall Quality Control during Environmental Stress. mBio. 11: e02456-20. doi:10.1128/mBio.02456-20

49. Aliashkevich A, Cava F. LD-transpeptidases: the great unknown among the peptidoglycan cross-linkers. The FEBS Journal. n/a. doi:10.1111/febs.16066

50. Malinverni JC, Silhavy TJ. An ABC transport system that maintains lipid asymmetry in the Gram-negative outer membrane. Proceedings of the National Academy of Sciences. 2009;106: 8009–8014. doi:10.1073/pnas.0903229106

51. Sklar JG, Wu T, Kahne D, Silhavy TJ. Defining the roles of the periplasmic chaperones SurA, Skp, and DegP in Escherichia coli. Genes Dev. 2007;21: 2473–2484. doi:10.1101/gad.1581007

52. Dufour YS, Imam S, Koo B-M, Green HA, Donohue TJ. Convergence of the Transcriptional Responses to Heat Shock and Singlet Oxygen Stresses. PLOS Genetics. 2012;8: e1002929. doi:10.1371/journal.pgen.1002929

53. Depuydt M, Leonard SE, Vertommen D, Denoncin K, Morsomme P, Wahni K, et al. A Periplasmic Reducing System Protects Single Cysteine Residues from Oxidation. Science. 2009;326: 1109–1111. doi:10.1126/science.1179557

54. Grimaud R, Ezraty B, Mitchell JK, Lafitte D, Briand C, Derrick PJ, et al. Repair of Oxidized Proteins: IDENTIFICATION OF A NEW METHIONINE SULFOXIDE REDUCTASE *. Journal of Biological Chemistry. 2001;276: 48915–48920. doi:10.1074/jbc.M105509200

55. Typas A, Banzhaf M, Gross CA, Vollmer W. From the regulation of peptidoglycan synthesis to bacterial growth and morphology. Nat Rev Microbiol. 2012;10: 123–136. doi:10.1038/nrmicro2677

56. Hara H, Yasuda S, Horiuchi K, Park JT. A promoter for the first nine genes of the Escherichia coli mra cluster of cell division and cell envelope biosynthesis genes, including ftsI and ftsW. Journal of Bacteriology. 1997;179: 5802–5811. doi:10.1128/jb.179.18.5802-5811.1997

57. Williams KP, Sobral BW, Dickerman AW. A Robust Species Tree for the Alphaproteobacteria. Journal of Bacteriology. 2007;189: 4578–4586. doi:10.1128/JB.00269-07

58. Hördt A, López MG, Meier-Kolthoff JP, Schleuning M, Weinhold L-M, Tindall BJ, et al. Analysis of 1,000+ Type-Strain Genomes Substantially Improves Taxonomic Classification of Alphaproteobacteria. Frontiers in Microbiology. 2020;11: 468. doi:10.3389/fmicb.2020.00468

59. Ferla MP, Thrash JC, Giovannoni SJ, Patrick WM. New rRNA Gene-Based Phylogenies of the Alphaproteobacteria Provide Perspective on Major Groups, Mitochondrial Ancestry and Phylogenetic Instability. PLOS ONE. 2013;8: e83383. doi:10.1371/journal.pone.0083383

60. Muñoz-Gómez SA, Hess S, Burger G, Lang BF, Susko E, Slamovits CH, et al. An updated phylogeny of the Alphaproteobacteria reveals that the parasitic Rickettsiales and Holosporales have independent origins. Rokas A, Wittkopp PJ, Irisarri I, editors. eLife. 2019;8: e42535. doi:10.7554/eLife.42535

61. Pechter KB, Gallagher L, Pyles H, Manoil CS, Harwood CS. Essential Genome of the Metabolically Versatile Alphaproteobacterium Rhodopseudomonas palustris. J Bacteriol. 2015;198: 867–876. doi:10.1128/JB.00771-15

62. Lemmer KC, Alberge F, Myers KS, Dohnalkova AC, Schaub RE, Lenz JD, et al. The NtrYX Two-Component System Regulates the Bacterial Cell Envelope. Harwood CS, editor. mBio. 2020;11. doi:10.1128/mBio.00957-20

63. Senadheera M. Dilani, Guggenheim Bernard, Spatafora Grace A., Huang Yi-Chen Cathy, Choi Jison, Hung David C. I., et al. A VicRK Signal Transduction System in Streptococcus mutans Affects gtfBCD, gbpB, and ftf Expression, Biofilm Formation, and Genetic Competence Development. Journal of Bacteriology. 2005;187: 4064–4076. doi:10.1128/JB.187.12.4064-4076.2005

64. Bisicchia P, Noone D, Lioliou E, Howell A, Quigley S, Jensen T, et al. The essential YycFG two-component system controls cell wall metabolism in Bacillus subtilis. Mol Microbiol. 2007;65: 180–200. doi:10.1111/j.1365-2958.2007.05782.x

65. Saha S, Lach SR, Konovalova A. Homeostasis of the Gram-negative cell envelope. Current Opinion in Microbiology. 2021;61: 99–106. doi:10.1016/j.mib.2021.03.008

66. Typas A, Banzhaf M, van den Berg van Saparoea B, Verheul J, Biboy J, Nichols RJ, et al. Regulation of peptidoglycan synthesis by outer membrane proteins. Cell. 2010;143: 1097–1109. doi:10.1016/j.cell.2010.11.038

67. Gerding MA, Ogata Y, Pecora ND, Niki H, De Boer PAJ. The trans-envelope Tol–Pal complex is part of the cell division machinery and required for proper outer-membrane invagination during cell constriction in E. coli. Molecular Microbiology. 2007;63: 1008–1025. doi:10.1111/j.1365-2958.2006.05571.x

68. Szczepaniak J, Holmes P, Rajasekar K, Kaminska R, Samsudin F, Inns PG, et al. The lipoprotein Pal stabilises the bacterial outer membrane during constriction by a mobilisation-and-capture mechanism. Nat Commun. 2020;11: 1305. doi:10.1038/s41467-020-15083-5

69. Yakhnina AA, Bernhardt TG. The Tol-Pal system is required for peptidoglycan-cleaving enzymes to complete bacterial cell division. Proc Natl Acad Sci USA. 2020;117: 6777–6783. doi:10.1073/pnas.1919267117

70. Gray AN, Egan AJ, van't Veer IL, Verheul J, Colavin A, Koumoutsi A, et al. Coordination of peptidoglycan synthesis and outer membrane constriction during Escherichia coli cell division. Storz G, editor. eLife. 2015;4: e07118. doi:10.7554/eLife.07118

71. Yeh Y-C, Comolli LR, Downing KH, Shapiro L, McAdams HH. The Caulobacter Tol-Pal Complex Is Essential for Outer Membrane Integrity and the Positioning of a Polar Localization Factor. Journal of Bacteriology. 2010;192: 4847–4858. doi:10.1128/JB.00607-10

72. Godessart P, Lannoy A, Dieu M, Van der Verren SE, Soumillion P, Collet J-F, et al. β-Barrels covalently link peptidoglycan and the outer membrane in the α-proteobacterium Brucella abortus. Nat Microbiol. 2021;6: 27–33. doi:10.1038/s41564-020-00799-3

73. Szczepaniak J, Press C, Kleanthous C. The multifarious roles of Tol-Pal in Gram-negative bacteria. FEMS Microbiol Rev. 2020;44: 490–506. doi:10.1093/femsre/fuaa018

74. Shrivastava R, Jiang X, Chng S-S. Outer membrane lipid homeostasis via retrograde phospholipid transport in Escherichia coli. Mol Microbiol. 2017;106: 395–408. doi:10.1111/mmi.13772

75. Krol E, Yau HCL, Lechner M, Schäper S, Bange G, Vollmer W, et al. Tol-Pal System and Rgs Proteins Interact to Promote Unipolar Growth and Cell Division in Sinorhizobium meliloti. mBio. 11: e00306-20. doi:10.1128/mBio.00306-20

76. Konovalova A, Grabowicz M, Balibar CJ, Malinverni JC, Painter RE, Riley D, et al. Inhibitor of intramembrane protease RseP blocks the σ^E response causing lethal accumulation of unfolded outer membrane proteins. Proc Natl Acad Sci USA. 2018;115: E6614. doi:10.1073/pnas.1806107115

77. Vianney A, Muller MM, Clavel T, Lazzaroni JC, Portalier R, Webster RE. Characterization of the tol-pal region of Escherichia coli K-12: translational control of tolR expression by TolQ and identification of a new open reading frame downstream of pal encoding a periplasmic protein. Journal of Bacteriology. 1996;178: 4031–4038. doi:10.1128/jb.178.14.4031-4038.1996

78. Clavel T, Lazzaroni JC, Vianney A, Portalier R. Expression of the tolQRA genes of Escherichia coli K-12 is controlled by the RcsC sensor protein involved in capsule synthesis. Mol Microbiol. 1996;19: 19–25. doi:10.1046/j.1365-2958.1996.343880.x

79. Green HA, Donohue TJ. Activity of Rhodobacter sphaeroides RpoHII, a Second Member of the Heat Shock Sigma Factor Family. J Bacteriol. 2006;188: 5712–5721. doi:10.1128/JB.00405-06

80. Nuss AM, Adnan F, Weber L, Berghoff BA, Glaeser J, Klug G. DegS and RseP Homologous Proteases Are Involved in Singlet Oxygen Dependent Activation of RpoE in Rhodobacter sphaeroides. PLOS ONE. 2013;8: e79520. doi:10.1371/journal.pone.0079520

81. Csonka LN. Physiological and genetic responses of bacteria to osmotic stress. Microbiol Rev. 1989;53(1):121-47. doi: 10.1128/mr.53.1.121-147.1989.

82. Daitch AK, Orsburn BC, Chen Z, Alvarez L, Eberhard CD, Sundararajan K, et al. EstG is a novel esterase required for cell envelope integrity. Microbiology; 2022 Apr. doi:10.1101/2022.04.12.488081

83. Kiley PJ, Kaplan S. Molecular genetics of photosynthetic membrane biosynthesis in Rhodobacter sphaeroides. 1988;52: 20. doi: 10.1128/mr.52.1.50-69.1988.

84. LaSarre B, Kysela DT, Stein BD, Ducret A, Brun YV, McKinlay JB. Restricted Localization of Photosynthetic Intracytoplasmic Membranes (ICMs) in Multiple Genera of Purple Nonsulfur Bacteria. mBio. 9: e00780-18. doi:10.1128/mBio.00780-18

85. Ryan KR, Shapiro L. Temporal and Spatial Regulation in Prokaryotic Cell Cycle Progression and Development. Annu Rev Biochem. 2003;72: 367–394. doi:10.1146/annurev.biochem.72.121801.161824

86. Brown PJB, de Pedro MA, Kysela DT, Van der Henst C, Kim J, De Bolle X, et al. Polar growth in the Alphaproteobacterial order Rhizobiales. Proc Natl Acad Sci U S A. 2012;109: 1697–1701. doi:10.1073/pnas.1114476109

87. Watarai M, Makino S, Fujii Y, Okamoto K, Shirahata T. Modulation of Brucella-induced macropinocytosis by lipid rafts mediates intracellular replication. Cellular Microbiology. 2002;4: 341–355. doi:10.1046/j.1462-5822.2002.00195.x

88. Howell M, Aliashkevich A, Sundararajan K, Daniel JJ, Lariviere PJ, Goley ED, et al. Agrobacterium tumefaciens divisome proteins regulate the transition from polar growth to cell division. Molecular Microbiology. 2019;111: 1074–1092. doi:10.1111/mmi.14212

89. Sohlenkamp C, Geiger O. Bacterial membrane lipids: diversity in structures and pathways. FEMS Microbiology Reviews. 2016;40: 133–159. doi:10.1093/femsre/fuv008

90. Otten C, Brilli M, Vollmer W, Viollier PH, Salje J. Peptidoglycan in obligate intracellular bacteria. Mol Microbiol. 2018;107: 142–163. doi:10.1111/mmi.13880

91. Atwal S, Chuenklin S, Bonder EM, Flores J, Gillespie JJ, Driscoll TP, et al. Discovery of a Diverse Set of Bacteria That Build Their Cell Walls without the Canonical Peptidoglycan Polymerase aPBP. mBio. 2021;12: e0134221. doi:10.1128/mBio.01342-21

92. Pawlowski K, Klosse U, de Bruijn FJ. Characterization of a novel Azorhizobium caulinodans ORS571 two-component regulatory system, NtrY/NtrX, involved in nitrogen fixation and metabolism. Molec Gen Genet. 1991;231: 124–138. doi:10.1007/BF00293830

93. Calatrava-Morales N, Nogales J, Ameztoy K, van Steenbergen B, Soto MJ. The NtrY/NtrX System of Sinorhizobium meliloti GR4 Regulates Motility, EPS I Production, and Nitrogen Metabolism but Is Dispensable for Symbiotic Nitrogen Fixation. MPMI. 2017;30: 566–577. doi:10.1094/MPMI-01-17-0021-R

94. López MF, Hegel VA, Torres MJ, García AH, Delgado MJ, López-García SL. The Bradyrhizobium diazoefficiens two-component system NtrYX has a key role in symbiotic nitrogen fixation of soybean plants and cbb3 oxidase expression in bacteroids. Plant Soil. 2019;440: 167–183. doi:10.1007/s11104-019-04067-0

95. Atack JM, Srikhanta YN, Djoko KY, Welch JP, Hasri NHM, Steichen CT, et al. Characterization of an ntrX Mutant of Neisseria gonorrhoeae Reveals a Response Regulator That Controls Expression of Respiratory Enzymes in Oxidase-Positive Proteobacteria. Journal of Bacteriology. 2013;195: 2632–2641. doi:10.1128/JB.02062-12

96. Carrica M del C, Fernandez I, Martí MA, Paris G, Goldbaum FA. The NtrY/X two-component system of Brucella spp. acts as a redox sensor and regulates the expression of nitrogen respiration enzymes. Molecular Microbiology. 2012;85: 39–50. doi:10.1111/j.1365-2958.2012.08095.x

97. Wang D, Xue H, Wang Y, Yin R, Xie F, Luo L. The Sinorhizobium meliloti ntrX Gene Is Involved in Succinoglycan Production, Motility, and Symbiotic Nodulation on Alfalfa. Applied and Environmental Microbiology. 2013;79: 7150–7159. doi:10.1128/AEM.02225-13

98. Charles TC, Nester EW. A chromosomally encoded two-component sensory transduction system is required for virulence of Agrobacterium tumefaciens. J Bacteriol. 1993;175: 6614–6625. doi:10.1128/jb.175.20.6614-6625.1993

99. Sola-Landa A, Pizarro-Cerdá J, Grilló MJ, Moreno E, Moriyón I, Blasco JM, et al. A two-component regulatory system playing a critical role in plant pathogens and endosymbionts is present in Brucella abortus and controls cell invasion and virulence. Mol Microbiol. 1998;29: 125–138. doi:10.1046/j.1365-2958.1998.00913.x

100. Yao S-Y, Luo L, Har KJ, Becker A, Rüberg S, Yu G-Q, et al. Sinorhizobium meliloti ExoR and ExoS proteins regulate both succinoglycan and flagellum production. J Bacteriol. 2004;186: 6042–6049. doi:10.1128/JB.186.18.6042-6049.2004

101. Wu C-F, Lin J-S, Shaw G-C, Lai E-M. Acid-Induced Type VI Secretion System Is Regulated by ExoR-ChvG/ChvI Signaling Cascade in Agrobacterium tumefaciens. PLOS Pathogens. 2012;8: e1002938. doi:10.1371/journal.ppat.1002938

102. Sistrom WRY 1960. A Requirement for Sodium in the Growth of Rhodopseudomonas spheroides. Microbiology. 22: 778–785. doi:10.1099/00221287-22-3-778

103. Schäfer A, Tauch A, Jäger W, Kalinowski J, Thierbach G, Pühler A. Small mobilizable multi-purpose cloning vectors derived from the Escherichia coli plasmids pK18 and pK19: selection of defined deletions in the chromosome of Corynebacterium glutamicum. Gene. 1994;145: 69–73. doi:10.1016/0378-1119(94)90324-7

104. . Simon R, Priefer U, Pühler AA. A broad range mobilization system for in vivo genetic engineering: transposon mutagenesis in Gram-negative bacteria. Nat Biotechnol. 1983;(1):784-791. doi: 10.1038/nbt1183-784.

105. Schindelin J, Arganda-Carreras I, Frise E, Kaynig V, Longair M, Pietzsch T, et al. Fiji: an open-source platform for biological-image analysis. Nat Methods. 2012;9: 676–682. doi:10.1038/nmeth.2019

106. Ducret A, Quardokus EM, Brun YV. MicrobeJ, a tool for high throughput bacterial cell detection and quantitative analysis. Nat Microbiol. 2016;1: 1–7. doi:10.1038/nmicrobiol.2016.77

107. Wickham H. ggplot2. New York, NY: Springer New York; 2009. doi:10.1007/978-0-387-98141-3

108. Gall DL, Ralph J, Donohue TJ, Noguera DR. A Group of Sequence-Related Sphingomonad Enzymes Catalyzes Cleavage of β-Aryl Ether Linkages in Lignin β-Guaiacyl and β-Syringyl Ether Dimers. Environ Sci Technol. 2014;48: 12454–12463. doi:10.1021/es503886d

109. Doherty AJ, Ashford SR, Brannigan JA, Wigley DB. A superior host strain for the over-expression of cloned genes using the T7 promoter based vectors. Nucleic Acids Res. 1995;23: 2074–2075. doi:10.1093/nar/23.11.2074

110. Wood WB. Host specificity of DNA produced by Escherichia coli: bacterial mutations affecting the restriction and modification of DNA. J Mol Biol. 1966;16: 118–133. doi:10.1016/s0022-2836(66)80267-x

111. Bolger AM, Lohse M, Usadel B. Trimmomatic: a flexible trimmer for Illumina sequence data. Bioinformatics. 2014;30: 2114–2120. doi:10.1093/bioinformatics/btu170

112. Langmead B, Salzberg SL. Fast gapped-read alignment with Bowtie 2. Nat Methods. 2012;9: 357–359. doi:10.1038/nmeth.1923

113. Anders S, Pyl PT, Huber W. HTSeq—a Python framework to work with high-throughput sequencing data. Bioinformatics. 2015;31: 166–169. doi:10.1093/bioinformatics/btu638

114. Robinson MD, McCarthy DJ, Smyth GK. edgeR: a Bioconductor package for differential expression analysis of digital gene expression data. Bioinformatics. 2010;26: 139–140. doi:10.1093/bioinformatics/btp616

115. McCarthy DJ, Chen Y, Smyth GK. Differential expression analysis of multifactor RNA-Seq experiments with respect to biological variation. Nucleic Acids Research. 2012;40: 4288–4297. doi:10.1093/nar/gks042

116. Benjamini Y, Hochberg Y. Controlling the False Discovery Rate: A Practical and Powerful Approach to Multiple Testing. Journal of the Royal Statistical Society: Series B (Methodological). 1995;57: 289–300. doi:10.1111/j.2517-6161.1995.tb02031.x

117. Karp PD, Billington R, Caspi R, Fulcher CA, Latendresse M, Kothari A, et al. The BioCyc collection of microbial genomes and metabolic pathways. Briefings in Bioinformatics. 2019;20: 1085–1093. doi:10.1093/bib/bbx085

118. Institute B. Picard Toolkit. 2019. https://github.com/broadinstitute/picard.

119. Li H, Handsaker B, Wysoker A, Fennell T, Ruan J, Homer N, et al. The Sequence Alignment/Map format and SAMtools. Bioinformatics. 2009;25: 2078–2079. doi:10.1093/bioinformatics/btp352

120. Sun G, Chung D, Liang K, Keleş S. Statistical Analysis of ChIP-seq Data with MOSAiCS. In: Shomron N, editor. Deep Sequencing Data Analysis. Totowa, NJ: Humana Press; 2013. pp. 193–212. doi:10.1007/978-1-62703-514-9_12

121. Althammer S, González-Vallinas J, Ballaré C, Beato M, Eyras E. Pyicos: a versatile toolkit for the analysis of high-throughput sequencing data. Bioinformatics. 2011;27: 3333–3340. doi:10.1093/bioinformatics/btr570

122. Valouev A, Johnson DS, Sundquist A, Medina C, Anton E, Batzoglou S, et al. Genome-wide analysis of transcription factor binding sites based on ChIP-Seq data. Nat Methods. 2008;5: 829–834. doi:10.1038/nmeth.1246

123. Homann OR, Johnson AD. MochiView: versatile software for genome browsing and DNA motif analysis. BMC Biology. 2010;8: 49. doi:10.1186/1741-7007-8-49

124. Myers KS, Noguera DR, Donohue TJ. Promoter Architecture Differences among Alphaproteobacteria and Other Bacterial Taxa. mSystems. 6: e00526-21. doi:10.1128/mSystems.00526-21

125. Altschul SF, Gish W, Miller W, Myers EW, Lipman DJ. Basic local alignment search tool. J Mol Biol. 1990;215: 403–410. doi:10.1016/S0022-2836(05)80360-2

126. Camacho C, Coulouris G, Avagyan V, Ma N, Papadopoulos J, Bealer K, et al. BLAST+: architecture and applications. BMC Bioinformatics. 2009;10: 421. doi:10.1186/1471-2105-10-421

127. Tamura K, Stecher G, Peterson D, Filipski A, Kumar S. MEGA6: Molecular Evolutionary Genetics Analysis version 6.0. Mol Biol Evol. 2013;30: 2725–2729. doi:10.1093/molbev/mst197

128. Edgar RC. MUSCLE: multiple sequence alignment with high accuracy and high throughput. Nucleic Acids Research. 2004;32: 1792–1797. doi:10.1093/nar/gkh340

129. Talavera G, Castresana J. Improvement of Phylogenies after Removing Divergent and Ambiguously Aligned Blocks from Protein Sequence Alignments. Systematic Biology. 2007;56: 564–577. doi:10.1080/10635150701472164

130. Price MN, Dehal PS, Arkin AP. FastTree 2 – Approximately Maximum-Likelihood Trees for Large Alignments. PLOS ONE. 2010;5: e9490. doi:10.1371/journal.pone.0009490

131. Benítez-Bellón E, Moreno-Hagelsieb G, Collado-Vides J. Evaluation of thresholds for the detection of binding sites for regulatory proteins in Escherichia coli K12 DNA. Genome Biol. 2002;3: RESEARCH0013. doi:10.1186/gb-2002-3-3-research0013

132. Crooks GE, Hon G, Chandonia J-M, Brenner SE. WebLogo: a sequence logo generator. Genome Res. 2004;14: 1188–1190. doi:10.1101/gr.849004

133. Lord SJ, Velle KB, Mullins RD, Fritz-Laylin LK. SuperPlots: Communicating reproducibility and variability in cell biology. Journal of Cell Biology. 2020;219. doi:10.1083/jcb.202001064

134. Ind AC, Porter SL, Brown MT, Byles ED, de Beyer JA, Godfrey SA, Armitage JP. Inducible -Expression Plasmid for Rhodobacter sphaeroides and Paracoccus denitrificans. Appl. Environ. Microbiol. 2009;75:6613–6615. doi: 10.1128/AEM.01587-09.

Table 2-1. The CenKR Regulon

CENTER OF PEAK (bp)[a]	ChIP-seq FOLD ENRICHMENT (IP/INPUT)				DOWNSTREAM GENE		Transmembrane Domain(s)[b]	Signal Peptide[c]	Predicted DNA-binding motif: TGA-N8-TGA	TRANSCRIPT FOLD CHANGE (log_2)[d]					REGULATORY ROLE[e]	Essential[f]
	D56E	WT	ΔcenK	D56A	ID	GENE NAME	ANNOTATION				cenR(D56E)	FDR	ΔcenK	FDR	cenR(D56A)	FDR		
Cell envelope, transport, and extracytoplasmic targeted proteins																		
2597500	1.4	--	--	--	RSP_0847	*RSP_0847*	two component transcriptional regulator winged helix family	N	N	ACAcGGAGGGGCGGAGa	0.49	9.1E-07	-5.16	5.9E-07	-4.34	1.1E-06	+	Y
2413901	4.5	3.2	1.6	1.6	RSP_0672	*toiQ*	Cell division and transport-associated protein ToiQ	Y	N	TGAcGGAGATGCTGATt	2.51	2.3E-03	-0.58	6.7E-03	n.s.	n.s.	+	Y
392575	3.8	1.7	--	--	RSP_1807	*RSP_1807*	putative secreted protein	N	Y	TCGcGAAAACCTGAAAt	2.72	4.1E-06	-2.04	1.4E-04	-1.97	8.0E-05	+	N
426084	2.8	2.3	--	--	RSP_1834	*RSP_1834*	Beta-lactamase superfamily	N	Y	TGAcGGACGCTGTGAAa	2.47	4.4E-06	-5.56	1.7E-05	-5.43	2.8E-07	+	N
2970115	2.9	2.2	--	--	RSP_1199	*RSP_1199*	L,D-transpeptidases/carboxypeptidases	N	Y	TGAcGCGGGGCGTGAAa	2.47	4.4E-05	-1.98	9.9E-05	-1.39	5.1E-04	+	N
2970115*	2.9*	2.2*	--	--	RSP_1200	*RSP_1200*	uncharacterized protein with SCP/PR1 domains	Y	Y	TGAcTTGCATTTGAAa	0.52	1.6E-05	-0.52	3.7E-03	n.s.	n.s.	+	N
478200	2.0	1.6	--	--	RSP_1880	*RSP_1880*	peptidoglycan-binding domain-containing protein	N	Y	TGAcATGGCGGTGTTt	-1.80	4.6E-06	1.24	5.3E-03	n.s.	n.s.	-	N
2933000	1.8	1.4	--	--	RSP_1168	*surA*	PpiC-type peptidyl-prolyl cis-trans isomerase	N	Y	TGAcATGATCGTGTTt	3.40	2.8E-06	-1.48	9.1E-04	-0.74	1.1E-02	+	N
2933000*	1.8*	1.4*	--	--	RSP_1169	*secA*	protein translocase subunit secA	N	N	TCGcGGGACGTTGAAc	1.80	3.0E-06	-0.94	1.7E-03	n.s.	n.s.	+	Y
435330	2.0	--	--	--	RSP_1844	*RSP_1844*	putative periplasmic protein	N	Y	TGGcGGAGGGGTGAAc	1.25	2.2E-05	n.s.	n.s.	n.s.	n.s.	+	N
1368770	2.0	--	--	--	RSP_2718	*RSP_2718*	putative outer membrane protein	Y	Y	TCAcCCTCCTGGTGAAg	3.09	8.2E-04	-4.76	5.9E-07	-6.49	2.9E-07	+	N
2641460	1.8	--	--	--	RSP_0890	*mlaC*	Intermembrane phospholipid transport system binding protein	N	Y	TCAcATACTTGGTGAAT	2.47	1.7E-03	-0.74	2.2E-03	-1.14	6.9E-04	+	N
2473818	3.2	1.9	--	--	RSP_0730	*RSP_0730*	TIGR02302 family protein	N	Y	TCAcCTTCCCGGTCAAT	2.23	2.0E-04	-1.63	3.7E-04	-0.63	1.5E-02	+	N
2450500	2.0	1.4	--	--	RSP_0704	*RSP_0704*	ABC peptide transporter substrate binding protein	Y	Y	TCAcCGAATCGCAAc	1.77	2.1E-05	-0.62	4.0E-03	n.s.	6.6E-04	+	N
458700	1.6	1.7	--	--	RSP_1860	*RSP_1860*	cell wall hydrolyses involved in spore germination	N	Y	TGGcAAAAATGCTCAc	1.42	2.1E-03	-0.61	1.1E-02	-1.25		+	N
1458970	1.6	1.6	1.6	1.6	RSP_2847	*RSP_2847*	putative lipoprotein (predicted lipid binding domain)	Y	Y	TCTTCGTCCCCTGAAC	-1.20	1.1E-03	0.97	2.7E-02	n.s.	n.s.	-	N
2665900	1.5	--	--	--	RSP_0915	*RSP_0915*	putative periplasmic protein	N	Y	TGAcAAAGGTGTTAGc	1.43	5.7E-04	n.s.	n.s.	n.s.	n.s.	+	N
606400	1.6	--	--	--	RSP_2006	*RSP_2006*	uncharacterized protein involved in outer membrane biogenesis	N	Y	TCAcCGAATCCTGAAC	0.67	7.9E-04	n.s.	n.s.	n.s.	n.s.	+	N
930800 (chr2)	1.7	1.6	--	--	RSP_1413	*RSP_1413*	TRAP-T family transporter periplasmic binding component	Y	Y	TCAcCAAATGCATTAGC	-1.34	1.2E-02	0.89	5.8E-02	n.s.	n.s.	-	N
1207306	2.7	1.8	--	1.5	RSP_2561	*exoP*	putative succinoglycan biosynthesis transport protein ExoP	Y	N	TCAcGATCCCTCTCAGc		n.s.	n.s.	n.s.	-0.60	4.2E-02	+	N
278100	1.7	-	--	--	RSP_1024	*RSP_1024*	Putative MoxR family protein	Y	N	TCAcGATCATTTGTGc	0.85	9.1E-05	-0.56	6.1E-03	-0.84	3.8E-03	+	N
2758300	2.8	1.5	--	--	RSP_1000	*dsbC*	Disulfide bond corrector protein DsbC	N	Y	TGGcGATCATTTGTGAc	2.48	5.9E-06	-1.64	1.9E-03	-2.07	8.8E-05	+	N
2758300*	2.8*	1.5*	--	--	RSP_0999	*RSP_0999*	putative transcriptional regulator	N	N	TCGcGCGGACTCTGGGC	1.37	4.5E-05	n.s.	n.s.	n.s.	n.s.	+	N
1273100	1.6	--	--	--	RSP_2633	*ccmF*	Cytochrome c maturation protein CcmF	Y	N	TCGcGGGAAGCGATGAC	1.06	3.2E-02	-0.21	3.0E-02	n.s.	n.s.	+	Y
1330900	2.2	--	--	--	RSP_2685	*cycH*	Putative cytochrome c-type biogenesis protein cycH	Y	N	TGAcGGGATATTGCAc	0.79	1.1E-04	n.s.		-0.89	1.6E-02	+	Y
1330900*	2.2*	--	--	--	RSP_2686	*soxB*	putative sarcosine oxidase beta subunit	N	N	TCGcAACTCGGTGATt	3.76	6.0E-05	-1.21	5.5E-04	n.s.	n.s.	+	N
51549	1.9	1.5	--	--	RSP_1465	*RSP_1465*	putative aminoglycoside phosphotransferase	N	N	TCAcGGATCTTTTTt	0.78	4.5E-05	-1.14	1.2E-03	-1.42	1.6E-03	+	N
106900 (chr2)	1.6	--	--	--	RSP_3067	*RSP_3067*	hypothetical protein	Y	N	TCGcAGGATCTTGTAT	4.51	1.9E-06	n.s.	n.s.	-1.27	8.0E-03	+	N
84880	2.5	1.6	--	--	RSP_1496	*RSP_1496*	Lysozome-like putative lipoprotein	N	Y	TCGcGTTTTTCTGGAAt	1.37	1.3E-03	n.s.	n.s.	n.s.	n.s.	+	N
Cytoplasmic proteins																		
1039245	4.1	2.5	--	--	RSP_2410	*rpoHI*	RNA polymerase sigma 32 subunit - RpoH	N	N	TTGcCATTCGGCGTGAT	3.20	3.2E-04	-3.38	1.4E-06	-2.30	4.6E-06	+	N
2296600	1.6	--	--	--	RSP_0559	*msrA*	Peptide methionine sulfoxide reductase	N	N	TGGcGCGAGCCGTGAT	3.11	8.92-06	-1.78	1.6E-04	-1.41	4.1E-04	+	N

a Chromosomal position of ChIP-seq peak (chr2 - chromosome 2)

b Transmembrane domain predicted using TMHMM 2.0 [132]

c Signaling transit peptides identified using SignalP 5.0 [133]; scores ≥ 0.6 were interpreted to have predicted transit peptides

d log_2(Fold-Change) are reported relative to WT (i.e. mutant/WT)

e Regulatory role of CenR based on changes in gene expresion between TCS mutants relative to WT cells. (+) positively regulated by CenR, (-) negatively regulated by CenR, (NA) Not assigned from data

f Essentiality determined previously by Tn-seq analysis [33]

-- No significant ChIP enrichment

* Peak located between differentially expressed genes

n.s. Not significant, RNA FDR p-value > 0.05 cutoff

Table 2-2. Extended CenKR Regulon

CENTER OF PEAK (bp)[a]	ChIP-seq FOLD ENRICHMENT (IP/INPUT)				DOWNSTREAM GENE			Transmembrane Domain(s)[b]	Signal Peptide[c]	Sequence Logo Predicted DNA-binding motif: TGA-N8-TGA	TRANSCRIPT FOLD CHANGE (log2)[d]						REGULATORY ROLE[e]	Essential[f]
	D56E	WT	ΔcenK	D56A	ID	GENE NAME	ANNOTATION				cenR(D56E)	FDR	ΔcenK	FDR	cenR(D56A)	FDR		
Cell envelope, transport, and extracytoplasmic targeted proteins																		
2597500	1.4	--	--	--	RSP_0847	*RSP_0847*	two component transcriptional regulator winged helix family	N	N		0.49	9.1E-07	-5.16	5.9E-07	-4.34	1.1E-06	+	Y
2413901	4.5	3.2	1.6	1.6	RSP_0672	*tolQ*	Cell division and transport-associated protein TolQ	Y	N		2.51	2.3E-03	-0.58	6.7E-03	n.s.	n.s.	+	Y
392575	3.8	1.7	--	--	RSP_1807	*RSP_1807*	putative secreted protein	N	Y		2.72	4.1E-06	-2.04	1.4E-04	-1.97	8.0E-05	+	N
426084	2.8	2.3	--	--	RSP_1834	*RSP_1834*	Beta-lactamase superfamily	N	Y		2.47	4.4E-06	-5.56	1.7E-05	-5.43	2.8E-07	+	N
2970115	2.9	2.2	--	--	RSP_1199	*RSP_1199*	L,D-transpeptidases/carboxypeptidases	N	Y		2.47	4.4E-05	-1.98	9.9E-05	-1.39	5.1E-04	+	N
2970115*	2.9*	2.2*	--	--	RSP_1200	*RSP_1200*	uncharacterized protein with SCP/PR1 domains	Y	Y		0.52	1.6E-05	-0.52	3.7E-03	n.s.	n.s.	+	N
478200	2.0	1.6	--	--	RSP_1880	*RSP_1880*	peptidoglycan-binding domain-containing protein	N	Y		-1.80	4.6E-06	1.24	5.3E-03	n.s.	n.s.	-	N
2933000	1.8	1.4	--	--	RSP_1168	*surA*	PpiC-type peptidyl-prolyl cis-trans isomerase	N	Y		3.40	2.8E-06	-1.48	9.1E-04	-0.74	1.1E-02	+	N
2933000*	1.8*	1.4*	--	--	RSP_1169	*secA*	protein translocase subunit secA	N	N		1.80	3.0E-06	-0.94	1.7E-03	n.s.	n.s.	+	Y
435330	2.0	--	--	--	RSP_1844	*RSP_1844*	putative periplasmic protein	N	Y		1.25	2.2E-05	n.s.	n.s.	n.s.	n.s.	+	N
1368770	2.0	--	--	--	RSP_2718	*RSP_2718*	putative outer membrane protein	Y	Y		3.09	8.2E-04	-4.76	5.9E-07	-6.49	2.9E-07	+	N
2641460	1.8	--	--	--	RSP_0890	*mlaC*	Intermembrane phospholipid transport system binding protein	N	Y		2.47	1.7E-03	-0.74	2.2E-03	-1.14	6.9E-04	+	N
2473818	3.2	1.9	--	--	RSP_0730	*RSP_0730*	TIGR02302 family protein	Y	N		2.23	2.0E-04	-1.63	3.7E-04	-0.63	1.5E-02	+	N
2450500	2.0	1.4	--	--	RSP_0704	*RSP_0704*	ABC peptide transporter substrate binding protein	Y	Y		1.77	2.1E-05	-0.62	4.0E-03	n.s.	n.s.	+	N
458700	1.6	1.7	--	--	RSP_1860	*RSP_1860*	cell wall hydrolyses involved in spore germination	N	Y		1.42	2.1E-03	-0.61	1.1E-02	-1.25	6.6E-04	+	N
1458970	1.6	1.6	--	1.6	RSP_2847	*RSP_2847*	putative lipoprotein (predicted lipid binding domain)	Y	Y		-1.20	1.1E-03	0.97	2.7E-02	n.s.	n.s.	-	N
2665900	1.5	--	--	--	RSP_0915	*RSP_0915*	putative periplasmic protein	N	Y		1.43	5.7E-04	n.s.	n.s.	n.s.	n.s.	+	N
606400	1.6	--	--	--	RSP_2006	*RSP_2006*	uncharacterized protein involved in outer membrane biogenesis	Y	N		0.67	7.9E-04	n.s.	n.s.	n.s.	n.s.	+	N
930800 (chr2)	1.7	1.6	--	--	RSP_1413	*RSP_1413*	TRAP-T family transporter periplasmic binding component	Y	Y		-1.34	1.2E-02	0.89	5.8E-02	n.s.	n.s.	-	N
1207306	2.7	1.8	--	1.5	RSP_2561	*exoP*	putative succinoglycan biosynthesis transport protein ExoP	Y	N		n.s.	n.s.	n.s.	n.s.	-0.60	4.2E-02	+	N
278100	1.7	--	--	--	RSP_1024	*RSP_1024*	Putative MoxR family protein	Y	N		0.85	9.1E-05	-0.56	6.1E-03	-0.84	3.8E-03	+	N
2758300	2.8	1.5	--	--	RSP_1000	*dsbC*	Disulphide bond corrector protein DsbC	N	Y		2.48	5.9E-06	-1.64	1.9E-03	-2.07	8.8E-05	+	N
2758300*	2.8*	1.5*	--	--	RSP_0999	*RSP_0999*	putative transcriptional regulator	N	N		1.37	4.5E-05	n.s.	n.s.	n.s.	n.s.	+	N
1273100	1.6	--	--	--	RSP_2633	*ccmF*	Cytochrome c maturation protein CcmF	Y	N		1.06	3.2E-02	-0.21	3.0E-02	n.s.	n.s.	+	Y
1330900	2.2	--	--	--	RSP_2685	*cycH*	Putative cytochrome c-type biogenesis protein cycH	Y	N		0.79	1.1E-04	n.s.	n.s.	-0.89	1.6E-02	+	Y
1330900*	2.2*	--	--	--	RSP_2686	*soxB*	putative sarcosine oxidase beta subunit	N	N		3.76	6.0E-05	-1.21	5.5E-04	n.s.	n.s.	+	N
51549	1.9	1.5	--	--	RSP_1465	*RSP_1465*	putative aminoglycoside phosphotransferase	N	N		0.78	4.5E-05	-1.14	1.2E-03	-1.42	1.6E-03	+	N
106900 (chr2)	1.6	--	--	--	RSP_3067	*RSP_3067*	hypothetical protein	Y	N		4.51	1.9E-06	n.s.	n.s.	-1.27	8.0E-03	+	N
84880	2.5	1.6	--	--	RSP_1496	*RSP_1496*	Lysozome-like putative lipoprotein	N	Y		1.37	1.3E-03	n.s.	n.s.	n.s.	n.s.	+	N
694770	3.6	2.6	3.0	3.1	RSP_2095	*mraZ*	Putative MraZ protein	N	N		-1.00	8.0E-02	n.s.	n.s.	n.s.	n.s.	-	N
706700	2.0	2.3	2.5	2.5	RSP_2106	*ftsW*	cell division protein FtsW	Y	N		-2.25	1.2E-03	1.18	1.3E-02	0.92	1.6E-03	-	Y
711700	7.2	9.9	7.5	5.7	RSP_2111	*ddlA*	D-alanine--D-alanine ligase	N	N		-1.06	2.4E-03	1.57	3.6E-03	0.49	1.9E-02	-	Y
2889120	2.6	1.8	--	--	RSP_1125	*mltB*	Membrane bound lytic murein transglycosylase B	N	Y		1.98	6.5E-06	n.s.	n.s.	n.s.	n.s.	+	N
2430800	1.6	1.7	2.1	1.8	RSP_0688	*dacC*	D-alanyl-D-alanine carboxypeptidase	Y	Y		-0.96	3.2E-03	1.09	1.5E-02	0.49	2.0E-02	-	Y
1622411	2.3	2.4	2.7	2.7	RSP_2942	*RSP_2942*	sporulation and cell division-related protein	Y	N		-0.53	1.4E-03	1.55	8.0E-03	0.83	3.2E-03	-	Y
239600 (chr2)	1.5	1.8	1.7	1.7	RSP_3186	*RSP_3186*	putative transmembrane protein	Y	N		-1.42	2.3E-02	n.s.	n.s.	n.s.	n.s.	-	N
1360340	1.7	1.8	1.6	1.6	RSP_2711	*RSP_2711*	Beta-barrel assembly machine subunit BamA	Y	Y		-0.42	3.7E-02	n.s.	n.s.	n.s.	n.s.	-	Y
1184160	2.3	1.8	1.7	1.7	RSP_2540	*tatA*	twin-arginine translocation system protein TatA	Y	N		1.96	4.3E-03	-0.43	1.1E-02	n.s.	n.s.	+	N
1193700	1.6	--	--	--	RSP_2549	*exoQ*	putative polysaccharide polymerase	Y	N		1.04	9.9E-03	n.s.	n.s.	n.s.	n.s.	+	N
1190291	2.5	3.1	2.9	2.9	RSP_2547	*exoY*	exopolysaccharide production protein exoY	Y	N		1.26	5.3E-03	n.s.	n.s.	-1.04	2.8E-03	+	N
1426500	2.1	3.2	2.5	2.2	RSP_2778	*RSP_2778*	Invasion protein B involved in pathogenesis	N	Y		0.55	8.3E-03	-0.29	1.3E-02	n.s.	n.s.	+	N
1670913	2.6	2.4	--	--	RSP_2980	*aspAT*	Putative aspartate aminotransferase A	N	N		-1.44	7.1E-03	n.s.	n.s.	n.s.	n.s.	-	N
1670913*	2.6*	2.4*	--	--	RSP_2981	*RSP_2981*	Putative protein-disulfide isomerase	N	Y		2.25	3.0E-06	-1.42	6.0E-04	-0.60	5.0E-02	+	N
889240	2.5	2.1	--	--	RSP_2271	*RSP_2271*	putative lipoprotein	N	Y		1.64	2.8E-02	-0.84	7.2E-03	n.s.	n.s.	+	N
2682500	1.8	--	--	--	RSP_0932	*cspA*	Peptidase family S41	Y	Y		1.54	7.0E-05	-0.35	1.7E-02	n.s.	n.s.	+	N
2856500	1.9	1.5	--	--	RSP_1097	*pqqL*	putative zinc protease	N	Y		3.36	1.8E-05	-1.15	3.5E-03	-1.04	1.0E-03	+	N
740875	3.0	3.2	2.8	2.6	RSP_2140	*RSP_2140*	Protein of unknown function (DUF1194)	N	Y		-1.28	1.6E-05	1.67	4.3E-02	n.s.	n.s.	-	N
1472000	2.1	2.2	1.9	1.8	RSP_2839	*ntrY*	NtrY Signal transduction histidine kinase	Y	N		-1.46	6.4E-03	0.78	5.4E-02	0.58	3.8E-02	-	N
742800	1.9	1.6	1.8	1.6	RSP_2141	*RSP_2141*	ABC polyamine transporter periplasmic substrate-binding protein	N	Y		1.11	9.4E-05	-0.46	1.2E-02	n.s.	n.s.	+	N
1371600	1.5	1.7	1.6	1.5	RSP_2721	*RSP_2721*	hypothetical protein	N	Y		-0.56	2.0E-02	1.10	1.3E-02	0.87	1.3E-03	-	N
Cytoplasmic proteins																		
1039245	4.1	2.5	--	--	RSP_2410	*rpoH1*	RNA polymerase sigma 32 subunit - RpoH	N	N		3.20	3.2E-04	-3.38	1.4E-06	-2.30	4.6E-06	+	N
2296600	1.6	--	--	--	RSP_0559	*msrA*	Peptide methionine sulfoxide reductase	N	N		3.11	8.9E-06	-1.78	1.6E-04	-1.41	4.1E-04	+	N
165500	1.5	--	--	--	RSP_1572	*RSP_1572*	Heat shock protein Hsp20 family	N	N		0.46	1.4E-02	-0.39	6.4E-03	-0.78	1.2E-02	+	N
1511300	1.8	1.6	--	--	RSP_2806	*Lon*	ATP-dependent proteinase	N	N		1.08	1.8E-03	-0.54	7.1E-03	n.s.	n.s.	+	N
67000 (chr2)	1.9	2.3	2.1	2.2	RSP_4110	*wbyL*	glycosyl transferase	N	N		0.86	5.1E-02	n.s.	n.s.	n.s.	n.s.	+	N
2526668	2.7	3.3	3.0	2.7	RSP_0782	*RSP_0782*	Ppx/GppA phosphatase	N	N		-1.52	1.2E-02	0.89	2.6E-02	n.s.	n.s.	-	N
62100 (chr2)	1.8	2.1	1.8	1.7	RSP_3989	*RSP_3989*	NAD-dependent epimerase/dehydratase	N	N		-2.32	8.8E-04	1.30	7.1E-03	n.s.	n.s.	-	N
1418670	3.4	4.1	3.7	3.3	RSP_2771	*RSP_2771*	putative Exopolyphosphatase	N	N		-1.01	4.5E-02	1.26	4.9E-03	n.s.	n.s.	-	N
2931800	1.6	--	--	--	RSP_1167	*argJ*	glutamate N-acetyltransferase	N	N		1.92	2.3E-04	-1.02	1.7E-03	-0.47	4.3E-02	+	N

a Chromosomal position of ChIP-seq peak (chr2 - chromosome 2)
b Transmembrane domain predicted using TMHMM 2.0 [132]
c Signaling transit peptides identified using SignalP 5.0 [133], scores ≥ 0.6 were interpreted to have predicted transit peptides
d $\log_2$(Fold-Change) are reported relative to WT (i.e. mutant/WT)
e Regulatory role of CenR based on changes in gene expression between TCS mutants relative to WT cells. (+) positively regulated by CenR, (-) negatively regulated by CenK, (NA) Not assigned from data
f Essentiality determined previously by Tn-seq analysis [33]
-- No significant ChIP enrichment
* Peak located between differentially expressed genes
n.s. Not significant, RNA FDR p-value > 0.05 cutoff

Table 2-3. Primers, plasmids, and strains lists.

A. Primers

Name	Sequence	Purpose
BDL3-3	TAGAAAGCCAGTCCGCAGAAAC	PCR Linearization of pk18mobsacB
BDL3-4	CTGTCGTGCCAGCTGCATTAATGAATCG	
BDL77-2	TTAATGCAGCTGGCACGACAGCCTGACGAACGAGACG	PCR upstream flank for RSP1056 deletion vector
BDL78-2	CCGACAGATCAGATCTTGTCCTTCCGAC	
BDL79-2	GACAAGATCTGATCTGTCGGCCCCTC	PCR downstream flank for RSP1056 deletion vector
BDL80-2	CTGCGGACTGGCTTTCTACGATCCGCGCGGGCTCG	
BDL1-3	ATCCCCTGATTCTGTGGATAACCGTATTACCG	PCR amplification of pk18mobsacB cloning site
BDL2-3	CCCAGTCTAGCTATCGCCATGTAAGCC	
BDL74-1	GCTCAACGAACTGTCGAAAC	Sequencing primers of RSP1056 deletion
BDL75-1	CCGGTTCGCTTCTGATGAT	
BDL77-3	TAATGCAGCTGGCACGACAGATTGAGATAGAGGAGCACG	PCR amplification of upstream flank for RSP0847 deletion vector
BDL78-3	CTTAATTTGATCCGGTCACTCCTTCGTTCGTG	
BDL79-3	AGGAGTGACCGGATCAAATTAAGGATCACACTC	PCR amplification of downstream flank for RSP0847 deletion vector
BDL80-3	TTCTGCGGACTGGCTTTCTAGTAGGACCACCAGGAATAGAG	
BDL43-3 (cenR_seq_F)	TCGATGGCGTAATGTTCTTCGC	Sequencing primers of RSP0847 deletion
BDL4-4 (cenR_seq_R)	GACCGAGTTGATGTTCCAGGTG	

BDL77-3	TAATGCAGCTGGCACGACAGATTGAGATAGAGGAGCACG	PCR RSP0847D56A upstream flank for pk18mobsacB
BDL37-4	AGACCCACGGCGAGGATCACGAGGTCGTAGAG	
BDL36-4	TGATCCTCGCCGTGGGTCTGCCGGACAC	PCR RSP0847D56A downstream flank for pk18mobsacB
BDL11-4	TTCTGCGGACTGGCTTTCTACCGTTGTAGCTCTTCTGTC	
BDL77-3	TAATGCAGCTGGCACGACAGATTGAGATAGAGGAGCACG	PCR RSP0847D56E upstream flank for pk18mobsacB
BDL9-4	AGACCCACCTCGAGGATCACGAGGTCGTAGAG	
BDL10-4	TGATCCTCGAGGTGGGTCTGCCGGACAC	PCR RSP0847D56E downstream flank for pk18mobsacB
BDL11-4	TTCTGCGGACTGGCTTTCTACCGTTGTAGCTCTTCTGTC	
BDL12-4	CTTTCCGCTTCTTCCTAGCCAG	Sequencing primers for RSP0847 variants
BDL13-4	GAAGGGCTTCGTCACATAGTCG	
BDL1-5	ATTTTCAGAGCGCGATCGCAGGAATGACCGCCTATGCCGAAGCG	RSP1056-cyto (truncated at M195) insertion into pVP302K with N-terminal H8-TEV tag
BDL2-5	TTGTTATTTTCGGCTTTCTGTCAGACGAGGGCGCTGAGACC	
BDL3-5	GAGGAGAAATTAACCATGGCTTCCCTGAAGAAGATCC	RSP0847 (WT, D56A) insertion into pVP302K with C-terminal TEV-H8
BDL4-5	TTCGCTTCCTGCGATCGCCGCAACAAGCCTGTAGCC	
BDL7-5	AAAGAGGAGAAATTAACCATGACCTCCGACACGACGC	RSP1274 insertion into pVP302K with C-terminal TEV-H8
BDL8-5	TTTTCGCTTCCTGCGATCGCGGCGCTGAGCGTTTCGGTCG	
BDL9-5	AAGAGGAGAAATTAACCATGGTCCCGTGCATTCTTGCGCTC	RSP1083 insertion into pVP302K with C-terminal TEV-H8
BDL10-5	TTTTCGCTTCCTGCGATCGCGCCGGCGAAGGTGTAGCC	

BDL11-5	ACATTTCCCCGAAAAGTGCCAC	pVP302K sequencing primers
BDL12-5	CTTTGTTAGCAGCCGGATCAGC	
BDL41-1	CATATGTAATTTCTCCTC	ATW linearization of pIND5$_{spec}$
BDL42-1	GGATCCAGATCTCATCACCATC	
BDL75-3	AAGAGGAGAAATTACATATGGCTTCCCTGAAGAAGATCC	Amplification of the coding region of *cenR* for assembly into pIND5$_{spec}$
BDL76-3	GATGAGATCTGGATCCTCCTCACGCAACAAGCCTGTAGCCG	
BDL33-1	CTTGTGAGCGGATAACAATGATAC	Sequencing primers for pIND5$_{spec}$
BDL34-1	CAACCGAGCGTTCTGAACAAATCC	
BDL16-8	CGAACTTCACGGTGAGCGTTG	Amplification of tolQ promoter region for EMSA
BDL17-8	GCATCCTCCTCGATCAGGAG	
BDL18-8	CAAGCTCTCGCCGAAGG	Amplification of rpoH1 promoter region for EMSA
BDL19-8	TGTAAGTGCTCATTCGTTGAC	
BDL20-8	CCGTCCCTTCGACCCGCCTC	Amplification of RSP2175 promoter region for EMSA
BDL21-8	GCAGGTGGCGGAACCGGGAG	
BDL22-8	CAGAAAGCCGAAAATAACAAAG	Linearization of pVP302K with N-terminal H_8 tag
BDL23-8	TCCTGCGATCGCGCTCTGAAAATAC	
BDL24-8	GTATTTTCAGAGCGCGATCGCAGGAATGGCTTCCCTGAAGAAGATCC	Amplification of 0847D56E gene for cloning into pVP302K-N
BDL25-8	AACTTTGTTATTTTCGGCTTTCTGTCACGCAACAAGCCTGTAGC	
BDL26-8	ATCCTCGAGGTGGGTCTGCCGGACACC	ATW linearization primers to make pVP302K-N-0847 from pVP302K-N-0847D56E
BDL27-8	AGACCCACCTCGAGGATCACGAGGTCG	

B. Plasmids

Name	Description	Source
pk18mobsacB	Broad host range mobilizable vector; Km^R oriT(RP4) mobT *sacB lacZα*	[103]
pk18mobsacB-RSP1056	*R. sphaeroides* genomic region flanking *RSP1056* Gibson assembled into pk18; Km^R; for deletion of *RSP1056*	This work
pk18mobsacB-RSP0847	*R. sphaeroides* genomic region flanking *RSP0847* Gibson assembled into pk18; Km^R; for deletion of *RSP0847*	This work
pk18mobsacB-RSP0847(D56A)	*R. sphaeroides* genomic regions containing the *RSP0847*D56A allele and genomic regions flanking the gene Gibson assembled into pk18; Km^R; for allelic exchange within RSP0847	This work
pk18mobsacB-RSP0847(D56E)	*R. sphaeroides* genomic regions containing the *RSP0847*D56E allele and genomic regions flanking the gene Gibson assembled into pk18; Km^R; for allelic exchange within RSP0847	This work
$pIND5_{spec}$	Replicable plasmid used for protein expression in *Rb. sphaeroides*.	[134]
pIND5spec-0847	Ectopic expression of *RSP0847* (*cenR*)	This work
pVP302K-N/C	Protein expression vector; Km^R lac promoter lacI, Tev site *rtxA* (*V. cholera*) coding sequence for 8×His-tag	[108]
$pVP302K\text{-}N\text{-}RSP1056_{cyto}$	pVP302K containing truncated *RSP1056* at M195	This work
pVP302K-C-RSP0847	pVP302K containing *RSP0847*	This work
pVP302K-C-RSP0847(D56A)	pVP302K containing *RSP0847* variant D56A	This work
pVP302K-C-RSP1274	pVP302K containing *RSP1274*	This work
pVP302K-C-RSP1083	pVP302K containing *RSP1083*	This work
pVP302K-N-0847D56E	pVP302K containing *RSP0847* variant D56E with N-terminal H_8 tag	This work
pVP302K-N-0847	pVP302K containing *RSP0847* with N-terminal H_8 tag	This work

C. Strains

Strains	Relevant characteristics	Reference
***Rhodobacter sphaeroides* strains**		
2.4.1	Wild-type strain	ATCC 17023
BDL021	Δ*RSP1056* (Δ*cenK*)	This work
BDL072	*RSP0847*D56A (*cenR* D56A)	This work
BDL019	*RSP0847*D56E (*cenR* D56E)	This work
BDL020	*RSP0847*D56E Δ*RSP1056* (*cenR* D56E Δ*cenK*)	This work
BDL013	pIND5$_{spec}$-*cenR*	This work
BDL121	pIND5$_{spec}$-*cenR* Δ*cenR*	This work
***Escherichia coli* strains**		
DH5α	F- Φ80*lacZ*ΔM15 Δ(*lacZYA-argF*) U169 *recA*1 *endA*1 *hsdR*17 (rK–, mK+) *phoA supE*44 λ– *thi*-1 *gyrA*96 *relA*1	New England Biolabs
S17-1	*TpR SmR recA1 thiE1 pro-82 hsdR17 RP4-2-Tc::Mu-Km::Tn7* λpir	[104]
NEB 5-alpha competent *E. coli*	*fhu*A2 Δ(*argF-lacZ*)U169 *phoA gln*V44 Φ80 Δ(*lacZ*)M15 *gyrA*96 *recA*1 *relA*1 *endA*1 thi-1 *hsdR*17	New England Biolabs
B834	F- *hsdS metE gal ompT*	[109,110]
BL21 (DE3) pLysS CodonPlus	E. coli str. B F– *ompT gal dcm lon hsdSB*(rB–mB–) λ(DE3 [*lacI* lacUV5-T7p07 *ind1 sam7 nin5*]) [*malB*+]K-12(λS) pLysS[T7p20 orip15A](CmR) argU (AGA, AGG), ileY (AUA), leuW (CUA)	Novagen

Table 2-4. Genbank accession numbers for all protein sequences used in CenK/R phylogeny (Fig 2-12).

Organism	CenK homolog	CenR homolog
Rhodobacter sphaeroides 2.4.1	ABA80240.1	ABA80028.1
Rhodobacter ovatus	WP_097029852.1	WP_097029114.1
Cereibacter changlensis	PZX58573.1	WP_107663473.1
Defluviimonas denitrificans	WP_105515131.1	WP_105516383.1
Pseudorhodobacter aquimaris	WP_083444869.1	WP_050526965.1
Pseudorhodobacter wandonensis	WP_050524403.1	WP_050523141.1
Roseibacterium elongatum	WP_025311819.1	WP_025311137.1
Paracoccus aminovorans	WP_062561073.1	WP_074969281.1
Rhodobacter capsulatus	WP_055211899.1	WP_136906601.1
Roseicitreum antarcticum	WP_092887326.1	WP_092887229.1
Gemmobacter megaterium	WP_083701327.1	WP_076533744.1
Meinhardsimonia_xiamenensis	WP_092500460.	WP_092497609.1
Pararhodobacter aggregans	WP_107753170.1	WP_107752404.1
Paracoccus zeaxanthinifaciens	WP_022708257.1	WP_022707883.1
Pontivivens insulae	WP_108783177.1	WP_108783392.1
Oceanicella actignis	WP_211356277.1	WP_072746865.1
Maricaulis maris	WP_121209738.1	WP_041637067.1
Hirschia maritima	WP_155826066.1	WP_018997296.1
Hyphomonas oceanitis	WP_051624558.1	WP_035538430.1
Ponticaulis koreensis	WP_022695910.1	WP_022693572.1
Henriciella algicola	WP_119455183.1	WP_119453332.1
Bradyrhizobium erythrophlei	WP_074272850.1	WP_072818367.1
Parvularculaceae bacterium	MCB2096247.1	MAW81539.1
Amphiplicatus metriothermophilus	WP_089410642.1	WP_089410979.1
Marinicaulis flavus	WP_104828836.1	WP_104829420.1
Caulobacter crescentus (vibrioides)	WP_010918418.1	WP_024266002.1
Caulobacter segnis	WP_013077599.1	PZR32001.1
Caulobacter henricii	WP_035045754.1	WP_062151853.1
Phenylobacterium haematophilum	WP_183772596.1	WP_183775692.1
Asticcacaulis endophyticus	GGZ27123.1	WP_189484874.1
Brevundimonas bacteroides	WP_029414873.1	WP_029417475.1
Oceanicaulis alexandrii	WP_022701438.1	WP_009802422.1

Ruegeria atlantica	NOD30888.1	WP_058279748.1
Ruegeria litorea	WP_085794123.1	WP_085797046.1 (*sp.*)
Ruegeria pomeroyi	WP_011046299.1	WP_011049109.1
Thalassobius activus	WP_058313840.1	WP_209358005.1
Roseobacter cerasinus	WP_159974535.1	WP_159975066.1
Roseobacter denitrificans	WP_011567720.1	WP_011566403.1 (*sp.*)
Sulfitobacter pontiacus	WP_064215825.1	WP_005850360.1
Lutimaribacter pacificus	WP_149789044.1	WP_149788025.1
Roseovarius aestuarii	WP_085800950.1	WP_085800306.1
Nitratireductor aquibiodomus	WP_065816343.1	WP_065816950.1
Nitratireductor pacificus	WP_040676576.1	WP_008596599.1
Hoeflea phototrophica	WP_007199885.1	WP_007199422.1
Phyllobacterium phragmitis	WP_105743815.1	WP_105741337.1
Phyllobacterium leguminum	WP_110752236.1	WP_110749900.1
Agrobacterium tumefaciens	KIQ02346.1	AMD60228.1
Sinorhizobium meliloti	RVJ02864.1	WP_100672725.1
Chelativorans alearense	WP_163266599.1	WP_163265216.1
Pseudovibrio denitrificans	WP_054784296.1	WP_041767864.1
Azorhizobium caulinodans	WP_043879669.1	WP_012168621.1
Bosea robiniae	WP_091856047.1	WP_061966680.1
Pararhizobium polonicum	WP_099050751.1	WP_068955266.1
Mesorhizobium albiziae	WP_188130341.1	WP_149759750.1
Neorhizobium galegae	WP_046664845.1	WP_210105920.1
Brucella rhizophere	WP_094579191.1	WP_094578402.1
Brucella abortus	WP_002963438.1	WP_002965068.1
Brucella melitensis	SPU63212.1	WP_070997026.1
Labrenzia (*Roseibium*) *alba*	WP_055675062.1	WP_055677803.1
Labrenzia (*Roseibium*) *aggregate*	WP_206904135.1	WP_190291169.1
Nitrobacter winogradskyi	WP_141383471.1	WP_011313424.1
Nitrobacter hamburgensis	WP_011512071.1	WP_011508702.1
Rhodopseudomonas palustris	WP_044412660.1	MBI5130782.1
Sneathiella sp.	PHQ71087.1	PHQ71627.1
Sneathiella litorea	MZR29347.1	WP_161314357.1
Sneathiella chinensis	WP_169559456.1	WP_169559000.1
Kiloniella majae	WP_085900939.1	WP_047764063.1
Kiliella laminaria	WP_020590891.1	WP_020590402.1

Skermanella rosea	WP_203096208.1	WP_203098182.1
Denitrobaculum tricleocarpae	WP_142894422.1	WP_142896990.1
Fodinicurvata sediminis	WP_022727682.1	WP_022727791.1
Roseospirillum parvum	WP_092616041.1	WP_092621908.1
Novispirillum itersonii	WP_184264282.1	WP_184262290.1
Ferruginivarius sediminum	WP_114583718.1	WP_114580497.1
Azospirillum halopraeferens	WP_029009133.1	WP_029010793.1
Azospirillum lipoferum	WP_085554914.1	WP_085555599.1
Thalassospira profundimaris	WP_114112327.1	WP_114100359.1
Thalassospira povalilytica	WP_206926285.1	WP_062950084.1 (*sp.*)
Thalassospira xiamenensis	WP_097053219.1	WP_101246657.1 (*sp.*)
Curvivirga aplysinae	WP_155157144.1	WP_155154090.1
Aestuariispira insulae	WP_115938537.1	WP_115936241.1
Oceanibaculum pacificum	WP_067557655.1	WP_067551072.1

Table 2-5. PatSer motif search (Fig 2-12) and PWM for CenR binding motif in *Rhodobacter sphaeroides* 2.4.1

A. PatSer motif search

Identified gene[1]	Position (distance from start codon)[2]	Score[3]	ln(p-value)	Sequence
***Rhodobacter sphaeroides* 2.4.1**				
cenR	183	7.4	-9.45	TTGCAGGAAATTGAA
msrA	199	9.98	-12.6	TGGCGCGAGCGTGAT
RSP1807	231	8.59	-10.77	TCGCAAAACCTTGAT
RSP1860	177	7.11	-9.16	TGGCAAAAATGTCAC
surA	142	9.01	-11.28	TGACATGATCGTGTG
tolQ	213	9.98	-12.6	TGACGCAGATGTGTT
***Agrobacterium tumefaciens* BIM B-1315G**				
cenR (IAI05_12475)	65	8.44	-10.6	TCACGAGATTTTGCT
msrA (IAI05_13425)	101	8.46	-10.62	TGGCGCTTCATTGAA
RSP1807 (IAI05_12080)	197	10.11	-12.79	TGACTTTCTATTGAA
RSP1860 (IAI05_01710)	171	9.5	-11.91	ACACATTAACGTGAA
surA (IAI05_17235)	239	3.26	-5.89	TGGAAGTTTTTTCAG
tolQ (IAI05_18005)	240	7.88	-9.96	TAACACGCGTTTGAA
***Brucella abortus* 2308**				
cenR (BAB1_2006)	121	4.33	-6.68	TCAAGGTCTTTCGAG
msrA (BAB2_1029)	116	7.5	-9.55	AGAAGCGACCGTGAC
RSP1807 (BAB1_0088)	146	7.66	-9.73	TGAATTCCTATTGAT
RSP1860 (BAB1_0408)	94	5.39	-7.55	TAGCAATGGTCTGAT

surA (BAB1_1944)	160	7.32	-9.37	TTGCTTCAAAGTGAT
tolQ (BAB1_1712)	238	5.9	-8	TAACGGATTTGCGAT
***Caulobacter crescentus* NA1000**				
cenR (*CCNA_03859*)	195	4.02	-6.44	TCCCGCAAGCTCGAA
msrA (*CCNA_01046*)	65	3.7	-6.21	AGAGAGGGATTCGAA
RSP1807 (*CCNA_03780*)	259	8.04	-10.14	TCACGGCCTCGTGAA
RSP1860 (*CCNA_03062*)	125	6.32	-8.39	TCAAGTGCTTGCGAG
surA (*CCNA_03163*)	145	3.6	-6.13	TGGTGTCAACGCGAA
tolQ (CCNA_03341)	66	2.49	-5.36	TGAGGTGCTGTTCGA
***Rhodopseudomonas palustris* RCB100**				
cenR (RPA0283)	55	5.73	-7.85	ACAATCGCGCGTGAT
msrA (RPA4834)	100	7.19	-9.02	TGAAATTGAGTTGAG
RSP1807 (RPA0201)	108	5.82	-7.93	TGAGTGGCAGGTGAA
RSP1860 (RPA0201)	NA	NA	NA	NA
surA (RPA0511)	83	6.60	-8.65	TTTCATCATTTTGAC
tolQ (RPA1117)	143	7.19	-9.24	TGACAGGGGATTGAG

[1]blastn search to identify homologs of each *Rb. sphaeroides* gene (locus tag listed).
[2]Identified in 300bp genomic region upstream of start codon using in search.
[3]Scores determined by comparison of the base position in the sequence to the same position in the PWM (below). Scores for each position are summed for the length of the sequence, larger score means more positions matched more frequent bases in the PWM.
NA - could not identify a homolog with high sequence homology.

B. PWM CenR binding motif in *Rhodobacter sphaeroides* 2.4.1 (Fig 2-8A) formatted for Patser

nucleotide	Logo Position														
	1	**2**	**3**	**4**	**5**	**6**	**7**	**8**	**9**	**10**	**11**	**12**	**13**	**14**	**15**
A	1	0	7	1	2	2	2	3	2	1	0	0	0	8	3
C	0	3	0	8	0	4	1	2	2	4	1	1	0	0	4
G	0	6	3	1	6	1	5	3	3	1	6	0	10	1	1
T	9	1	0	0	1	3	2	2	3	4	2	9	0	1	3

CHAPTER 3:

Coordination of *Rhodobacter sphaeroides* cell elongation and division

This chapter will be submitted to mBio for publication:

Bryan D. Lakey, François Alberge[*], Daniel Parrell[*], Elizabeth R. Wright, Daniel Noguera, Timothy J. Donohue.

[*]Indicates equal contribution

BDL was responsible for conceptualization, construction of strains and plasmids, fluorescence and bright field microscopy. FDAA experiments and analysis performed by BDL and FA, cryogenic electron microscopy and analysis performed by DP. The manuscript was written by BDL and TJD. Editing and revisions provided by all.

Abstract

Cell elongation and division are essential aspects of the bacterial life cycle that must be coordinated for viability and replication. The impacts of mis-regulation of these essential processes are not well understood as these systems are often not amenable to traditional genetic manipulation. Recently, we reported on a two-component system, CenKR, in *Rhodobacter sphaeroides* that is genetically tractable, widely conserved in α-proteobacteria, and directly regulates expression of components of the bacterial lifecycle, including genes encoding subunits of the Tol-Pal complex that play a crucial role in division. In this work we show that by overexpressing *cenK*, we can increase the activity of this TCS and observe disruptions of cell elongation and division. Cryo-electron microscopy analysis images of cells overexpressing *cenK* show that they failed to complete cell division and maintain outer membrane connection at division septum. By monitoring the localization of Pal, peptidoglycan biosynthesis, and the bacterial cytoskeletal proteins MreB and FtsZ in wild type cells and those overexpressing *cenKR*, we develop a model for how increased CenKR activity leads to changes in cell elongation and division. This model predicts that Pal localization is key for normal cell elongation and division in *Rb. sphaeroides*. It further predicts that disruption of outer membrane constriction in cells overexpressing *cenK* alters the mid-cell positioning of MreB and FtsZ, thereby interfering with the spatial regulation of nascent peptidoglycan biosynthesis that occurs in wild type cells. We propose that the knowledge gained from the genetic manipulation of CenKR activity has and can continue to provide new insight into previously uncharacterized processes in cell elongation and division in α-proteobacteria and other bacteria.

Introduction

Gram-negative cells contain a diderm membrane system consisting of an inner membrane (IM) phospholipid bilayer and an outer membrane (OM) that is composed of an inner leaflet of phospholipids and an outer leaflet of lipopolysaccharide (LPS) molecules (1). These two membranes are separated by a periplasmic space containing a thin layer of peptidoglycan (PG) that is closely associated with, and covalently connected to, the OM (1). The synthesis of new cell envelope materials, specifically PG, is critical for cell shape, elongation, and division. While much is known about the function, assembly, and spatiotemporal movement of complexes (the elongasome (2) and divisome (3)) that are essential for cell elongation and division in some bacteria, little is known about the coordination of these processes. We are interested in the coordination of these processes in α-proteobacteria that display a wide variety of cell elongation or division patterns, have properties of biomedical, environmental, agricultural and industrial importance (4), and lack homologous regulators of the systems that have been described in *Escherichia coli* and other Gram-negative bacteria (5–7).

There is considerable knowledge about cell elongation and division in the γ-proteobacterium *E. coli.* In this bacterium, the IM TolQRA complex is localized to the midcell during septum formation by interactions with subunits of the divisome (8, 9). At the time of cell division, TolQRA interacts with the Pal lipoprotein to populate the division septum by promoting diffusion of this lipoprotein from the TolB-Pal complex, thereby allowing Pal to bind PG (8, 9). These events are followed by constriction of the OM at the site of septum formation through non-covalent interactions of Pal with newly synthesized PG during the late stages of cell division (8, 9). The dynamic localization of TolQRA also regulates the activity of lateral PG synthesis

complexes (PBP1B-LpoB-CpoB) during cell elongation (6) as well as the hydrolysis of cell septum PG strands ensuring separation of the daughter cells during cell division (10). While the role of the Tol-Pal complex has been described in *E. coli*, α-proteobacteria lack homologs to several of the genes encoding proteins implicated in these events. In addition, unlike the situation in *E. coli* which divide by binary fission (11), α-proteobacteria display a wide-variety of budding morphologies, midcell constriction, as well as asymmetric or polar growth, which possibly requires fundamental differences in cell elongation and division (4). The diversity of cell properties may also explain why the genes encoding several subunits of the Tol-Pal complex (*tolQ*, *tolA*, *tolR*, *tolB*, and *pal*) are known or predicted to be essential in *Rb. sphaeroides* (12) and other α-proteobacteria (13, 14), unlike the case in *E. coli* and several other well-studied bacteria.

Often, important insights into cell envelope processes have come from analyzing the role of two-component systems (TCSs). However, well-studied TCS(s) that impact the expression of cell envelope genes in *E. coli* (15, 16), are not typically conserved outside of γ-proteobacteria. Moreover, TCSs that directly regulate the expression of cell wall processes have been described in few microbes and generally not well conserved (17–20). The essential nature of TCSs that regulate cell cycle dynamics in some α-proteobacteria has made it difficult to dissect specific roles in cell envelope biosynthesis and division due to pleiotropic effects. Consequently, less is known about envelope biosynthesis and the broad impacts of TCSs on cell elongation and division in α-proteobacteria.

Recently, we reported on the cell envelope kinase and response regulator, CenKR, in *Rhodobacter sphaeroides*, a TCS that is conserved in many α-proteobacteria and regulates transcription of genes encoding subunits of the TolQRAB complex and those proteins known or predicted to function in cell envelope biogenesis and division (Chapter 2 and (21)). In this work, we take advantage of the features of the *Rb. sphaeroides* CenKR TCS to study the dynamics of cell elongation and division in this α-proteobacterium. We show that ectopic expression of *cenK* increases the activity of the CenKR TCS, leading to filamentation, as well as changes in the morphology of the periplasm and the OM. Fluorescence microscopy was used to track changes in the temporal and spatial dynamics of PG biosynthesis, movement of Pal, and localization of cell elongation (MreB) and cell division (FtsZ) proteins between wild type and those with increased CenKR activity. Our results have provided important new insight into the processes of cell elongation and division in *Rb. sphaeroides* and allow us to propose how increased CenKR activity leads to the observed morphological changes. This work also lays a foundation for future studies to obtain a deeper understanding of cell elongation and division in this and other α-proteobacteria.

Results

Overexpression of *cenK* is sufficient to increase CenKR TCS activity *in vivo*. To expand our understanding of the role of *Rb. sphaeroides* CenKR, we examined the effects of increasing expression of either *cenR* or *cenK*. Based on previous observations and what is known about other TCSs, we hypothesized that increased expression of one or both genes would result in changes in cell length (21). To test this hypothesis, we cloned either *cenR* or *cenK* into a low copy-number plasmid, pIND5, under the control of an isopropyl- β-D-thiogalactopyranoside

(IPTG) inducible promoter (22). Mobilization of pIND5-*cenR* or pIND5-*cenK* into wild type cells produced no significant change in cell length (2.16 ± 0.17 µm and 2.23 ± 0.27 µm, respectively) compared with a control strain (pIND5-empty, 1.96 ± 0.11 µm) when cells were grown in the absence of IPTG (Fig 3-1A-B). However, in the presence of IPTG, cells containing pIND5-*cenR* were longer (2.86 ± 0.07 µm) than the control strain (Fig 3-1A-B), as expected since previous work indicated that cells containing amino acid changes in CenR that increase its function were longer than their wild type counterparts (21).

In contrast, we found that cells containing pIND5-*cenK* when grown in the presence of IPTG, exhibited a more severe morphological changes, producing cell filaments with lengths of 7.51 ± 1.40 µm (Fig 3-1A-B). To test if increased CenK was sufficient for filament formation in a CenR-dependent manner, we analyzed the impact of a D56A amino acid substitution in CenR which has previously been shown to block phosphorylation by CenK (21). Mobilization of pIND5-*cenK* into a strain containing a *cenR*(D56A) allele in the genome produced cells with no significant difference in cell length in the presence or absence of IPTG compared to the control strain (Fig 3-1A-B). From this, we can conclude that increased levels of CenK is sufficient to stimulate TCS activity as phosphorylation of the CenR protein by CenK is required to produce the morphological changes observed when *cenK* is overexpressed.

Cells containing a CenR protein in which aspartate residue 56 has been changed to a glutamate have altered growth rates in liquid cultures, presumably since the amino acid substitution at this phospho-acceptor residue mimics phosphorylation of this response regulator (21, 25). Testing the effects of *cenR*/*cenK* overexpression on growth rates in the absence of IPTG, we observed no

Figure 3-1. Overexpression of *cenK* is sufficient to increase CenKR activity *in vivo*. A. Bright-field microscopy measurements of cell length, displayed as bee swarm plots (23). Mean length values (μm) from each of the three biological replicates (grey circles, blue squares, orange triangles) and mean length for each strain (black bar) are shown. For each biological replicate >500 cells were analyzed. Unpaired t-tests were used to compare pooled cell length data from the mean values of each biological replicate (n =3) (23). Significant *P* values < 0.01 (*) are indicated by an asterisk (N.S. indicate a *p*-value > 0.05 and no significant difference). WT = wild type, +IPTG = ectopic expression of *cenK* induced by addition of 10 μM IPTG. **B.** Representative bright-field micrographs of each strain analyzed. Scale bar = 2 μm. **C.** Cell density (Klett units) of *Rb. sphaeroides* cultures grown aerobically (1 Klett unit is equal to ~1 x 10^7 cells/mL for WT *Rb. sphaeroides* (24)).

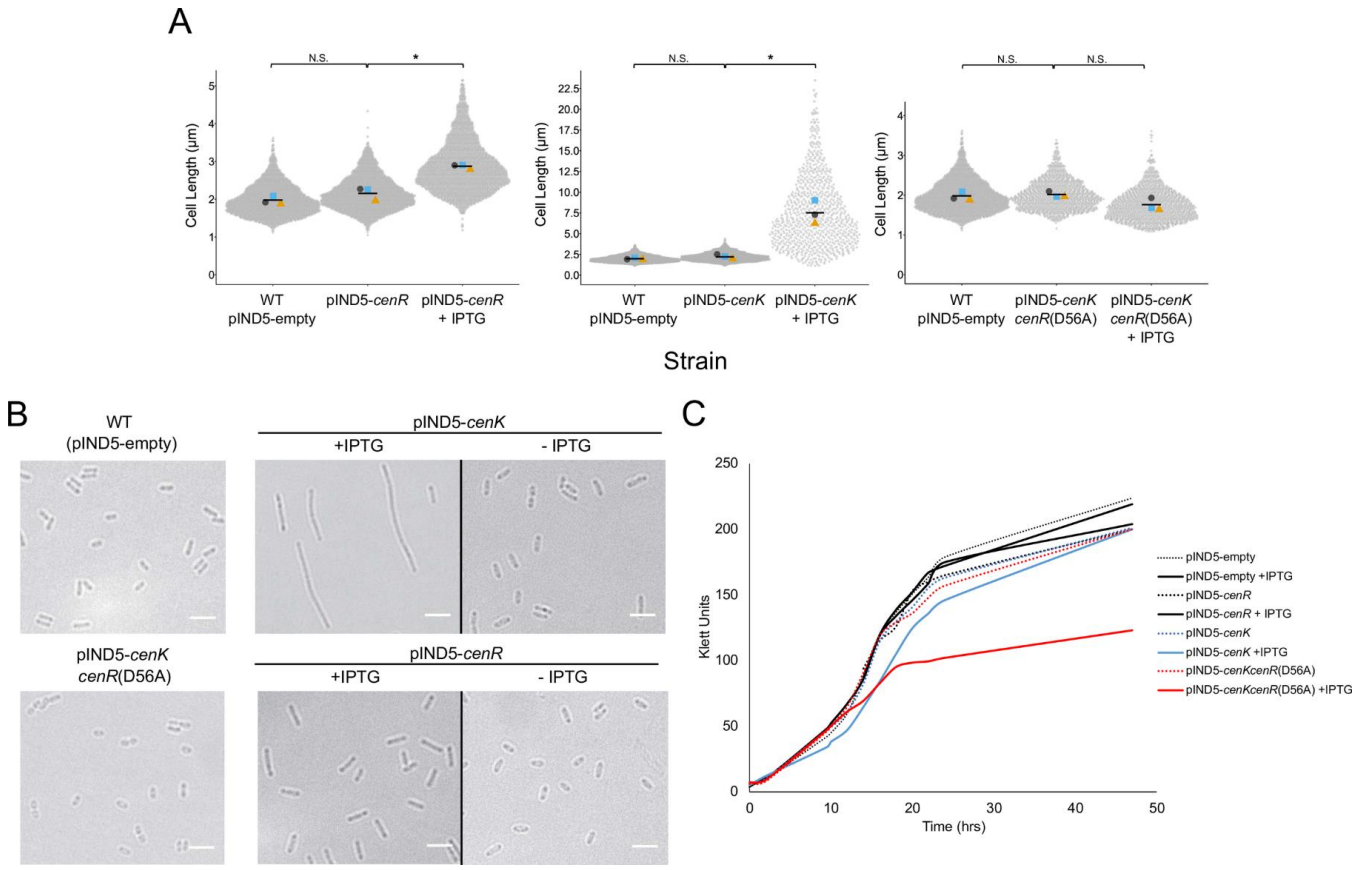
A
N.S.
*
Cell Length (µm)
WT pIND5-empty
pIND5-cenR
pIND5-cenR + IPTG
pIND5-cenK
pIND5-cenK + IPTG
pIND5-cenK cenR(D56A)
pIND5-cenK cenR(D56A) + IPTG
Strain
B
WT (pIND5-empty)
pIND5-cenK
+IPTG
- IPTG
pIND5-cenK cenR(D56A)
pIND5-cenR
C
Klett Units
Time (hrs)
pIND5-empty
pIND5-empty +IPTG
pIND5-cenR
pIND5-cenR + IPTG
pIND5-cenK
pIND5-cenK +IPTG
pIND5-cenKcenR(D56A)
pIND5-cenKcenR(D56A) +IPTG

impact on either growth or final cell density of wild type cells containing either pIND5-*cenR* or pIND5-*cenK*, and only a slight decline in generation time after IPTG was added to cells containing pIND5-*cenK* (Fig. 3-1C). In contrast, there was both a significant increase in generation time, and an early cessation of growth (as measured by increases in cell density) after IPTG is added to cells containing the *cenR*(D56A) allele in the genome and the pIND5-*cenK* plasmid, compared to other strains analyzed (Fig. 3-1C). Combined, these data support the hypothesis that ectopic overexpression of *cenK* is sufficient to both increase activity of the CenKR TCS and produce the observed changes in cell length. Moreover, the results show that the filamentation of cells that overexpress *cenK* requires phosphotransfer to its cognate RR CenR. Below, we present the results of experiments that seek to gain insight into how increased CenKR activity due to overexpression of *cenK* produces these changes in cell morphology.

Visualizing the impact of increased CenKR activity on cell morphology. Previous analysis of the CenKR regulon has shown that this TCS directly or indirectly controls the expression of genes that are required for PG synthesis, cell elongation and division (21). Thus, we used high-resolution microscopy to visualize the impact of *cenK* overexpression on cell morphology. Negative stain electron microscopy revealed that the filaments found when CenKR activity is increased consist of cell chains containing incomplete cell division septa (Fig 3-2A). We also observed surface protrusions that extend into the media originating from many of these incomplete cell division septa (Fig 3-2A), suggesting that there is improper OM migration during the late stages of cell division in cells with increased CenKR activity.

To visualize morphological changes associated with increased CenKR activity at higher resolution, we used cryogenic electron microscopy (Cryo-EM). For these experiments, we analyzed a *Rb. sphaeroides* mutant that cannot synthesize poly-β-hydroxybutyrate storage granules (Δ*RSP_0382* (26)) in order to better visualize internal cellular features. In this Δ*RSP_0382* strain, a tomographic reconstruction of the Cryo-EM images revealed that the IM separated to form two cytoplasmic compartments connect by a continuous OM layer prior to the formation of daughter cells (Fig 3-2B). In addition, during IM fission, separate PG layers appear prior to OM separation and formation of daughter cells. These events are typical of IM and OM co-migration during midcell constriction and cell division in bacteria (Fig 3-2B).

In Cryo-EM images of Δ*RSP_0382* cells that ectopically overexpress *cenK* from the same plasmid used in the above experiments, we observed an increased distance between the IM and OM throughout the length of the cell, at the cell poles, and throughout the cell cycle (Fig 3-2C top panel, 3-2E middle panel). We also observed a periodic difference in the spacing between the IM and OM along the length of the cell (Fig 3-2C, middle panel). Tomographic reconstructions of these data predict periodic constriction of the IM along the length of the cell, while the properties of the OM and PG layers remaining relatively unchanged in cells with increased CenKR activity (Fig 3-2C bottom panel). Measurement of the average distance between the IM and OM or IM and PG layers (excluding the regions of extended periplasmic width) indicates that the width of the periplasmic space in the cells overexpressing *cenK* (33.9 ± 4.8 nm) is increased along the length of the cell relative to that measured in the parent cells (27.3 ± 1.8 nm) (Fig 3-2D). The distance between the OM and PG layer were not found to be significantly different in cells overexpressing *cenK* when compared to the control strain (Fig 3-2D).

Figure 3-2. Morphological changes in cells with increased CenKR activity. A. Electron micrographs of negatively stained cells overexpressing *cenK*. **B.** Cryo-EM images of parent cells (Δ*RSP_0382*). (Top panel) A central slice through a tomographic reconstruction of the parent strain showing IM, PG cell wall, and OM. (Bottom panel) A central slice through a tomographic reconstruction of the division plane within parent cells showing constriction of OM and PG layers closely associated with the IM separation. **C.** Central slices through tomographic reconstructions of cells overexpressing *cenK* (20,000x magnification) showing extended gaps (red lines) between the IM and OM at the cell pole (top panel) and along the length of the cell (middle panel). Gaps range from ~65-115 nm along the cell body and from ~120-285 nm at the cell pole. The bottom panel is a central slice through the same cell in the middle panel at 48,000x magnification. **D.** The periplasmic space is wider in cells with *cenK* overexpression. The distances between the layers of the cell envelope were measured using a central slice through a tomographic reconstruction of the parent strain (left image, green box plots) and *cenK* overexpression strain (right image, purple box plots). Box plots for each strain representing the median (black lines) and inter quartile range (boxes) of measurements for the distance between the IM and OM or IM and PG or OM and PG (nm). Data points for the individual measurements are overlayed to represent the range. * = p-value < 0.01. **E.** Thin slice tomographic reconstructions showing the impact of *cenK* overexpression on cell division, OM/PG migration, and membrane blebbing. Cryo-EM images of cells induced for ectopic expression of *cenK*. (Left panel) Visualization of the division plane shows dissociation of the IM and OM/PG layers. White arrows indicate membrane structure protruding from the division septum of the cells. (Middle panel) A second slice through the same cell indicating a thin connection between the IMs of separating cells correlating with delayed OM constriction. (Right panel) Visualization of

the cell poles show retraction of the IM from the OM/PG layers. White arrows indicate membrane blebbing from various sites along the cell envelope. **F.** (Left panel) A 4,800x magnified cryo-electron microscopy image of cells overexpressing *cenK*. (Middle panel) A central slice from a cryoelectron tomograph of the same cell at 19,500x magnification. A chain of extracellular lipids is seen budding from the cell septum and appears to originate from the OM. (Right panel) A 3-dimensional model of the same cell depicting the OM (blue), IM (green), and extracellular vesicles (orange).

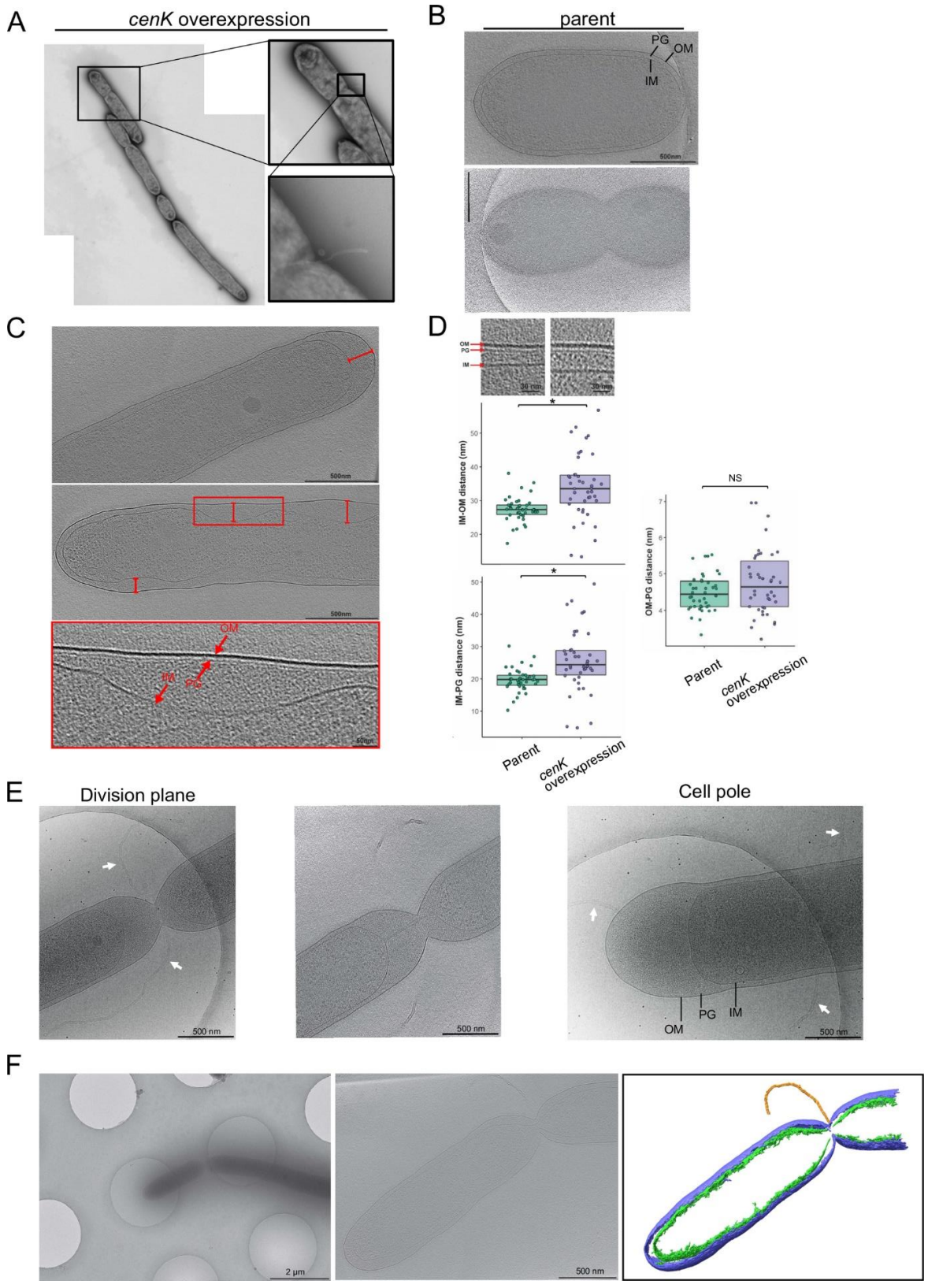
A
cenK overexpression
B
parent
PG
OM
IM
500nm
C
500nm
500nm
OM
IM
PG
50nm
D
OM
PG
IM
30 nm
30 nm
*
IM-OM distance (nm)
50
40
30
20
*
IM-PG distance (nm)
50
40
30
20
10
Parent
cenK overexpression
NS
OM-PG distance (nm)
7
6
5
4
Parent
cenK overexpression
E
Division plane
500 nm
500 nm
Cell pole
OM
PG
IM
500 nm
F
2 µm
500 nm

We also created high resolution tomographic reconstructions of the cell division sites in cells with increased CenKR activity (Fig 3-2E). These reconstructions showed instances where the IM had completed fission, dissociated from the OM, and increased the distance between the cytoplasmic compartments of daughter cells compared to the control strain where the IM, PG, and OM are tightly associated at the time of cell division. These reconstructions also provided evidence for protrusions located at either the sites of IM fission (Fig 3-2E left panel) or the cell poles (Fig 3-2E right panel) in *cenK* overexpression strains that were not present in reconstruction of the parent strain. Observations of cell envelope structure at stalled division sites indicated that the OM failed to invaginate contiguously with the IM as in WT cells. Within these filamentous cells, we also observed a thin, continued interconnection between the IMs of daughter cells despite retraction of the rest of the IMs from one another suggesting the normal mechanisms of cytokinesis were disrupted (Fig 3-2E, middle panel). When we constructed a segmentation model from these tomograms (Fig 3-2F), it predicted the OM as the origin of the surface protrusions, leading us to propose that cells which overexpress *cenK* have altered interactions between the OM, PG cell wall, and surface components. Because of these findings, we performed additional experiments to provide more insight into the observed morphological changes in cells that have increased CenKR activity.

Increased CenKR activity leads to mislocalization of the Tol-Pal complex. The previous results suggest that cells with increased CenKR activity have defects in cell division. We know that the RR CenR binds to and activates the expression of the *tolQRAB* genes that encode subunits of the Tol-Pal complex (Fig. 3-3A-B) (21). We hypothesized that increased expression of the *tolQRAB* genes in cells with increased CenKR activity leads to elevated levels of the

TolQRA subunits of the divisome and that this leads to mis-localization of the Tol-Pal component of the cell division machinery. To test this hypothesis, we compared Pal localization throughout the cell cycle in wild type and *cenK* overexpression strains (Fig 3-3). To do this, we fused the gene encoding mCherry to the Pal coding region to generate a C-terminal fusion of Pal-mCherry expressed from the *pal* locus in both strains. Using this reporter, we observed fluorescence of the Pal-mCherry protein at the poles of wild type cells using fluorescence and bright field microscopy (Fig 3-4). Additionally, wild type cells containing this Pal-mCherry construct exhibited no observable filamentation, chaining, or other cell envelope phenotypes suggesting the presence of this Pal-mCherry translational fusion had no major impact on Tol-Pal activity or function of this part of the divisome.

To model the intracellular localization of Pal-mCherry in wild type cells, we performed a demograph analysis (Fig 3-3C, left panel). Sorting cells by length allowed us to simulate cell cycle dynamics, assuming that length is a suitable indicator of cell cycle progression (29). During the elongation phase of wild type cells, Pal-mCherry fluorescence was focused between the new cell pole and the midcell, while it begins accumulating at the midcell during septum formation. Immediately following cell division in wild type cells, Pal-mCherry fluorescence is predominantly localized at the newly formed cell pole before it begins to diffuse along the length of the cell during elongation. Similar pole-to-midcell localization dynamics have been observed in other Gram-negative bacteria (8, 9, 13) suggesting that the pattern of cell cycle Tol-Pal localization is conserved in *Rb. sphaeroides*.

Figure 3-3. Increased CenKR activity affects the topological localization of the Pal outer membrane lipoprotein. A. Schematic of Tol-Pal OM complex function (27). The interaction of Pal (yellow) with PG and its diffusion through the periplasm is facilitated by interactions with TolB (red). During cell division, recruitment of TolQRA to the midcell sequesters Pal to the septum. **B.** The *tol* and *pal* operons. The *tolQRAB* genes and *pal-cpoB-RSP_0660* are in two transcriptional units in *Rb. sphaeroides*, with known transcriptional start sites indicated (28). Expression of the transcriptional unit containing *tolQRAB* (green) is increased by CenKR activity (show this with a CenR and + sign on the figure). **C.** Pal-mCherry spatial localization during the cell cycle as visualized by fluorescence microscopy. (Left) Demographs of Pal-mCherry displaying normalized fluorescence intensity profiled over the length of wild type cells (y-axis). Heat maps for each cell were combined and sorted by length to model growth and division throughout the cell cycle (x-axis). (Right) Representative micrographs with dotted line showing outlines the shape of cells, scale bar = 2 µm. Accumulation of Pal-mCherry at the division plane is indicated by arrows. **C.** Pal-mCherry localization when cells containing pIND5-*cenR* are grown in the presence of 10 µM IPTG. (Left) Demograph displaying Pal-mCherry normalized fluorescence intensity profiles. (Right) Representative micrographs of cells overexpressing *cenK*, white arrows indicate accumulation of Pal at cell poles and stalled division septum, scale bar = 2 µm.

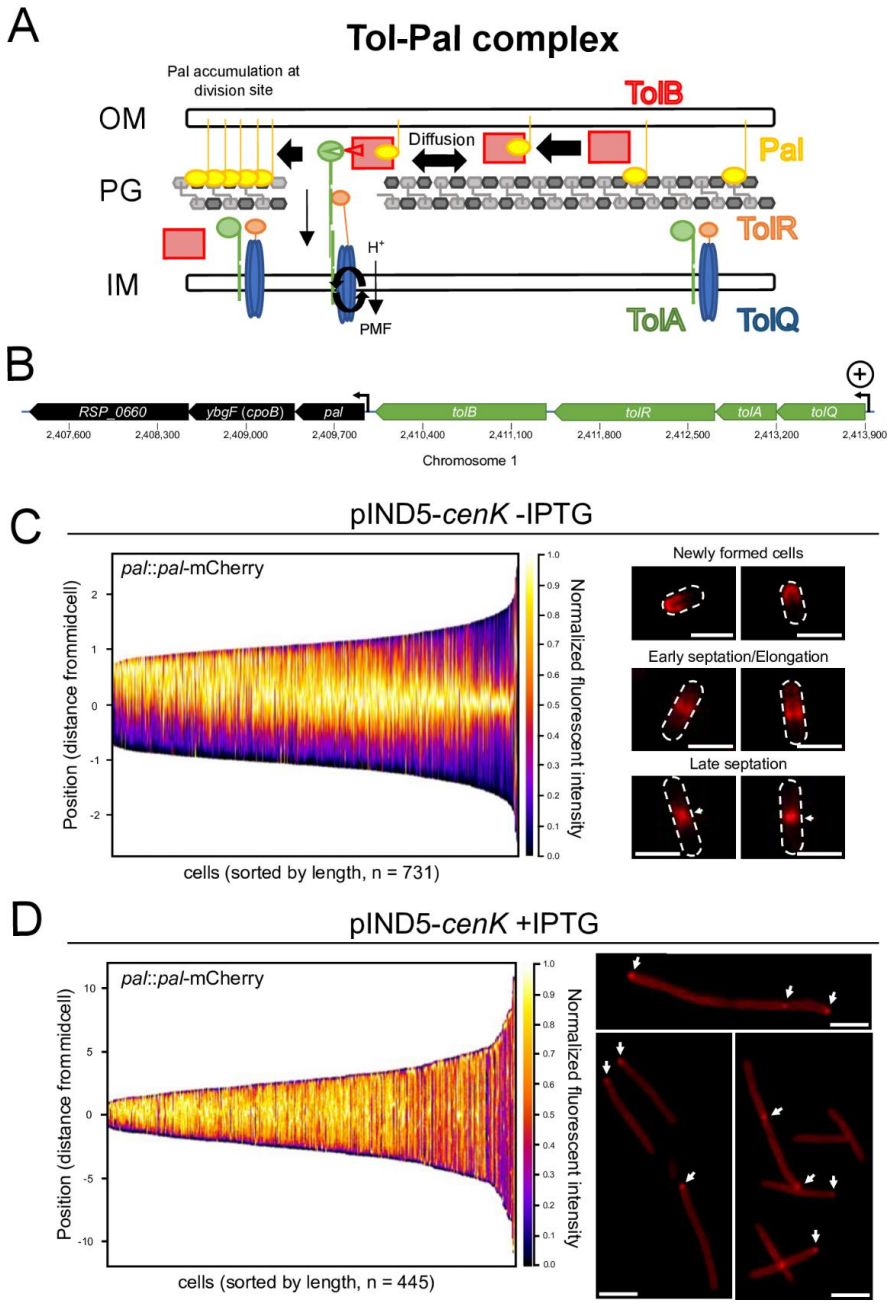
A
Tol-Pal complex
Pal accumulation at division site
TolB
OM
Diffusion
Pal
PG
TolR
H+
IM
PMF
TolA
TolQ
B
RSP_0660
ybgF (cpoB)
pal
tolB
tolR
tolA
tolQ
2,407,600
2,408,300
2,409,000
2,409,700
2,410,400
2,411,100
2,411,800
2,412,500
2,413,200
2,413,900
Chromosome 1
C
pIND5-cenK -IPTG
pal::pal-mCherry
Position (distance from midcell)
Normalized fluorescent intensity
cells (sorted by length, n = 731)
Newly formed cells
Early septation/Elongation
Late septation
D
pIND5-cenK +IPTG
pal::pal-mCherry
Position (distance from midcell)
Normalized fluorescent intensity
cells (sorted by length, n = 445)

Figure 3-4. Pal localization in wild type *Rb. sphaeroides*.

Pal-mCherry spatial localization during the cell cycle as visualized by fluorescence microscopy. (Left) Demographs of Pal-mCherry displaying normalized fluorescence intensity profiled over the length of wild type cells (y-axis). Heat maps for each cell were combined and sorted by length to model growth and division throughout the cell cycle (x-axis). (Right) Representative micrographs with dotted line showing outlines the shape of cells, scale bar = 2 µm. Accumulation of Pal-mCherry at the division plane is indicated by an arrow.

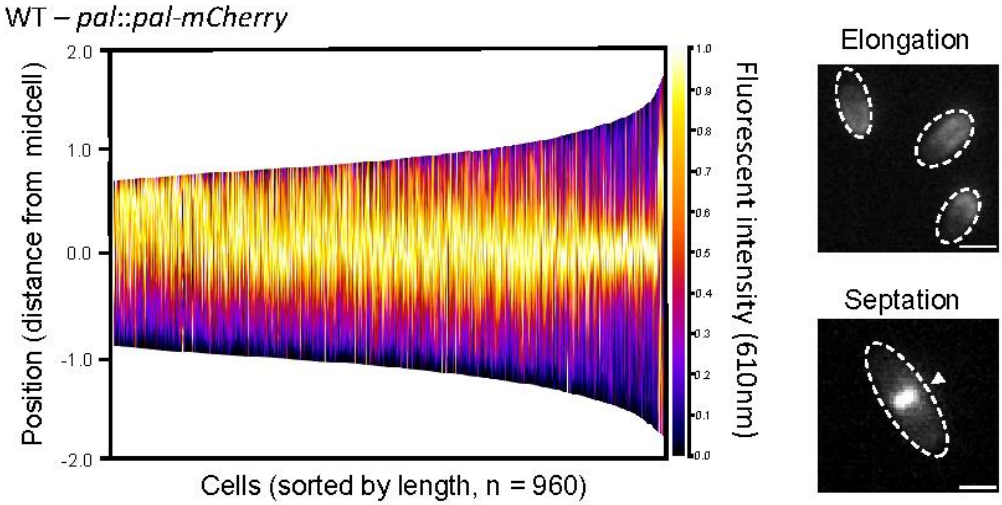

When we monitored localization of Pal-mCherry in cells containing increased CenKR activity (Fig 3-3D), we observed a different pattern of fluorescence. In this strain, a significant fraction of the Pal-mCherry protein was localized at the poles of these filamentous cells (Fig 3-3D, white arrows). We also found that ~75% of the apparent division septa in cells with increased CenKR activity lacked evidence for the accumulation of Pal-mCherry fluorescence. Taken together, these data suggest that the defect in cell division in cells containing increased CenKR activity is associated with a failure to move Pal away from the poles of newly formed cells and relocalize during the cell cycle (Fig 3-3D right panel). Reconstruction of a demograph for cells containing increased CenKR activity predicts that there is widespread distribution of Pal-mCherry fluorescence throughout the cell and suggests a reduced rate of Pal diffusion during the cell cycle in these filaments.

Increased CenKR activity alters PG synthesis. We also know that the CenKR TCS increases the expression of genes encoding members of the elongasome, such as MreB, PBP2, MreC, and RodZ (21). Rod shaped bacteria like *Rb. sphaeroides* often utilize the cytoskeletal homolog MreB to coordinate the localization of the elongation specific transpeptidase (TPase) penicillin-binding protein 2 (PBP2) in order to maintain a rod shape (7, 30). Given the changes in gene expression and the increase in cell length observed when *cenK* is overexpressed, we hypothesized there were changes in PG and cell wall deposition in this strain compared with wild type cells. To test this hypothesis, we first wanted to compare nascent PG synthesis in wild type cells to those with increased CenKR activity. In one approach, we monitored PG biosynthesis by growing cells in the presence of HADA (a fluorescent hydroxycoumarin moiety linked to 3-amino-D-alaine) that can be incorporated into PG via periplasmic enzymes (31, 32). Analyzing

the pattern of fluorescence in exponentially growing wild type cells after a ~30 minute ($1/5^{th}$ doubling time) 'short' pulse with HADA (Fig 3-5A), we observed fluorescence at the midcell that radiates towards the poles as a function of time. During cell division, HADA fluorescence localizes to the septum of wild type cells where the IM and cell wall invaginate prior to OM separation, as predicted from the Cryo-EM analysis. Following cell division, HADA fluorescence localizes to the cell poles of daughter cells before PG synthesis returns to the midcell during cell elongation. The use of a demograph from the HADA incorporation data predicts that PG synthesis is localized to the region between the midcell and the newly synthesized cell pole (Fig 3-5A) consistent with previous analysis of HADA incorporation in wild type *Rb. sphaeroides* (33).

The polar localization of HADA in newly formed wild type cells displayed fluorescence at the cell poles (Fig 3-5A) is consistent with studies in other α-proteobacteria (commonly *Rhizobiales*) that utilize polar synthesis of PG for cell elongation (34). However, it has been shown that MreB localization in *Rb. sphaeroides* is primarily constrained to the midcell (35, 36). It is known that incorporation of HADA reports on the periplasmic activity of D,D-TPases (PBPs) and L,D-TPases that add this fluorescent reporter into the tetrapeptide stems of PG (32). Therefore, we hypothesized that fluorescence at newly formed cell poles may represent residual activity of PG crosslinking enzymes rather than nascent PG synthesis. To test this hypothesis, we used a second method to visualize the process and sites of PG synthesis by cytoplasmic precursor molecules. In this case, we analyzed time-dependent RADA (5-carboxytetramethylrhodamine conjugated to 3-amino-D-alanine) fluorescence. Treatment of exponentially growing wild type cells with a longer pulse of RADA led to uniform PG labelling (Fig 3-5B). By monitoring growth of these labeled

Figure 3-5. Spatial and temporal PG biosynthesis in *Rb. sphaeroides*. A, C. Demographs of HADA normalized fluorescence intensity profiled over cell length (y-axis). Heat maps for each cell were combined and sorted by length to model growth and division throughout the cell cycle (x-axis). Representative micrographs of WT cells (A) those overexpressing *cenK* (C), dotted lines outline the shape of cells, white arrow indicated division septum, scale bar = 2 μm. **B, D.** Time lap microscopy of FDAA (RADA) incorporation (pulse) and dispersion due to nascent PG synthesis (chase) over several cell cycles in WT cells (B) and cells overexpressing *cenK* (D). FDAA heat map intensity profiles and complementary bright field images are shown (dotted red outline of cell shape).

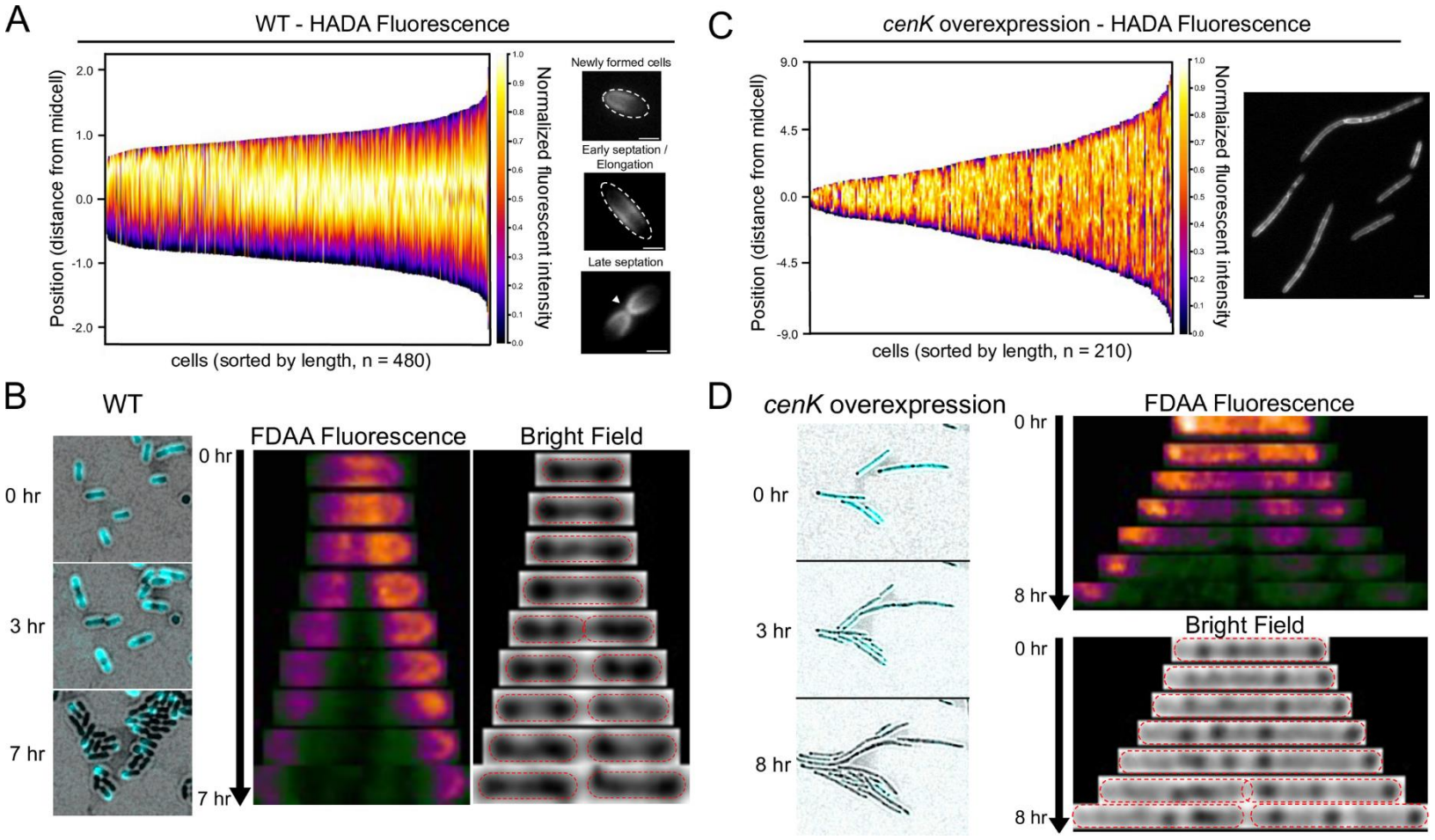
A
WT - HADA Fluorescence
Position (distance from midcell)
cells (sorted by length, n = 480)
Normalized fluorescent intensity
Newly formed cells
Early septation / Elongation
Late septation
C
cenK overexpression - HADA Fluorescence
Position (distance from midcell)
cells (sorted by length, n = 210)
Normlaized fluorescent intensity
B
WT
0 hr
3 hr
7 hr
FDAA Fluorescence
Bright Field
D
cenK overexpression
0 hr
3 hr
8 hr
FDAA Fluorescence
Bright Field

cells after removal of RADA (chase), we observed loss of fluorescence at the midcell expanding towards the poles. Following cell division, the previous poles of each daughter cell retained RADA fluorescence with new PG synthesis (as monitored by increased RADA fluorescence) appearing to initiate from the new midcells (Fig 4B). Combined, these data suggest that wild type *Rb. sphaeroides* uses medial PG synthesis for elongation throughout the cell cycle (Fig 3-5B).

Expanding these analyses to cell overexpressing *cenK*, we observed a different pattern in PG synthesis and cycling using HADA as a reporter (Fig 3-5C). In this strain, the entire length of the cells showed evidence of HADA fluorescence, suggesting that cells with increased CenKR activity are synthesizing PG throughout the cell and have uncoupled elongasome activity from the cell cycle. Indeed, the pattern of HADA fluorescence predicts PG synthesis and separation at the sites of incomplete cell division in the filaments of cells with increased CenKR activity (Fig 3-5C, right pane), similar to the pattern observed for wild type cells at the late stages of septum formation (Fig 3-5A). Further examining spatial synthesis of PG in cells overexpressing *cenK* by monitoring RADA fluorescence (Fig 3-5D), we again observed broad incorporation of RADA throughout the cell length. During the period after RADA was removed, loss fluorescence was observed from several sites suggesting cells with increased CenKR activity initiates and directs PG synthesis and assembly from multiple locations. We also observed a general loss of RADA fluorescence throughout the length of these cells over the course of the analysis. We propose that this loss of RADA fluorescence could reflect increased activity of PG carboxypeptidases or hydrolases that are known CenKR target genes (21) and have been reported to promote PG turnover in other bacteria (32, 37).

Cells with increased CenKR activity are sensitive to PG-active drugs. It has been shown that loss of CenKR activity alters their sensitivity to β-lactam antibiotics that block nascent PG synthesis and detergents that permeabilize the OM (38). Given the observed pattern of PG biosynthesis in cells with increased CenKR activity, we asked if these cells also have altered sensitivity to β-lactam antibiotics. To do this, cells containing the pIND5-*cenK* plasmid were serial diluted and spotted onto plates containing amdinocillin (also known as mecillinam which specifically inhibits PBP2 in *Rb. sphaeroides* (33, 35, 36)) or ampicillin (which inhibits several PBPs (39)) in the presence (+) or absence (-) of IPTG (Fig 3-6A). We found that cells induced for *cenK* expression by growth in the presence of IPTG were more sensitive to either antibiotic compared to control cells and when grown in the absence of IPTG (Fig 3-6A). Many Gram-negative bacteria are naturally resistance to PG active compounds like β-lactam antibiotics, therefore sensitivity to these drugs in cells containing increased CenKR activity supports the conclusion that these cells have defects in OM integrity.

Inhibiting the activity of PBP2 in *Rb. sphaeroides* results in midcell swelling consistent with defects in PG synthesis in this (33, 35, 36) and other Gram-negative bacteria (40, 41). Given the results of analyzing the process of PG synthesis, we asked how this swelling differs in cells with basal and increased CenKR activity. Addition of sub-MIC concentrations of amdinocillin to cells containing pIND5-*cenK* in the absence of IPTG resulted in midcell swelling (Fig 3-6B) consistent with previous analysis of wild type cells (33, 35, 36). Treatment of this same strain with amdinocillin in the presence of IPTG produced filamentous cells and showed evidence for midcell swelling (Fig 3-6B). In the presence of amdinocillin, we observed only one region of swelling per cell following exposure in cells with increased CenKR activity. When this result is

Figure 3-6. Antibiotic treatment of cells overexpressing *cenK*. A. Parent and cells containing pIND5-*cenK* were tested for sensitivity to β-lactam antibiotics in the presence or absence of IPTG. **B, C.** Acute antibiotic treatment of cells with amdinocillin. Bright field and fluorescence micrographs of cells uninduced (-IPTG, Top) and induced (+IPTG, Bottom) for ectopic expression of *cenK*. Scale bar = 2 µm. (A) Amdinocillin (0.5 µg/mL). (B) A22 (10 µg/mL).

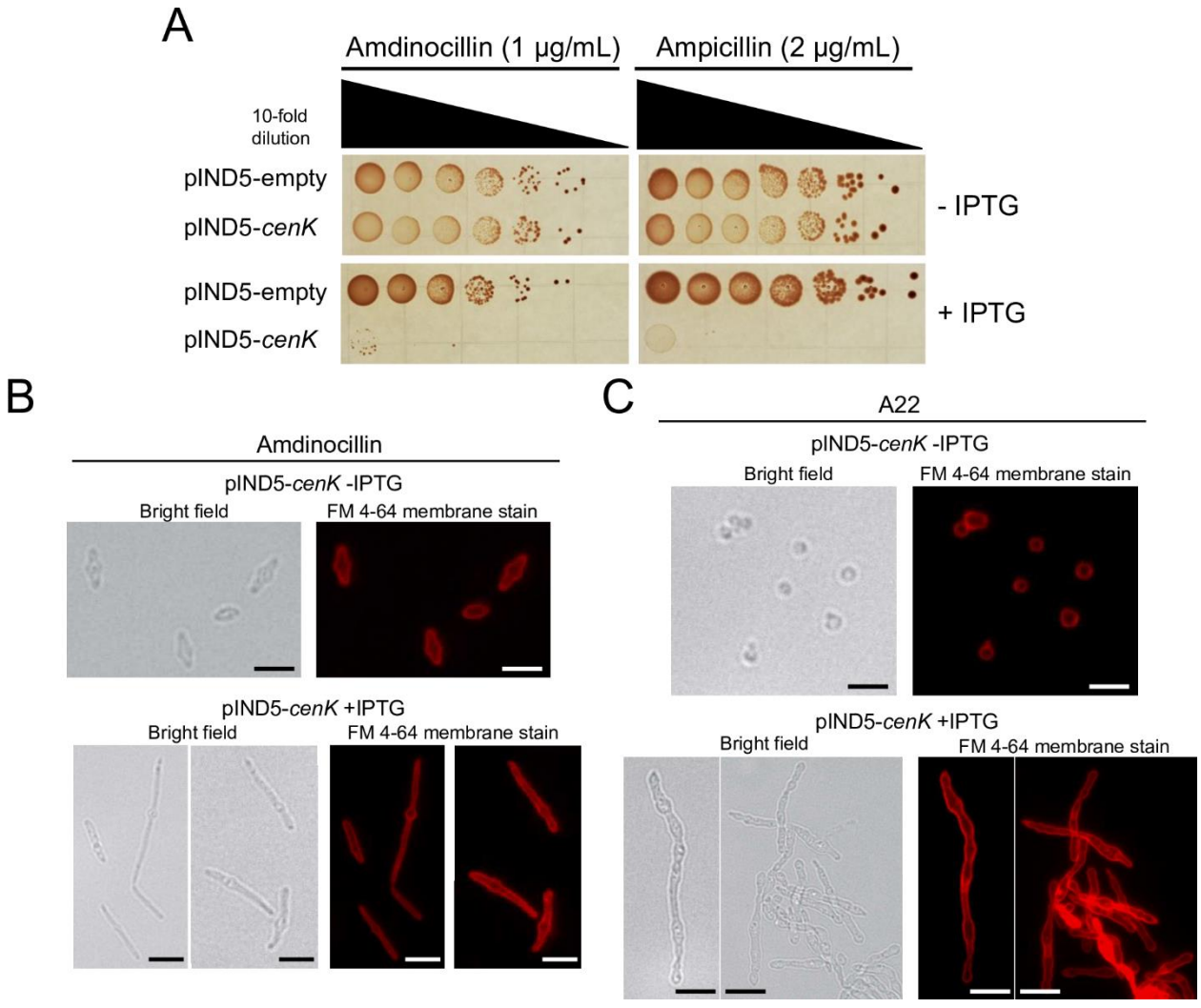

combined with those form fluorescent labelling experiments, it suggests that, while cells with increased CenKR activity appear to initiate PG assembly from several sites (Fig 3-5C-D), PBP2 activity and localization is not required for this behavior.

Others have proposed that swelling of wild type cells treated with amdinocillin was correlated with the localization of the cytoskeletal protein MreB directing PG synthesis at the elongasome (36). Based on this, we tested the impact of treatment with A22, which blocks polymerization of MreB filaments in *Rb. sphaeroides* (33) and other Gram-negative bacteria (42, 43), on wild type cells and those overexpressing *cenK*. We found that treatment of cells containing pIND5-*cenK* with A22 in the absence of IPTG produced small round cells that cannot elongate, consistent with published analysis of wild type cells (33). However, treatment of the cells containing pIND5-*cenK* that were grown in the presence of IPTG with A22 led to filamentous cells with irregular widths (Fig 3-6C). The response of cells with increased CenKR activity to amdinocillin and A22 suggests that PBP2 does not colocalize with MreB in cells overexpressing *cenK*. Furthermore, these data suggest that MreB polymerization occurs throughout the length of the filaments in cells with increased CenKR activity.

Increased CenKR activity alters MreB localization. In many bacteria, MreB is an integral component of the elongasome that serves to localize PG synthesis during cell elongation (3, 44). Given the observed pattern of PG synthesis and the cell swelling produced by A22, we tested if increased CenKR activity affected MreB localization. To do this, we monitored the cellular position of a translational fusion of mCherry-MreB expressed from the native *mreB* locus. Analysis of wild type cells containing this mCherry-MreB fusion shows foci of fluorescence

positioned at the midcell (Fig 3-7A, B top panel). Analysis of the mCherry-MreB fluorescence pattern in wild type cells suggest that MreB remains at the midcell until septum formation after which it moves to the midcell of daughter cells (Fig 6B top panel, D left panel), confirming previous analyses of MreB localization in *Rb. sphaeroides* (35, 36). In cells with increased CenKR activity, we observed mCherry-MreB fluorescence at numerous locations along the length of the filament (Fig 3-7A), and we failed to observe a pattern of opposing foci similar to those seen in wild type cells. Instead, the pattern of mCherry-MreB fluorescence along the entire length of cells with increased CenKR activity predicts that the organization of MreB filaments is mislocalized, providing a likely explanation for the unusual pattern of PG synthesis, initiation, and turnover that was observed in this strain.

FtsZ localization is altered in cells with increased CenKR activity. In *E. coli*, the assembly and position of MreB filaments is proposed to be dependent on the tubulin homolog FtsZ during septation (45–48). The published cell cycle localization pattern of *Rb. sphaeroides* MreB suggest there is also a cooperative relationship between the elongasome and divisome in this bacterium (49). However, the cell division and Pal localization defects observed in cells overexpressing *cenK* prompted us to compare FtsZ localization in wild type cells and this strain. In wild type cells, FtsZ-mCherry fluorescence was observed at the new pole of recently formed daughter cells. During cell elongation, FtsZ fluorescence shifts to the midcell, forming a single band through the midcell plane, at early stages of septum formation which persists throughout cytokinesis and late stages of cell division in wild type cells (Fig 3-7C, B bottom panel). This pattern of fluorescence predicts there is an expected dynamic positioning of FtsZ throughout the

Figure 3-7. Accumulation and localization of MreB and FtsZ in wild type cells and those with increased CenKR activity. A. Fluorescence microscopy of mCherry-MreB localization in cells uninduced (-IPTG) and induced (+IPTG) for ectopic expression of *cenK*. Dotted lines indicate cell boundaries, white arrows indicate location of mCherry-MreB foci, scale bar = 2 μm. **B.** Heat maps of normalized fluorescence maxima intensities of mCherry-MreB (top), HADA (middle), or FtsZ-mCherry (bottom). Cells were binned into four categories based on cell length to simulate cell cycle progression. Representative cell perimeters are displayed by the white boundary lines for each plot. Position of fluorescent maximum was identified for each cell, data were pooled, and relative position and abundance was determined and plotted as a heat map. **C.** Fluorescence microscopy images of FtsZ-mCherry localization in cells uninduced (-IPTG) and induced (+IPTG) for ectopic expression of *cenK*. Dotted lines indicate cell boundaries, white arrows indicate FtsZ-mCherry foci, scale bar = 2 μm. **D.** Density plots of fluorescence maxima for (left) mCherry-MreB (purple), HADA (pink) and (right) FtsZ-mCherry (red). Individual cells were sorted by length to simulate cell cycle progression (y-axis) and the position of the fluorescence maximum along the length of the cell relative to the mid-cell (x-axis = 0) was plotted. Relative density of clustered data points is indicated.

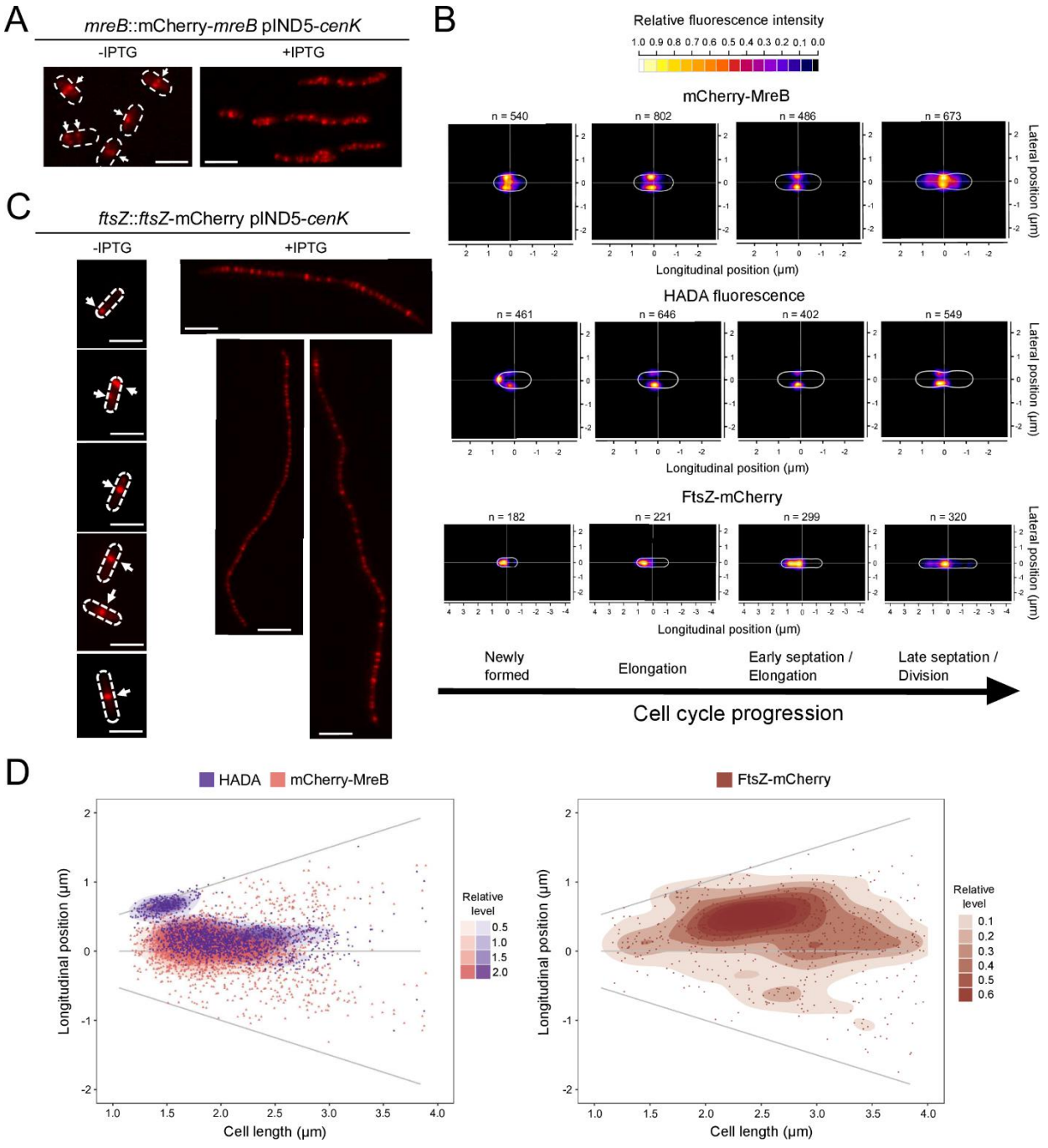
A
mreB::mCherry-mreB pIND5-cenK
-IPTG
+IPTG
B
Relative fluorescence intensity
1.0 0.9 0.8 0.7 0.6 0.5 0.4 0.3 0.2 0.1 0.0
mCherry-MreB
n = 540
n = 802
n = 486
n = 673
Lateral position (µm)
Longitudinal position (µm)
HADA fluorescence
n = 461
n = 646
n = 402
n = 549
Lateral position (µm)
Longitudinal position (µm)
FtsZ-mCherry
n = 182
n = 221
n = 299
n = 320
Lateral position (µm)
Longitudinal position (µm)
Newly formed
Elongation
Early septation / Elongation
Late septation / Division
Cell cycle progression
C
ftsZ::ftsZ-mCherry pIND5-cenK
-IPTG
+IPTG
D
HADA
mCherry-MreB
Longitudinal position (µm)
Cell length (µm)
Relative level
0.5
1.0
1.5
2.0
FtsZ-mCherry
Longitudinal position (µm)
Cell length (µm)
Relative level
0.1
0.2
0.3
0.4
0.5
0.6

cell cycle in wild type cells (Fig 3-7C, D right panel), as has been reported in studies using a FtsZ-YFP translational fusion that was ectopically expressed from a plasmid (49, 50).

In contrast, analysis of FtsZ-mCherry localization in cells overexpressing *cenK* showed fluorescence at regularly spaced intervals along the length of the cell (Fig 3-7C). Moreover, cells containing both the FtsZ-mCherry reporter and pIND5-*cenK* contain even longer filaments when grown in the presence of IPTG (Fig 3-7C) than those lacking the FtsZ fusion, suggesting there is an additive relationship between the CenKR TCS and the function of the FtsZ-mCherry protein during cell division.

Discussion

This work sought to gain additional insight into how previously observed changes in the activity of the essential CenKR envelope stress response TCS activity affects cell morphology in *Rb. sphaeroides* (21). Specifically, we focused on analyzing cell elongation and division scaffolding machinery since the CenKR TCS was previously shown to regulate transcription of many genes that are involved in these systems. Below, we summarize the major new information that has been obtained by analyzing the role of *Rb. sphaeroides* CenKR in cell elongation and division. We also present a working model for how overexpression of the *cenK* impacts cell shape, elongation, and division in *Rb. sphaeroides* (Figure 3-8) and compare the behavior of this α-proteobacterium to what is known in other Gram-negative bacteria. Given the conservation of CenKR and its predicted target genes across α-proteobacteria, we expect that major concepts gleaned from analyzing *Rb. sphaeroides* will be translatable to other bacterial species.

Overexpression of *cenK* is sufficient to increase CenKR TCS activity. We found that ectopic overexpression of *cenK* was sufficient to increase activity of this TCS in a CenR-dependent manner (Fig 1). This observation reveals a somewhat unusual feature of the CenKR TCS since overexpression of a HK often has no impact or lowers activity of a TCS even in the presence of an activating stimulus (51, 52). Rather, canonical TCS are typically sensitive to the levels of RR (53). Indeed, we found that cells overexpressing *cenR* have an increased cell length, likely due to the known binding of non-phosphorylated CenR to promoter sequences (21, 54) or transient phosphorylation by small molecule donors (55). Since overexpression of *cenK* is sufficient to stimulate TCS activity (Fig 1), we propose that the activity of CenK is inhibited by an unknown signal in *Rb. sphaeroides* (Fig 3-8A), as has been reported for some other TCSs (56–58) as well as ones that control several bacterial cell envelope processes (59, 60). CenKR is a direct transcriptional regulator of cell elongation and division, given its role in expression of genes encoding subunits of the Tol-Pal complex (Fig 3-3B), and this TCS activity affects the transcription of cell wall biosynthesis genes (21). Therefore, it is possible that CenKR responds to a signal that is derived from a normal or abnormal temporal cell cycle process. While overexpression of *cenK* is sufficient to stimulate TCS activity in *Rb. sphaeroides* this is not the case in *C. crescentus*, the other α-proteobacterium where CenKR activity has been studied (61). This suggests that the activity of these homologous TCSs is modulated differently between organisms that utilize different modes of cell division (i.e. midcell constriction in *Rb. sphaeroides* vs stalked budding for *C. crescentus*). Additional work is needed to identify the signal(s) that controls CenKR activity and how it may differ among α-proteobacteria, but we were able to analyze cells that overexpress *cenK* to better understand the function of this essential TCS in cell elongation and division.

Figure 3-8. Model for how CenKR activity impacts PG biosynthesis, and cell division machinery in *Rb. sphaeroides*. A. A putative and unknown cell envelope derived ligand blocks CenK activity (see Discussion) **B.** Model for localization of PG biosynthesis, MreB, and FtsZ throughout the cell cycle. **C.** Model to explain the presence of a proposed stalled division septum in cells overexpressing *cenK*. In cells with increased CenKR activity the elevated levels of TolQRAB alter interactions between the IM TolQRA complex and periplasmic TolB, thereby preventing diffusion of Pal throughout the cell length. This interaction between TolQRA and TolB prevents Pal accumulation at division septum leading to disassociation of the IM, OM, and PG layers and incomplete division. Thus, FtsZ is unable to disassemble from the divisome while MreB migrates to the newly-formed midcells and begins another cycle of elongation as in (B).

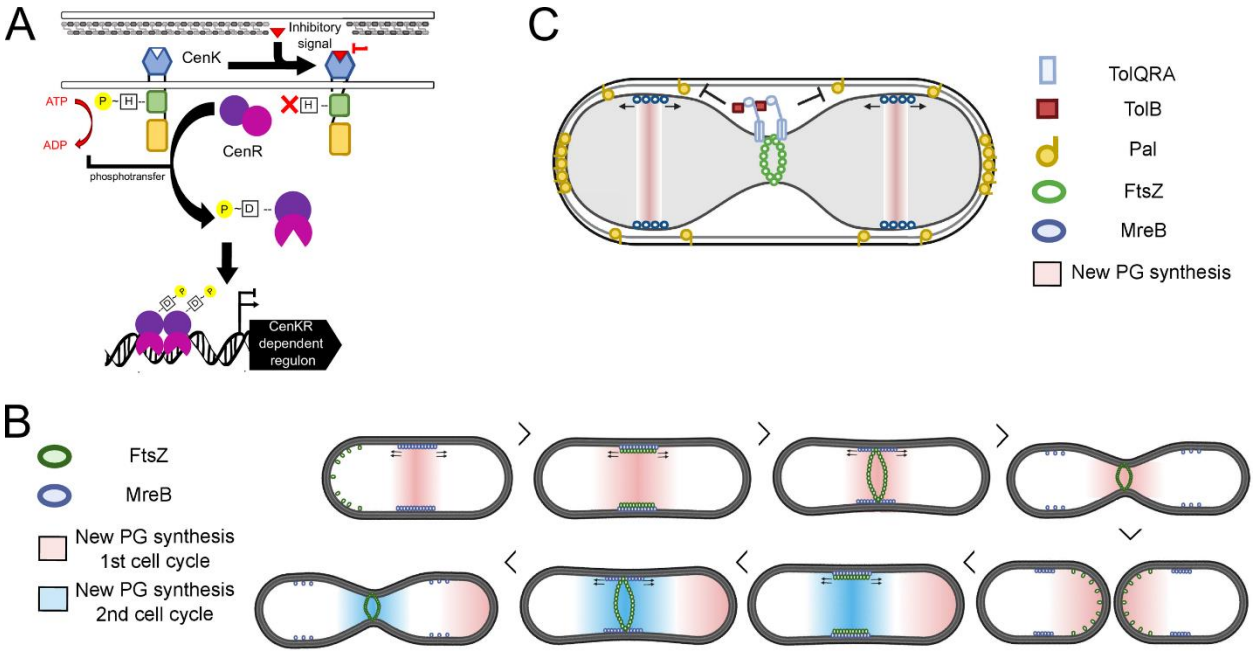

The process of cell elongation and division in *Rb. sphaeroides.* Our analysis of wild type cells agrees with previously reported differences in MreB and FtsZ localization in *Rb. sphaeroides* (35, 36, 49, 50) from that of *E. coli* (45) and *C. crescentus* (46, 47). By tracking MreB, FtsZ, and nascent PG synthesis (Fig 3-5, 3-7) in wild type cells we present the following model for cell elongation and division in *Rb. sphaeroides* (Fig 3-8B).

Both MreB and PG synthesis are localized to the midcell during early stages of cell elongation while FtsZ is localized at the cell pole. As wild type cells elongate, FtsZ repositions to be colocalized with MreB and components of the elongasome at the midcell. In the late stages of cell division, the septum forms and initiates the process of cell envelope invagination. During this process, MreB moves from the 'old' midcell to the midcells of each daughter cell while PG synthesis persists at the pre-existing midcell. Finally, following separation of the daughter cells, MreB redirects PG synthesis and cell elongation from the new midcells while FtsZ is retained at the new poles of each daughter cell.

In other Gram-negative bacteria, FtsZ and MreB interactions are required for septal PG synthesis or at least are heavily colocalized for midcell growth (45, 48, 62). In *E. coli* and *C. crescentus*, FtsZ filaments are proposed to recruit MreB from the lateral cell wall to the midcell, likely promoting function of PBP2, PBP1A, or other proteins required for pre-septal PG synthesis (45). Our data suggests a similar synergistic relationship exists among MreB, FtsZ and pre-septal PG synthesis in *Rb. sphaeroides* (Fig 3-7B). Furthermore, the movement of *Rb. sphaeroides* MreB to the daughter cell midpoles during late stages of cell septation supports a conclusion that MreB plays an important early, but not late, role in directing midcell PG biosynthesis which is directed

by FtsZ. In *C. crescentus* and other α-proteobacteria, MreB midcell localization during septation appears to be conserved (40, 43, 46, 62). However, the dynamic movement of *Rb. sphaeroides* FtsZ from the midcell to the new pole and the relatively continual presence of MreB at the midcell, suggests MreB may facilitate migration of FtsZ to the midcell at the time of cell division (Fig 3-7). Furthermore, our data supports the interconnected function of these two scaffolding proteins and suggest that while cell elongation and division are often thought of as two distinct processes, we speculate that in *Rb. sphaeroides*, these modes of PG synthesis are synergistic.

The impacts of increased CenKR activity on cell elongation and division. In cells with increased CenKR activity, we observed filamentous and chained cells along with evidence of asymmetric cell division (Fig 3-2). In other bacteria, filamentation is associated with a delay in initiating cell division (63), while chaining is a phenotype commonly linked to loss of Tol-Pal function (13, 64–67). Consistent with this, we observed Pal retention at cell poles and immobilization along the length of the cell in cells overexpressing *cenK* (Fig 3-3), a property normally attributed to TolA or TolB loss of function mutants in *E. coli* (8, 68, 69). The known increase in *tolQRAB* transcript levels in cells with increased CenKR activity (21) leads us to propose that increasing TolQRA-B complex levels prevent TolB from forming a normal TolB-Pal complex that can diffuse through the cells, as predicted by the mobilization-capture model of Tol-Pal function (8, 69). When individual components of the Tol-Pal system were overexpressed in *E. coli*, the filamentation observed when *tolQ* was overexpressed was proposed to represent a defect in septum PG synthesis caused by TolQ sequestration of FtsN (70). By increasing the activity of CenKR, we are able observe the predicted impacts of increasing TolQRAB complexes and how this alters function of the Tol-Pal complex.

We propose that the failure of cells overexpressing *cenK* to sequester Pal at the division septum delays OM migration and comigration with the IM during midcell constriction. In cells with increased CenKR activity, we also observed instances where the inner membranes of daughter cells remain connected through narrow channels suggesting that OM migration is vital to finish cytokinesis. In this strain, cells continue to elongate, initiate cell division, and assemble PG along the length of the cells a product of the continued dynamics of MreB and FtsZ repositioning. Thus, cells overexpressing *cenK* assemble PG along the length of the cells despite having not finished the separation of daughter cells in the prior cell cycle. This observation is consistent with our previous finding that the CenKR TCS affects transcription of PG biosynthetic genes clusters, activating genes encoding elongasome components while repressing genes encoding known subunits of the divisome (21).

Given the observed changes in the localization of the Pal lipoprotein and division septum in cells with increased CenKR activity, we propose that overexpression of *cenK* delays cell division by promoting Pal-PG interconnectivity away from the midcell. Lipoprotein-PG interconnection are known to be vital for the normal interactions between the OM and PG layers as well as regulating periplasmic width (1). However, the *E. coli* Lpp protein which provides this function in this and many other Gram-negative bacteria has no known homolog in α-proteobacteria. Disruption of Lpp and OM-PG interconnectivity has been linked in changes in periplasmic distance (71), but in α-proteobacteria periplasmic width has been proposed to result from linkage of β-barrel proteins to PG in *Rhizobiales* (72). While additional work is needed to understand the interactions of PG synthesis during cell elongation and division, our data suggests that the

impacts of CenKR activity on Pal localization plays an important role in PG synthesis and the state of the periplasm in *Rb. sphaeroides*. It is possible that CenKR activity is regulated by the interaction of the CenK kinase with an envelope derived ligand to ensures or responds to Pal-PG and OM-interactions during cell elongation and division.

In other bacteria, genetic or other changes that inhibit MreB-FtsZ interactions block division, cause filamentation, and result in regularly spaced FtsZ-rings along the length of the cell (45, 73). The produces a similar phenotype to what we observed in cells overexpressing *cenK* in which Z-rings appear to be 'locked' along the length of the cell (Fig 3-7). In *E coli* and *C. crescentus*, these regularly spaced FtsZ-rings can result in improper recruitment of PBPs and MreB-directed TPases such as PBP2 that are required for early septation (45, 46). In contrast, when we treat cells overexpressing *cenK* with antibiotics that block MreB polymerization we observed cell elongation suggesting that FtsZ accumulation is sufficient to allow cell elongation in the absence of MreB filaments. Furthermore, treatment of cells overexpressing *cenK* with antibiotics that block PBP2 activity results in a localized cellular response suggesting that altered localization of MreB alone is not sufficient to affect PBP2 activity or its movement during elongation (Fig 3-6). Taken together, this suggests that completion of cell division and OM constriction in *Rb. sphaeroides* is required for FtsZ ring depolymerization and elongasome movement. Additionally, these 'locked' Z-rings configuration is sufficient to continue PG synthesis and cell elongation in a PBP2 independent manner suggesting redundant functions of FtsZ coordinated PBPs in *Rb. sphaeroides*.

In sum, our studies have provided new insights, posed additional questions and provided approaches which can be used to dissect cell elongation and division in α-proteobacteria. Given the phenotypes observed in cells overexpressing *cenK* and the number of genes encoding IM, periplasmic or OM proteins that are direct or indirect targets of CenKR activity, we propose that the analysis of other regulon members can provide new insights into the dynamic localization of PG biosynthesis, MreB/FtsZ positioning and depolymerization, secondary functions of Tol-Pal, independent movement and function of PBP2, and other division associated processes. For example, α-proteobacteria like *Rb. sphaeroides*, encodes CpoB (which is co-transcribed with *pal*) but lack genes encoding homologs of the OM lipoproteins LpoA/LpoB. Thus, the proposed role for the Tol complex in the regulation of CpoB-LpoB connection and PBP1b's TPase activity at division septum (6) might not be applicable to *Rb. sphaeroides* and other α-proteobacteria. Interestingly, genes encoding a number of lipoproteins of unknown function are differentially expressed in CenKR mutants (21), including one (*RSP_1200*) which when disrupted results in protrusions from the midcell septum suggesting a role in division (38). In addition, disruptions in Tol-Pal interactions in other bacteria have been reported to lead to vesicle secretion (67, 74) similar to what we observed either in cells overexpressing *cenK* or in high lipid mutants that contain mutations blocking CenKR function (38). Thus, additional analysis of how CenKR activity impacts cellular processes can provide important new insights into the lifestyle of *Rb. sphaeroides*, other α-proteobacteria, and additional Gram-negative bacteria.

Materials and Methods

Bacterial strains and growth conditions. *Rb. sphaeroides* strains (Table 3-1B) were grown in Sistrom's (SIS) minimal medium (75). Unless specified, cultures of 10 mL were grown in 125

mL flasks with shaking at 200 rpm, at 30°C for ~18 hours until cells reached an OD_{600} of ~0.5 (mid exponential growth). *E. coli* strains (Table 3-1B) were grown at 37°C in Luria-Bertani medium. As needed, media was supplemented with 50 µg/mL kanamycin and/or 10 µM IPTG. For growth experiments, cell density was measuring using a Klett-Summerson colorimeter equipped with a number 66 filter.

For treatment with previously determined (33) sub-MIC A22 (10 µg/mL, Caymen Chemical) or amdinocillin (mecillinam 0.5 µg/mL, Fisher Scientific) a single colony of *Rb. sphaeroides* was grown in SIS medium overnight. Cell cultures were then diluted to an OD_{600} ~ 0.05 with the addition of antibiotic and IPTG (10 µM) as appropriate. Cells were grown for 6 hrs (~2 doubling times) before imaging. For FM 4-64 stain (Setareh Biotech) a final concentration of 1 µg/mL was added to a small portion of culture before imaging (see below).

***Strain construction*.** All strains, primers, and plasmids used in this study are listed in Table 3-1. Construction of pIND5-*cenR* or pIND5-*cenK* was performed by PCR amplification of *cenR* or *cenK* from *Rb. sphaeroides* genomic DNA using Herculse II Fusion DNA Polymerase (Agilent). PCR products were assembled into PCR linearized pIND5 vector by Gibson Assembly (New England BioLabs) and transformed into DH5α cells (New England BioLabs). Transformants were screened by colony PCR and sequenced to confirm there were no mutations in coding regions. Plasmids were mobilized into *Rb. sphaeroides* via conjugal mating with *E. coli* S17-1 (76). Colony PCR of Kan^R *Rb. sphaeroides* colonies was used to confirm successful mobilization of pIND5-*cenR* or pIND5-*cenK*. Translational fusions to fluorescent reporters were constructed by allelic exchange using the suicide vector pk18mobsacB (77) as described previously (21).

Gene insertions were confirmed by colony PCR of chromosomal loci and sequencing of genomic DNA with gene specific primers (Table 3-1A).

***Serial dilution spot titer assays*.** A single colony of *Rb. sphaeroides* was inoculated into 5 mL SIS medium with antibiotic as needed and was grown with shaking at 30°C overnight. Once cultures reached an OD_{600} of 0.4-0.6, they were diluted to an OD_{600} of 0.3 in 1 mL SIS. In a 96-well plate, 10 µL of dilute culture was serially diluted into 90 µL SIS. On SIS agar plates containing ampicillin (2 µg/mL), amdinocillin (1 µg/mL), and when appropriate IPTG (10 µM), 5 µL of the dilution series was spotted, allowed to dry, and then incubated at 30°C until growth was observed (~ 2 days). Spot titer SIS plates were made fresh the day they were used, antibiotics were added directly to melted SIS agar. Plates were dried at RT for 3 hrs before use. Spot titers were performed in triplicate.

***Fluorescence microscopy*.** All strains were grown as described above to an OD_{600} ~ 0.5. Cells (1 µL of culture) was immobilized on a coverslip with a 1.5% agarose gel pad. Images were taken using an EVOS FL microscopy with 100X oil immersion PLAN Apochromat objective (numerical aperture, 1.40). The EVOS light cube Texas Red (for mCherry signal) was used to capture fluorescence signals. For cell segmentation, all pictures were treated in FIJI (78): bandpass (large filter, 40 pixels; small filter, 2 pixels), background subtraction (rolling ball radius = 20 pixels), and contrast enhancing with normalization (0.1%). When required, Z-stacks from different channels were taken one immediately following another. Segmentation was performed using the plugin MicrobJ (79) and cell segmentation errors were manually removed.

Cell shape parameters were extracted, figures and statistical analysis were performed in Rstudio using ggplot2 package (80).

***Cryo-electron microscopy*.** A 5 μL sample of each culture was deposited three times onto glow discharged 200 mesh R2/1 copper Quantifoil grids for 1 min. The first two 5 μL applications were manually blotted away after 1 min using Whatman number 1 filter paper before the next 5 μL application. The third 5 μL sample was applied along with 4 uL of 10 nm BSA Gold tracers (Electron Microscopy Sciences). After a 1 min incubation the sample was blotted and plunge frozen in liquid ethane using a Vitrobot Mark IV (ThermoScientific). Cryo-electron microscopy (cryo-EM) and cryo-electron tomography (cryo-ET) data were collected using a Titan Krios TEM (ThermoScientific) operated at 300 kV, equipped with a Bioquantum energy filter and a K3 direct electron detector (Gatan). Single axis tilt series were acquired bidirectionally using SerialEM (81), with a tilt increment of 2° covering −60° to +60° and a cumulative dose under 120 e-/Å2 at a nominal defocus range between −4 and −10 μm.

***Cell measurements and segmentation models*.** Tomograms were reconstructed using IMOD/eTomo (82). Post processing of tomograms used low pass filtered to 80 angstroms using imod or were processed with the SIRT-like filter equivalent to 6 iterations using etomo. Measurements of the distance between the IM, OM and PG layer were collected using the measurement tools in IMOD. 3-Dimensional rendering of cells was performed using EMAN2 neural network segmentation training (83). Between 20 to 80 boxes from each tomogram were segmented per feature (OM, IM, and extracellular vesicles) and the neural networks trained using

the recommended settings provided in the EMAN2 segmentation tutorial. Models were visualized in chimeraX (84).

***HADA and RADA labeling*.** A single colony of *Rb. sphaeroides* was inoculated into SIS medium with appropriate antibiotic and grown overnight. Cells were then diluted to an OD_{600} of 0.05 in 10 mL SIS medium, with antibiotic and IPTG when appropriate, and grown to early log phase OD_{600} ~ 0.2. To the culture, a final concentration of 0.5 mM HADA (Tocris Bioscience) was added and incubated for 30 min with shaking at 30°C. Then, 1 mL of cells was pelleted and washed with PBS three times to remove excess dye, resuspended in 200 µL PBS and visualized by microscopy as described above. DAPI (4′,6-diamidino-2-phenylindole) EVOS light cube was used to capture fluorescence signal.

For RADA (Tocris Bioscience) time-lapse, a single colony of *Rb. sphaeroides* was inoculated into SIS medium and grown overnight. Cultures were grown as described above. Following dilution, once cells reached early log phase OD_{600} ~ 0.2 to the culture a final concentration of 100 µM RADA was added and incubated for 30 min with shaking at 30°C. Then 1 mL of cells was pelleted and washed with SIS medium three times to remove excess dye. Cells were resuspended in 1 mL of SIS with kanamycin when appropriate. 2 µL of culture was placed inside an Ibidi slide chamber under a 1.5% agarose pad containing SIS medium and supplemented with 50 µg/mL kanamycin and 10 µM IPTG when appropriate. Cells were imaged by microscopy as described above. Texas Red Evos light cube was used to capture fluorescence signal.

Acknowledgements.

We thank Rachelle A. Lemke (UW – Madison), Kevin S. Myers (UW – Madison), and Katherine J. Wozniak (University of Michigan), as well as other members of the lab for helpful discussion and feedback. This work was supported by the Great Lakes Bioenergy Research Center (https://www.glbrc.org), U.S. Department of Energy, Office of Science, Office of Biological and Environmental Research (https://www.energy.gov/science/ber/biological-and-environmental-research) (award DE-SC0018409 to T. J. D.). Additional funding provided by the National Science Foundation Graduate Research Fellowship Program (Grant No. DGE-1747503 to B.D.L. (https://www.nsfgrfp.org)), National Institute of Health Genetics Predoctoral Training Program award (T32 GM007133 to B.D.L.), and the Foster Wisconsin Idea Fellowship, UW-Madison, Department of Bacteriology (to B.D.L.).

References

1. Silhavy TJ, Kahne D, Walker S. 2010. The Bacterial Cell Envelope. Cold Spring Harb Perspect Biol 2:a000414.

2. Levin PA, Janakiraman A. 2021. Localization, Assembly, and Activation of the Escherichia coli Cell Division Machinery. EcoSal Plus 9:eESP00222021.

3. Liu X, Biboy J, Consoli E, Vollmer W, Blaauwen T den. 2020. MreC and MreD balance the interaction between the elongasome proteins PBP2 and RodA. PLOS Genetics 16:e1009276.

4. Williams MA, Kysela DT, Brown PJB. 2022. Diversity of Growth Patterns in the Alphaproteobacteria, p. 185–220. *In* Biondi, E (ed.), Cell Cycle Regulation and Development in Alphaproteobacteria. Springer International Publishing, Cham.

5. Typas A, Banzhaf M, van den Berg van Saparoea B, Verheul J, Biboy J, Nichols RJ, Zietek M, Beilharz K, Kannenberg K, von Rechenberg M, Breukink E, den Blaauwen T, Gross CA, Vollmer W. 2010. Regulation of peptidoglycan synthesis by outer membrane proteins. Cell 143:1097–1109.

6. Gray AN, Egan AJ, van't Veer IL, Verheul J, Colavin A, Koumoutsi A, Biboy J, Altelaar AFM, Damen MJ, Huang KC, Simorre J-P, Breukink E, den Blaauwen T, Typas A, Gross CA, Vollmer W. 2015. Coordination of peptidoglycan synthesis and outer membrane constriction during Escherichia coli cell division. eLife 4:e07118.

7. Egan AJF, Errington J, Vollmer W. 2020. Regulation of peptidoglycan synthesis and remodelling. 8. Nat Rev Microbiol 18:446–460.

8. Petiti M, Serrano B, Faure L, Lloubes R, Mignot T, Duché D. 2019. Tol Energy-Driven Localization of Pal and Anchoring to the Peptidoglycan Promote Outer-Membrane Constriction. Journal of Molecular Biology 431:3275–3288.

9. Szczepaniak J, Holmes P, Rajasekar K, Kaminska R, Samsudin F, Inns PG, Rassam P, Khalid S, Murray SM, Redfield C, Kleanthous C. 2020. The lipoprotein Pal stabilises the bacterial outer membrane during constriction by a mobilisation-and-capture mechanism. Nat Commun 11:1305.

10. Yakhnina AA, Bernhardt TG. 2020. The Tol-Pal system is required for peptidoglycan-cleaving enzymes to complete bacterial cell division. Proc Natl Acad Sci USA 117:6777–6783.

11. Chien A-C, Hill NS, Levin PA. 2012. Cell Size Control in Bacteria. Curr Biol 22:R340–R349.

12. Burger BT, Imam S, Scarborough MJ, Noguera DR, Donohue TJ. Combining Genome-Scale Experimental and Computational Methods To Identify Essential Genes in Rhodobacter sphaeroides. mSystems 2:e00015-17.

13. Yeh Y-C, Comolli LR, Downing KH, Shapiro L, McAdams HH. 2010. The Caulobacter Tol-Pal Complex Is Essential for Outer Membrane Integrity and the Positioning of a Polar Localization Factor. Journal of Bacteriology 192:4847–4858.

14. Krol E, Yau HCL, Lechner M, Schäper S, Bange G, Vollmer W, Becker A. Tol-Pal System and Rgs Proteins Interact to Promote Unipolar Growth and Cell Division in Sinorhizobium meliloti. mBio 11:e00306-20.

15. Saha S, Lach SR, Konovalova A. 2021. Homeostasis of the Gram-negative cell envelope. Current Opinion in Microbiology 61:99–106.

16. Grabowicz M, Silhavy TJ. 2017. Envelope Stress Responses: An Interconnected Safety Net. Trends in Biochemical Sciences 42:232–242.

17. Zahrt TC, Deretic V. 2000. An Essential Two-Component Signal Transduction System in Mycobacterium tuberculosis. Journal of Bacteriology 182:3832–3838.

18. Gorla P, Plocinska R, Sarva K, Satsangi AT, Pandeeti E, Donnelly R, Dziadek J, Rajagopalan M, Madiraju MV. 2018. MtrA Response Regulator Controls Cell Division and Cell Wall Metabolism and Affects Susceptibility of Mycobacteria to the First Line Antituberculosis Drugs. Front Microbiol 9:2839.

19. Dörr T, Alvarez L, Delgado F, Davis BM, Cava F, Waldor MK. 2016. A cell wall damage response mediated by a sensor kinase/response regulator pair enables beta-lactam tolerance. Proc Natl Acad Sci U S A 113:404–409.

20. Dubrac S, Bisicchia P, Devine KM, Msadek T. 2008. A matter of life and death: cell wall homeostasis and the WalKR (YycGF) essential signal transduction pathway. Molecular Microbiology 70:1307–1322.

21. Lakey BD, Myers KS, Alberge F, Mettert EL, Kiley PJ, et al. (2022) The essential Rhodobacter sphaeroides CenKR two-component system regulates cell division and envelope biosynthesis. PLOS Genetics 18(6): e1010270.

22. Ind AC, Porter SL, Brown MT, Byles ED, de Beyer JA, Godfrey SA, Armitage JP. 2009. Inducible-Expression Plasmid for Rhodobacter sphaeroides and Paracoccus denitrificans. Appl Environ Microbiol 75:6613–6615.

23. Lord SJ, Velle KB, Mullins RD, Fritz-Laylin LK. 2020. SuperPlots: Communicating reproducibility and variability in cell biology. Journal of Cell Biology 219.

24. Tai SP, Kaplan S. 1985. Intracellular localization of phospholipid transfer activity in Rhodopseudomonas sphaeroides and a possible role in membrane biogenesis. Journal of Bacteriology 164:181–186.

25. Smith JG, Latiolais JA, Guanga GP, Pennington JD, Silversmith RE, Bourret RB. 2004. A search for amino acid substitutions that universally activate response regulators. Molecular Microbiology 51:887–901.

26. Yilmaz LS, Kontur WS, Sanders AP, Sohmen U, Donohue TJ, Noguera DR. 2010. Electron Partitioning During Light- and Nutrient-Powered Hydrogen Production by Rhodobacter sphaeroides. Bioenerg Res 3:55–66.

27. Szczepaniak J, Press C, Kleanthous C. 2020. The multifarious roles of Tol-Pal in Gram-negative bacteria. FEMS Microbiol Rev 44:490–506.

28. Myers KS, Vera JM, Lemmer KC, Linz AM, Landick R, Noguera DR, Donohue TJ. Genome-Wide Identification of Transcription Start Sites in Two Alphaproteobacteria, Rhodobacter sphaeroides 2.4.1 and Novosphingobium aromaticivorans DSM 12444. Microbiology Resource Announcements 9:e00880-20.

29. Taheri-Araghi S, Bradde S, Sauls JT, Hill NS, Levin PA, Paulsson J, Vergassola M, Jun S. 2015. Cell-Size Control and Homeostasis in Bacteria. Current Biology 25:385–391.

30. Typas A, Banzhaf M, Gross CA, Vollmer W. 2012. From the regulation of peptidoglycan synthesis to bacterial growth and morphology. Nat Rev Microbiol 10:123–136.

31. Hsu Y-P, Rittichier J, Kuru E, Yablonowski J, Pasciak E, Tekkam S, Hall E, Murphy B, Lee TK, Garner EC, Huang KC, Brun YV, VanNieuwenhze MS. 2017. Full color palette of fluorescent D-amino acids for in situ labeling of bacterial cell walls. Chem Sci 8:6313–6321.

32. Kuru E, Radkov A, Meng X, Egan A, Alvarez L, Dowson A, Booher G, Breukink E, Roper DI, Cava F, Vollmer W, Brun Y, VanNieuwenhze MS. 2019. Mechanisms of Incorporation for D -Amino Acid Probes That Target Peptidoglycan Biosynthesis. ACS Chem Biol 14:2745–2756.

33. Lin T-Y, Gross WS, Auer GK, Weibel DB. 2019. Cardiolipin Alters Rhodobacter sphaeroides Cell Shape by Affecting Peptidoglycan Precursor Biosynthesis. mBio 10:e02401-18.

34. Williams MA, Aliashkevich A, Krol E, Kuru E, Bouchier JM, Rittichier J, Brun YV, VanNieuwenhze MS, Becker A, Cava F, Brown PJB. 2021. Unipolar Peptidoglycan Synthesis in the Rhizobiales Requires an Essential Class A Penicillin-Binding Protein. mBio 12:e02346-21.

35. Slovak PM, Wadhams GH, Armitage JP. 2005. Localization of MreB in Rhodobacter sphaeroides under Conditions Causing Changes in Cell Shape and Membrane Structure. Journal of Bacteriology 187:54–64.

36. Slovak PM, Porter SL, Armitage JP. 2006. Differential Localization of Mre Proteins with PBP2 in Rhodobacter sphaeroides. Journal of Bacteriology 188:1691–1700.

37. Peters K, Kannan S, Rao VA, Biboy J, Vollmer D, Erickson SW, Lewis RJ, Young KD, Vollmer W. 2016. The Redundancy of Peptidoglycan Carboxypeptidases Ensures Robust Cell Shape Maintenance in Escherichia coli. mBio 7:e00819-16.

38. Lemmer KC, Zhang W, Langer SJ, Dohnalkova AC, Hu D, Lemke RA, Piotrowski JS, Orr G, Noguera DR, Donohue TJ. Mutations That Alter the Bacterial Cell Envelope Increase Lipid Production. mBio 8:e00513-17.

39. Kong K-F, Schneper L, Mathee K. 2010. Beta-lactam Antibiotics: From Antibiosis to Resistance and Bacteriology. APMIS 118:1–36.

40. Wagner JK, Galvani CD, Brun YV. 2005. Caulobacter crescentus Requires RodA and MreB for Stalk Synthesis and Prevention of Ectopic Pole Formation. J Bacteriol 187:544–553.

41. Spratt BG. 1977. The mechanism of action of mecillinam. Journal of Antimicrobial Chemotherapy 3:13–19.

42. Bean GJ, Flickinger ST, Westler WM, McCully ME, Sept D, Weibel DB, Amann KJ. 2009. A22 disrupts the bacterial actin cytoskeleton by directly binding and inducing a low-affinity state in MreB. Biochemistry 48:4852–4857.

43. Takacs CN, Poggio S, Charbon G, Pucheault M, Vollmer W, Jacobs-Wagner C. 2010. MreB Drives De Novo Rod Morphogenesis in Caulobacter crescentus via Remodeling of the Cell Wall. J Bacteriol 192:1671–1684.

44. Egan AJF, Errington J, Vollmer W. 2020. Regulation of peptidoglycan synthesis and remodelling. 8. Nat Rev Microbiol 18:446–460.

45. 2013. Direct interaction of FtsZ and MreB is required for septum synthesis and cell division in Escherichia coli. The EMBO Journal 32:1953–1965.

46. Figge RM, Divakaruni AV, Gober JW. 2004. MreB, the cell shape-determining bacterial actin homologue, co-ordinates cell wall morphogenesis in Caulobacter crescentus. Molecular Microbiology 51:1321–1332.

47. Gitai Z, Dye N, Shapiro L. 2004. An actin-like gene can determine cell polarity in bacteria. Proceedings of the National Academy of Sciences 101:8643–8648.

48. Vats P, Rothfield L. 2007. Duplication and segregation of the actin (MreB) cytoskeleton during the prokaryotic cell cycle. Proceedings of the National Academy of Sciences 104:17795–17800.

49. Chiu S-W, Roberts MAJ, Leake MC, Armitage JP. 2013. Positioning of chemosensory proteins and FtsZ through the Rhodobacter sphaeroides cell cycle. Molecular Microbiology 90:322–337.

50. Dubarry N, Willis CR, Ball G, Lesterlin C, Armitage JP. 2019. In Vivo Imaging of the Segregation of the 2 Chromosomes and the Cell Division Proteins of Rhodobacter sphaeroides Reveals an Unexpected Role for MipZ. mBio 10:e02515-18.

51. Batchelor E, Goulian M. 2003. Robustness and the cycle of phosphorylation and dephosphorylation in a two-component regulatory system. Proceedings of the National Academy of Sciences 100:691–696.

52. Shinar G, Milo R, Martínez MR, Alon U. 2007. Input–output robustness in simple bacterial signaling systems. Proceedings of the National Academy of Sciences 104:19931–19935.

53. Lazar JT, Tabor JJ. 2021. Bacterial two-component systems as sensors for synthetic biology applications. Current Opinion in Systems Biology 28:100398.

54. Gao R, Bouillet S, Stock AM. 2019. Structural Basis of Response Regulator Function. Annual Review of Microbiology 73:175–197.

55. Lukat GS, McCleary WR, Stock AM, Stock JB. 1992. Phosphorylation of bacterial response regulator proteins by low molecular weight phospho-donors. Proc Natl Acad Sci USA 89:718–722.

56. Heermann R, Jung K. 2010. The complexity of the 'simple' two-component system KdpD/KdpE in Escherichia coli. FEMS Microbiology Letters 304:97–106.

57. David M, Daveran M-L, Batut J, Dedieu A, Domergue O, Ghai J, Hertig C, Boistard P, Kahn D. 1988. Cascade regulation of nif gene expression in Rhizobium meliloti. Cell 54:671–683.

58. Wang B, Zhao A, Novick RP, Muir TW. 2014. Activation and Inhibition of the Receptor Histidine Kinase AgrC Occurs through Opposite Helical Transduction Motions. Molecular Cell 53:929–940.

59. Wall EA, Majdalani N, Gottesman S. 2020. IgaA negatively regulates the Rcs Phosphorelay via contact with the RcsD Phosphotransfer Protein. PLOS Genetics 16:e1008610.

60. Hews CL, Cho T, Rowley G, Raivio TL. 2019. Maintaining Integrity Under Stress: Envelope Stress Response Regulation of Pathogenesis in Gram-Negative Bacteria. Frontiers in Cellular and Infection Microbiology 9.

61. Skerker JM, Prasol MS, Perchuk BS, Biondi EG, Laub MT. 2005. Two-Component Signal Transduction Pathways Regulating Growth and Cell Cycle Progression in a Bacterium: A System-Level Analysis. PLOS Biology 3:e334.

62. van Teeseling MCF. 2021. Elongation at Midcell in Preparation of Cell Division Requires FtsZ, but Not MreB nor PBP2 in Caulobacter crescentus. Frontiers in Microbiology 12.

63. Bos J, Zhang Q, Vyawahare S, Rogers E, Rosenberg SM, Austin RH. 2015. Emergence of antibiotic resistance from multinucleated bacterial filaments. Proceedings of the National Academy of Sciences 112:178–183.

64. Heilpern AJ, Waldor MK. 2000. CTXφ Infection of Vibrio cholerae Requires the tolQRA Gene Products. Journal of Bacteriology 182:1739–1747.

65. Llamas MA, Ramos JL, Rodríguez-Herva JJ. 2000. Mutations in Each of the tol Genes ofPseudomonas putida Reveal that They Are Critical for Maintenance of Outer Membrane Stability. Journal of Bacteriology 182:4764–4772.

66. Gerding MA, Ogata Y, Pecora ND, Niki H, De Boer PAJ. 2007. The trans-envelope Tol–Pal complex is part of the cell division machinery and required for proper outer-membrane invagination during cell constriction in E. coli. Molecular Microbiology 63:1008–1025.

67. Bernadac A, Gavioli M, Lazzaroni J-C, Raina S, Lloubès R. 1998. Escherichia coli tol-pal Mutants Form Outer Membrane Vesicles. Journal of Bacteriology 180:4872–4878.

68. Meury J, Devilliers G. 1999. Impairment of cell division in tolA mutants of Escherichia coli at low and high medium osmolarities. Biology of the Cell 91:67–75.

69. Szczepaniak J, Holmes P, Rajasekar K, Kaminska R, Samsudin F, Inns PG, Rassam P, Khalid S, Murray SM, Redfield C, Kleanthous C. 2020. The lipoprotein Pal stabilises the bacterial outer membrane during constriction by a mobilisation-and-capture mechanism. 1. Nat Commun 11:1305.

70. Teleha MA, Miller AC, Larsen RA. 2013. Overexpression of the Escherichia coli TolQ protein leads to a null-FtsN-like division phenotype. MicrobiologyOpen 2:618–632.

71. Miller SI, Salama NR. 2018. The gram-negative bacterial periplasm: Size matters. PLoS Biol 16:e2004935.

72. Godessart P, Lannoy A, Dieu M, Van der Verren SE, Soumillion P, Collet J-F, Remaut H, Renard P, De Bolle X. 2021. β-Barrels covalently link peptidoglycan and the outer membrane in the α-proteobacterium Brucella abortus. Nat Microbiol 6:27–33.

73. The structure of FtsZ filaments in vivo suggests a force-generating role in cell division. https://www.embopress.org/doi/epdf/10.1038/sj.emboj.7601895. Retrieved 22 June 2022.

74. Avila-Calderón ED, Ruiz-Palma M del S, Aguilera-Arreola MaG, Velázquez-Guadarrama N, Ruiz EA, Gomez-Lunar Z, Witonsky S, Contreras-Rodríguez A. 2021. Outer Membrane Vesicles of Gram-Negative Bacteria: An Outlook on Biogenesis. Frontiers in Microbiology 12.

75. Sistrom WRY. 1960. A Requirement for Sodium in the Growth of Rhodopseudomonas spheroides. Microbiology 22:778–785.

76. Simon R, Priefer U, Puhler A. 1983. A broad range mobilization system for in vivo genetic engineering: transposon mutagenesis in Gram-negative bacteria. Nat Biotechnol. 1:784-791.

77. Schäfer A, Tauch A, Jäger W, Kalinowski J, Thierbach G, Pühler A. 1994. Small mobilizable multi-purpose cloning vectors derived from the Escherichia coli plasmids pK18 and pK19: selection of defined deletions in the chromosome of Corynebacterium glutamicum. Gene 145:69–73.

78. Schindelin J, Arganda-Carreras I, Frise E, Kaynig V, Longair M, Pietzsch T, Preibisch S, Rueden C, Saalfeld S, Schmid B, Tinevez J-Y, White DJ, Hartenstein V, Eliceiri K, Tomancak P, Cardona A. 2012. Fiji: an open-source platform for biological-image analysis. Nat Methods 9:676–682.

79. Ducret A, Quardokus EM, Brun YV. 2016. MicrobeJ, a tool for high throughput bacterial cell detection and quantitative analysis. Nat Microbiol 1:1–7.

80. Wickham H. 2009. ggplot2. Springer New York, New York, NY. http://link.springer.com/10.1007/978-0-387-98141-3.

81. Mastronarde DN. 2005. Automated electron microscope tomography using robust prediction of specimen movements. J Struct Biol 152:36–51.

82. Kremer JR, Mastronarde DN, McIntosh JR. 1996. Computer Visualization of Three-Dimensional Image Data Using IMOD. Journal of Structural Biology 116:71–76.

83. Chen M, Dai W, Sun SY, Jonasch D, He CY, Schmid MF, Chiu W, Ludtke SJ. 2017. Convolutional neural networks for automated annotation of cellular cryo-electron tomograms. 10. Nat Methods 14:983–985.

84. Pettersen EF, Goddard TD, Huang CC, Meng EC, Couch GS, Croll TI, Morris JH, Ferrin TE. 2021. UCSF ChimeraX: Structure visualization for researchers, educators, and developers. Protein Science 30:70–82.

Table 3-1 Primers, plasmids, and strains list

A. Primers

Name	Sequence	Purpose
BDL29-1	GGAGGATCCAGATCTCATCAC	PCR linearization of pIND5
BDL30-1	CATATGTAATTTCTCCTCTTTAATTCTAG	
BDL75-3	AAGAGGAGAAATTACATATGGCTTCCCT GAAGAAGATCC	PCR amplification of *cenR* (*RSP_0847*) for assembly into pIND5
BDL76-3	GATGAGATCTGGATCCTCCTCACGCAACA AGCCTGTAGCCG	
BDL31-1	AAGAGGAGAAATTACATATGTTGCGGCGGT TCCTGAAC	PCR amplification of *cenK* (*RSP_1056*) for assembly into pIND5
BDL32-1	TGAGATCTGGATCCTCCTCAGACGAGGGCGC TGAG	
BDL33-1	CTTGTGAGCGGATAACAATGATAC	pIND5 cloning site sequencing and amplification
BDL34-1	CAACCGAGCGTTCTGAACAAATCC	
BDL3-3	TAGAAAGCCAGTCCGCAGAAAC	PCR linearization of pk18mobsacB
BDL3-4	CTGTCGTGCCAGCTGCATTAATGAATCG	
BDL9-7	TTAATGCAGCTGGCACGACAGATGGCACTCAA CCTCATGATG	PCR upstream flank for pk18 *ftsZ-mCherry* with GSRS linker
BDL50-7	ATAGATCTGGATCCGTTTGCCTGACGCCGCAGGAAC	
BDL49-7	AACGGATCCAGATCTATGGTGAGCAAGGGCGAGG	PCR amplification of *mCherry* for pk18 *ftsZ-mCherry* with GSRS linker
BDL10-7	GATGTGAACGGATCATTACTTGTACAGCTCGTC	
BDL53-7	GCTGCCAGCCAGCATTAC	PCR of the 3' *ftsZ* locus
BDL55-7	GTCCTTTCCGGCTTGTGGTC	
FA204	tacgaattcCGCTCGGGCGGC	PCR upstream flank for pk18 *pal*-mCherry
FA205	cttgcatgcGCAGGGGTGGGC	
FA206	tgtacaagtaatgaTCCCATGCGCACCCT	PCR amplification of *mCherry* for pk18 *pal-mCherry*
FA207	CTTGCTCACGACCCCCGCACCCAT	

FA208	GCGGGGGTCGTGAGCAAGGGCGAGGAGGATAA CATGG	PCR downstream flank for pk18 *pal-mCherry*
FA209	CGCATGGGAtcattacttgtacagctcgtcCATGCC	
BDL66-7	TGCCGTGACATGACATG	PCR of *pal* locus
BDL67-7	GATCTCGGCCTTGATGTCG	
FA169	tcgagctcggtacccggTCGGCACGGCGATCC	PCR upstream flank for pk18 *mCherry-mreB*
FA170	aacgacggccagtgccCGCCCGAGATCCGGCCGAC	
FA172	ggaggggggcTCGTTTCTCACCGGCCTCTTCT	PCR amplification of *mCherry* for pk18 *mCherry-mreB*
FA173	TGCTCACCATGCTCTGCTGATCCTGTCCTGCGA	
FA174	TCAGCAGAGCATGGTGAGCAAGGGCGAGG	PCR downstream flank for pk18 *mCherry-mreB*
FA175	TGAGAAACGAgccccctccgctgcc	
BDL81-7	GCGCACCCTTCCTATAAGC	PCR of *mreB* locus
BDL82-7	GCCAGATCAGGAAGATCCC	

B. Plasmids

Name	**Description**	**Source**
pk18mobsacB	Broad host range mobilizable vector; Km^R oriT(RP4) mobT *sacB lacZα*	(77)
pIND5	Replicable plasmid used for IPTG-inducible expression; Km^R.	(22)
pIND5-*cenR*	pIND5 containing *cenR* (*RSP_0847*)	This work
pIND5-*cenK*	pIND5 containing *cenK* (*RSP_1056*)	This work
pk18mobsacB-*pal*-mCherry	pk18 containing the genomic regions directly flanking the 3' end of *pal* for the insertion of mCherry before the stop codon	This work

pk18mobsacB-*ftsZ*-mCherry	pk18 containing the genomic regions directly flanking the 3' end of *ftsZ* for the insertion of mCherry before the stop codon	This work
pk18mobsacB-mCherry-*mreB*	pk18 containing the genomic regions directly flanking the 5' end of *mreB* for the insertion of mCherry before the start codon	This work

C. Strains

Strains	Relevant characteristics	Source
***Rhodobacter sphaeroides* strains**		
2.4.1	Wild type	ATCC-17023
BDL008	pIND5-*cenR* in 2.4.1 background	This work
BDL003	pIND5-*cenK* in 2.4.1 background	This work
BDL072	*cenR*(D56A)	(21)
BDL098	pIND5-*cenK cenR*(D56A)	This work
TD000322	Δ*RSP_0382* (Δ*phaC*)	(26)
BDL007	pIND5-*cenK* Δ*RSP_0382*	This work
BDL134	*pal*::*pal-mCherry*	This work
BDL139	pIND5-*cenK pal*::*pal-mCherry*	This work
BDL144	*mreB*::*mCherry-mreB*	This work
BDL142	pIND5-*cenK mreB*::*mCherry-mreB*	This work
BDL141	*ftsZ*::*ftsZ-mCherry*	This work
BDL140	pIND5-*cenK ftsZ*::*ftsZ-mCherry*	This work
***Escherichia coli* strains**		
DH5α	F- Φ80*lacZ*ΔM15 Δ(*lacZYA-argF*) U169 *recA*1 *endA*1 *hsdR*17 (rK–, mK+) *phoA supE*44 λ– *thi*-1 *gyrA*96 *relA*1	Bethesda Research Laboratories

S17-1	*TpR SmR recA1 thiE1 pro-82 hsdR17 RP4-2-Tc::Mu-Km::Tn7* λpir	(76)
NEB 5-alpha competent *E. coli*	*fhu*A2 Δ(*argF-lacZ*)U169 *phoA gln*V44 Φ80 Δ(*lacZ*)M15 *gyrA*96 *recA*1 *relA*1 *endA*1 thi-1 *hsdR*17	New England Biolabs

Chapter 4:

Conclusions and Future Directions

Conclusions

Before my thesis work, the Donohue lab had performed a forward genetic screen to identify loss of function mutations that led to increased lipid production in *Rhodobacter sphaeroides* [1]. The motivation of this work was to provide insights into the native ability of *Rb. sphaeroides* to accumulate lipids (Fig 1-5) needed to produce intracytoplasmic membrane vesicles (ICMs) at reduced oxygen tensions [2,3]. This screen was performed at high oxygen tensions where *Rb. sphaeroides* does not produce ICM vesicles, since previous results predicted one could identify mutations to uncouple the anoxic requirements for ICM synthesis, and lipid synthesis from photopigments needed for a functional ICM [2]. For example, while the PrrBA TCS that is known to control synthesis of ICM pigments [4,5] was important for lipid accumulation, it was predicted that other pathways were required to increase lipid synthesis at reduced oxygen tensions.

This screen identified strains with loss of function in two separate two-component systems (TCSs) that produced high lipid levels at oxygen tensions that repress ICM synthesis in wild type cells (Fig 1-6) [1]. Since most bacterial TCSs modulate transcription (Fig 1-7), the analysis of these mutants was predicted to help understand the systems that control lipid production in *Rb. sphaeroides*. Neither of these two TCSs had been previously studied in *Rb. sphaeroides*, but the sensitivity of these mutants to membrane active antibiotics and detergents suggested that these regulators had a role in maintaining cell envelope integrity [1]. Given the envelope remodeling

that that accompanies ICM formation by *Rb. sphaeroides*, it was proposed that the study of these TCSs would provide important new insight into transcriptional networks in this bacterium.

When I began my thesis work, I choose to study the high lipid mutant, HLM04, which was previously shown to contain a transposon insertion in the gene *RSP_1056*, an uncharacterized locus that was predicted to encode a membrane-bound histidine kinase (HK). While I demonstrated that creating an in-frame deletion of the *RSP_1056* gene recapitulated the high lipid phenotype of HLM04, the cognate response regulator (RR) of this predicted TCS was unknown. Below I summarize some of the significant findings from my analysis of the *RSP_1056* gene.

RSP_1056 is part of the essential CenKR TCS

The experiments described Chapter 2 show that RSP_1056 is a homolog of a **c**ell **e**nvelope **k**inase, CenK, and that a recombinant version of the CenK protein is capable of both autophosphorylation and phosphotransfer to a cognate response regulator, CenR (Fig 2-1, 2-2). I found that *cenR* is essential in *Rb. sphaeroides* as it has been reported in other α-proteobacteria [6–8] suggesting that this TCS may regulate the expression of other essential genes. Leveraging a series of *cenR* alleles that increase, *cenR*(D56E), or decrease, *cenR*(D56A), activity of this RR allowed me to identify direct targets for the transcription factor CenR. Of note, analysis of cells containing the CenR(D56E) was required to identify the *tol-pal* operon as a direct CenR target since comparison of gene expression in Δ*cenK, cenR*(D56A) and wild type cells revealed no significant change in levels of transcripts from these essential genes (Fig 2-10B). Using ChIP-seq analysis, we showed that there was binding of both CenR and CenR(D56A) to the *tol-pal* operon

promoter, which I propose is sufficient for basal expression of these essential genes in the absence of phosphorylation. In contrast, RNA-seq and ChIP-seq analysis of cells containing CenR(D56E) showed increased expression and enrichment at promoter elements, respectively, compared to WT cells. Had I not analyzed cells containing the *cenR*(D56E) allele and instead relied solely on analysis of wild type and loss of function *cenK/cenR* strains, I would not have identified CenKR as a new, and direct regulator of *tol-pal* operon transcription. In addition to explaining why CenKR is an essential TCS in *Rb. sphaeroides* and other α-proteobacterias, my data reinforce why analysis of transcriptional networks solely by a comparison of deletion and wild type strains may not be sufficient to uncover the role and regulation of these systems, especially when the signal that controls their function is often transient and unknown.

The CenKR TCS is a global regulator of processes needed for cellular survival

I showed that CenR is a direct activator of *tol-pal* and *rpoHI* expression, and a repressor of genes encoding peptidoglycan (PG) biosynthesis enzymes (Fig 2-10) [9]. Consequently, I predict that CenKR plays an essential role in PG and OM biosynthesis, cell envelope assembly, and cell division. The data in Chapter 3, leads me to propose that by increasing the expression of TolQRAB, the CenKR TCS reduces diffusion of Pal, and promotes interactions between Pal-PG, a mechanism that cells use to allow OM-PG interconnections that are needed for normal cell elongation and division (Fig 3-3).

The direct control of expression of the gene encoding the heat shock sigma factor RpoHI by the CenKR links this envelope TCS to the general cellular stress response. Indeed, CenR and RpoHI has been shown to directly regulate the expression of genes encoding proteins involved in heat

shock, membrane stress, and protein misfolding, as well as the expression of each other, facilitating feed-forward transcriptional regulation to promote cell survival in response to a variety of stress signals [10]. The increased expression of genes encoding periplasmic chaperones and proteases by CenKR also illustrates the function of this TCS in cell envelope stress and is reminiscent of well-studied *E. coli* envelope stress response responses that are controlled by TCSs which do not exist in *Rb. sphaeroides* and other α-proteobacteria [11,12].

In *E. coli,* it is well known that the number of Lpp-PG crosslinks is inversely correlated with OM vesicle production [13]. Furthermore, overexpression of Pal in a Lpp null strain of *E. coli* prevents the overproduction of OM vesicles that is associated with the loss of this lipoprotein [14]. *Rb. sphaeroides* and other α-proteobacteria lack a Lpp homolog, so I propose that CenKR's control of *tolQRAB* expression stabilizes the OM, and that the membrane protrusions that are found in cells that overexpress *cenK* results from the destabilization of the cell envelope in this strain (Chapter 3).

I found that Δ*cenK* and *cenR*(D56A) cells are shorter, rounder (Fig 2-5), and have both increased cellular and extracellular lipid [2,9]. Based on my data, I propose that a reduction in the activity of the CenKR TCS leads to the accumulation of misfolded or improperly trafficked proteins as well as the accumulation of PG precursor molecules in the periplasmic space. The production of OM vesicles in other Gram-negative bacteria has been shown to be a product of accumulating such molecules in the periplasm [13]. This provides one possible explanation for the increased lipid production in Δ*cenK* and *cenR*(D56A) cells. Other processes that are predicted to be controlled by CenKR include retrograde transport of lipids from the OM to the IM (Mla

complex), assembly of OM proteins (Bam complex), and Sec-dependent translocation of proteins from the cytoplasm to the envelope; defects in these functions likely result in pleiotropic effects that inhibit proper assembly of the OM leading to instability and accumulation of lipids in the OM of Δ*cenK* and *cenR*(D56A) cells (Table 2-1). The hypothesis that altered CenKR activity causes changes to the periplasm and cell envelope is supported by the increase in sensitivity of these strains to a broad range of PG-active antibiotics that require increased OM permeability membrane to gain access to the periplasmic enzymes that represent their sites of action (Appendix A and [1]). My work has provided several new insights into cell envelope function in *Rb. sphaeroides* and provides a model for how the CenKR TCS impacts cell elongation, morphology, and lipid production. Given the conservation of CenKR and many known target genes in α-proteobacteria, my results provide a list of genes of unknown function that likely play a role in cell envelope biogenesis in these and possibly other bacteria.

CenKR and NtrYX lesions each lead to lipid overproduction and cell envelope alterations

Based on the work in my thesis and others in the lab, we now know of two TCSs, CenKR and NtrYX, that control transcription of genes encoding proteins that are needed for normal cell envelope function. Each of these TCSs were discovered because mutations which inactivate these signal transduction networks exhibited a high lipid phenotype, secreted lipids into the media, and were sensitive to antibiotics and compounds that act at the membrane [1]. It is now known that the RR NtrX functions as a direct transcriptional regulator of genes needed for PG synthesis in *Rb. sphaeroides* [15]. Additionally, it was shown that Δ*ntrYX* mutants had defects in LPS accumulation and OM permeability [15]. This is not surprising given what is known about the shared transporters for lipopolysaccharide (LPS) and PG precursor molecules via Lipid II

[16]. The PG/LPS defects in Δ*ntrYX* cells directly impacts OM function and can explain the pleiotropic impact of these mutations on reducing growth rate, formation of filamentous cells, and stalled cell division septum [15]. However, additional information is needed to provide a mechanistic understanding for the high lipid secretion of Δ*ntrYX* mutants.

The direct activation of genes encoding PG biosynthetic enzymes by NtrYX is in contrast to the repression of genes encoding PG precursor biosynthesis enzymes and subunits of the elongasome (Rod complex) by CenKR (Figure 2-10D, 2-11). These findings suggest that CenKR and NtrYX activity work together to coordinate the proper expression of PG gene clusters in α-proteobacteria (Appendix A). In some Gram-negative bacteria, the highly conserved protein MraZ, encoded by the first gene in the division and cell wall biosynthesis (*dcw*) gene cluster, acts as a transcriptional repressor of the *dcw* gene cluster [17]. Aside from MraZ, few transcriptional regulators, none of which are conserved outside of specific bacterial orders, have been shown to regulate the expression of *dcw* gene clusters [12]. The *E. coli* envelope stress response systems Cpx, Rcs, Bae, σ^E, and Psp are reported to respond to cell wall damage or antibiotic stress, however none of these systems are known to directly control the expression of PG biosynthesis genes [11,12,18–21]. In addition, homologs of these cell envelope master regulators are not found in *Rb. sphaeroides* and many other α-proteobacteria, suggesting the existence of different systems for sensing and responding to envelope changes across the phylogeny. Based on these data in my thesis and elsewhere, I propose that CenKR and NtrYX have conserved functions in *Rb. sphaeroides* and other α-proteobacteria that contain homologues of these TCSs.

My analysis of *Rb. sphaeroides* CenKR function led to the identification of several unexpected properties of this TCS. For example, the finding that overexpression of *cenK,* but not *cenR,* was sufficient to stimulate TCS activity suggested that CenK is unusual. Specifically, TCS are typically more sensitive to expression levels of the RR rather than the HK [22]. Due to this, my data predicts that an unknown ligand acts to negatively regulates autophosphorylation of the CenK HK rather than an activating signal for canonical TCSs. In addition, the ability of CenR to activate transcription of genes encoding subunits of both the divisome and the elongasome provided an opportunity to explore new aspects of *Rb. sphaeroides* cell division in both wild type cells and those with increased CenKR activity (Chapter 3).

Overexpression of *cenK* produced phenotypes consist with, but more severe than phosphomimic hyperactivation by a single amino acid change at the site of RR phosphorylation, CenR(D56E), so I studied the morphological changes due of *cenK* overexpression. In a collaboration with Daniel Parrell of the Wright Lab, cryogenic electron microscopy allowed us to observe the impact of *cenK* overexpression on the cell envelope. This analysis found a significant increase in periplasmic width, disassociation of the OM and IM during cell division, and formation of vesicle protrusions from the stalled division septa in cells overexpressing *cenK* (Fig 3-2).

In other well-studied bacteria, the Tol-Pal complex is need for the OM to invaginate during cell division [23–26]. I found that CenKR is a direct activator of the *tolQRAB* operon and that the Tol complex did not move to the cell septa in cells overexpressing *cenK* (Fig 3-3). Based on these observations, I propose that the failure to form a Tol-Pal complex at the septum in cells overexpressing *cenK* can be linked to filamentation and cell division defects in this strain.

Using a combination of fluorescence microscopy and antibiotics that inhibit known enzymes in cell elongation, I showed that Z-ring accumulation was a key driver for cell elongation in an MreB and PBP2 independent manner (Fig 3-6, 3-7). Analysis of wild type cells showed that during PG synthesis, MreB and FtsZ were each present at the midcell throughout the wild type cell cycle, where these two proteins likely function together during pre-septal PG synthesis as is found in other bacteria [27,28]. Later, MreB leaves FtsZ at the 'old' midcell and moves to promote cell elongation at the 'new' midcells of daughter cells, while FtsZ facilitates the completion of cell division. A similar analysis of *cenK* overexpression strains suggest that FtsZ depolymerization is dependent on completion of OM separation (a process that is mediated by Tol-Pal) and formation of the new cell poles. In other words, the inability of cells overexpressing *cenK* to divide likely can be attributed to FtsZ and MreB accumulation along the length of the cell, presumably at new midcell sites (Fig 3-7). In all, this suggests a novel mechanism for MreB mediated recruitment and interactions with FtsZ as well as FtsZ driven elongation in *Rb. sphaeroides*. Further, our observations suggest other (Tol-)Pal mediated processes are required for completion of cell division in addition to OM invagination in *Rb. sphaeroides*.

Future Directions

Elucidating the function of genes regulated by CenKR.

Analysis of the CenR direct and indirect regulon provided important insight into the phenotypes we observed for CenKR mutant strains. As with most genomic analyses, included in our list of direct *cenR* targets are many genes encoding proteins with predicted or unknown functions (Table 2-1, 2-2). However, the majority of these direct *cenR* target genes encode proteins that are

predicted to be lipoproteins, periplasmic and OM β-barrel proteins, or possibly secreted to the media [9]. Thus, we predict that many of these uncharacterized *cenR* gene products likely have a role in cell envelope maintenance or assembly and serve as excellent candidates for understanding this process in α-proteobacteria and other Gram-negative bacteria. Below I note some members of the direct CenR regulon of interest for future analysis given my data and the features of *Rb. sphaeroides.*

- *RSP_1200,* which encodes a putative lipoprotein, was also identified as gene which when mutated produced a high lipid phenotype [1].Transcription of *RSP_1200* and neighboring *RSP_1199,* which encodes a predicted L,D-transpeptidase that typically functions in crosslinking PG peptide stems, is predicted to be increased by CenKR activity.
- *RSP_1880,* encoding a protein with a predicted PG binding domain that could be involved in cell wall remodeling, is predicted to be repressed by CenKR activity.
- *RSP*_0730 is predicted to be an IM protein containing a large periplasmic domain with no clear functional domains and is predicted to be activated by CenKR activity.
- *RSP_2847* is predicted to be repressed by CenKR activity and encodes a putative lipoprotein with a predicted lipid-binding domain.
- *RSP_1860* encodes a predicted PG hydrolase that is upregulated by CenKR activity. It has been shown that Tol-Pal activity is important for the hydrolysis of septal PG during division in *E. coli* [26]. Given the role of CenKR in the regulation of the *tol* operon, it is tempting to speculate that other Tol-Pal driven processes may also be differentially expressed in this data set.

- Of relation to the formation of ICM vesicles by *Rb. sphaeroides* and other bacteria, is *RSP_2718*, which is predicted upregulated by CenKR. This gene encodes a homologue of a subunit of the Bam complex that is needed for assembly of OM proteins in other Gram-negative bacteria. Recently posted data suggests that a BamA homologue interacts with *RSP_6207* (*mic60*) and *RSP_1508* (*orf52*) to facilitate ICM formation in α-proteobacteria via a process analogous to that used for mitochondrial cristae formation [29].

Evidence for post-translational regulation of PG synthesis in α-proteobacteria.

In *E. coli* the lipoproteins LpoA and LpoB are key to modulating the bifunctional activity of class A PBPs (PBP1A and PBP1B) as PG transglycolases and hydroylases [30]. The *Rb. sphaeroides* is not predicted to encode homologs to either lipoprotein, suggesting the existence of an alternate post-translational mechanism for modulating the function of these PG biosynthetic enzymes. Given that PG synthesis appears to occur exclusively at the midcell in *Rb. sphaeroides*, and not in spatiotemporally distinct regions as in *E. coli*, perhaps the function of MreCD or FtsN is sufficient to modulate PBP1A and PBP1B activity, respectively. Alternatively, RSP_1200 and other putative lipoproteins may play a similar, but previously unknown, role in the post-translational control of PG synthesis. Given the predicted essentiality of *pal* in *Rb. sphaeroides* [6] and the multiple roles of Tol-Pal in other organisms [31], it is also possible that Pal plays a role in post-translational control of PG synthesis in this and other bacteria. I propose that screening an existing *Rb. sphaeroides* Tn-seq library [6] for fitness defects when grown in the presence of β-lactam, glycopeptide antibiotics, globomycin (inhibitor of lipoprotein trafficking), or other antibiotics could prove useful for identification of genes that

encode lipoproteins or other gene products that are involved in the post-translational control of PG synthesis, as previously demonstrated for other bacteria [30,32,33].

Identification of signal(s) that regulate CenK and NtrY activity.

The two HKs NtrY and CenK are each predicted to be integral membrane proteins with significant periplasmic domains that are flanked by trans-membrane alpha-helices. CenK is predicted to contain 2 transmembrane alpha-helices and a 124-residue periplasmic domain with no significant amino acid sequence similarity to other known ligand binding domains. The NtrY periplasmic domain is predicted to be 80 amino acid residues with no similarity to known ligand binding domains, it is flanked by two transmembrane domains on the N- and C-termini, and resembles canonical NtrY sensory domains in other proteins that are reported to function involved in nitrogen fixation and metabolism [34].

Recently, it was shown that the phosphatase activity of *Caulobacter crescentus* NtrY is repressed by NtrZ, a small periplasmic protein [35], but the nature and location of the signal that controls this TCS is unknown. In some other bacteria, NtrY is proposed to act as a redox sensor monitoring oxygen tensions through a heme cofactor [36]. It is therefore tempting intriguing that such a signal could be related to ICM formation, increased lipid synthesis and envelope remodeling that occurs at low oxygen development in *Rb. sphaeroides*.

In the case of CenK, no information is available on signals that control its HK activity. By analogy to NtrY, a number of small periplasmic proteins that are direct CenKR targets (encoded by *RSP_1807*, *RSP_1844*, *RSP_0915*, *RSP_3068* as well as others) could bind to and control

CenK activity in response to an unknown signal or stress. Moreover, differences in *cenK* essentiality, particularly between *Rb. sphaeroides* (not essential) [9] and *C. crescentus* (essential) [7] where this TCS has been studied, suggest different regulation and signal recognition mechanisms for each HK. This raises an interesting question regarding the biology and evolution of orphaned bacterial TCSs. If orphaned TCSs arise through gene duplications [37], but do not increase cross-talk between related HK-RR pairs [7,37,38], then perhaps differences between homologous orphaned systems is reflective of the adaptation to different sensory inputs. Alternatively, as the essentiality of RR's appear to remain intact, perhaps this difference is reflective of promoter architecture and binding to fine tune the expression of direct targets independent of HK regulation. Regardless, the differential essentiality, activity, and morphology of *Rb. sphaeroides* and *C. crescentus* offers a model for the comparison of homologous orphaned TCSs.

Future experiments to identify sensory inputs that control CenK and NtrY activity in *Rb. sphaeroides* could rely on high throughput systems using the DNA binding motifs and native transcriptional elements that I [9] and others have identified [15]. Such a system could be used to screen for proteins or other ligands that alter expression of a reporter system in a CenK- or NtrY-dependent manner by taking advantage of success in similar previous experiments [22,39–42]. Of note, these systems have been useful for the detection of signals that are typically small, soluble molecules or sensors of pH, temperature, or light. Therefore, careful consideration needs to be taken to assay molecules or peptides that are excluded by the Gram-negative OM.

Isolation of high(er) lipid mutants.

The overarching goal of the research that led to my thesis was to provide new information on lipid production in *Rb. sphaeroides* towards designing new types of oleaginous microbes. This work has shown that manipulation of cell envelope processes is a promising approach for identification of strains that secrete bacterial lipids. In the future, it will be interesting to test combinations of high lipid mutants identified previously to increase lipid secretion in this and other industrial relevant bacteria.

In an attempt to do so, I sought to construct a double Δ*cenK* Δ*ntrYX* mutant. However, I was unsuccessful in recovering such a strain, suggesting loss of both of these TCSs was synthetically lethal. Overexpression of *cenK* and loss of Δ*ntrYX* results in increased transcription of PG biosynthetic genes (Appendix A), so I hypothesized that combining these alleles might increase lipid secretion. When I introduced the pIND5-*cenK* expression plasmid into a Δ*ntrYX* strain, I saw morphological changes including filamentous cells with abnormal cell width when cells were grown in the presence of IPTG (Appendix A). Negative stain cryo-EM analysis of this strain when grown in the presence of IPTG to increase *cenK* expression revealed many cells surface changes and an increased formation of lipid-rich protrusions than the Δ*ntrYX* control strain (Appendix A). Further analysis is needed to obtain information on how these two TCS might function to produce these changes and quantify the impact of these two traits on lipid secretions and growth.

Other published approaches for generating oleaginous microbes have centered around genetic and metabolic engineering of fatty acid and lipid biosynthesis pathways [43,44]. In the future, it

would be useful to test if published or predicted [45] biosynthetic or regulatory changes can be used to generate oleaginous bacteria with increase titers, rates and yields of lipid production. Thus, future work to improve lipid yields should focus on combining metabolic and cell envelope engineering strategies for development of oleaginous bacteria.

The impact of cenK overexpression on photosynthetic growth of *Rb. sphaeroides*.

Growth of *Rb. sphaeroides* by photosynthesis (anaerobiosis with light) requires formation of ICM invaginations and remodeling of the cell envelope at low oxygen tensions (Fig 1-5). It seems likely that CenKR has an impact on photosynthetic growth in some capacity given the myriad of cell envelope function that are impacted directly or indirectly by this TCS. I have found that cells containing either the Δ*cenK* or *cenR*(D56A) alleles have increased pigment production compared to wild type cells when grown under photosynthetic conditions, while cells containing the *cenK*(D56E) allele (which increases CenKR activity) are less pigmented under the same conditions (Appendix A). While there are many possible explanations for these observations, it is tempting to speculate that these phenotypes reflect a previously unknown role for CenKR in the *Rb. sphaeroides* photosynthetic lifestyle. To explore these phenotypes further, I grew the *cenK* overexpression strains in the presence of IPTG under photosynthetic conditions (Appendix A). After a long growth lag, I found that these *cenK* overexpressing cells formed clumps and settled in the absence of shaking (Appendix A). It would be interesting to analyze cellular and secreted lipid yields, the formation of photopigments and ICM structures in the *cenK* overexpression strain relative to wild type cells to see if growth under low oxygen or anaerobic conditions provides a way to secrete higher levels of lipids in the media.

Deciphering genetic connections between *Rb. sphaeroides* lipid and ICM production.

The previous screen for high lipid mutants relied on isolating loss of function mutants under aerobic conditions when cells normally lack the additional need for lipids as part of the ICM bilayer. While the analysis of these high lipid mutants provided new insight into regulators or components of the cell envelope that when inactivated can increase lipids production in *Rb. sphaeroides*, many of these gene products do not have a clear connection to the process or regulation of lipid or ICM synthesis. The screen was also based on the assumption that loss of a negative regulator would increase lipid synthesis. In the future, consideration for additional screens for gain of function or other mutations that increase lipid or ICM membrane synthesis is warranted.

The previous screen for high lipid mutants depended on the use of Nile Red, a hydrophobic fluorescent dye as a proxy for accumulation of hydrophobic (lipid) molecules. While excellent at detecting substantial changes in the presence of hydrophobic molecules, it cannot accurately report on small changes in fluorescence, especially since Nile Red staining is often irregular, surface focused and may not report on changes to internal lipids or membrane accumulation in *Rb. sphaeroides*. In the future it might be advantageous to consider dyes like MitoTracker Green that have been shown to stain the inner membrane in *E. coli* [46,47]. It would be interesting to test if *Rb. sphaeroides* cells that contain ICM have increased MitoTracker Green fluorescence compared to cells which lack this increased IM surface area. Depending on the results of this analysis, a FACS screen could be developed to identify cells that have increased MitoTracker Green fluorescence in a randomly mutagenized cell population. Subsequent genome sequencing,

plus biochemical and microscopic analysis of cells with increased fluorescence could be used to identify point and other mutations that lead to increased lipid production.

In another approach, previous analysis of *Rb. sphaeroides* [6] identified two AsnC family transcriptional regulators (encoded by *RSP_1866* and *RSP*_1867), that are essential for photosynthetic growth. In the future it would be interesting to analyze whether cells lacking each of these genes produce increased levels of lipids under the low oxygen conditions needed to form ICM vesicles. Depending on the analysis of these strains, additional studies could be planned to define the direct targets of these putative transcriptional regulators, their impact on ICM formation, and determine if these gene products are conserved and play similar roles in other different species of purple non-sulfur bacteria that house their photosynthetic apparati in membranes that range from small circular vesicles to extensive lamellae systems [48]. Therefore, this raises the question of what aspects of ICM regulation and development are conserved throughout these bacteria.

Summary

In all, I have combined biochemical, imaging, and genetic techniques to identify the CenKR TCS and show that this essential TCS in *Rb. sphaeroides* is amenable to genetic manipulation. I used these features to probe transcriptional regulation directed by CenR. Using genomic techniques, I identified CenKR as a newly identified and direct regulator of the *tol* operon as well as PG biosynthesis enzymes and cell division. These findings represent the first direct transcriptional regulator of *tol* expression in Gram-negative bacteria and establish CenR as a global regulator of cell division. I was also able to use a set of CenKR mutants with different phenotypes to develop

an understanding the spatial and temporal regulation of cell elongation and cell division in *Rb. sphaeroides*. Together, this work builds a foundation for understanding cell envelope biosynthesis, remodeling, homeostasis, and cell division in *Rb. sphaeroides* and other bacteria. I hope that this work will establish an appreciation for using this model system for analyzing these processes in other well studied organisms and that these techniques can be applied to building a holistic understanding of the myriad of morphological features and growth patterns in α-proteobacteria.

References

1. Lemmer KC, Zhang W, Langer SJ, Dohnalkova AC, Hu D, Lemke RA, et al. Mutations That Alter the Bacterial Cell Envelope Increase Lipid Production. mBio. 8: e00513-17. doi:10.1128/mBio.00513-17

2. Lemmer KC, Dohnalkova AC, Noguera DR, Donohue TJ. Oxygen-Dependent Regulation of Bacterial Lipid Production. Journal of Bacteriology. 2015;197: 1649–1658. doi:10.1128/JB.02510-14

3. Kiley PJ, Kaplan S. Molecular genetics of photosynthetic membrane biosynthesis in Rhodobacter sphaeroides. 1988;52: 20.

4. Mackenzie C, Eraso JM, Choudhary M, Roh JH, Zeng X, Bruscella P, et al. Postgenomic Adventures with *Rhodobacter sphaeroides*. Annu Rev Microbiol. 2007;61: 283–307. doi:10.1146/annurev.micro.61.080706.093402

5. Zeilstra-Ryalls J, Gomelsky M, Eraso JM, Yeliseev A, O'Gara J, Kaplan S. Control of Photosystem Formation in Rhodobacter sphaeroides. J Bacteriol. 1998;180: 2801–2809.

6. Burger BT, Imam S, Scarborough MJ, Noguera DR, Donohue TJ. Combining Genome-Scale Experimental and Computational Methods To Identify Essential Genes in Rhodobacter sphaeroides. mSystems. 2: e00015-17. doi:10.1128/mSystems.00015-17

7. Skerker JM, Prasol MS, Perchuk BS, Biondi EG, Laub MT. Two-Component Signal Transduction Pathways Regulating Growth and Cell Cycle Progression in a Bacterium: A System-Level Analysis. PLOS Biology. 2005;3: e334. doi:10.1371/journal.pbio.0030334

8. Pechter KB, Gallagher L, Pyles H, Manoil CS, Harwood CS. Essential Genome of the Metabolically Versatile Alphaproteobacterium Rhodopseudomonas palustris. J Bacteriol. 2015;198: 867–876. doi:10.1128/JB.00771-15

9. Lakey BD, Myers KS, Alberge F, Noguera DR, Donohue TJ. The essential Rhodobacter sphaeroides CenKR two-component system regulates cell division and envelope biosynthesis. PLOS Genetics. 2022;In preprint.

10. Dufour YS, Imam S, Koo B-M, Green HA, Donohue TJ. Convergence of the Transcriptional Responses to Heat Shock and Singlet Oxygen Stresses. PLOS Genetics. 2012;8: e1002929. doi:10.1371/journal.pgen.1002929

11. Saha S, Lach SR, Konovalova A. Homeostasis of the Gram-negative cell envelope. Current Opinion in Microbiology. 2021;61: 99–106. doi:10.1016/j.mib.2021.03.008

12. Delhaye A, Collet J-F, Laloux G. A Fly on the Wall: How Stress Response Systems Can Sense and Respond to Damage to Peptidoglycan. Frontiers in Cellular and Infection Microbiology. 2019;9. Available: https://www.frontiersin.org/article/10.3389/fcimb.2019.00380

13. Schwechheimer C, Kuehn MJ. Outer-membrane vesicles from Gram-negative bacteria: biogenesis and functions. Nat Rev Microbiol. 2015;13: 605–619. doi:10.1038/nrmicro3525

14. Cascales E, Bernadac A, Gavioli M, Lazzaroni J-C, Lloubes R. Pal Lipoprotein of Escherichia coli Plays a Major Role in Outer Membrane Integrity. Journal of Bacteriology. 2002;184: 754–759. doi:10.1128/JB.184.3.754-759.2002

15. Lemmer KC, Alberge F, Myers KS, Dohnalkova AC, Schaub RE, Lenz JD, et al. The NtrYX Two-Component System Regulates the Bacterial Cell Envelope. Harwood CS, editor. mBio. 2020;11. doi:10.1128/mBio.00957-20

16. Ruiz N. Lipid Flippases for Bacterial Peptidoglycan Biosynthesis. Lipid Insights. 2016;8: 21–31. doi:10.4137/LPI.S31783

17. Eraso JM, Markillie LM, Mitchell HD, Taylor RC, Orr G, Margolin W. The Highly Conserved MraZ Protein Is a Transcriptional Regulator in Escherichia coli. Journal of Bacteriology. 2014;196: 2053–2066. doi:10.1128/JB.01370-13

18. Masi M, Pinet E, Pagès J-M. Complex Response of the CpxAR Two-Component System to β-Lactams on Antibiotic Resistance and Envelope Homeostasis in Enterobacteriaceae. Antimicrobial Agents and Chemotherapy. 2020;64: e00291-20. doi:10.1128/AAC.00291-20

19. Bernal-Cabas M, Ayala JA, Raivio TL. The Cpx Envelope Stress Response Modifies Peptidoglycan Cross-Linking via the l,d-Transpeptidase LdtD and the Novel Protein YgaU. Journal of Bacteriology. 2015;197: 603–614. doi:10.1128/JB.02449-14

20. Callewaert L, Vanoirbeek KGA, Lurquin I, Michiels CW, Aertsen A. The Rcs Two-Component System Regulates Expression of Lysozyme Inhibitors and Is Induced by Exposure to Lysozyme. Journal of Bacteriology. 2009;191: 1979–1981. doi:10.1128/JB.01549-08

21. Konovalova A, Grabowicz M, Balibar CJ, Malinverni JC, Painter RE, Riley D, et al. Inhibitor of intramembrane protease RseP blocks the σ^E response causing lethal accumulation of unfolded outer membrane proteins. Proc Natl Acad Sci USA. 2018;115: E6614. doi:10.1073/pnas.1806107115

22. Lazar JT, Tabor JJ. Bacterial two-component systems as sensors for synthetic biology applications. Current Opinion in Systems Biology. 2021;28: 100398. doi:10.1016/j.coisb.2021.100398

23. Gerding MA, Ogata Y, Pecora ND, Niki H, De Boer PAJ. The trans-envelope Tol–Pal complex is part of the cell division machinery and required for proper outer-membrane invagination during cell constriction in E. coli. Molecular Microbiology. 2007;63: 1008–1025. doi:10.1111/j.1365-2958.2006.05571.x

24. Szczepaniak J, Holmes P, Rajasekar K, Kaminska R, Samsudin F, Inns PG, et al. The lipoprotein Pal stabilises the bacterial outer membrane during constriction by a mobilisation-and-capture mechanism. Nat Commun. 2020;11: 1305. doi:10.1038/s41467-020-15083-5

25. Petiti M, Serrano B, Faure L, Lloubes R, Mignot T, Duché D. Tol Energy-Driven Localization of Pal and Anchoring to the Peptidoglycan Promote Outer-Membrane Constriction. Journal of Molecular Biology. 2019;431: 3275–3288. doi:10.1016/j.jmb.2019.05.039

26. Yakhnina AA, Bernhardt TG. The Tol-Pal system is required for peptidoglycan-cleaving enzymes to complete bacterial cell division. Proc Natl Acad Sci USA. 2020;117: 6777–6783. doi:10.1073/pnas.1919267117

27. Figge RM, Divakaruni AV, Gober JW. MreB, the cell shape-determining bacterial actin homologue, co-ordinates cell wall morphogenesis in Caulobacter crescentus. Molecular Microbiology. 2004;51: 1321–1332. doi:10.1111/j.1365-2958.2003.03936.x

28. Direct interaction of FtsZ and MreB is required for septum synthesis and cell division in Escherichia coli. The EMBO Journal. 2013;32: 1953–1965. doi:10.1038/emboj.2013.129

29. Muñoz-Gómez SA, Cadena LR, Gardiner AT, Leger MM, Sheikh S, Connell L, et al. The development of intracytoplasmic membranes in alphaproteobacteria involves the conserved mitochondrial crista-developing Mic60 protein. bioRxiv; 2022. p. 2022.06.14.496148. doi:10.1101/2022.06.14.496148

30. Typas A, Banzhaf M, van den Berg van Saparoea B, Verheul J, Biboy J, Nichols RJ, et al. Regulation of peptidoglycan synthesis by outer membrane proteins. Cell. 2010;143: 1097–1109. doi:10.1016/j.cell.2010.11.038

31. Szczepaniak J, Press C, Kleanthous C. The multifarious roles of Tol-Pal in Gram-negative bacteria. FEMS Microbiol Rev. 2020;44: 490–506. doi:10.1093/femsre/fuaa018

32. Gurnani Serrano CK, Winkle M, Martorana AM, Biboy J, Morè N, Moynihan P, et al. ActS activates peptidoglycan amidases during outer membrane stress in Escherichia coli. Molecular Microbiology. 2021;116: 329–342. doi:10.1111/mmi.14712

33. Genomewide phenotypic analysis of growth, cell morphogenesis, and cell cycle events in Escherichia coli. Molecular Systems Biology. 2018;14: e7573. doi:10.15252/msb.20177573

34. Pawlowski K, Klosse U, de Bruijn FJ. Characterization of a novel Azorhizobium caulinodans ORS571 two-component regulatory system, NtrY/NtrX, involved in nitrogen fixation and metabolism. Molec Gen Genet. 1991;231: 124–138. doi:10.1007/BF00293830

35. Stein BJ, Fiebig A, Crosson S. The ChvG-ChvI and NtrY-NtrX Two-Component Systems Coordinately Regulate Growth of Caulobacter crescentus. Journal of Bacteriology. 2021;203: e00199-21. doi:10.1128/JB.00199-21

36. Carrica M del C, Fernandez I, Martí MA, Paris G, Goldbaum FA. The NtrY/X two-component system of Brucella spp. acts as a redox sensor and regulates the expression of nitrogen respiration enzymes. Molecular Microbiology. 2012;85: 39–50. doi:10.1111/j.1365-2958.2012.08095.x

37. Capra EJ, Laub MT. Evolution of Two-Component Signal Transduction Systems. Annual Review of Microbiology. 2012;66: 325–347. doi:10.1146/annurev-micro-092611-150039

38. Laub MT, Goulian M. Specificity in Two-Component Signal Transduction Pathways. Annu Rev Genet. 2007;41: 121–145. doi:10.1146/annurev.genet.41.042007.170548

39. Baumgartner JW, Kim C, Brissette RE, Inouye M, Park C, Hazelbauer GL. Transmembrane signalling by a hybrid protein: communication from the domain of chemoreceptor Trg that recognizes sugar-binding proteins to the kinase/phosphatase domain of osmosensor EnvZ. Journal of Bacteriology. 1994;176: 1157–1163. doi:10.1128/jb.176.4.1157-1163.1994

40. Hirakawa H, Inazumi Y, Masaki T, Hirata T, Yamaguchi A. Indole induces the expression of multidrug exporter genes in Escherichia coli. Molecular Microbiology. 2005;55: 1113–1126. doi:10.1111/j.1365-2958.2004.04449.x

41. Wu C-F, Lin J-S, Shaw G-C, Lai E-M. Acid-Induced Type VI Secretion System Is Regulated by ExoR-ChvG/ChvI Signaling Cascade in Agrobacterium tumefaciens. PLOS Pathogens. 2012;8: e1002938. doi:10.1371/journal.ppat.1002938

42. Inada S, Okajima T, Utsumi R, Eguchi Y. Acid-Sensing Histidine Kinase With a Redox Switch. Frontiers in Microbiology. 2021;12. Available: https://www.frontiersin.org/article/10.3389/fmicb.2021.652546

43. Kosa M, Ragauskas AJ. Lipids from heterotrophic microbes: advances in metabolism research. Trends in Biotechnology. 2011;29: 53–61. doi:10.1016/j.tibtech.2010.11.002

44. Liang M-H, Jiang J-G. Advancing oleaginous microorganisms to produce lipid via metabolic engineering technology. Progress in Lipid Research. 2013;52: 395–408. doi:10.1016/j.plipres.2013.05.002

45. Imam S, Noguera DR, Donohue TJ. Global insights into energetic and metabolic networks in Rhodobacter sphaeroides. BMC Systems Biology. 2013;7: 89. doi:10.1186/1752-0509-7-89

46. Shi H, Westfall CS, Kao J, Odermatt PD, Anderson SE, Cesar S, et al. Starvation induces shrinkage of the bacterial cytoplasm. Proc Natl Acad Sci U S A. 2021;118: e2104686118. doi:10.1073/pnas.2104686118

47. Vadia S, Tse JL, Lucena R, Yang Z, Kellogg D, Wang JD, et al. Fatty acid availability sets cell envelope capacity and dictates microbial cell size. Curr Biol. 2017;27: 1757-1767.e5. doi:10.1016/j.cub.2017.05.076

48. LaSarre B, Kysela DT, Stein BD, Ducret A, Brun YV, McKinlay JB. Restricted Localization of Photosynthetic Intracytoplasmic Membranes (ICMs) in Multiple Genera of Purple Nonsulfur Bacteria. mBio. 9: e00780-18. doi:10.1128/mBio.00780-18

Appendix A: Addendum to the characterization of the CenKR TCS in *Rhodobacter sphaeroides*.

Summary.

The inclusion of this work in my thesis is meant to supplement experiments presented in Chapters 2 & 3 and encourage future analysis of CenKR. These experiments where either discontinued due to time or disconnected from the analyses described elsewhere in my thesis. I show that cells containing different *cenK* and *cenR* alleles are sensitive to a wide variety of PG active compounds and produce more pigments aerobically (Fig AA1). Growing these strains under anaerobic conditions with light for photosynthesis, I observed that hyperactivation of *cenR*(D56E) or overexpression of *cenK* resulted in a sever lag in growth (Fig AA2). Overexpression of *cenK* produced an additional phenotype in that cells would grow in large clumps amassed at the bottom of growth tubes (Fig AA2).

Comparing differentially expressed genes in Δ*cenK* and Δ*ntrYX* strains relative to wild type cells, I observed opposite changes in the levels of transcripts for genes encoding PG biosynthesis enzymes and divisome proteins (Fig AA3). Construction of a strain containing both pIND5-*cenK* and the Δ*ntrYX* allele and growth in the presence of IPTG produced cells with morphological changes and increased secretion of lipid structures.

Results.

Previous chemical genomic analysis of a *cenK* transposon mutant showed these cells were sensitive to ampicillin and membrane detergents [1]. To expand on this analysis, I challenged

cells containing different *cenK* and *cenR* alleles with several antibiotics that affects aspects of peptidoglycan (PG) synthesis. This sensitivity analysis demonstrated that cells with an inactive CenKR TCS were sensitive to drug that inhibit processes that occur in the periplasmic space, but not sensitive to drugs that inhibit cytoplasmic processes (Fig AA1). Observation of mutants on plates and in liquid culture provide evidence that Δ*cenK* and *cenR*(D56A) strains appear to produce more pigments aerobically than WT cells (Fig AA2A-B). This suggests that CenKR or disruption of genes regulated by CenKR activity could play a role in regulating or the production of pigments or ICM vesicles in *Rb. sphaeroides*.

Comparing Δ*cenK* (Chapter 2) and Δ*ntrYX* [2]strain lengths, Δ*cenK* cells were shorter than wild type and Δ*ntrYX* cells were longer than wild type. Additionally, cells containing the *cenR*(D56E) allele that increases activity of this RR produced cells that were longer than wild type cells. Given the role of PG in determining cells shape and width, I hypothesized that CenKR and NtrYX may have different effects on transcription of these genes. Comparison of existing RNA-seq data sets in this thesis and those generated previously [2] shows that transcripts from genes within the division and cell wall gene clusters were increased in the Δ*cenK* strain and decreased in the Δ*ntrYX* strain (Fig AA3). This suggests that together the CenKR and NtrYX TCSs may play a role in tuning the expression of these genes in *Rb. sphaeroides*. This activity is reminiscent to tuning roles of WalRK and PhoPQ in the Gram-positive bacterium *Bacillus subtilis* to increase or decrease, respectively, expression of PG biosynthesis enzymes and assembly machinery in response to different stimuli [3]. These findings led me to consider that CenKR and NtrYX play similar roles in *Rb. sphaeroides* and possibly other Gram-negative bacteria. To test this hypothesis, I attempted to construct a double mutant of Δ*cenK* Δ*ntrYX* but

was unsuccessful, suggesting that altered regulation of one or more target genes for these TCS was synthetically lethal. However, I was able to mobilize the plasmid for expression of *cenK* (pIND5-*cenK*) into cells containing the Δ*ntrYX* allele (Fig AA4). Since both the *cenK* overexpression strains and Δ*ntrYX* strains exhibited morphological defects, I asked if this also true in this strain. Growing the strain pIND5-*cenK* Δ*ntrYX* in the presence of IPTG produced cell morphology defects that differed from strains with either pIND5-*cenK* or Δ*ntrYX*. Additionally, in a collaboration with Daniel Parrell of the Wright lab, we observed increased lipid protrusions from the membrane into the media. Together, these experiments suggest an epistatic relationship between *cenKR* and *ntrYX*, possibly due to their impact on PG biosynthesis or other direct target genes.

Materials and Methods.

Bacterial strains and growth conditions. *Rb. sphaeroides* strains (Table AA) were grown in Sistrom's (SIS) minimal medium [4]. For aerobic growth, cells were grown in 5 mL of SIS with shaking at 200 rpm at 30°C. For anaerobic growth, a single colony of *Rb. sphaeroides* was used to inoculate SIS media and grown overnight. Phototubes were filled completely with media and diluted to an OD_{600} ~ 0.05. Tubes were sealed with a screw cap and wrapped in parafilm and grown in front of a light box ~100 W/m^2. Cell growth was monitored by Klett units (1 klett ~ $1x10^9$ cells).

Serial dilution spot titer assays. Spot assays were performed as described previously (Chapter 3). Fresh SIS antibiotic plates were made day of using the antibitoics at the indicated concentrations (Fig AA1).

Construction of pIND5-*cenK* Δ*ntrYX*.

The plasmid pIND5-*cenK* was transformed in *E. coli* S17-1 [5] and then mobilized in Δ*ntrYX* via conjugal mating. Colony PCR of Kan^R *Rb. sphaeroides* colonies was used to confirm successful mobilization of pIND5*cenK*.

Fluorescence and cryogenic electron microscopy. These experiments were performed as described previously (Chapter 3 materials and methods).

Table AA. Strains

Strain	Relevant characteristics	Source
Rhodobacter sphaeroides		
2.4.1	Wild type	ATCC-17023
BDL021	Δ*cenK*	[6]
BDL072	*cenR*(D56A)	[6]
BDL019	*cenR*(D56E)	[6]
BDL020	*cenR*(D56E) Δ*cenK*	[6]
TD000140	Δ*ntrYX*	[2]
Escherichia coli		
S17-1	*TpR SmR recA1 thiE1 pro-82 hsdR17 RP4-2-Tc::Mu-Km::Tn7* λpir	[5]

Figure AA1. Inactivation of the CenKR TCS results in antibiotic sensitivity.

Strains containing alleles that inactivate (Δ*cenK* or *cenR*(D56A)) or hyperactivate (*cenR*(D56E)) the CenKR TCS were tested for sensitivity to PG active compounds compared to wild type (WT) cells. β-lactam antibiotics Aztreonam inhibits PBP3, Ampicillin inhibits multiple PBPs, Amdinocillin inhibits PBP2; Vancomycin inhibits D-Ala-D-Ala crosslinking, Ramoplanin inhibits transglycosylation, Nisin inhibits Lipid II and DNA replication and repair, Bacitracin blocks Lipid II recycling; Globomycin inhibits LspA necessary for lipoprotein maturation; Fosfomycin blocks MurA activity the first committed step to cytoplasmic PG biosynthesis, D-cycloserine blocks DdlA activity preventing cytoplasmic addition of pentapeptide stems.

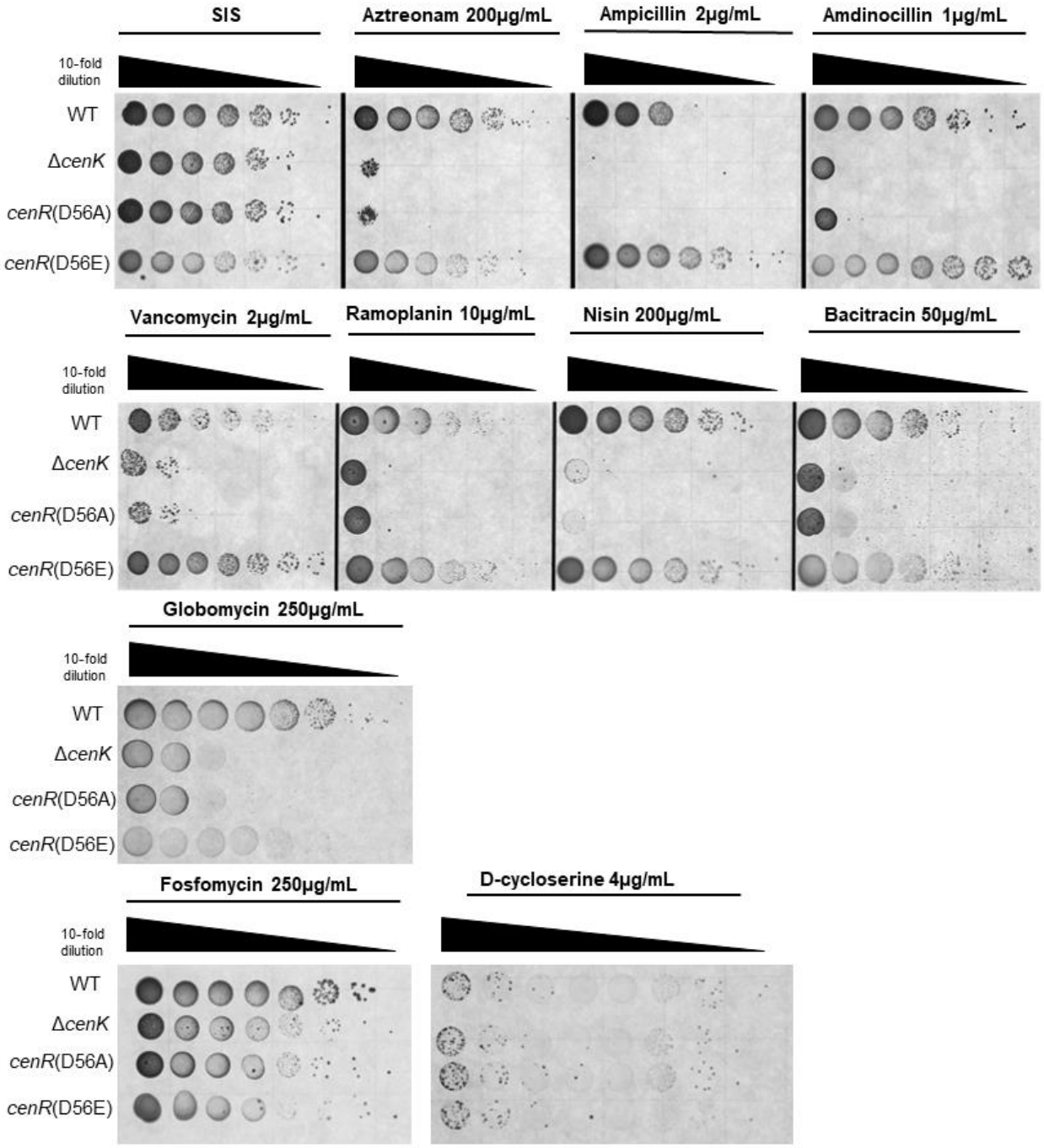
SIS
Aztreonam 200μg/mL
Ampicillin 2μg/mL
Amdinocillin 1μg/mL
10-fold dilution
WT
ΔcenK
cenR(D56A)
cenR(D56E)
Vancomycin 2μg/mL
Ramoplanin 10μg/mL
Nisin 200μg/mL
Bacitracin 50μg/mL
10-fold dilution
WT
ΔcenK
cenR(D56A)
cenR(D56E)
Globomycin 250μg/mL
10-fold dilution
WT
ΔcenK
cenR(D56A)
cenR(D56E)
Fosfomycin 250μg/mL
D-cycloserine 4μg/mL
10-fold dilution
WT
ΔcenK
cenR(D56A)
cenR(D56E)

Figure AA2. Pigment and photosynthesis phenotypes of *cenK* and *cenR* mutants

(A) Wild type, Δ*cenK*, and *cenR*(D56E) cells grown on SIS plates in the presence of oxygen. (B) Comparison of aerobically grown wild type and Δ*cenK* cultures. (C) Growth of wild type and indicated mutants in anaerobic + light conditions. Cells containing the *cenR*(D56E) allele displayed slower growth compared to wild type and strains with reduced CenKR activity. (D) Growth of cells containing pIND5-*cenK* in anaerobic + light conditions in the presence (+) or absence (-) of IPTG. Photos of *cenK* overexpression strains (+IPTG) represent early and late exponential growth.

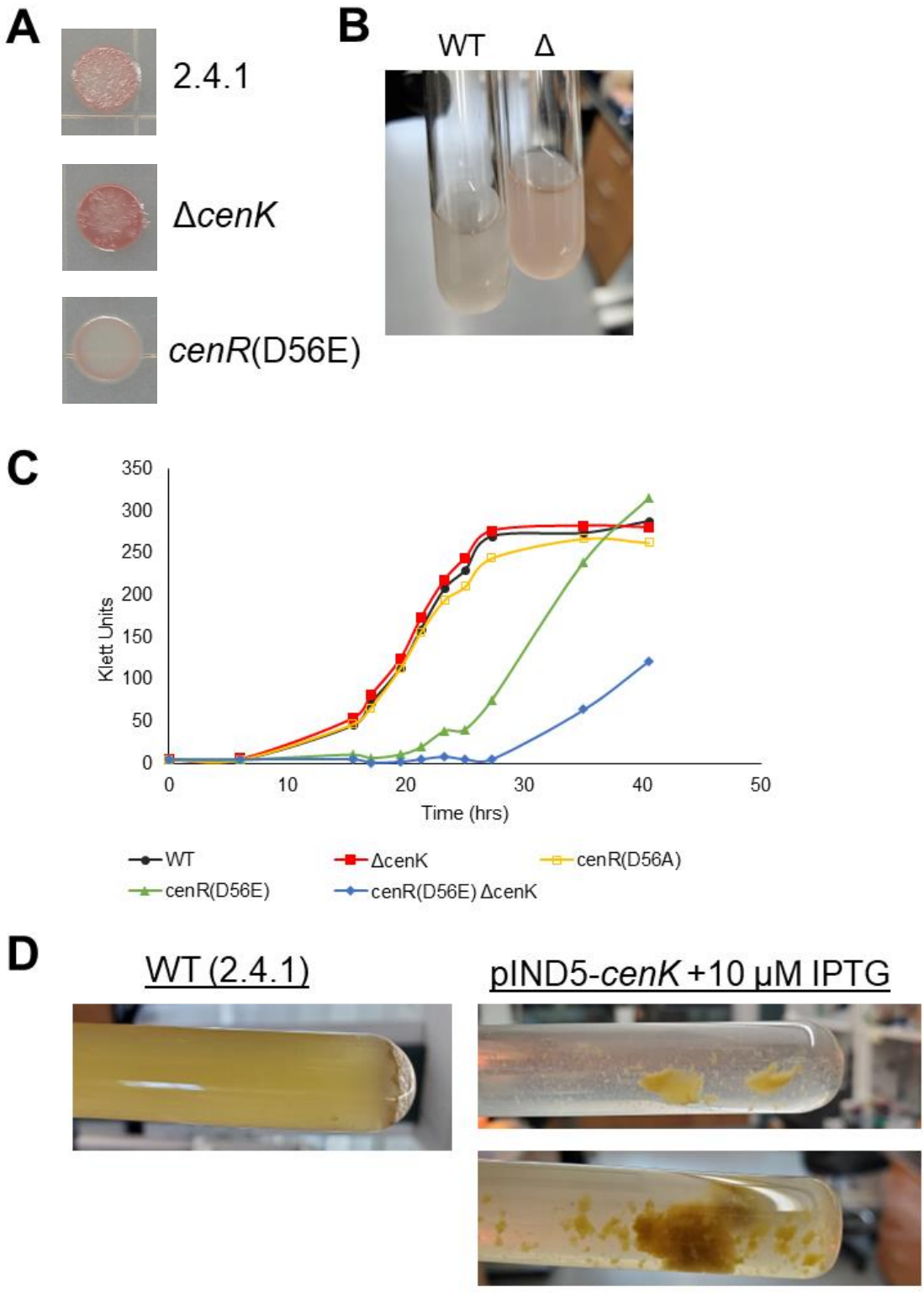
A
2.4.1
ΔcenK
cenR(D56E)
B
WT
Δ
C
Klett Units
350
300
250
200
150
100
50
0
0
10
20
30
40
50
Time (hrs)
WT
ΔcenK
cenR(D56A)
cenR(D56E)
cenR(D56E) ΔcenK
D
WT (2.4.1)
pIND5-cenK +10 µM IPTG

Figure AA3. NtrYX and CenKR synergistically regulate divisome machinery and cytoplasmic synthesis of peptidoglycan.

Differential expression of the *dcw* gene clusters (*mraZ-ftsA*; *RSP_2095 – RSP_2113*) in Δ*cenK* and Δ*ntrYX* strains relative to wild type cells determined by RNA-seq. The *dcw* gene clusters are negatively regulated by CenKR (blue) and positively regulated by NtrYX (orange) activity. (*ftsZ*, encoded on a separate downstream transcriptional unit was not differentially expressed, data not shown)

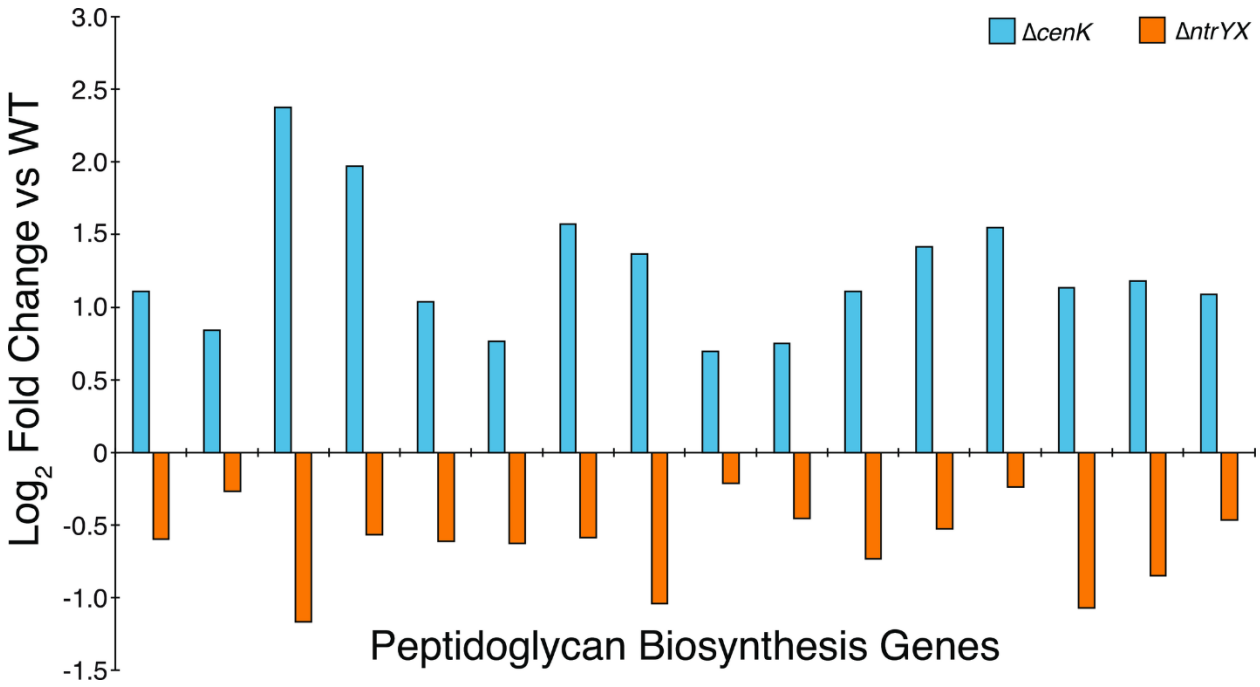

Figure AA4. Changes in morphology due to increased CenKR activity and loss of NtrYX

(Top panels) Bright field and fluorescence microscopy of pIND5-*cenK* Δ*ntrYX* grown in the presence (+) or absence (-) of IPTG to induce *cenK* expression. For fluorescence microscopy, cells were stained with FM 4-64 to better visual changes in cell envelope morphology. Scale bar =2 µm. (Bottom panel) Negative strain cryogenic electron microscopy images of this strain grown in the presence of IPTG. These cells exhibit large increases in extracellular lipid secretions. Scale bar = 500 nm.

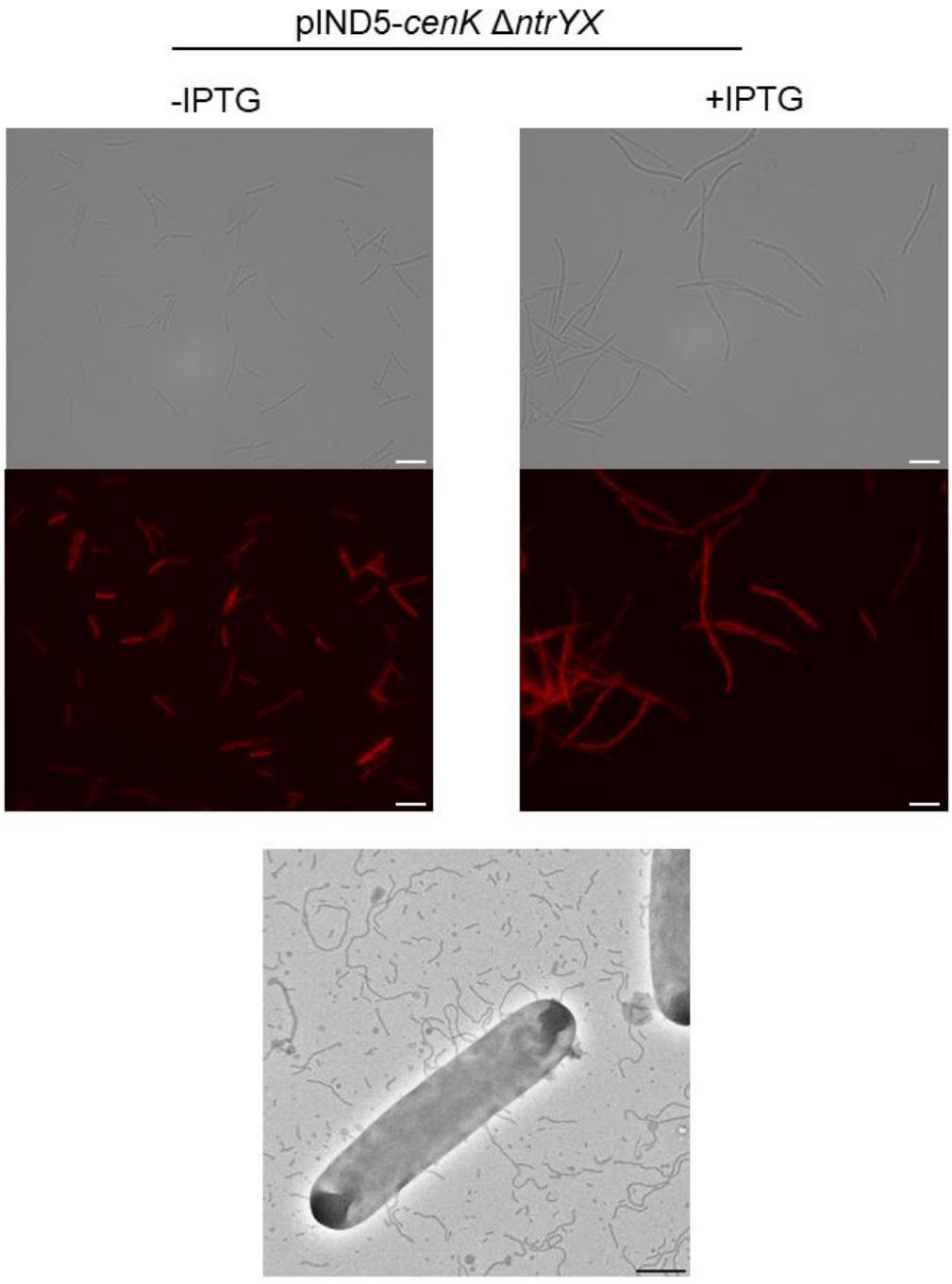
pIND5-*cenK* Δ*ntrYX*
-IPTG
+IPTG

References

1. Lemmer KC, Zhang W, Langer SJ, Dohnalkova AC, Hu D, Lemke RA, et al. Mutations That Alter the Bacterial Cell Envelope Increase Lipid Production. mBio. 8: e00513-17. doi:10.1128/mBio.00513-17
2. Lemmer KC, Alberge F, Myers KS, Dohnalkova AC, Schaub RE, Lenz JD, et al. The NtrYX Two-Component System Regulates the Bacterial Cell Envelope. Harwood CS, editor. mBio. 2020;11. doi:10.1128/mBio.00957-20
3. Bisicchia P, Lioliou E, Noone D, Salzberg LI, Botella E, Hübner S, et al. Peptidoglycan metabolism is controlled by the WalRK (YycFG) and PhoPR two-component systems in phosphate-limited Bacillus subtilis cells. Molecular Microbiology. 2010;75: 972–989. doi:10.1111/j.1365-2958.2009.07036.x
4. Sistrom WRY. A Requirement for Sodium in the Growth of Rhodopseudomonas spheroides. Microbiology. 1960;22: 778–785. doi:10.1099/00221287-22-3-778
5. Simon R, Priefer U, Pühler AA. A broad range mobilization system for in vivo genetic engineering: transposon mutagenesis in Gram-negative bacteria. Nat Biotechnol. 1983;(1):784-791. doi: 10.1038/nbt1183-784.
6. Lakey BD, Myers KS, Alberge F, Mettert EL, Kiley PJ, et al. (2022) The essential Rhodobacter sphaeroides CenKR two-component system regulates cell division and envelope biosynthesis. PLOS Genetics 18(6): e1010270. doi: 10.1371/journal.pgen.1010270

Appendix B: Analysis of the predicted essential *Rhodobacter sphaeroides* iron-sulfur cluster regulatory protein RSP_0443

Summary.

Below, I briefly highlight experiments performed to elucidate the role of RSP_0443 in *Rb. sphaeroides*. This work was performed in collaboration with the Kiley Lab and will be continued by Isabel Flores, Rachelle Lemke, and Kevin Myers.

Purple non-sulfur microbes can grow via aerobic respiration, anaerobic respiration, fermentation, and anaerobic photosynthesis [1,2]. As a part of this metabolic flexibility, *Rb. sphaeroides* relies on a different sets of iron-sulfur (Fe-S) proteins to support these and other metabolic and cellular functions [3]. Specifically, synthesis of tetrapyrrole molecules (porphyrins) required for heme biosynthesis as well as specialized bacteriochlorophyll accumulation required for anaerobic photosynthesis in *Rb. sphaeroides*, relies on proteins that coordinate Fe-S clusters [4]. Moreover, the cytochrome *bc1* complex that is necessary for photosynthetic electron transport requires a Fe-S cluster [5]. Consistent with this need, *Rb. sphaeroides* encodes genes of the Suf (sulfur formation) Fe-S biogenesis pathway directly downstream (*RSP_0442-RSP_0431*) of the gene encoding a predicted Rrf2 regulatory protein, RSP_0443. This IscR-like protein, has 44% amino acid identity to the well-studied *E. coli* IscR protein that directly regulates the expression of the *suf* operon [6] as well as other genes vital for Fe-S biogenesis (*isc* operon) [7]. Furthermore, the RSP_0443 protein contains a predicted DNA binding domain with amino acids that are known or predicted to be required for binding of the *E. coli* IscR protein to a Type 2 target site.

Rb. sphaeroides RSP_0443 is encoded directly upstream of the *suf* and this bacterium is not predicted to to contain a homologous *isc* operon (*iscSUA-hscBA-fdx*). Finally, unlike *E. coli* IscR that is well known to coordinate a 2Fe-2S cluster within the C-terminal domain [8], RSP_0443 lacks the key cysteine residues required for the ligation of this cluster. Thus, if and how RSP_0443 DNA binding activity is regulated in *Rb. sphaeroides*, what, if any, cofactor it coordinates, and how it controls expression of Fe-S biosynthesis and other target genes is not well understood.

This work sought to address these questions and characterize this IscR-like regulatory protein in order to provide much needed insight into how *Rb. sphaeroides* balances metabolic flexibility with Fe-S biosynthesis and other metabolic functions. We used a strain containing a C-terminally Myc-tagged version of the *RSP_0443* gene in the chromosome and Myc-specific antibodies in a ChIP-Seq analysis to show that it binds DNA and identify potential binding sites for this protein in the genome. We found that *RSP_0443* is essential in *Rb. sphaeroides* and loss of this protein often results in the accumulation of suppressor mutations in *chrR*, a gene that encodes the anti-sigma factor that controls the photooxidative stress response sigma factor σ^E. Based on this, we propose that activation of the σ^E regulon compensates for loss of the RSP_0443 protein, possibly by altering levels of Fe-S containing enzymes or by preventing cell damage by one or more reactive oxygen species that accumulate in the Δ*RSP_0443* mutant. Finally, we have preliminary evidence that RSP_0443 binds heme or other tetrapyrrole that could potentially be a newly identified strategy to regulate the DNA-binding activity of this transcription factor.

Results.

To identify the genes directly controlled by *Rb. sphaeroides* IscR (RSP_0443), I sought to delete this gene and compare the global transcript profiles in Δ*RSP_0443* strain relative to WT cells. Previous Tn-seq analysis suggests that *RSP_0443* is an essential gene in both aerobic and anaerobically grown *Rb. sphaeroides* since this genome-scale mutant library did not contain any strains with insertions in this gene or those of the neighboring *suf* operon [9]. To test the role of RSP_0443 directly, I constructed pk18mobsacB-Δ*RSP_0443* containing the homologous regions directly upstream of the 5' and directly downstream of the 3' regions encoding *RSP_0443* (see chapter 2 for deletion scheme diagram). Following mobilization into a wild type strain and sucrose counter selection to remove the pk18mobsacB suicide plasmid from the genome, I was able to isolate two separate strains containing an in-frame deletion of *RSP_0443* that I confirmed via colony PCR and sequencing (Fig AB-1A). These Δ*RSP_0443* deletion strains appeared as small colonies, growing slower than wild type cells. However, following outgrowth on plates or in liquid media, multiple colony morphologies were observed for each isolate suggesting the accumulation of suppressor mutations in the Δ*RSP_0443* strains (Fig AB-1C). In addition, incubation of the Δ*RSP_0443* strains on plates under anaerobic photosynthetic conditions (0% O_2 and ~100 W/m^2 Light) revealed that the Δ*RSP_0443* strain was unable to grow under these conditions (Fig AB-1B). Together, these data suggest that *RSP_0443* is an essential gene in *Rb. sphaeroides* under both aerobic and anaerobic conditions.

RNA-seq analysis of global transcript levels in Δ*RSP_0443* cells compared to WT cells grown in aerobic conditions identified 506 differentially expressed genes with $\log_2$ fold change greater than 1 or less than -1 and a false discovery rate (FDR) of less than 0.05. While this analysis is

confounded by the accumulation of suppressor mutations, the data suggests that RSP_0443 controls expression of the *suf* genes that lie directly downstream of *RSP_0443* (*RSP_0442-RSP_0431*).

To better assess the potential direct targets of RSP_0443 I assayed where in the genome this transcriptional regulator is bound by ChIP-seq. To do this, I constructed a strain containing a translational fusion of RSP_0443 to tandem Myc peptides (2xMyc) inserted at the C-terminal end (opposite the N-terminal DNA-binding motif) within the native *RSP_0443* genomic locus. Construction of this strain and analysis of growth in aerobic and anaerobic photosynthetic conditions showed that cells containing the RSP_0443-Myc tagged protein had colony and growth phenotypes that were comparable to that of a wild type strains, suggesting that the presence of this C-terminal tag did not have an adverse effect on cell growth (Fig AB-2). Furthermore, western blot analysis with antibody against the Myc-tag confirmed the accumulation of the _0443-Myc tagged protein in cell lysates (Fig AB-1D).

I used this strain to perform ChIP-seq experiments and analyze the binding of the RSP_0443-2xMyc to genomic DNA, *in vivo*, under both aerobic and anaerobic photosynthetic conditions. We identified a single major RSP_0443 enrichment site within the genome (~300 fold higher than negative and unenriched controls) directly upstream of the *RSP_0443-RSP_0431* operon suggesting that RSP_0443 regulates the expression of this *suf* operon in a manner consistent with *E. coli*. The ChIP-seq analysis also identifies other potential sites for RSP_0443 binding in the genome, but the fold-enrichment of this protein at these other positions compared to the background control is such that additional experiments are needed to make definitive conclusions

about any role of this transcription factor in controlling expression of these other genes. While the ChIP-seq dataset predict that RSP_0443 has a direct role in controlling transcription of the *RSP_0443-suf* transcription unit, the products of this operon only accounts for 9 of the 506 differentially expressed genes in the datasets obtained from Δ*RSP_0443* cells. Thus, it seems likely that RSP_0443 directly or indirectly impacts transcription from additional to be identified genes.

To gain additional insight into the role of RSP_0443, I utilized whole genome sequencing in order to identify SNPs within suppressors that were isolated under aerobic conditions. Following genomic DNA purification, library preparation, and sequencing, we identified 13 SNPs distributed across eight independent isolates (Table AB-1). Of these, 3 strains had the identical SNP that is predicted to result in a frame shift mutation within the gene encoding the anti-sigma factor ChrR. Based on what is know about ChrR, this mutation disrupts the function of the N-terminal region of this anti-sigma factor and is predicted to result in the activation of the stress response alternate sigma factor σ^E [10]. Given the importance of σ^E in *Rb. sphaeroides* for the mitigation of oxidative stress [11], this finding suggests that deletion of *RSP_0443* results in increased oxidative stress in the Δ*RSP_0443* strain. Indeed, it is well known that Fe-S clusters react with oxygen to produce toxic reactive oxygen species [12]. Together, this analysis leads to a hypothesis that RSP_0443 represses Fe-S protein biosynthesis and that derepression of these genes by loss of RSP_0443 results in accumulation of Fe-S clusters in oxygenic conditions, oxidative stress, and can lead to cell death. Furthermore, this analysis confirms the essentially of this regulator in *Rb. sphaeroides* as previously suggested [9]. As the σ^E regulon has been extensively characterized, construction of a Δ*RSP_0443* Δ*chrR* strain maybe provide us a chassis

to study a stable deletion of *RSP_0443* and best determine differentially expressed genes regulated by this IscR-like regulator.

In *E. coli*, IscR activity is governed by the occupancy (holo) or absence (apo) of the Fe-S center coordinated by cysteine and other residues in the C-terminal domain of this regulator [8]. This modulation of activity governs its regulatory control of the *isc* operon, but not the *suf* operon [8]. Given the lack of this *isc* operon in *Rb. sphaeroides* and the absence of these cysteine residues (Fig AB-3), we sought to determine if RSP_0443 coordinates another ligand and how it may affect its regulatory control of the *Rb. sphaeroides suf* operon. Within the C-terminal domain of RSP_0443 (Figure AB-3) are several histidine residues (H92, H121, H127) that are known to be important for heme coordination in other bacterial proteins [13,14]. Heme is a tetrapyrrole molecule bound to a reduced Fe^{2+} atom which can be oxidized to Fe^{3+} thereby forming hemin. The redox chemistry of heme plays a significant role in many biological processes including sensing of gases like O_2 or NO, respiration, and electron transport, and can commonly function as a key prosthetic group in transcriptional regulators [14]. To test if RSP_0443 can bind heme, we sought to purify this protein anaerobically and determine if heme was present by spectroscopy. To do so, we first expressed a purified RSP_0443-GCFGG-streptavidin fusion protein in *E. coli* suf+ [15] containing the Rosetta plasmid for rare tRNAs. Incubation of this recombinant RSP_0443-GCFGG-streptavidin protein in the presence of heme and removal of excess heme by buffer exchange produced an absorbance spectrum consistent with the presence of heme in the RSP_0443 protein (Fig AB-4). We also sought to purify RSP_0443-GCFGG-streptavidin directly from *Rb. sphaeroides* in order to capture native heme coordinating activity. However, expression of this translational fusion from an ectopic, IPTG inducible pIND5 plasmid

mobilized into *Rb. sphaeroides* proved to be detrimental to cells as a frameshift or nonsense mutation was found in the RSP_0443-GCFGG-streptavidin coding regions in several independent exconjugants. Finally, we sought to purify RSP_0443-2xMyc endogenously expressed from the native *RSP_0443* locus. Purification of this protein on a mcy-affinity column yielded quantities of RSP_0443 only detectable by western blot (Figure AB-5), so future efforts will focus on growing larger amounts of cells to assay heme or other ligand binding to the tagged version of RSP_0443 when the protein is expressed in the native host. Finally, following identification of a putative RSP_0443 ligand, substitution of specific histidine residues to disrupt binding activity will be key to understanding the coordination of this molecule in the C-terminal domain. Further, this approach will be useful to understanding how the presence or absence of any ligand influences DNA binding of the *Rb. sphaeroides* RSP_0443 to one or more target sites predicted from ChIP-Seq and other experiments.

Materials and methods.

Bacterial strains and growth conditions. *Rb. sphaeroides* strains (Table AB-2) were grown in Sistrom's (SIS) minimal medium [16]. For aerobic growth, cells were grown in 5 mL of SIS with shaking at 200 rpm at 30°C. For anaerobic growth, SIS agar plates were placed into sealed canisters containing a GasPak EZ anaerobe container system packet (BD Biosciences), inclubated at room temperature in front of incandescent light with an intensity of 100 W/m^2. For RNA-seq and ChIP-seq growth, 500 mL of SIS was inoculated with *Rb. sphaeroides* at an OD_{600} of 0.01 and bubbled with either 69% N_2, 30% O_2, 1% CO_2 (aerobic), or 95% N_2, 5% CO_2 in front of incandescent light with an intensity of 100 W/m^2 (anaerobic) for ~18 hours until cells reached

an OD_{600} of ~0.5 (mid-log). *E. coli* strains (Table AB-2) were grown in LB supplemented with Kanamycin (25 µg/mL) and/or 10 µM IPTG as required.

Construction of Δ*RSP_0443* and *RSP_0443*::*RSP_0443-2xMyc*.

Cloning, assembly, mobilization, and selection (Km^R)/counter-selection (Km^S Suc^R) of pk18mobsacB-Δ*RSP_0443* or pk18mobsacB-*RSP_0443-2xMyc* in *Rb. sphaeroides* was performed as previously described (Chapter 2 Materials and Methods). Primers and plasmids are listed in Table AB-3. For deletion of *RSP_0443*, in-frame deletion was designed and confirmed by sequencing, to remove bases 2,174,826 (5' start codon of *RSP_0443*) – 2,174,359 (3' stop codon of *RSP_0443*).

Western blot analysis.

Confirmation of Myc or streptavidin RSP-0443 fusion protein was performed by harvesting exponentially growing cultures resuspended in 3x LDS samples buffer (ThermoFisher) supplemented with 100 µM DTT and heated at 95°C for 15 minutes. Samples were centrifuged to remove cell debris. Western blotting was performed as previously described [17] using anti-Myc (abcam) or anti-streptavidin (ThermoFisher). Secondary anti-goat or anti-rabbit, respectively, antibodies conjugated to HRP was used. Detection was performed with Fisher SuperSigal Western Pico Plus Chemiluminescent Detection Kit.

ChIP-seq and RNA-seq

Chromatin immunoprecipitation and sequencing was performed as previously described [18]. Immunoprecipitation of RSP_0443-2xMyc-DNA complexes was achieved using anti-Myc tag

antibody (ChIP Grade, abcam ab9132). Isolation of ab-0443-DNA complexes was achieved using protein G sepharose (Sigma). RNA isolation and sequencing was performed as previously described [18].

Genomic DNA extraction and whole genome sequencing.

15 mL of exponentially growing *Rb. sphaeroides* (OD_{600} ~ 0.5) was pelleted by centrifugation (8,000 x *g* for 5 minutes), resuspended in 200 µL of lysis buffer (50 mM Tris·HCl, pH 8.0, 10 mM EDTA pH 8.0, 1% Triton X-100, and 0.5 mg/mL RNase A), and incubated at 37°C for 30 minutes. 30 µL of 10% SDS and 25 µL protease K was added, mixed well by pipette, and incubated at 55°C for 30 minutes. To the lysis mixture, 600 µL PB buffer (Qiagen) was added, mixed by pipette, and loaded onto a silica spin column. The column was centrifuged at max speed for 1 minute, the flow through was discarded, the column was washed with 600 µL PB Buffer, and then with 750 µL PE Buffer (Qiagen). Following final flow through, the silica membrane was dried by a final centrifugation at max speed for 1 minute. Genomic DNA was eluted by addition of 75 µL of ddH_2O, incubated for 3 minutes at room temperature, and centrifuged at max speed for 1 minute. This was elution was repeated once more for a final volume of 150 µL.

For library preparation and sequencing, 250 ng of DNA was sheared by sonication to 200-300 bp in length. Library preparation was performed using the NEBNext Ultra II DNA Library Preparation Kit following the manufacturer's instructions (E7103L, New England BioLabs). Unique dual indexing primers were used for each library (NEBNext Multiplex Oligos for Illumina, E6440S). Library quality and integrity was confirmed by D1000 ScreenTape System

(Agilent) and quantified by Qubit HS dsDNA kit. Equal molar libraries were loaded onto NextSeq 1000 flow cell for sequencing. Data processing and analysis was performed by Kevin S. Myers using a previously described DNA sequencing pipeline.

Expression and purification of RSP_0443-GCFGG-streptavidin.

E. coli BL21(DE3) suf+ strain was modified to incorporate Rosetta plasmid (Cm^R). RSP_0443 was cloned into pET11a containing the linker GCFGG connected to streptavidin tag. Expression was induced with IPTG. Protein purification was performed using GE Healthcare ÄKTA Prime Plus FPLC system and 1 mL StrepTrap HP HiTrap prepacked column (GE). *E. coli* was lysed by sonication in harvest buffer (10 mM HEPES pH 7.4, 100 mM NaCl, 10% glycerol, 1 mM DTT), and centrifuged to remove debris before being loaded onto column. The column was washed with 10 mM HEPES pH 7.4, 100 mM NaCl, 10% glycerol, 1 mM DTT before protein was eluted with 10 mM HEPES pH 7.4, 100 mM NaCl, 10% glycerol, 1 mM DTT, 2.5 mM desthiobiotin. Protein was buffer exchanged (10 mM HEPES pH 7.4, 100 mM NaCl, 10% glycerol) and flash frozen for storage.

Batch purification of RSP_0443-2xMyc.

100 mL of exponentially growing cells (OD_{600} ~ 0.6) was harvested, pelleted by centrifugation, and resuspended in 2mL harvest buffer (same as above). Cells were lysed by sonication (10 cycles, 30s on, 30s off, 75%, on ice) and cell debris was cleared by centrifugation. A small sample was saved for protein gel analysis (L fraction). In a 2 mL Eppendorf tube, 400 µL of Pierce Anti-c-Myc Agarose (25% slurry) was washed three times with TBS for a bead volume of 100 µL. Protein preparation was done following manufacturer's instructions with some

exceptions. To the washed beads, the remaining volume of lysate was added and incubated at 4°C with gentle rocking overnight. Beads were collected by centrifuge 5,000 x *g* for 2 min at 4°C and supernatant removed and saves for analysis (F fraction). Beads were washed four times with one bead volume of TBS-T (0.05% Tween-20), beads were collected by centrifuge, and supernatant saved for analysis (W fractions). The c-Myc peptide (Pierce) was resuspended in TBS to a concentration of 1 mg/mL. To elute, one bead volume (~100 µL) of 1 mg/mL c-Myc peptide was added to the beads and incubated at room temperature for 30 minutes. Beads were centrifuged and elution fractions (E) were collected. This was repeated three times. Samples of each fraction were collected for analysis and the remaining volume (~400 µL) was concentrated to~50 µL for analysis.

Figure AB-1. Δ*RSP_0443* and *RSP_0443*::*RSP_0443-2xMyc* strains

(A) Isolation of Δ*RSP_0443* mutants. Patch plating of colonies following sucrose counter selection produced two, slow growing colonies ($Km^{S}Suc^{R}$), indicated by blue and red arrows. Colony PCR (primers listed in Table AB-3 confirmed in frame deletion of *RSP_0443* from the genome. (expected sizes of PCR products Δ ~ 650bp; WT ~ 1,050 bp) **(B)** Wild type, Δ*RSP_0443* and *RSP_0443*::*RSP_0443-2xMyc* strains were assayed for their ability to grown in anaerobic photosynthetic conditions. **(C)** Outgrowth of Δ*RSP_0443* in aerobic conditions produced multiple colonies types suggesting the accumulation of suppressor mutations in this strain. **(D)** Western blot confirming stable fusions of the tandem Myc tag to RSP_0443.

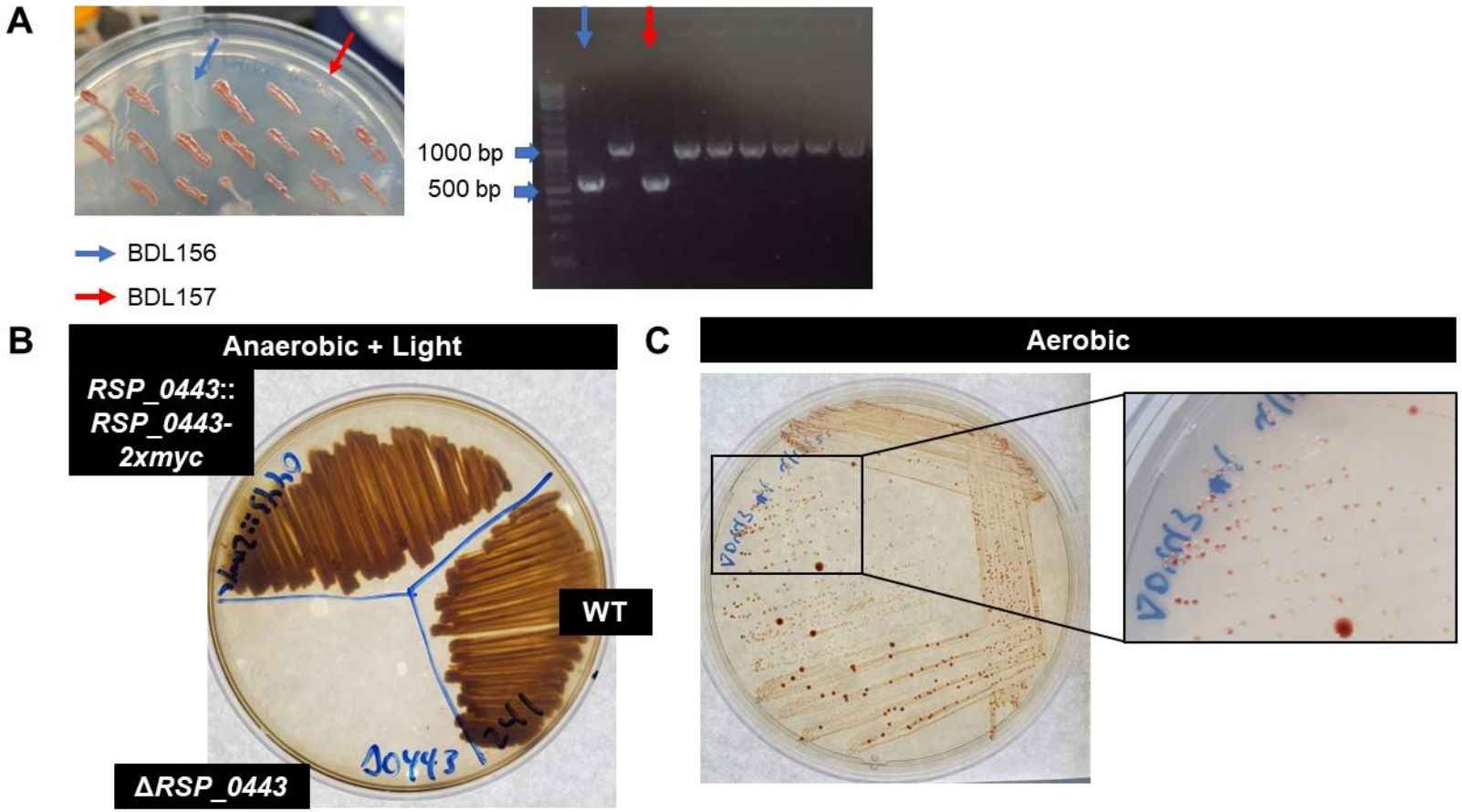
A
1000 bp
500 bp
BDL156
BDL157
B
Anaerobic + Light
RSP_0443::
RSP_0443-
2xmyc
WT
ΔRSP_0443
C
Aerobic

D

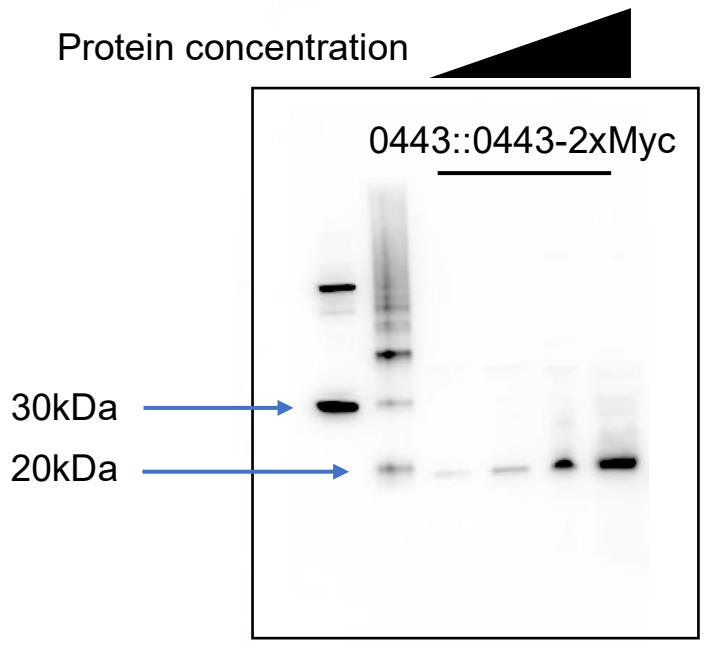

Expected size : 16.8 kDa (untagged)

: ~20 kDa (2xMyc)

Figure AB-2. ChIP-seq and RNA-seq data of *RSP_0443-RSP_0431* operon.

(A) ChIP-seq enrichment (top panel) shows binding of RSP_0443 directly upstream of the *Rb. sphaeroides suf* operon. Deletion of Δ*RSP_0443* results in increased *suf* transcript levels relative to WT cells (bottom panel). Transcription start sites (TSS) [19] for this transcriptional unit are also shown below each ChIP peak. Aero = aerobic 30% O_2, Photo = anaerobic 0% O_2 + Light.

(B) Sequence contained within the RSP_0443 enrichment peak. The motif CC-N_{13}-GG is highly conserved in genome wide binding motifs identified in *E. coli* [20]. Putative IscR binding site is in bold and underlined; +1 TSS indicated is in bold and red; gene coding sequence for *RSP_0443* is in the aqua box.

A

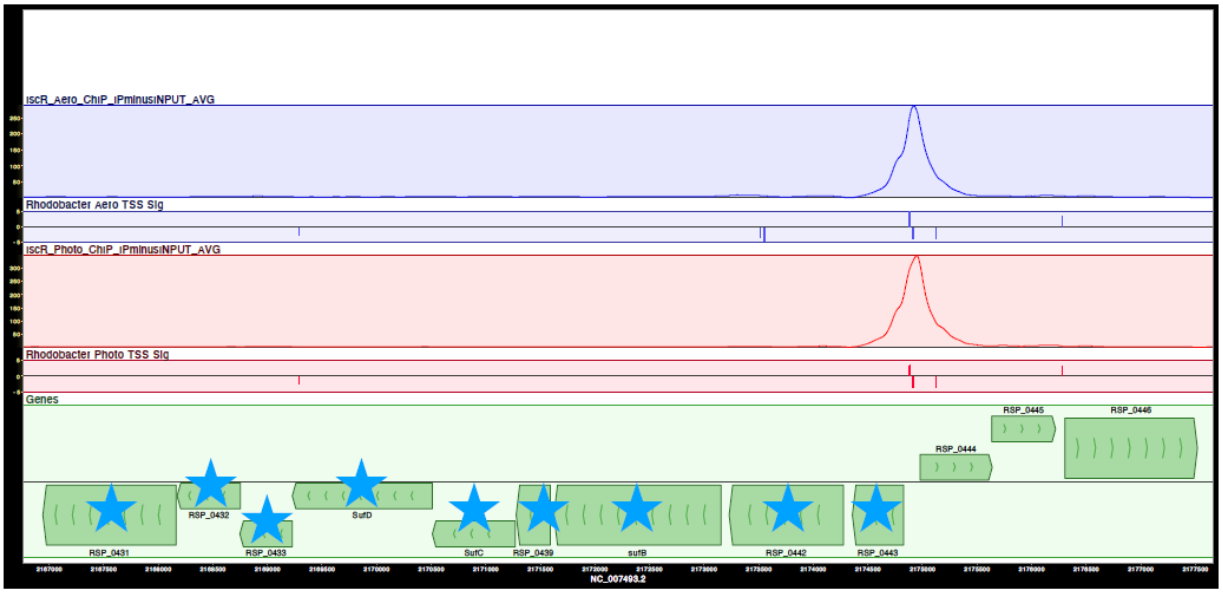

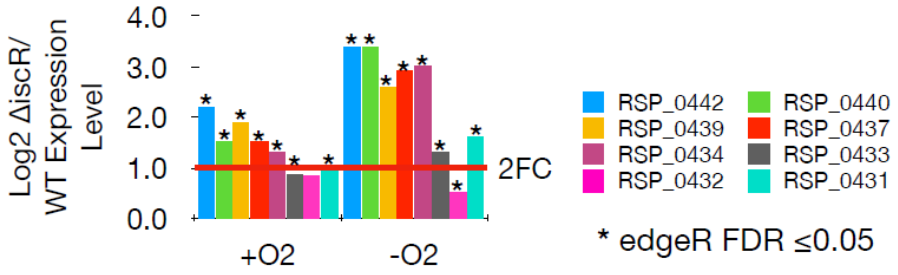

B

CGCCTCGCCTTGCCTGTTTCTTCCGCGGCGTAATCTTGACAAAAACGCTCGGATAAATT**AGAACCATTCC**
ACCTGGGCGGTGCATCCGCCCGGAACCGTAACGAGTTAAGCGGCCTGCCGCTTGGCGTCAATGGATTT
GGCGGGAACCGGAAA**ATGAAACTCTCGACCAAGGGTCGGTATGCGATGGTGGCGCT**

Potential IscR Type2 Site:

AGAACCATTCCACCTGGGCGG**TGCA**

Figure AB-3. Amino acid alignment of *E. coli* and α-proteobacterial IscR homologs

Important residues for DNA binding [21] are highlighted with red stars. Rrf2 highly conserved regions indicated by blue line. Green arrows indicate the position of conserved cysteine residues for Fe-S ligation. For amino acid alignment, asterisks (*) indicate identical residues in all four sequences, colons (:) indicate residues with strongly similar properties, periods (.) indicate residues with weakly similar properties (for more information, visit Clustal Omega FAQs). For *Rb. sphaeroides* contains three histidine residues (orange underline) within the C-terminal coordination domain, as well as a single cysteine residue (yellow box), suggesting that this domain may bind a heme or other tetrapyrrole-like molecule. IscR homologs identified in other α-proteobacteria of industrial relevance, *Zymomonas mobilis* and *Novosphingobium aromaticivorans* were included in this alignment. In each of these related bacteria, the cysteine residues within the C-terminal domain are highly conserved.

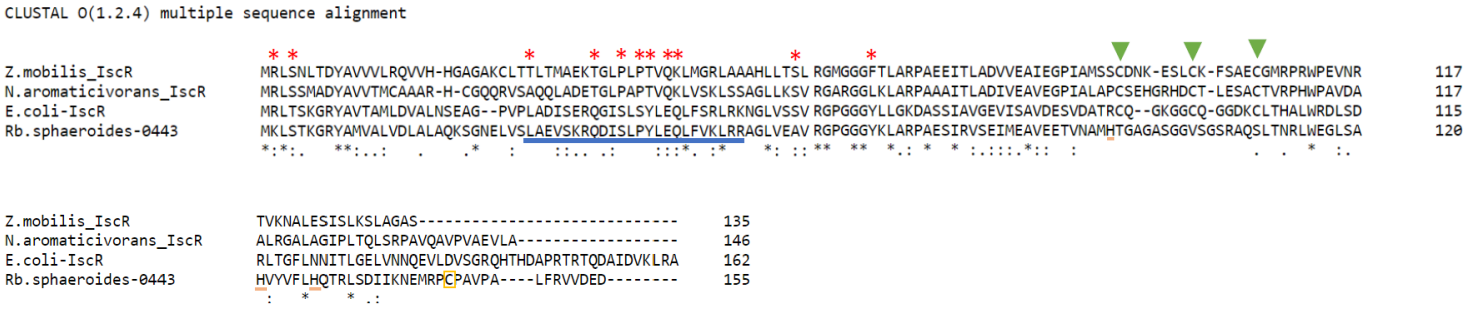
CLUSTAL O(1.2.4) multiple sequence alignment
Z.mobilis_IscR MRLSNLTDYAVVVLRQVVH-HGAGAKCLTTLTMAEKTGLPLPTVQKLMGRLAAAHLLTSL RGMGGGFTLARPAEEITLADVVEAIEGPIAMSSCDNK-ESLCK-FSAECGMRPRWPEVNR 117
N.aromaticivorans_IscR MRLSSMADYAVVTMCAAAR-H-CGQQRVSAQQLADETGLPAPTVQKLVSKLSSAGLLKSV RGARGGLKLARPAAAITLADIVEAVEGPIALAPCSEHGRHDCT-LESACTVRPHWPAVDA 117
E.coli-IscR MRLTSKGRYAVTAMLDVALNSEAG--PVPLADISERQGISLSYLEQLFSRLRKNGLVSSV RGPGGGYLLGKDASSIAVGEVISAVDESVDATRCQ--GKGGCQ-GGDKCLTHALWRDLSD 115
Rb.sphaeroides-0443 MKLSTKGRYAMVALVDLALAQKSGNELVSLAEVSKRQDISLPYLEQLFVKLRRAGLVEAV RGPGGGYKLARPAESIRVSEIMEAVEETVNAMHTGAGASGGVSGSRAQSLTNRLWEGLSA 120
Z.mobilis_IscR TVKNALESISLKSLAGAS---------- 135
N.aromaticivorans_IscR ALRGALAGIPLTQLSRPAVQAVPVAEVLA---------- 146
E.coli-IscR RLTGFLNNITLGELVNNQEVLDVSGRQHTHDAPRTRTQDAIDVKLRA 162
Rb.sphaeroides-0443 HVYVFLHQTRLSDIIKNEMRPCPAVPA----LFRVVDED-------- 155

Figure AB-4. Absorbance spectrum of RSP_0443 incubated with heme.

Purified RSP_0443 was incubated with heme for 20 minutes at room temperature and then buffer exchanged to remove excess heme. Absorbance was measured over a range from 260-700 nm. In both assays (protein at excess to heme and at equal molar quantities), an absorbance shift was detected compared to samples with protein (apo) or heme alone. Soret peaks with maxima at 361 and 421 nm are indicative of protein with heme-ligand bound.

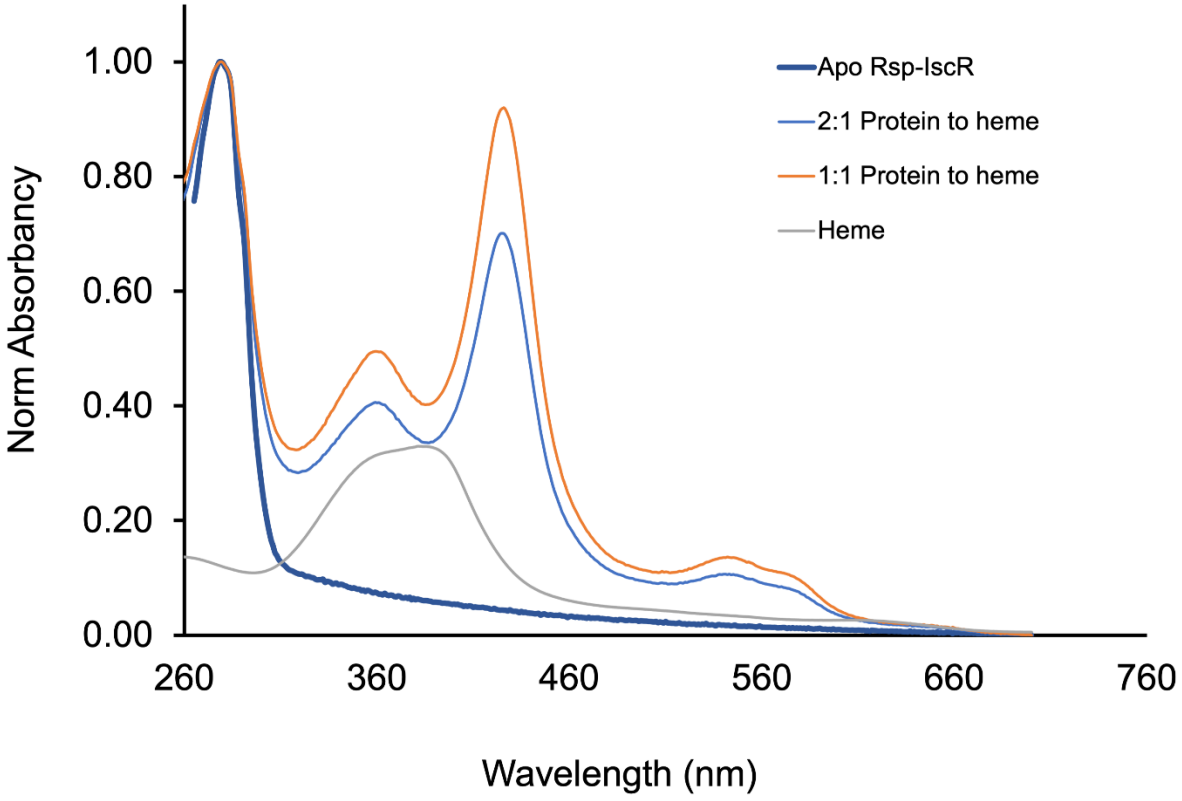

Figure AB-5. Purification of RSP_0443-2xMyc

Western blot (top) and coomassie stained protein gel (bottom) of RSP_0443-2xMyc purified using Myc affinity agarose. L – cell lysate; F – flow through collected after incubation with agarose slurry; W1-W3 wash fractions; E1-E4 elution fractions; C – concentrated protein.

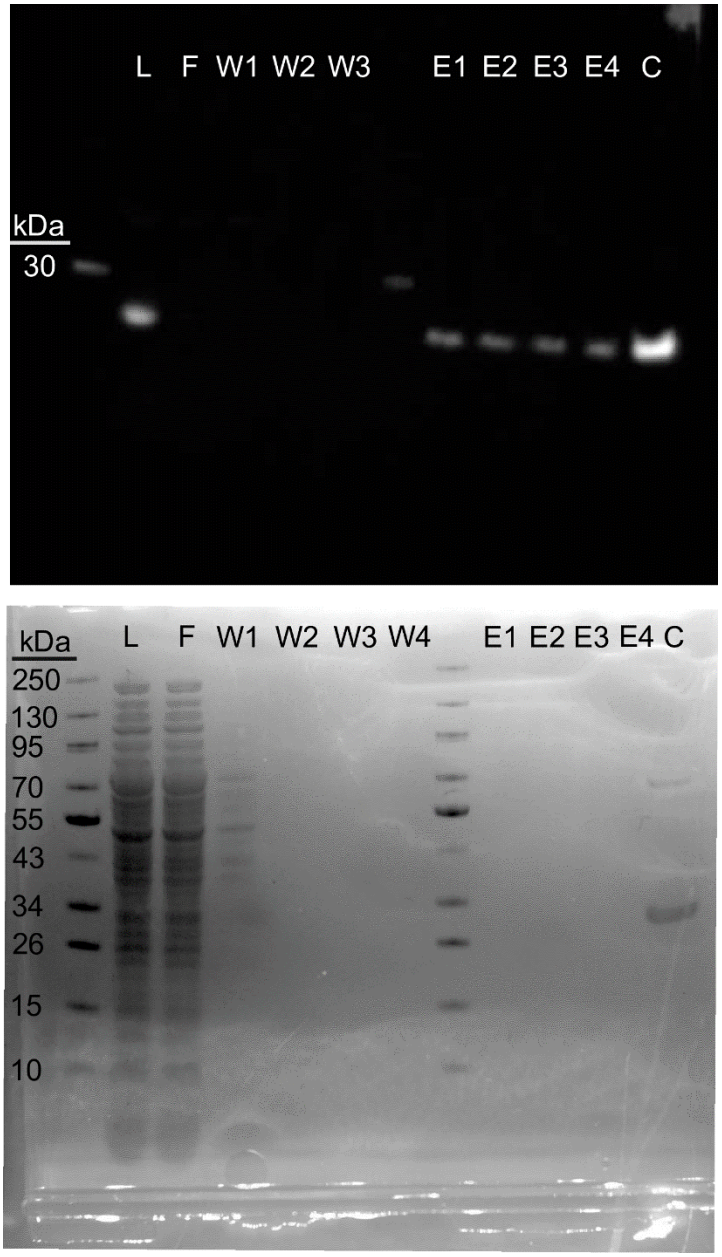

Table AB-1. Suppressor mutations identified within Δ*RSP_0443* isolates

Mutation	Annotation	Gene	WT	BL 1	BL 2	BL 3	BL 4	BL 5	BL 6	BL 7	BL 8
Δ468 bp	Original *RSP_0443* deletion	Δ*RSP_0443*		X	X	X	X	X	X	X	X
G→C	intergenic (+122/+69)	*RSP_3995* → / ← *RSP_3994*		X	X	X		X	X	X	
$(C)_{6\rightarrow7}$	coding (1126/1218 nt)	*RSP_7390* ←					X	X	X		
G→A	Q307Q (CAG→CAA)	*traC* →					X	X	X		
C→T	C343C (TGC→TGT)	*traC* →					X	X	X		
C→T	R45H (CGC→CAC)	*RSP_6006* ←					X	X	X		
$(G)_{6\rightarrow7}$	coding (149/642 nt) (At Gly50)	*chrR* →		X			X				X
A→G	S22P (TCC→CCC) (Ser22 to Pro22)	*RSP_6006* ←				X					
A→G	intergenic (-4/-234)	*RSP_7501* ← / → *RSP_1549*								X	
T→G	intergenic (-225/+73)	*RSP_2392* ← / ← *kdtA 1*						X			
C→G	intergenic (+11/+135)	*RSP_0247* → / ← *RSP_0248*			X						
Δ2 bp	Intergenic (+22/-281)	*RSP_0378* → / → *RSP_0379*			X						

A→G	Intergenic (-26/+26)	*RSP_3659* ← / ← *RSP_3661*			X						
C→G	intergenic (+30/+62)	*RSP_3705* → / ← *RSP_3706*			X						

Table AB-2. Strains

Strain	Relevant characteristics	Source
Rhodobacter sphaeroides		
2.4.1	Wild-type	ATCC 17023
BDL156 and BDL157	Δ*RSP_0443*	This work
BDL158	*RSP_0443*::*RSP_0443*-2xMyc (C-terminal tag)	This work
Escherichia coli		
NEB 5-alpha competent *E. coli*	*fhu*A2 Δ(*argF-lacZ*)U169 *phoA* *gln*V44 Φ80 Δ(*lacZ*)M15 *gyrA*96 *recA*1 *relA*1 *endA*1 thi-1 *hsdR*17	New England BioLabs
S17-1	*TpR SmR recA1 thiE1 pro-82 hsdR17 RP4-2-Tc::Mu-Km::Tn7* λpir	[22]
BDL256	S17-1 containing pK18mobsacB-0443	This work
BDL299	S17-1 containing pK18mobsacB-0443-2xMyc	This work

Table AB-3. Primer and Plasmids

A. Primers

Primer Name	Sequence	Purpose
pk18_0443_up_F2	TGCAGCTGGCACGACAGCATGGATGAGCAG CATG	Amplification of region 5' of *RSP_0443*
0443_down_up_R	GACAGCCACCGCCTTTCCGGTTCCCGCCAAA TC	
0443_up_down_F	GAACCGGAAAGGCGGTGGCTGTCGTGG	Amplification of the region 3' of *RSP_0443*
pk18_0443_down_R2	TTCTGCGGACTGGCTTTCTACCGGACGGCTT GATCCTTC	
BDL3-3	TAGAAAGCCAGTCCGCAGAAAC	PCR Linearization of pk18mobsacB
BDL3-4	CTGTCGTGCCAGCTGCATTAATGAATCG	
0443_confirm_F	ACTGTGAATCCCAGCCGATAGA	PCR and sequencing primers flanking *RSP_0443*
0443_confirm_R	ATCTTATGCGCCGAGACGAATC	
pk18_0443_up_F	TGCAGCTGGCACGACAGCATGGATGAGCAG CATG	Amplification of region 5' *RSP_0443* stop codon for insertion of tandem Myc tag
0443_gene_up_R	CCGCGCGAGCTTGTAGC	
0443_2xC-terminal Myc_gblock	TACAAGCTCGCGCGGCCCGCGGAGTCGATC CGGGTCAGCGAGATCATGGAAGCGGTGGAA GAGACGGTCAATGCGATGCATACCGGTGCT GGTGCAAGTGGAGGCGTTTCCGGCTCGCGT GCACAATCCTTGACCAACCGGCTGTGGGAG GGCCTCTCGGCGCATGTCTATGTCTTCCTGC ACCAGACCCGTCTGTCGGACATCATCAAAA ACGAGATGCGTCCATGCCCGGCGGTGCCGG CGCTGTTTCGAGTGGTTGACGAGGACGGTTC GGAGCAGAAGCTGATCTCGGAGGAGGACCT	gBlock (IDT) containing the coding sequencing for the Myc tag. Using in Gibson cloning reaction for assembly of pK18mobsacB-0443-2xMyc

	GGAACAGAAGCTCATCAGCGAGGAGGACCT GTAGGGCGGTGGCTGT	
0443_gene-Myc_down_F	GGCGGTGGCTGTCGTGGC	Amplification of the region 3' *RSP_0443* stop codon
pk18_0443_down_R	TTCTGCGGACTGGCTTTCTACCGGACGGCTT GATCCTTC	
BDL1-3	ATCCCCTGATTCTGTGGATAACCGTATTACCG	PCR amplification of pk18mobsacB cloning site
BDL2-3	CCCAGTCTAGCTATCGCCATGTAAGCC	

B. Plasmids

Name	Description	Source
pK18mobsacB	Broad host range mobilizable vector; Km^R oriT(RP4) mobT *sacB lacZα*	[23]
pK18mobsacB-Δ*RSP_0443*	*Rb. sphaeroides* genomic regions flanking *RSP_0443* Gibson assembled into pk18, Km^R, for deletion of *RSP_0443*	This work
pK18mobsacB-*RSP_0443-2xMyc*	*Rb. sphaeroides* genomic regions flanking *RSP_0443* Gibson assembled into pk18, Km^R, for insertion of 2xMyc tag into genome	This work

References.

1. Imam S, Noguera DR, Donohue TJ. Global insights into energetic and metabolic networks in Rhodobacter sphaeroides. BMC Systems Biology. 2013;7: 89. doi:10.1186/1752-0509-7-89

2. Mackenzie C, Eraso JM, Choudhary M, Roh JH, Zeng X, Bruscella P, et al. Postgenomic Adventures with *Rhodobacter sphaeroides*. Annu Rev Microbiol. 2007;61: 283–307. doi:10.1146/annurev.micro.61.080706.093402

3. Fontecave M. Iron-sulfur clusters: ever-expanding roles. Nat Chem Biol. 2006;2: 171–174. doi:10.1038/nchembio0406-171

4. Zappa S, Li K, Bauer CE. The tetrapyrrole biosynthetic pathway and its regulation in Rhodobacter capsulatus. Adv Exp Med Biol. 2010;675: 229–250. doi:10.1007/978-1-4419-1528-3_13

5. Purvis DJ, Theiler R, Niederman RA. Chromatographic and protein chemical analysis of the ubiquinol-cytochrome c2 oxidoreductase isolated from Rhodobacter sphaeroides. Journal of Biological Chemistry. 1990;265: 1208–1215. doi:10.1016/S0021-9258(19)40179-8

6. Yeo W-S, Lee J-H, Lee K-C, Roe J-H. IscR acts as an activator in response to oxidative stress for the suf operon encoding Fe-S assembly proteins. Molecular Microbiology. 2006;61: 206–218. doi:10.1111/j.1365-2958.2006.05220.x

7. Schwartz CJ, Giel JL, Patschkowski T, Luther C, Ruzicka FJ, Beinert H, et al. IscR, an Fe-S cluster-containing transcription factor, represses expression of Escherichia coli genes encoding Fe-S cluster assembly proteins. Proceedings of the National Academy of Sciences. 2001;98: 14895–14900. doi:10.1073/pnas.251550898

8. Mettert EL, Kiley PJ. Coordinate Regulation of the Suf and Isc Fe-S Cluster Biogenesis Pathways by IscR Is Essential for Viability of Escherichia coli. Journal of Bacteriology. 2014;196: 4315–4323. doi:10.1128/JB.01975-14

9. Burger BT, Imam S, Scarborough MJ, Noguera DR, Donohue TJ. Combining Genome-Scale Experimental and Computational Methods To Identify Essential Genes in Rhodobacter sphaeroides. mSystems. 2: e00015-17. doi:10.1128/mSystems.00015-17

10. Anthony JR, Newman JD, Donohue TJ. Interactions Between the Rhodobacter sphaeroides ECF Sigma Factor, σE, and its Anti-sigma Factor, ChrR. J Mol Biol. 2004;341: 345–360. doi:10.1016/j.jmb.2004.06.018

11. Donohue TJ. Shedding light on a Group IV (ECF11) alternative σ factor. Mol Microbiol. 2019;112: 374–384. doi:10.1111/mmi.14280

12. Outten FW. Recent advances in the Suf Fe-S cluster biogenesis pathway: Beyond the Proteobacteria. Biochim Biophys Acta. 2015;1853: 1464–1469. doi:10.1016/j.bbamcr.2014.11.001

13. Rinaldo S, Castiglione N, Giardina G, Caruso M, Arcovito A, Longa S della, et al. Unusual Heme Binding Properties of the Dissimilative Nitrate Respiration Regulator, a Bacterial Nitric Oxide Sensor. Antioxidants & Redox Signaling. 2012;17: 1178–1189. doi:10.1089/ars.2011.4226

14. Tong Y, Guo M. Bacterial heme-transport proteins and their heme-coordination modes. Archives of Biochemistry and Biophysics. 2009;481: 1–15. doi:10.1016/j.abb.2008.10.013

15. Corless EI, Mettert EL, Kiley PJ, Antony E. Elevated Expression of a Functional Suf Pathway in Escherichia coli BL21(DE3) Enhances Recombinant Production of an Iron-Sulfur Cluster-Containing Protein. J Bacteriol. 2020;202: e00496-19. doi:10.1128/JB.00496-19

16. Sistrom WRY 1960. A Requirement for Sodium in the Growth of Rhodopseudomonas spheroides. Microbiology. 22: 778–785. doi:10.1099/00221287-22-3-778

17. Lennon CW, Lemmer KC, Irons JL, Sellman MI, Donohue TJ, Gourse RL, et al. A Rhodobacter sphaeroides Protein Mechanistically Similar to Escherichia coli DksA Regulates Photosynthetic Growth. mBio. 2014;5: e01105-14. doi:10.1128/mBio.01105-14

18. Lakey BD, Myers KS, Alberge F, Mettert EL, Kiley PJ, Noguera DR, et al. The essential Rhodobacter sphaeroides CenKR two-component system regulates cell division and envelope biosynthesis. PLOS Genetics. 2022;18: e1010270. doi:10.1371/journal.pgen.1010270

19. Myers KS, Vera JM, Lemmer KC, Linz AM, Landick R, Noguera DR, et al. Genome-Wide Identification of Transcription Start Sites in Two Alphaproteobacteria, Rhodobacter sphaeroides 2.4.1 and Novosphingobium aromaticivorans DSM 12444. Microbiology Resource Announcements. 9: e00880-20. doi:10.1128/MRA.00880-20

20. Nesbit AD, Giel JL, Rose JC, Kiley PJ. Sequence-specific binding to a subset of IscR regulated promoters does not require IscR Fe-S cluster ligation. J Mol Biol. 2009;387: 28–41. doi:10.1016/j.jmb.2009.01.055

21. Rajagopalan S, Teter SJ, Zwart PH, Brennan RG, Phillips KJ, Kiley PJ. Studies of IscR reveal a unique mechanism for metal-dependent regulation of DNA binding specificity. Nat Struct Mol Biol. 2013;20: 740–747. doi:10.1038/nsmb.2568

22. Simon R, Priefer U, Pühler AA. A broad range mobilization system for in vivo genetic engineering: transposon mutagenesis in Gram-negative bacteria. Nat Biotechnol. 1983;(1):784-791. doi: 10.1038/nbt1183-784

23. Schäfer A, Tauch A, Jäger W, Kalinowski J, Thierbach G, Pühler A. Small mobilizable multi-purpose cloning vectors derived from the Escherichia coli plasmids pK18 and pK19: selection of defined deletions in the chromosome of Corynebacterium glutamicum. Gene. 1994;145: 69–73. doi:10.1016/0378-1119(94)90324-7